Report No. FHWA-KS-08-9
FINAL REPORT

THE EFFECTS OF TEMPERATURE ON FIBER COMPOSITE BRIDGE DECKS

Mahesh Gajula Nagabhushanam
Guillermo Ramirez, Ph.D., P.E.
The University of Texas at Arlington
Arlington, Texas

January 2009

KANSAS DEPARTMENT OF TRANSPORTATION

Division of Operations
Bureau of Materials and Research

1 Report No. FHWA-KS-08-9	2 Government Accession No.	3 Recipient Catalog No.
4 Title and Subtitle The Effects of Temperature on Fiber Composite Bridge Decks		5 Report Date January 2009 6 Performing Organization Code
7 Author(s) Mahesh Gajula Nagabhushanam*, Guillermo Ramirez, Ph.D., P.E. *deceased		8 Performing Organization Report No.
9 Performing Organization Name and Address The University of Texas at Arlington Department of Civil Engineering 416 Yates Street, Suite 417 Arlington, Texas 76019-0308		10 Work Unit No. (TRAIS) 11 Contract or Grant No. C1607, IBRC 2002
12 Sponsoring Agency Name and Address Kansas Department of Transportation Bureau of Materials and Research 700 SW Harrison Street Topeka, Kansas 66603-3745		13 Type of Report and Period Covered Final Report May 2006 - Summer 2008 14 Sponsoring Agency Code RE-0330-01

15 Supplementary Notes
For more information write to address in block 9.

16 Abstract

In this study the fiber composite bridge decks were subjected to thermal gradients to obtain the temperature difference between the top and bottom surface of the decks and to determine the thermal properties of the deck. The fiber composite bridge decks were fabricated in sizes of 2 feet wide x 8 feet long x .5 feet deep and 4 feet wide x 8 feet long x .5 feet deep specimens by Kansas Structural Composites Inc. The project consisted of 3 specimens of size 2 feet in width x 8 feet in length x .5 feet in depth with ribs oriented along longitudinal direction, 3 specimens of size 2 feet in width x 8 feet in length x .5 feet in depth with ribs oriented along transverse direction and a specimen of size 4 feet in width x 8 feet in length x .5 feet in depth with ribs oriented along transverse direction. Two specimens with ribs oriented along longitudinal direction and two specimens with ribs oriented along transverse direction of size 2 feet in width x 8 feet in length x .5 feet in depth were subjected to temperature greater than 120˚ F with unrestrained ends. Four tests were carried out on two specimens having ribs oriented along longitudinal direction and two specimens having ribs oriented along transverse direction with the shorter ends restrained. The top surface was exposed to constant temperature until the temperature and the strain linearize at the bottom surface of the fiber composite deck to obtain the difference in temperature between the top and bottom surface of the deck. The decks were restrained using a mechanical setup made up of fiber composite sections. A single specimen of size 4 feet in width x 8 feet in length x .5 feet in depth was tested for thermal loads greater than 120˚ F with unrestrained ends. The strain readings were recorded using strain gage technology from Vishay Micro Measurements and the displacement was measured for specimens with restrained ends using cable extension displacement sensor at half span. A prototype of fiber composite deck was modeled using PRO-E and analyzed using ANSYS FEM software.

17 Key Words	18 Distribution Statement
Fiber Composite Bridge Decks, temperature change, honeycomb FRP	No restrictions. This document is available to the public through the National Technical Information Service, Springfield, Virginia 22161

19 Security Classification (of this report)	20 Security Classification (of this page)	21 No. of pages	22 Price
Unclassified	Unclassified	168	

Form DOT F 1700.7 (8-72)

THE EFFECTS OF TEMPERATURE ON FIBER COMPOSITE BRIDGE DECKS

Final Report

Prepared by

Mahesh Gajula Nagabhushanam
Guillermo Ramirez, Ph.D., P.E.
The University of Texas at Arlington
Arlington, Texas

A Report on Research Sponsored By

THE KANSAS DEPARTMENT OF TRANSPORTATION
TOPEKA, KANSAS

January 2009

NOTICE

The authors and the state of Kansas do not endorse products or manufacturers. Trade and manufacturers' names appear herein solely because they are considered essential to the object of this report.

This information is available in alternative accessible formats. To obtain an alternative format, contact the Office of Transportation Information, Kansas Department of Transportation, 700 SW Harrison Street, Topeka, Kansas 66603-3745 or phone (785) 296-3585 (Voice) (TDD).

DISCLAIMER

The contents of this report reflect the views of the authors who are responsible for the facts and accuracy of the data presented herein. The contents do not necessarily reflect the views or the policies of the state of Kansas. This report does not constitute a standard, specification or regulation.

ABSTRACT

The use of fiber composite honeycomb structures as bridge decks has gained importance because of its light weight and ease of installation.

In this study the fiber composite bridge decks were subjected to thermal gradients to obtain the temperature difference between the top and bottom surface of the decks and to determine the thermal properties of the deck. The fiber composite bridge decks were fabricated in sizes of 2 feet wide x 8 feet long x .5 feet deep and 4 feet wide x 8 feet long x .5 feet deep specimens by Kansas Structural Composites Inc. The project consisted of 3 specimens of size 2 feet in width x 8 feet in length x .5 feet in depth with ribs oriented along longitudinal direction, 3 specimens of size 2 feet in width x 8 feet in length x .5 feet in depth with ribs oriented along transverse direction and a specimen of size 4 feet in width x 8 feet in length x .5 feet in depth with ribs oriented along transverse direction. Two specimens with ribs oriented along longitudinal direction and two specimens with ribs oriented along transverse direction of size 2 feet in width x 8 feet in length x .5 feet in depth were subjected to temperature greater than 120˚F with unrestrained ends. Four tests were carried out on two specimens having ribs oriented along longitudinal direction and two specimens having ribs oriented along transverse direction with the shorter ends restrained. The top surface was exposed to constant temperature until the temperature and the strain linearize at the bottom surface of the fiber composite deck to obtain the difference in temperature between the top and bottom surface of the deck. The decks were restrained using a mechanical setup made up of fiber composite sections. A single specimen of size 4 feet in width x 8 feet in length x .5 feet in depth was tested for thermal loads greater than 120˚F with

unrestrained ends. The strain readings were recorded using strain gage technology from Vishay Micro Measurements and the displacement was measured for specimens with restrained ends using cable extension displacement sensor at half span. A prototype of fiber composite deck was modeled using PRO-E and analyzed using ANSYS FEM software.

ACKNOWLEDGEMENTS

I would like to express my gratitude to Dr Guillermo Ramirez, who conveyed a spirit of adventure in regard to research and scholarship and an excitement in regard to teaching. Without his guidance and help this project would not have been possible.

I would like to thank Dr John H. Matthys and Dr Shih-Ho Chao for serving on my committee. In addition, I would like to thank Mr. Paul Shover, technical lab assistant for his support during testing.

I would like to thank the Graduate School, University of Texas at Arlington for their financial assistance through “Graduate Deans Fellowship” and American Concrete Institute for awarding “American Concrete Institute Northeast Chapter Scholarship” for the term 2006-2007.

I would also like to thank the Kansas Department of Transportation (KDOT) for being a part of my project and for their financial support as well as the Federal Highway Administration (FHWA) for funding through the Innovative Research and Construction Program.

TABLE OF CONTENTS

LIST OF FIGURES

LIST OF TABLES

CHAPTER 1 - INTRODUCTION

1.1 Background

The United States has over 578,000 bridges on public roads. Over 112,000 of them are classified as substandard through deterioration according to a report from ASCE (2001). Fiber Reinforced Polymer (FRP) composites are a natural fit for building and retrofitting bridges, because they offer advantages such as:

- Reduced weight -- the reduced dead weight of the deck allows the bridge girders to carry an increased traffic load.

- Decreased Effects from Environment -- FRPs do not rust and are not affected by salts and other contaminants. They can be affected by ultraviolet radiation (UV) but that is easily resolved by adding pigments to the polymer when it is constructed. This reduces their maintenance costs and promises a longer lifespan.

- The FRP decks have relatively low self-weight (roughly 20% of regular reinforced concrete decks).

Speed in Installation -- Since FRP bridges can be built in a factory; they can be transported to a site and installed in considerably less time than it would take to build a bridge on site with other materials such as concrete. A bridge can be installed in hours or days instead of weeks or months. A large amount of work has been carried out in developing FRP bridges. It is estimated that over 30 million dollars has been spent by the federal government in developing composites for infrastructure usage; over half of

that has been spent on bridges. An extensive research has been carried out by various universities and private companies (NCHRP 503, 2003 and NCHRP 514, 2004).

1.2 Fiber Reinforced Polymer Honeycomb Structures.

The idea of honey comb structures originated in aerospace and automobile industries for their unique features like excellent energy absorption capability and higher mechanical performance with less material weight. The use of composites has gained importance in rehabilitation of structures and new construction in civil infrastructures.

The characteristics of composites influenced Plunkett (Plunkett, 1997) to develop a lightweight and heavy-duty fiber reinforced polymer honeycomb panels for highway bridges, with sinusoidal wave core configuration between top and bottom face laminates. A series of tests and field installations were conducted to determine the structural capacity of the FRP honeycomb structures. However, no design models could be generated due to its complicated honeycomb core geometry and optimize the FRP honeycomb structural panels.

In the recent years, an experimental study on FRP honeycomb panels with sinusoidal core suggesting an approximate analytical solution, which was affirmed by finite element analysis, was carried out by Davalos, et al. (Davalos, Qiao, Xu, Robinson, & Barth).

1.3 Geometry of Honeycomb Core

The FRP composite bridge decks used in this study were supplied by Kansas Structural Composites, Inc. The arrangement of sinusoidal wave ribs between the top and bottom face laminates was to improve the stiffness and buckling response by the

continuous support between sinusoidal wave ribs and the face laminates. Figure 1.1 shows a sample FRP composite bridge deck.

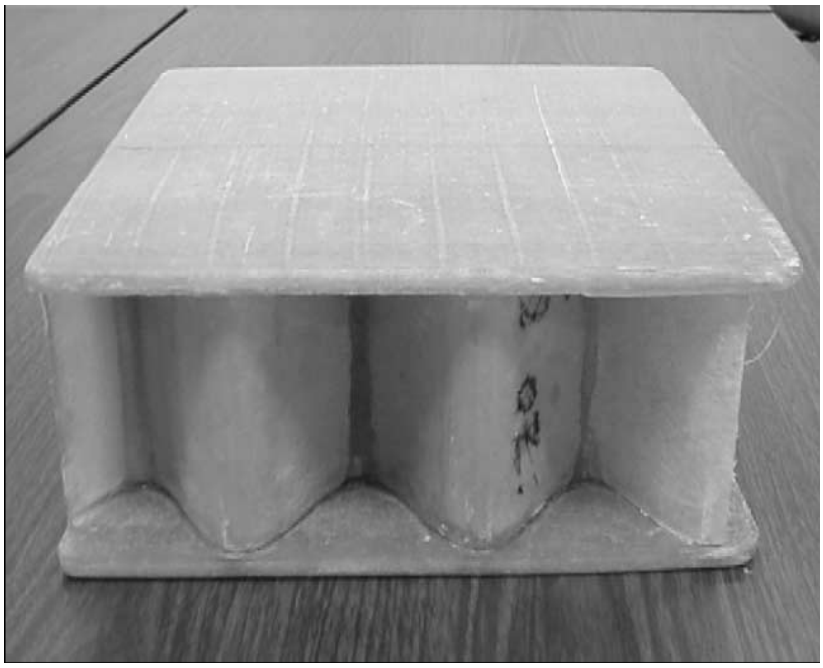

Figure 1.1: FRP Honeycomb Sandwich Panel Ref: 13

The core geometry of a bridge deck consists of closed honeycomb-type FRP cells. The thermosetting property of resin distinguishes honeycomb cores from their metal counterparts in both manufacturing and consequent corrugated shapes. Unlike traditional honeycomb sandwiches structures, the shape of the FRP corrugated cell wall is defined by a sinusoidal function in the plane. The combined flat and waved FRP cells are produced by sequential bonding a flat sheet to a corrugated sheet, which is similar to the processing of the paper resin sandwich panel. The assembled cellular core is then co-cured with the upper and bottom face laminates to build a sandwich panel.

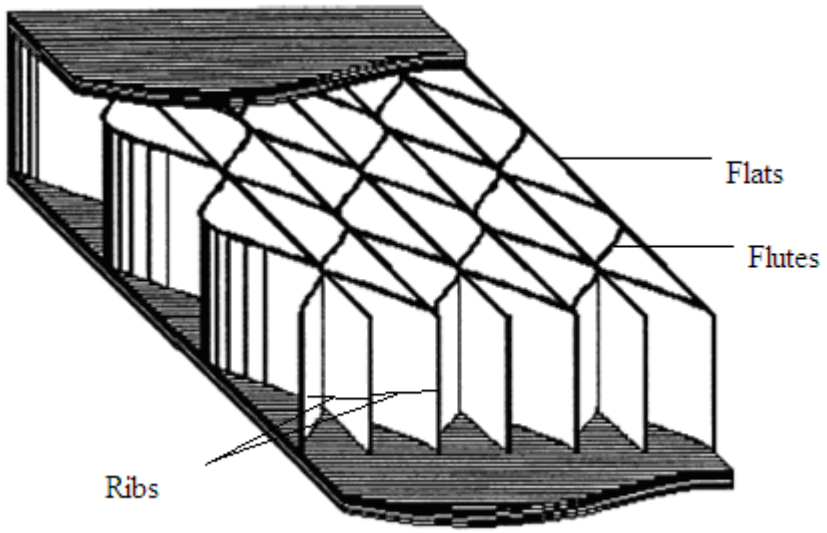

Figure 1.2: Configuration of Sandwich Panels Ref: 13

The waved flutes or core elements are produced by forming FRP sheets to a corrugated mold. As shown in Figure 1.2, the distance of adjoining crests represents the wavelength l, and the interval between two adjoining flats gives the amplitude 2h. In the coordinate system of Figure 1.3, the wave function of corrugated core wall can be defined as

$$y = h\left(1 - \cos\frac{2\pi x}{l}\right) \qquad \text{Equation 1.1}$$

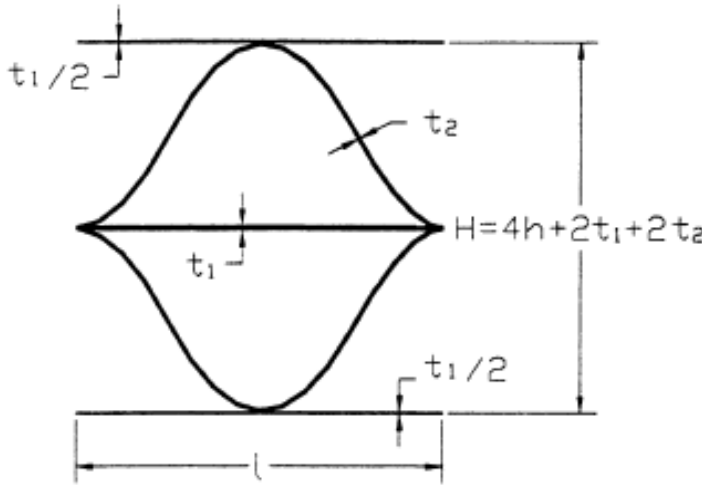

l: Wavelength, 2h: Amplitude, t_1: Thickness of Flat and t_2: Thickness of Flute

Figure 1.3: Part of Honeycomb Configuration Ref: 13

1.4 Coefficient of Thermal Expansion for Uni-directional Composites

The coefficient of thermal expansion can be defined as the change in length of a material to a degree of temperature change. It is the thermodynamic property of a material as given by Incropera & DeWitt (Schapery, 1986). The coefficient of thermal expansion would remain the same in all directions for an isotropic material and differ for a composite material made of different materials. In 1968 (Schapery, 1986) Schapery derived an expression for coefficient of thermal expansion for unidirectional composites.

$$\alpha_L := \frac{1}{E_L}\left(\alpha_f * E_f * V_f + \alpha_m * E_m * V_m\right) \qquad \text{Equation 1.2}$$

$$\alpha_T := (1+\nu_f) * \alpha_f * V_f + (1+\nu_m) * \alpha_m * V_m - \alpha_L * \nu_{LT} \qquad \text{Equation 1.3}$$

Where αL and αT are coefficients of thermal expansion along longitudinal and transverse direction. Ef and Em are modulus of elasticity of fiber and matrix

respectively. Vf and Vm are volume of fiber and matrix respectively. uf and um are possion’s ratio of fiber and matrix respectively.

CHAPTER 2 - LITERATURE SURVEY

2.1 Introduction

The concept of designing materials or civil structures is based upon the probability of the load intensity and different kinds of loads over time. Temperature loads are considered as a vital part of designing materials and structures, because the structural response varies with the thermal effect. Bridges experience a higher temperature difference on bridge deck slabs. Fiber-Reinforced Polymer Bridge decks undergo a higher temperature difference over the depth than the regular concrete bridge decks because the value of thermal conductivity of fiber material is much less than concrete. The temperature difference between the top and bottom surfaces would be around 3 times more in fiber reinforced bridge decks than in concrete bridge decks.

2.2 Behavior of Composite Decks Due to Thermal Loads.

An investigation by Jack H. Emanuel and J. Leroy Hulsey (Emauel & Hulsey, 1978) concluded that, the temperature distribution within a bridge structure is a function of ambient air temperature, the short wave radiation absorbed by the bridge deck, the heat transfer due to long wave thermal radiation, the film coefficient, and the thermal properties of the materials used. Higher thermal gradient with the bridge deck can be achieved by adding a thin layer of asphalt. The intensity of stresses in a composite bridge deck depends on the temperature distribution; the internal forces due to change in different coefficients of thermal expansion and the support conditions. The maximum temperature difference between the top and bottom of a concrete deck slab can be as high as 40˚F (22˚C) during the summer and as low as -10˚F (-6˚C) in the winter as

observed by Zuk (Zuk, Thermal Behavior of Composite Bridges-Insulated and Uninsulated, 1965). The field results obtained by Zuk over the Hardware River near Charlottesville, North Carolina on a composite bridge with a temperature difference between top and bottom ranged from +20˚F to 35˚F (11˚C to 19˚C) during the day, and -3˚F to -7˚F (-2˚C to -4˚C) during the night. In 1987 John B. Kennedy and Mohamed H. Soliman (Kennedy & Soliman, 1987) proposed a linear-uniform vertical temperature distribution through the composite bridge section of concrete deck slab-on-steel beams, which appeared to be realistic and simple to implement. The recommended values of temperature difference, ΔT are given in Table 2.1.

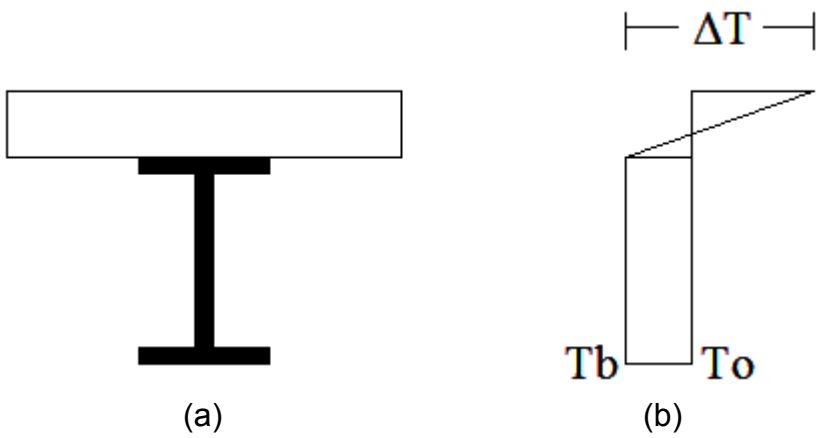

T_o = Temperature at Casting T_b = Mean Seasonal Temperature

Figure 2.1: (a) and (b): Linear-Uniform Vertical Temperature Distribution Ref: 3

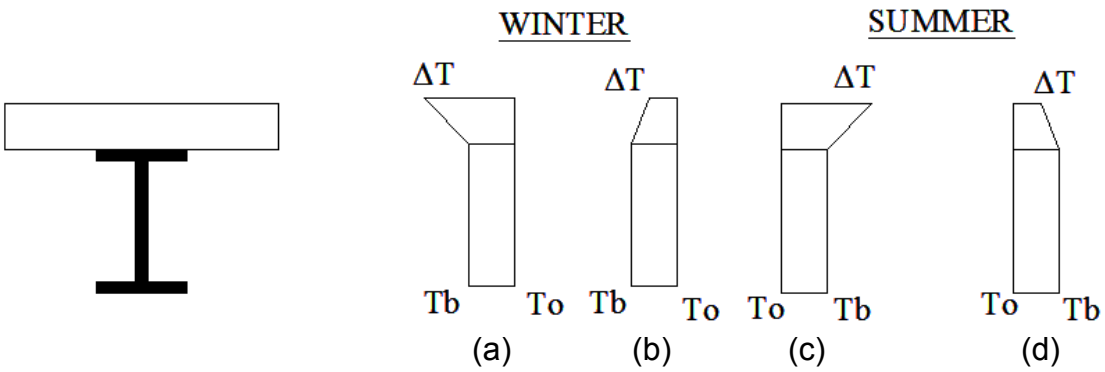

Figure 2.2 (a), (b), (c), (d): Critical Cases of Temperature Conditions for Design Ref: 3

Table 2.1: Recommended Values for Temperature Differential, ΔT

Season	Maximum ΔT (degrees Fahrenheit)	Maximum ΔT (degrees Fahrenheit)
Summer	40	-7.5
Winter	20	-7.5

According to Churchward and Sokal (Churchward & Sokal, 1981), structures are subjected to a non-uniform temperature distribution, which could be categorized into three different components of temperature strains as uniform, linear and nonlinear components. The uniform component is the average strain which will produce axial movement without stress if the movement is unrestrained. Total restrain of the axial movement would induce stress without strain, and partial restraint would produce some combination of stress and strain. The linear component is a curvature-inducing strain which will produce vertical deflections and curvature without stress if the vertical movement is completely unrestrained. Total restraint of vertical movement would induce stress without strain, and partial restraint would produce some combination of stress and strain. The nonlinear component of the temperature strain is a stress inducing strain with stresses resulting from the continuity of the cross section and the assumption that the plane sections remain plane. The nonlinear component may also be produced in

non-homogeneous and anisotropic material or in a composite beam as a result of nonlinear strains caused by different coefficients of thermal expansion with a linear temperature distribution.

2.3 Previous Studies on FRP Composite Decks Subjected to Thermal Loading

An experiment was conducted evaluating the performance of FRP Composite bridge deck prototypes under high and low temperature by Dutta, Kwon and Lopez-Anido (Dutta, Kwon, & Anido, 2003). The FRP composite bridge decks were subjected to simulated traffic loads that induce repetitive stress cycles under two extreme temperature conditions: -22˚F (-30˚C), and 122˚F (50˚C). Initially each prototype deck was subjected to one million simulated wheel load cycles at low temperature, -30˚C (-22˚F), and another one million cycles at a controlled high temperature, 50˚C (122˚F). Later, the decks were subjected to four million simulated wheel load cycles at -22˚F (-30˚C) and another four million cycles at 122˚F (50˚C). The fatigue performance of each FRP deck prototype was compared with the response of the conventional reinforced-concrete deck. The results signified the progressive degradation in stiffness of the FRP composite bridge decks under two extreme temperatures, -22˚F (-30˚C) and 122˚F (50˚C) with load cycles for all the decks. The stiffness of FRP composite bridge decks was more susceptible to two extreme temperature changes than to ten million cumulative load cycles.

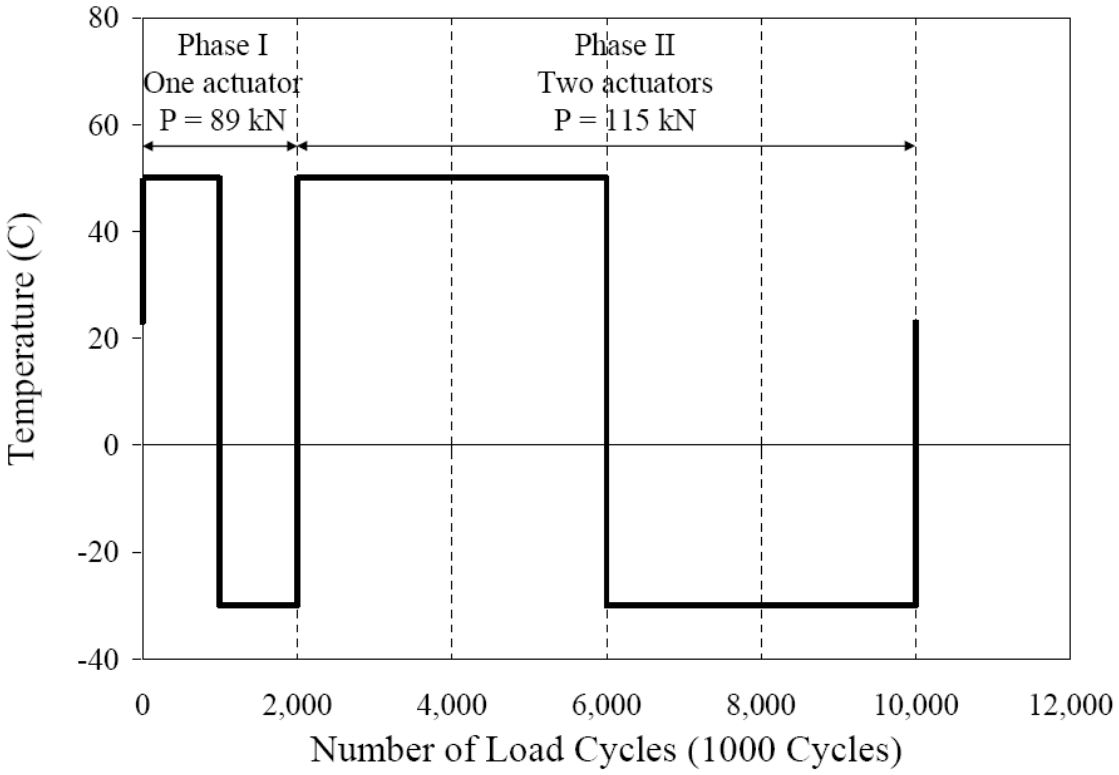

Figure 2.3: Load Cycling and Temperature History Ref: 7

Tests conducted by Kwon, et al. (Kwon, Dutta, Eum, Shin, & Lopez-Anido, 2004) exhibited higher stiffness in reinforced-concrete deck and the FRP-concrete hybrid deck than in FRP composite decks. Load deflection curves for each deck prototype after two million load cycles and after 10 million load cycles are shown as in Figures 2.4 to 2.6. The decrease in slope of the load deflection curves with number of fatigue cycles, indicate damage accumulation in the decks.

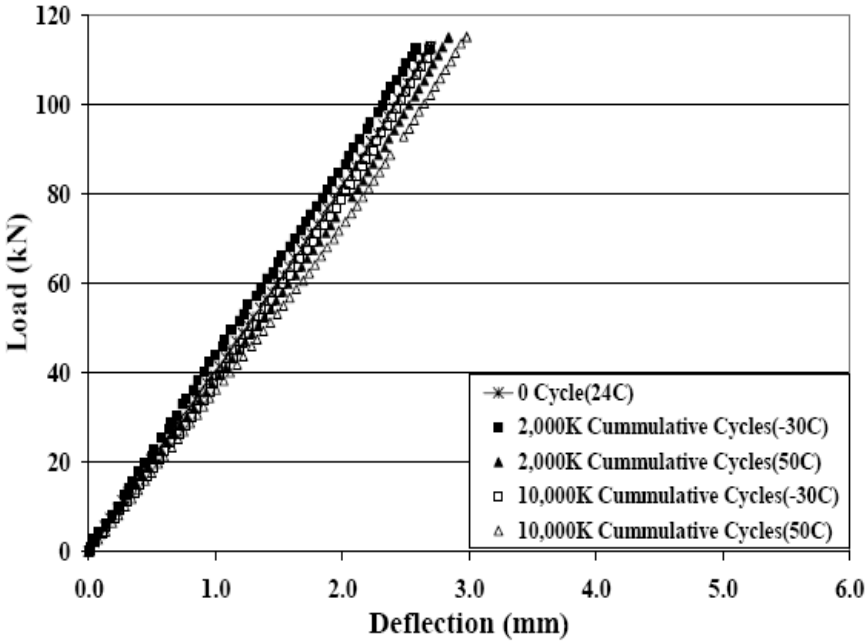

Bridge #1

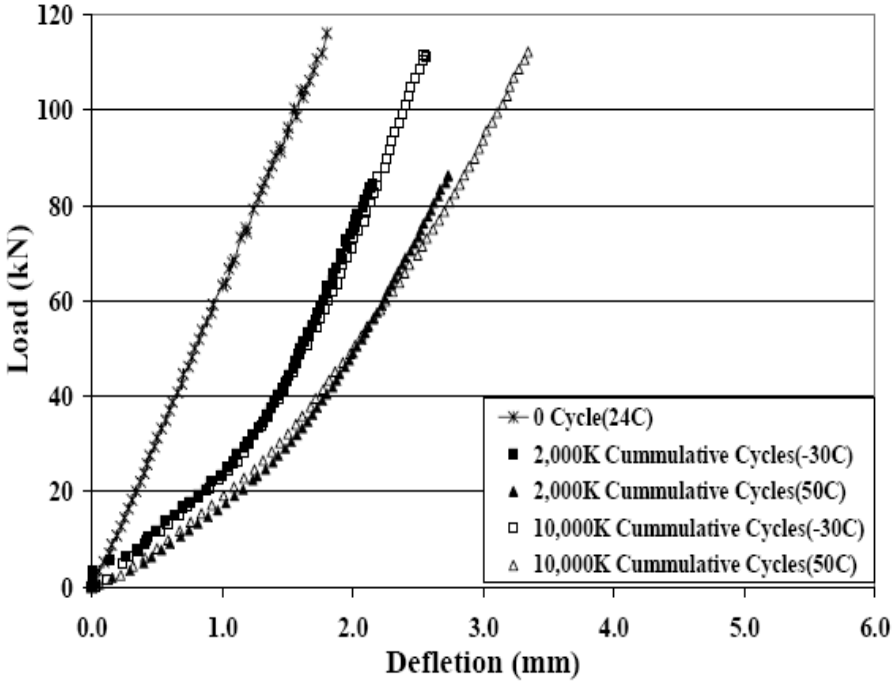

Bridge #2

Figure 2.4: Load-Deflection Curves for Bridge #1 and #2 Ref: 8

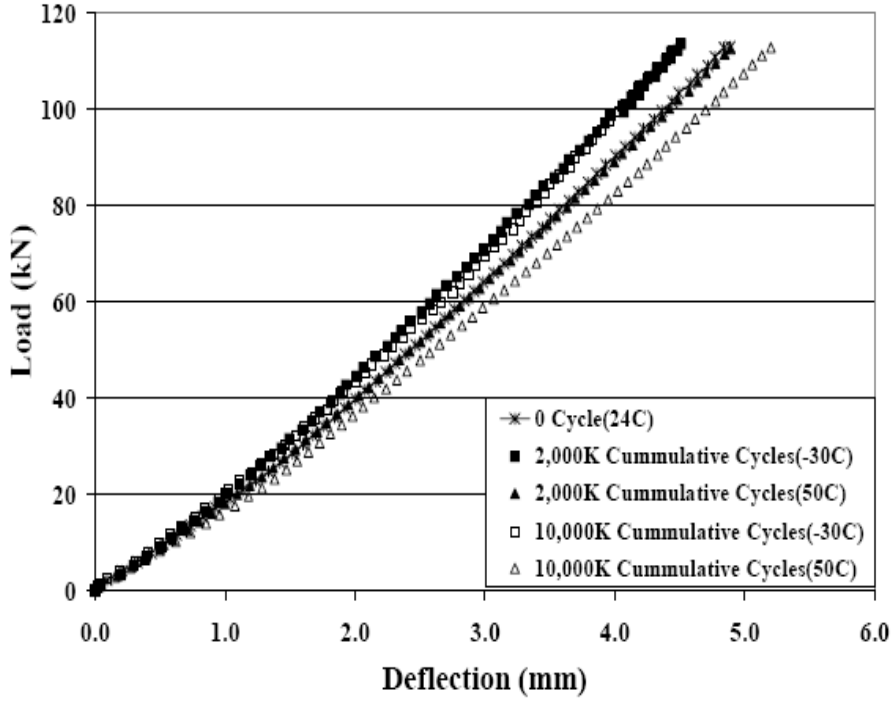

Bridge #3

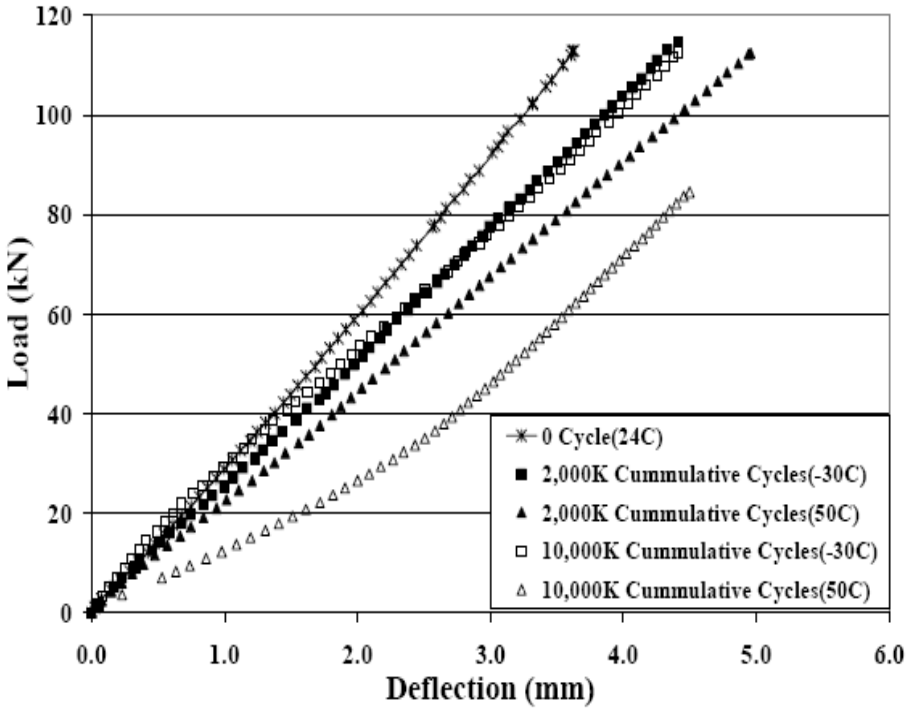

Bridge #4

Figure 2.5: Load-Deflection Curves for Bridge #3 and #4 Ref: 8

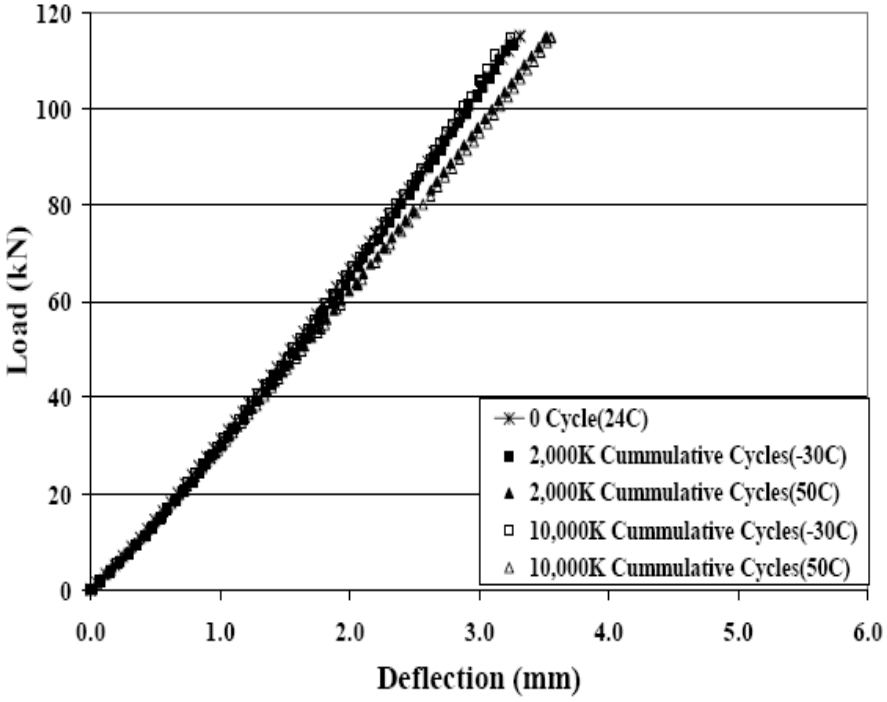

Bridge #5

Figure 2.6: Load-Deflection Curve for Bridge #5 Ref: 8

CHAPTER 3 - TEMPERATURE TESTS

3.1 Standards

3.1.1 Temperature Test Standard

A series of temperature tests were carried on the fiber composite bridge deck at University of Texas at Arlington (UTA). The tests were performed inside the UTA laboratory simulating the environmental conditions. Since, there were no specific standards available for temperature tests on fiber composite bridge deck, ”Standard Test Method for Thermal Conductivity of Unfired Monolithic Refractories” was used as a reference standard ASTM C 417-05. The temperature test methods were derived from ASTM C 417-05 as suitable for fiber composite bridge deck. The decks were either placed on 2 feet x 8 feet or 4 feet x 8 feet wood frame at 2.5 feet above the ground. The heaters were suspended at 1.5 feet above the top surface of the deck to a frame constructed using punched angles. The space between the heaters and the deck was covered with the insulation foil on tempered hardboards. The 2.5 feet height around the wood frame were covered with cardboard.

The tests were conducted on 7 specimens with a total of 9 tests. Two specimens were retested during the restrained end experiment. The heaters were controlled using a control panel with K type Thermocouple. Ibutton technology from Maxim Integrated products were used to record the temperature around the setup. The Tests carried out are tabulated in Table 3.1.

Table 3.1: Temperature Tests

Test No	Specimen Size (feet)	Orientation of Ribs	End Condition
1	2 x 8	Longitudinal	Unrestrained
2	2 x 8	Longitudinal	Unrestrained
3	2 x 8	Transverse	Unrestrained
4	2 x 8	Transverse	Unrestrained
5	2 x 8	Longitudinal	Restrained
6	2 x 8	Longitudinal	Restrained
7	2 x 8	Transverse	Restrained
8	2 x 8	Transverse	Restrained
9	4 x 8	Longitudinal	Unrestrained

Strain gages were installed and strain data were recorded by a data acquisition system. Two uni-axial strain gages were installed at quarter spans along longitudinal and transverse direction on top and bottom surfaces. A rectangular rosette and temperature strain gages were installed at half spans on top and bottom surfaces. A cable extension displacement sensor was used at half span on bottom surface during restrained end tests. Since the specimen was subjected to thermal load, both the specimen and strain gage expands. The acquired strain data is composed of strain due to Fiber composite deck and strain gage. In order to overcome the effect of thermal strain on strain gages, an excellent reference material ULE Titanium Silicate Code 7971 with property “absolute” expansion coefficient was used as per Vishay technical note TN-513-1. This particular glass has a very low thermal expansion over the temperature range -50˚F to +350˚F (-45˚C to +175˚C). Strain gage was installed on the specimen and the reference material. The reference material was placed in such a position to experience the same level of thermal loads as the specimen. The final strain was

calculated by subtracting the strain on the reference material from strain on Fiber composite deck.

$$\varepsilon = \varepsilon_{specimen} - \varepsilon_{reference\ material} \qquad \text{Equation 3.1}$$

The data from the temperature sensors were transferred to the acquisition system using a matching LST Network as specified in Vishay Tech note TN-506-3.

3.1.2 Standards for Coupon Testing:

The coupons of fiber composite deck and fiber composite tubular sections were tested for tensile properties. The dimensions of the coupons were derived from the ASTM D 3039/D 3039M -00 as it could be machined (See Appendix B). The results of the tension tests were recorded using strain gage technology.

3.2 Material

3.2.1 Fiber Composite Bridge Deck:

Six specimens of size 2 feet in width x 8 feet in length and 4 feet in width x 8 feet in length fiber composite bridge decks made of glass fiber were used for the testing. Two types of specimens were included in 2 feet in width x 8 feet in length specimens. The Type I specimen has fiber ribs oriented along longitudinal axis and Type II has fiber ribs oriented along transverse direction.

Figure 3.1: Fiber Composite Bridge Deck of Size 2 feet x 8 feet

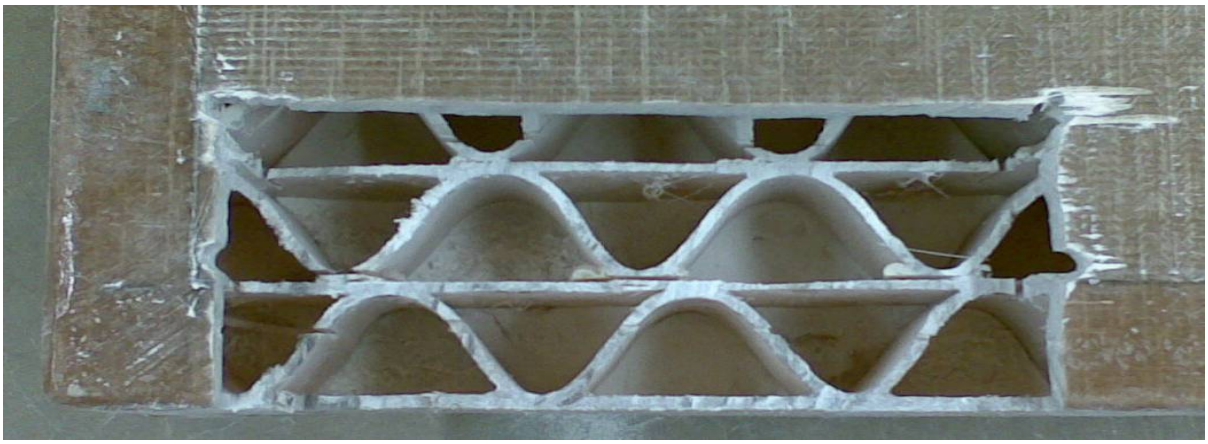

Figure 3.2: Cut Section of Type I Specimen

Fiber composite bridge decks are made up of flutes and flats. The fiber composite bridge decks are classified as Type I and Type II based upon the orientation of flutes in longitudinal and transverse direction respectively as shown in the Figure 3.4 and 3.5. The flutes are covered on all the sides by flats.

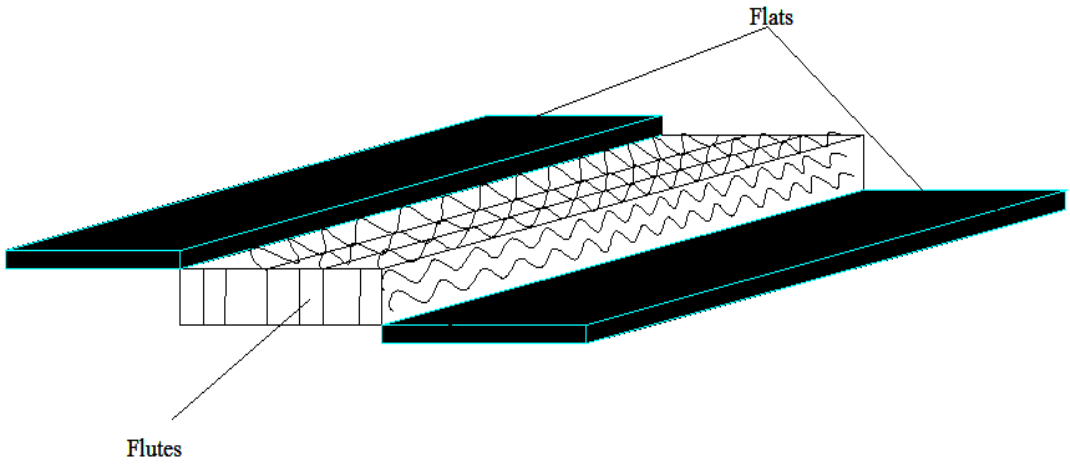

Figure 3.3: Components of Fiber Composite Bridge Deck

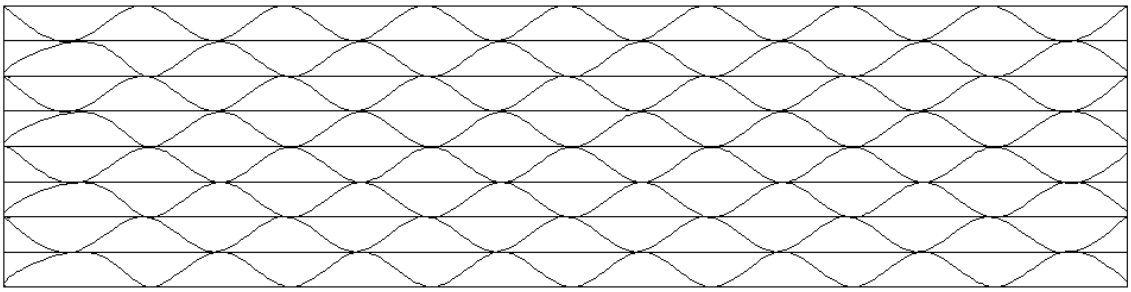

Figure 3.4: Type I Fiber Composite Bridge Deck

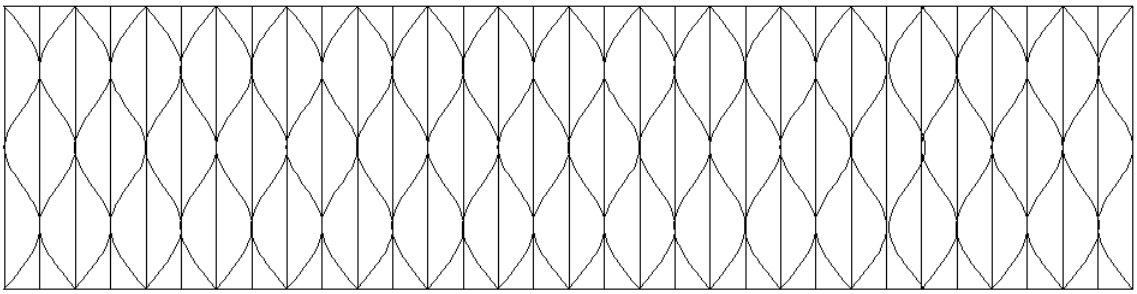

Figure 3.5: Type II Fiber Composite Bridge Deck

3.2.2 Types of Material

Chopped Strand Mat (CSM)

This is a very basic material that has been used thoroughly in industry for quite some time. The best asset of this material is its bonding ability with other layers and its secondary bond strength. This is the main reason the material is used next to the core or in areas where a stronger bond is needed. This is due to the materials ability to form around whatever shape it needs to, thus increasing the surfacing which increase the strength at which the material will begin to delaminate. Since most of the delamination is a product of the shear strength of the material, KSCI (Kansas Structural Composites Inc.) wants to maximize this contact area, thus the reason why CSM is used.

Biaxial (TVM)

The biaxial material used in this application is a basic interwoven fiber pattern in which there is a 50/50 mix of fibers orientated in both the principle direction, 0 degrees, and the transverse or lateral direction, 90 degrees. This provides for the same modulus in both directions.

Uniaxial (UM)

The uniaxial material consists of all fibers orientated in the principle direction.

3.2.3 Detailed Composition of Fiber Composite Bridge Deck

Table 3.2: Core Designation

Core Designations

	Flats					
Flutes	csm150	csm300	csm450	csm600	tvm3408	2@um1810
csm150	CM1515	CM3015	CM4515	CM6015	TM3415	UM3615
csm300	CM1530	CM3030	CM4530	CM6030	TM3430	UM3630

Table 3.3: Laminate Properties per Square Foot and per Board Foot of Core

Laminate Properties per Square Foot

Flat Laminates		Weight (lbs)		Glass	Nominal		Cost	
Layers	Description	Glass	Resin	Lamina	Percent	Thickness	Glass	Resin
1	csm150	0.094	0.141	0.234	40%	0.030	$0.12	$0.14
1	csm300	0.188	0.281	0.469	40%	0.060	$0.23	$0.27
1	csm450	0.281	0.422	0.703	40%	0.090	$0.35	$0.41
1	csm600	0.375	0.563	0.938	40%	0.120	$0.47	$0.54
1	tvm3408	0.283	0.332	0.615	46%	0.075	$0.52	$0.51
2	um1810	0.320	0.320	0.640	50%	0.076	$0.61	$0.43
Flute Laminates								
1	csm150	0.094	0.141	0.234	40%	0.030	$0.12	$0.14
1	csm300	0.188	0.281	0.469	40%	0.060	$0.23	$0.27
1	csm450	0.281	0.422	0.703	40%	0.060	$0.35	$0.41

Laminate Properties per Board Foot of Core

Flat Laminates		Weight (lbs)		Glass	Nominal		Cost	
Layers	Description	Glass	Resin	Lamina	Percent	Thickness	Glass	Resin
1	csm150	0.047	0.070	0.117	40%	0.030	$0.059	$0.068
1	csm300	0.094	0.141	0.234	40%	0.060	$0.117	$0.136
1	csm450	0.141	0.211	0.352	40%	0.090	$0.176	$0.204
1	csm600	0.188	0.281	0.469	40%	0.120	$0.234	$0.272
1	tvm3408	0.142	0.166	0.308	46%	0.075	$0.262	$0.254
2	um1810	0.160	0.160	0.320	50%	0.076	$0.307	$0.216
Flute Laminates								
1	csm150	0.066	0.098	0.164	40%	0.030	$0.082	$0.095
1	csm300	0.131	0.197	0.328	40%	0.030	$0.164	$0.191
1	csm450	0.197	0.295	0.492	40%	0.030	$0.246	$0.286

Table 3.3 defines different kinds of laminate and their physical properties which are used in preparing flats and flutes used in preparing the fiber composite deck. The Table 3.2 defines the core designations based upon the kind of flats and flutes used in preparing the ribs.

3.2.4 Fiber Composite Sections

An arrangement was made using fiber Composite tubular sections and W sections to restrain the bridge decks during restrain condition testing.

Figure 3.6: W Section

Figure 3.7: Tubular Sections

Figure 3.8: Restrained End Experiment

3.3 Equipment

3.3.1 Heaters

"O" Model Heaters from Intek Corporation

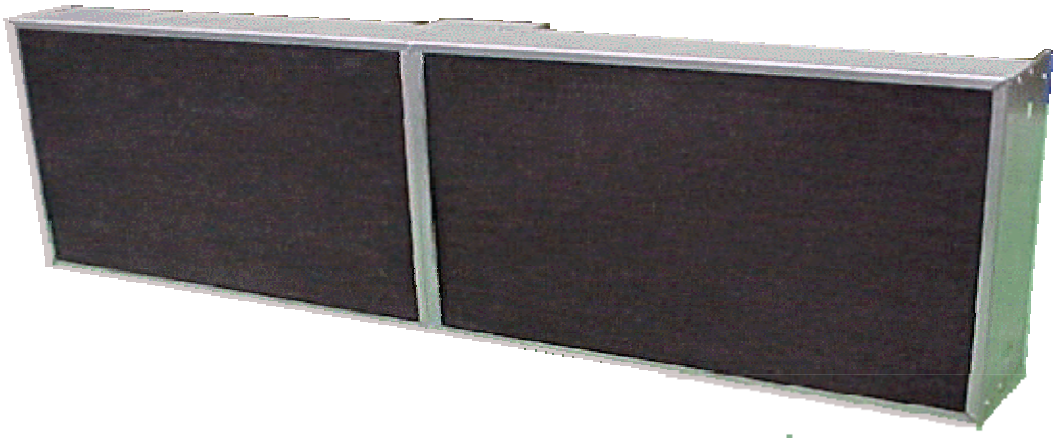

Figure 3.9: O model Heater Ref: 17

Table 3.4: Technical Specification of Heaters

Technical Specification

Output Surface	Dimensions	Watts	Volts	Amps	Shipping Weight
12" x 48"	12" x 48" x 5 ½ "	4800	230/460	21.0/10.5	35 lbs

The heaters were arranged for the experiments as shown in the figures below.

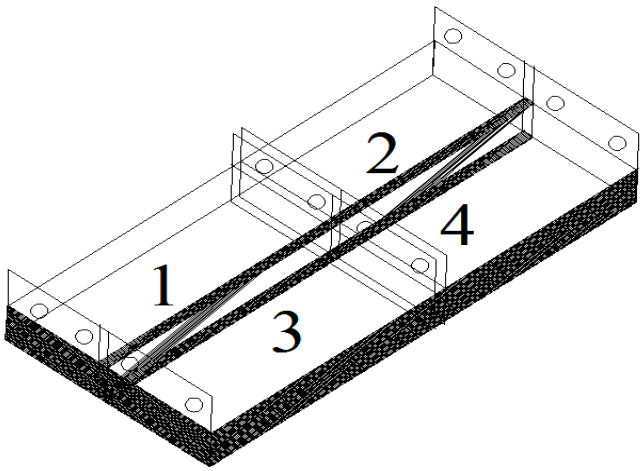

Figure 3.10: Describing the Heaters Setup for 2 feet x 8 feet Specimen.

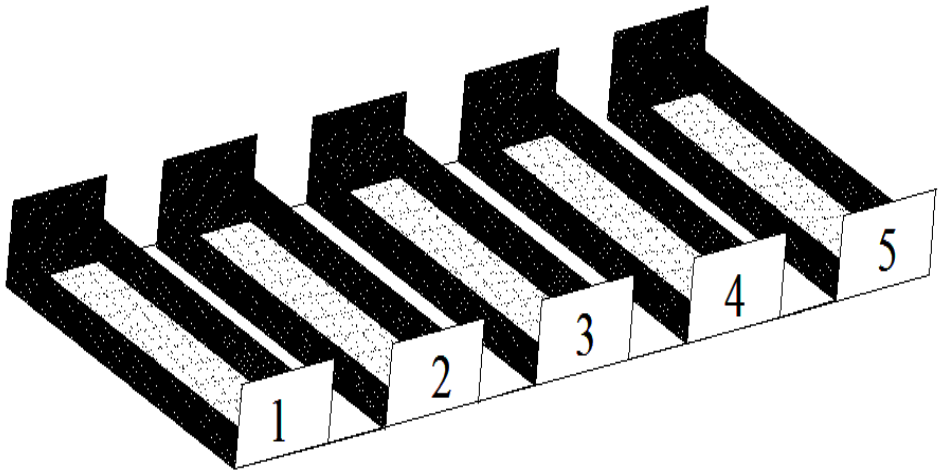

Figure 3.11: Describing the Heaters Setup for 4 feet x 8 feet Specimen.

1. The heaters were suspended using metal chain and hooks from framework made of punched angles.
2. Aluminized sheet baffles were placed in between the heaters to reduce the heat loss for 4 feet x 8 feet experimental setup.
3. Since each of the heaters included a built in junction box, Flex conduits were used in between the heaters and the control panel.
4. The heaters were interconnected in a delta network as advised by “Intek Corporation” using #12 THHN wires.
5. 6-3 NM WG wire was used to connect between external power supply and the Control panel.
6. K-type Thermocouple is fixed to the heaters to control the temperature.
7. The temperature can be controlled using a digital front panel on the control panel.

3.3.2 Control Panel

A custom made digital control panel with a K type thermocouple designed by Intek Corporation for 5 heaters with a requirement of 40 Amps from a three phase 480 volts electrical supply.

Figure 3.12: Control Panel

3.3.3 Technical Details:

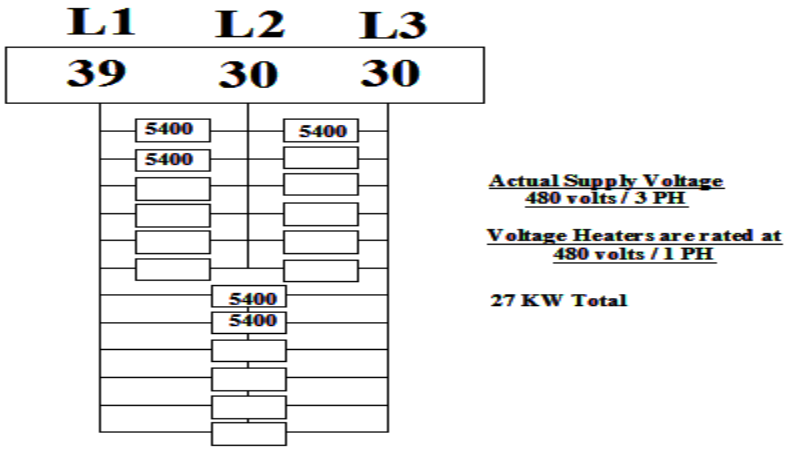

Figure 3.13: Actual Voltage Supply Diagram

Electrical Wires:

#12 TGGT wires

#8 THHT wires

3.3.4 Computer

Gateway Desktop PC Powered By, Intel Pentium III Processor, 646 MHZ, 192 MB of Ram, Microsoft Windows XP, Professional Version 2002 Service Pack2

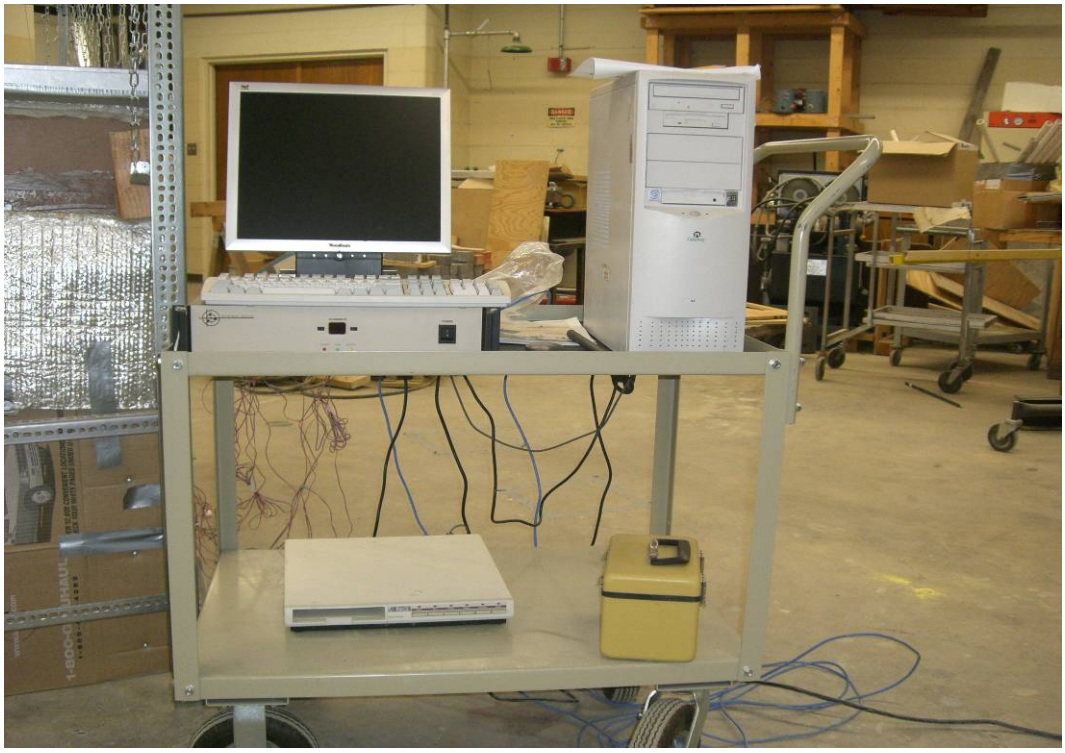

Figure 3.14: Computer

3.3.5 Strain Gage:

3.3.5.1 5100B Scanner

Figure 3.15 Model 5100B Scanner Front and Rear Panel Ref: 17

3.3.5.2 Uni-axial Strain Gage - C2A-06-250LR-350

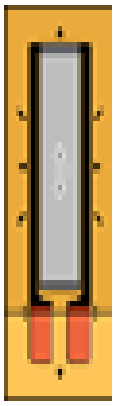

Figure 3.16: Uniaxial strain gage 250 LR Ref: 17

3.3.5.3 Rosette - C2A-060250LR-350

Figure 3.17: Rectangular Rosette 250 LR Ref: 17

3.3.5.4 Temperature Sensor - ETG-50B/W

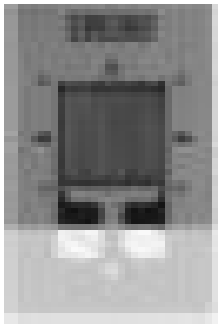

Figure 3.18: Temperature Sensor ETG-50 B/W Ref: 17

3.3.5.5 Cable Extension Displacement Sensor - CDS-20

Figure 3.19: Cable Extension Displacement Sensor

3.3.5.6 LST Matching Network - 10F-350D

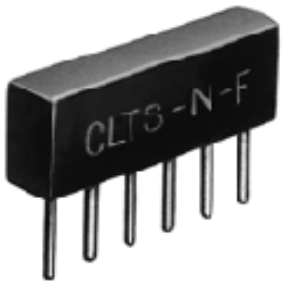

Figure 3.20 LST Network-10F-350D Ref: 17

3.3.5.7 M-Bond 200 Adhesive

Figure 3.21 M-Bond Adhesive Kit Ref: 17

3.3.6 Palm M105

Figure 3.22: Palm M105 Ref: 18

3.3.7 Temperature IButton

Figure 3.23: IButton Ref:19

3.4 Procedure

- Wood frame was built to place composite fiber decks.
- .125” Teflon was adhered on short sides of wood frame.
- Fiber composite bridge decks are strain gauged with uniaxial strain gages, rectangular rosettes and temperature strain gages.
- Uniaxial strain gages are bonded along longitudinal and transverse direction at quarter spans on top and bottom surface of fiber composite bridge deck.
- Rectangular rosettes are bonded at center spans on top and bottom surface of fiber composite bridge deck.
- Temperature gages are bonded at center spans on top and bottom surface of Fiber composite bridge deck.
- Displacement transducer was position at centre span for restrained condition testing of the specimen.
- Set up consisting of heaters on punched angle frame is moved on top of fiber composite bridge deck. It is sealed using duct tape.
- K-Type thermo couple is fixed in between the heaters and deck.
- IButtons are programmed using Palm M105 and placed at left, right and top of the setup.
- IButton is bonded at mid height of the deck using duck tape and placed in the lower encapsulated box below fiber composite bridge deck.
- The bridge decks are restrained using composite tubular and w sections. This step is carried out only for restrained end conditions.

- The test is started by switching on the control panel and the decks are subjected to a linear increase in temperature from room temperature to the maximum desired temperature.
- The decks were exposed to desired temperature until the strain values stabilized.
- The readings were retrieved using a 5100B scanner and recorded to a computer powered by Intel Pentium III processor.

CHAPTER 4 - RESULTS AND CONCLUSIONS

4.1 Introduction

The data (located in Appendix C) acquired from the heat and coupon experimental tests were plotted on a graph with time (hours) on the x-axis. Strain and temperature readings were plotted on the y-axis. In all the temperature tests, the top surface of the fiber deck was subjected to constant temperature, until the bottom surface stabilizes with the temperature, strain and deflection readings. The duration, number of scans, highest top surface temperature, highest bottom surface temperature, deflection and strain on restraining mechanism for each experiment has been listed below in the Table4.1

Table 4.1: Details of Temperature Tests

Test No	Duration Hours	Number of Scans	T_T (˚F)	T_B (˚F)	Deflection (mm)	Straining Strain
1	10.83	77948	125.4	91.2	-	-
2	69.18	24907	143.3	95.8	-	-
3	49.13	17686	134.9	94.1	-	-
4	48.39	17420	122.6	89.6	-	-
5	74.2	26712	125.2	94.3	1.0958	-70E-06
6	53.89	19401	131.9	88.2	2.4866	-74E-06
7	46.79	16845	147.4	99.5	1.8965	-218E-06
8	79.52	28629	147.6	98.5	4.1724	-219E-06
9	72.12	26176	145.3	101.1	-	-

The strain readings recorded for the specimens are corrected for thermal effect on strain gages using a reference material as stated earlier. The corrected strain readings were used to plot the graphs (located in Appendix C).

$$\varepsilon = \varepsilon_{specimen} - \varepsilon_{reference\ material} \qquad \text{Equation 4.1}$$

4.2 Coupons

The coupons of fiber composite deck and fiber composite tubular sections were tested for tensile properties. The dimensions of the coupons were derived from the ASTM D 3039/D 3039M -00 as it could be machined. The results of the tension tests were recorded using strain gage technology and can be found in Appendix C.

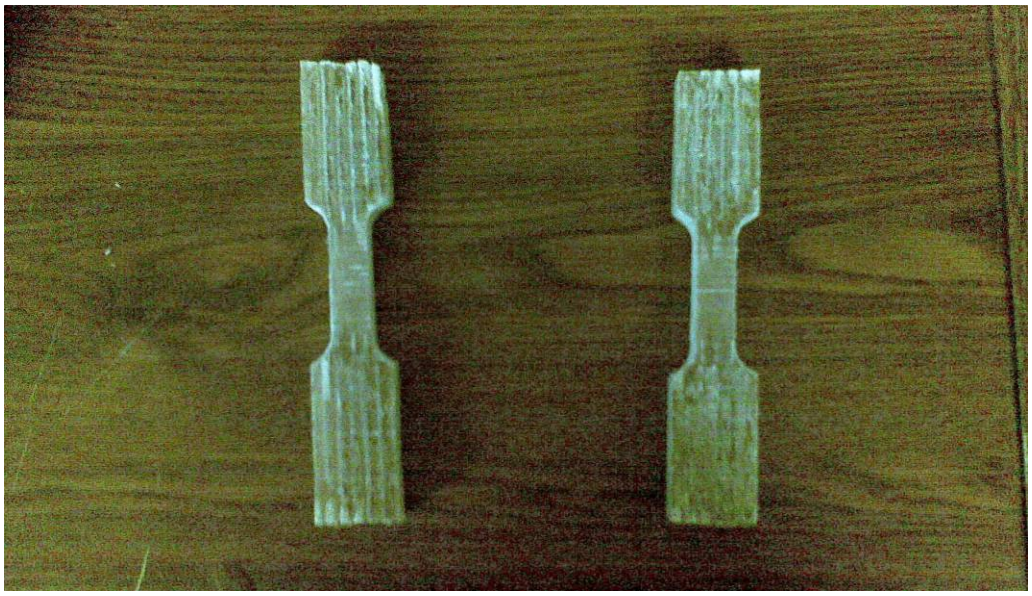

Figure 4.1: Fiber Composite Deck Coupons before Testing

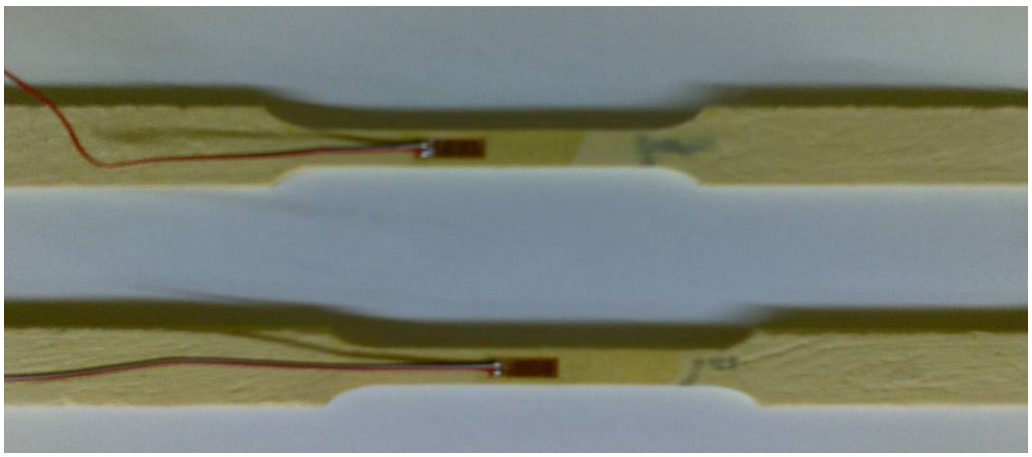

Figure 4.2: Fiber Composite Tubular Section Coupons before Testing

Figure 4.3: Fiber Composite Deck Coupon after Testing

Figure 4.4: Fiber Composite Tubular Section Coupon after Testing

The coupons failed by delamination of the lamina.

4.3 Four Point Bending Test on Fiber Decks Subjected to Temperature Tests.

The fiber composite decks, tested for temperature tests with ribs oriented along transverse and longitudinal directional were tested for four point bending test. The fiber composite decks which were tested for temperature tests in test numbers 2, 4, 6 and 8 were tested for structural response after the effect of temperature on fiber composite decks. The strain and displacement readings were recorded using strain gage technology. The strain gages were installed at half span on top and bottom surfaces of the fiber composite decks. The fiber composite decks were loaded at two points one foot from the center. The figure below shows the experimental setup.

Figure 4.5: Four Point Bending Test

The fiber decks were loaded to the point of failure. The results of the four point bending test for a fiber composite deck panel with ribs oriented in longitudinal direction and transverse direction are as follows.

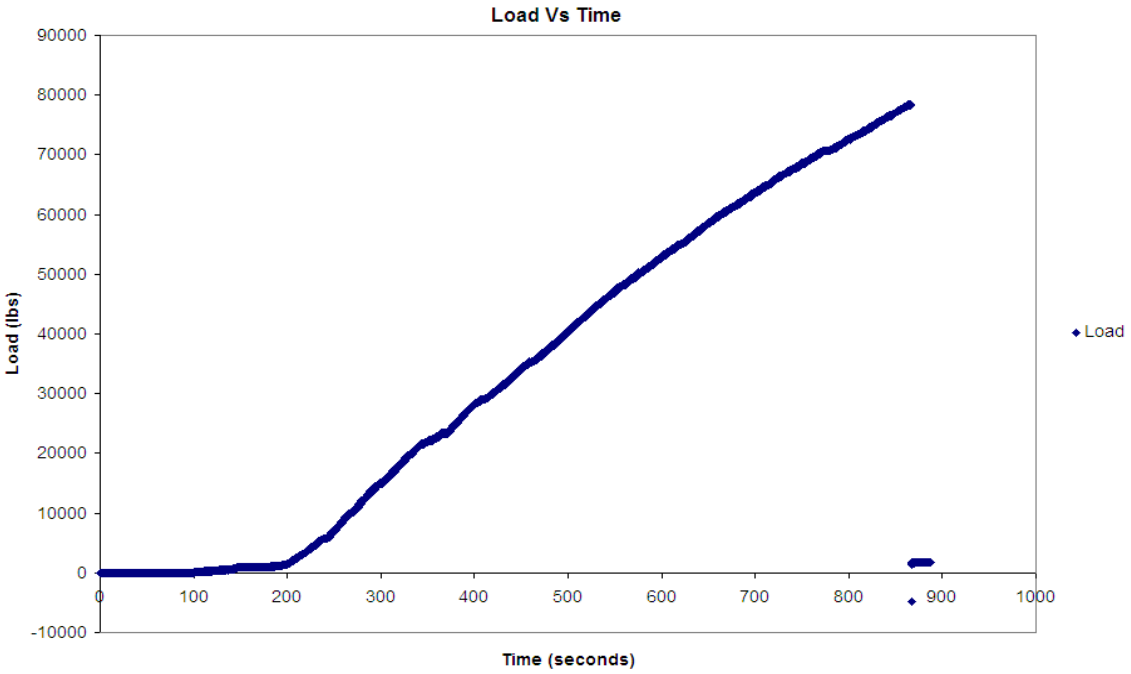

Figure 4.6: Load Vs Time for Fiber Deck with Longitudinal Ribs

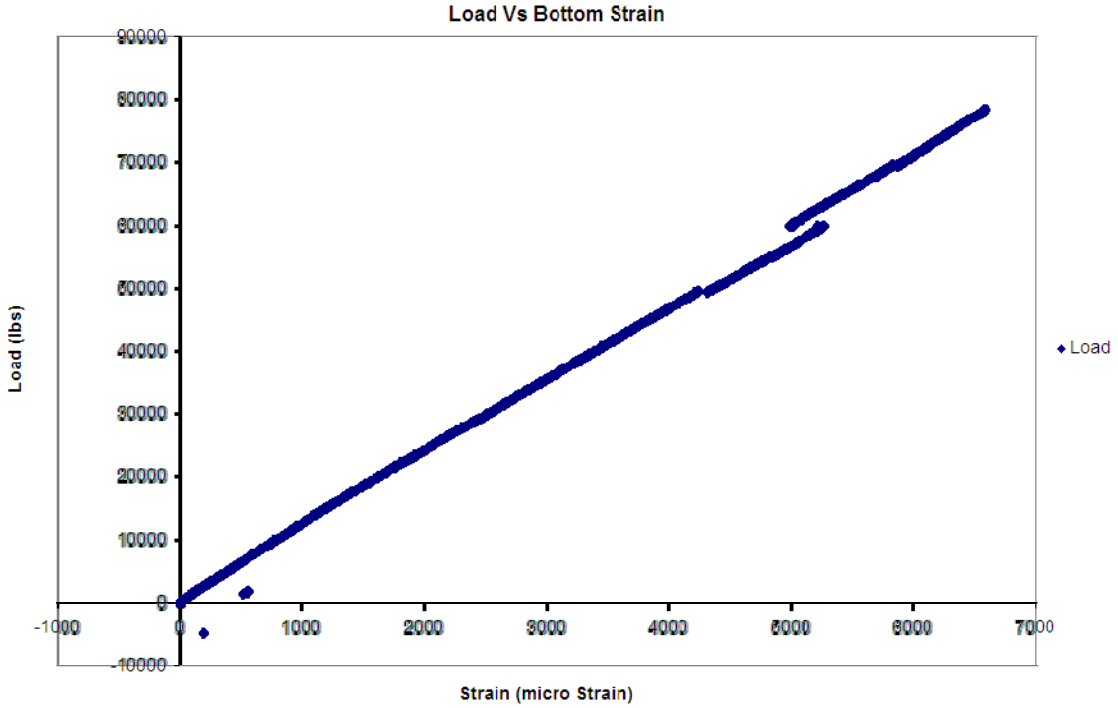

Figure 4.7: Load Vs Bottom Strain for Fiber Deck with Longitudinal Ribs

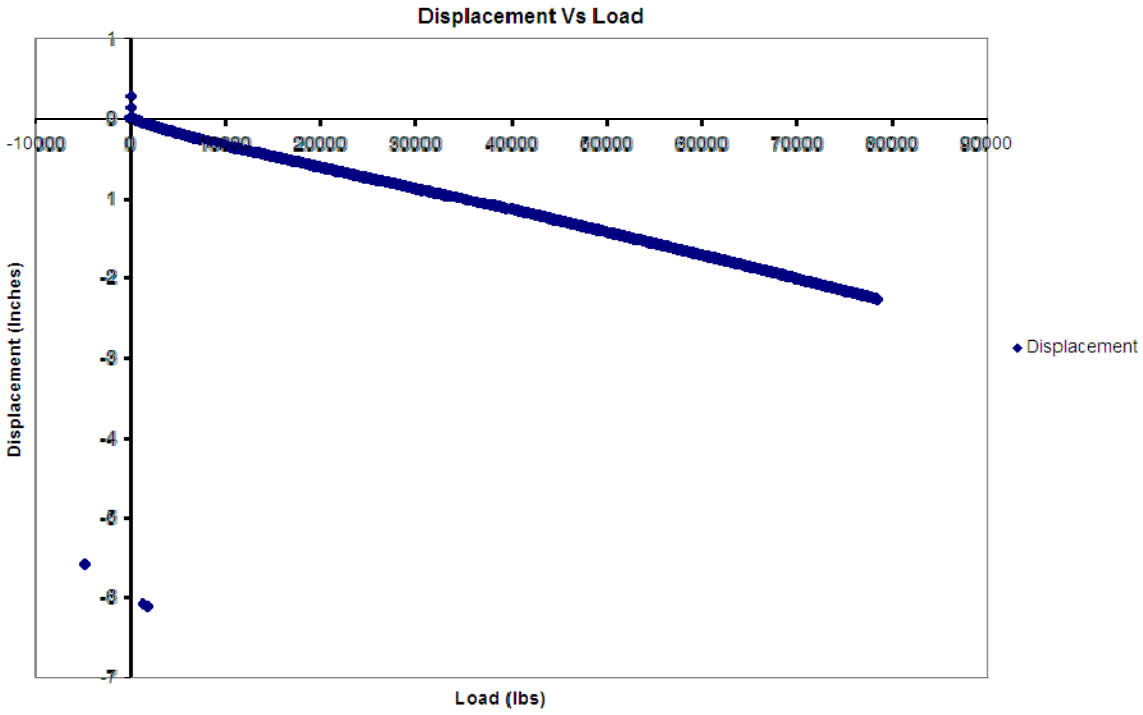

Figure 4.8: Displacement Vs Load for Fiber Deck with Longitudinal Ribs

Figure 4.9: Fiber Deck with Longitudinal Ribs at the Point of Failure

Figure 4.10: Fiber Deck with Longitudinal Ribs at the Point of Failure

The composite decks failed by shearing the laminate with a brittle failure.

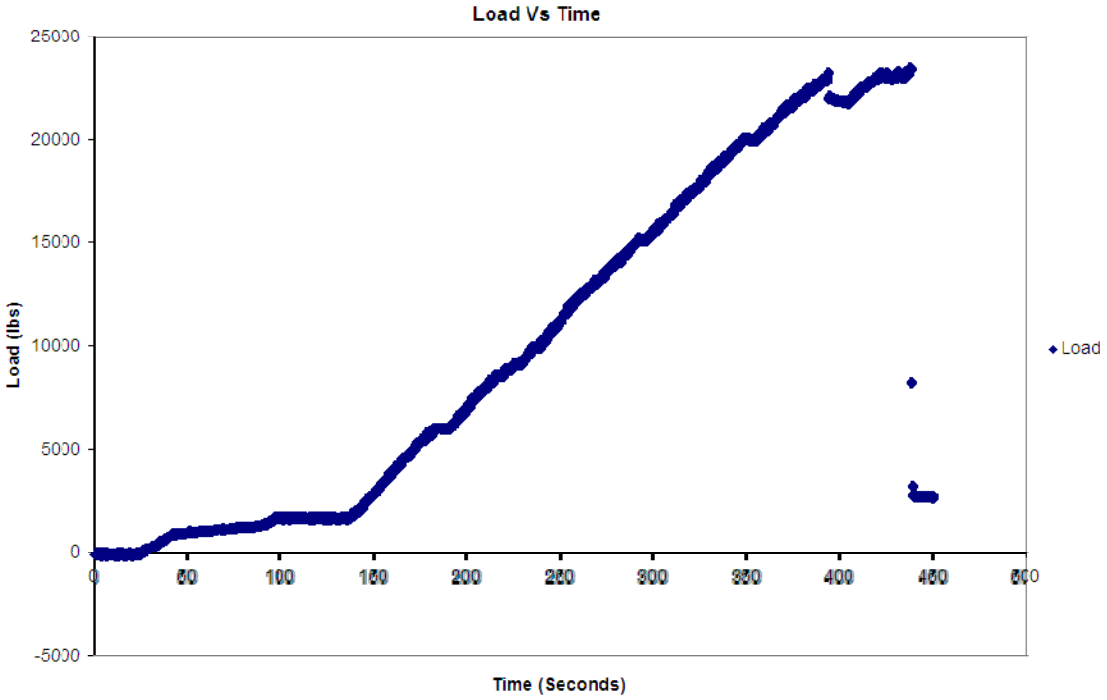

Figure 4.11: Load Vs Time for Fiber Deck with Transverse Ribs

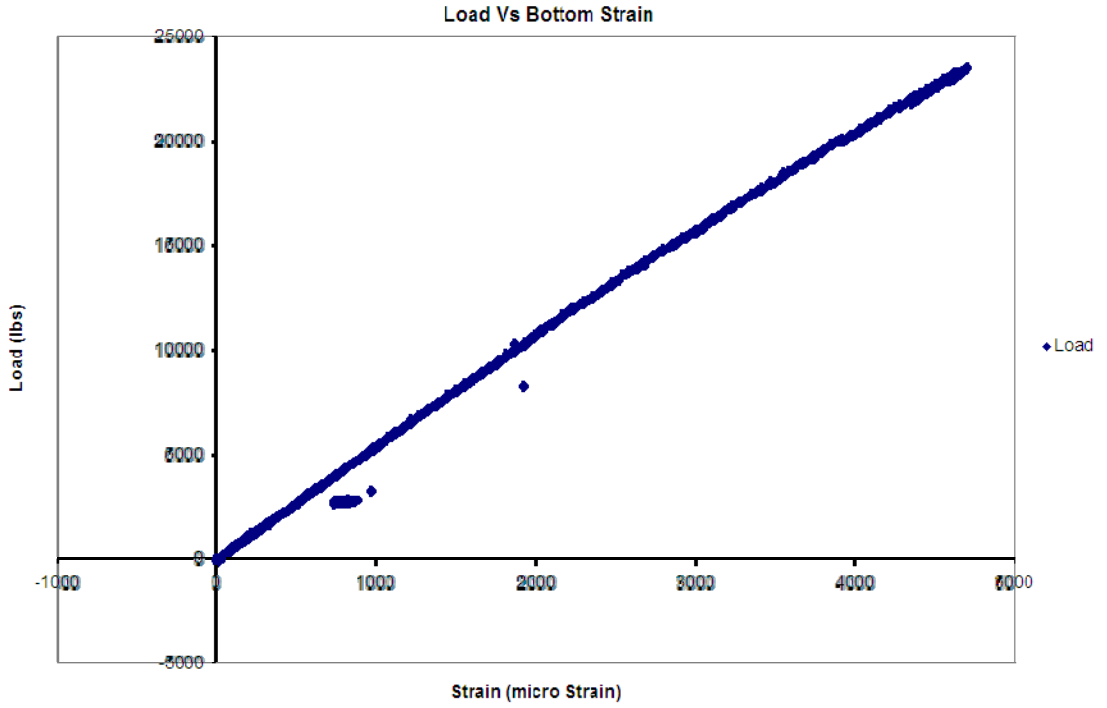

Figure 4.12: Load Vs Bottom Strain for Fiber Deck with Transverse Ribs

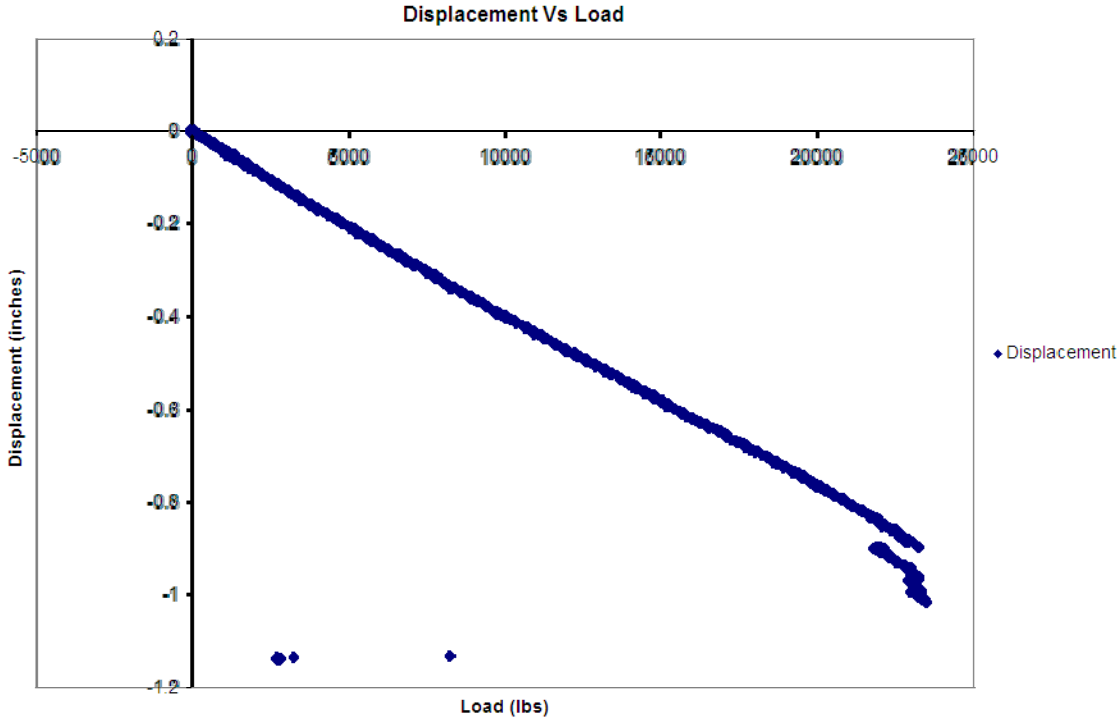

Figure 4.13: Displacement Vs Load for Fiber Deck with Transverse Ribs

Figure 4.14: Fiber Deck with Transverse Ribs at the Point of Failure

The fiber composite decks with ribs oriented along longitudinal and transverse direction failed by tearing the external thin CSM and at the connection between the honeycomb structure and the surrounding plates. The fiber Composite deck with longitudinal ribs carried a maximum load of 78544.499 lbs with a maximum deflection of 2.26 inches before failure. The Fiber Composite deck with transverse ribs carried a maximum load of 23449.103 lbs with a maximum deflection of 0.89 inches before failure.

4.4 Calculation of Rotation.

$$d\theta = \frac{(\alpha * T_m * dx)}{C} \qquad \text{Equation 4.2}$$

$d\theta$: Rotation of an element

α : Coefficient of Thermal Expansion in /°F

ΔT_m : Temperature Difference in F

dx : Small Element

c : Distance b/w the neutral axis and the extreme fiber

T_T : Temperature at Top

T_B : Temperature at Bottom

T_m : Mean Temperature

$\Delta T_m = T_T - T_m = T_m - T_B$

ΔT : Difference in temperature between the top and bottom surface of the decks is assumed to be linear.

Rotation for the entire span can be calculated by integrating over the entire length

$$\theta = \int_{-\frac{L}{2}}^{\frac{L}{2}} \frac{\alpha * \Delta T}{C} dx \qquad \text{Equation 4.3}$$

Table 4.2: Calculated Rotation Component for all the tests.

Test No	α	T_T (˚F)	T_B (˚F)	T_m (˚F)	ΔT_m (˚F)	C (in)	θ (Radians)
1	9.37672E-05	117.8	78.9	98.35	19.45	3	0.029
2	1.36229E-05	140.1	93	116.55	23.55	3	5.133E-03
3	1.30482E-05	134.9	94.1	113.5	21.7	3	4.53E-03
4	6.69028E-06	121.3	88	104.65	16.65	3	1.782E-03
5	1.55241E-05	123.7	92.3	108	15.7	3	3.9E-03
6	1.69454E-05	131.9	88.2	110.05	21.85	3	5.924E-03
7	2.14695E-05	145.3	95.7	120.5	24.8	3	8.519E-03
8	1.94984E-05	144.6	95.9	120.25	24.35	3	7.597E-03
9	1.087E-05	141.6	96.8	119.2	22.4	3	3.896E-03

4.5 Summary, Conclusions and Recommendations

4.5.1 Summary

The experimental tests conducted on specimens with ribs oriented along transverse and longitudinal direction with ends unrestrained or restrained resulted a mean temperature difference of 33˚F with a standard deviation of 2.1˚F for the 2 feet X 8 feet specimens. A temperature difference of 40.4˚F and 43˚F was obtained for the specimen of size 4 feet x 8 feet, when it was subjected to temperature of 120.2˚F and 143.3˚F at the top surface. The difference in temperature between the top and bottom surfaces for all the experimental tests has been tabulated in Table 4.4. The difference in temperature between the top and bottom surfaces stabilizes as the temperature stabilizes at the top surface.

The analysis of the composite deck, based on a finite element approach, rendered the values close to experimental results with a few variations. The temperature at the bottom surface of the fiber composite deck showed a slight constant increase in temperature at the bottom of the deck even after the temperature at the top

surface stabilized. This behavior is influenced by the ideal conditions adopted in the solution.

Table 4.3: Difference in Temperature from Finite Element Method Results at 120 ˚F

No	Type	Duration Seconds	Room Temperature	T_T (˚F)	T_B (˚F)	T_T- T_B (˚F)
1	I	72000	75.7	120	77.6	42.4
2	II	72000	75.7	120	77.7	42.3
3	III	72000	75.7	120	75.7	44.3
4	I	108000	75.7	120	77.4	42.6
5	I	275400	75.7	120	77.4	42.6
6	I	406800	75.7	120	77.5	42.5

For T_T- T_B, Mean $\bar{X}$ = 42.78 ˚F $\sigma = 0.75$ ˚F

Table 4.4: Difference in Temperature from Experimental Results

Test No	Orientation Of Ribs	Room Temperature	T_T (˚F)	T_B (˚F)	T_T- T_B (˚F)
1	Longitudinal	76	120	83.6	36.4
2	Longitudinal	75.7	119.2	86	33.2
3	Longitudinal	76.1	120.5	86.1	34.4
4	Longitudinal	72.2	120.4	87.9	32.5
5	Transverse	75.7	120.1	90.6	29.5
6	Transverse	72.3	119.8	87.4	32.4
7	Transverse	75.6	120	88.4	31.6
8	Transverse	71.7	120.2	79.8	40.4
9	Transverse	78.9	143.3	99.9	43.4

For T_T- T_B, Mean $\bar{X}$ = 33 ˚F $\sigma = 2.1$ ˚F for test no 1 to 8

Table 4.5: Difference in Temperature from Finite Element Method Results at 140 ˚F

No	Type	Duration Seconds	Room Temperature	T_T (˚F)	T_B (˚F)	T_T- T_B (˚F)
1	I	72000	75.7	140	86.7	53.3
2	II	72000	75.7	140	87.4	52.6
3	III	72000	75.7	140	80.8	59.2
4	I	108000	75.7	140	88.75	51.25
5	I	275400	75.7	140	97.5	42.5
6	I	406800	75.7	140	106	34

For T_T- T_B, Mean $\bar{X}$ = 48.08 ˚F $\sigma = 9.03$ ˚F

The fiber composite decks with ribs oriented along longitudinal and transverse direction with restrained or unrestrained ends are exposed to the temperature as shown in the figures 4.15 and 4.17. The resulting strain due to the temperature has been shown in figures 4.16 and 4.18. The longitudinal strain remained almost the same for the fiber composite decks, tested for the first time as obtained in test no 1, 2, 3, 4, 5 and 7. The re-testing of the decks in test no 6 and 8, which were the same decks as those tested in test no 1 and 3, yielded a higher value of longitudinal strain. The higher value of longitudinal strain in test no 6 and 8 is due to the heat absorbed in the initial tests 1 and 3. There is an exponential increase in strain for a short duration, when the temperature was increased on the top surface.

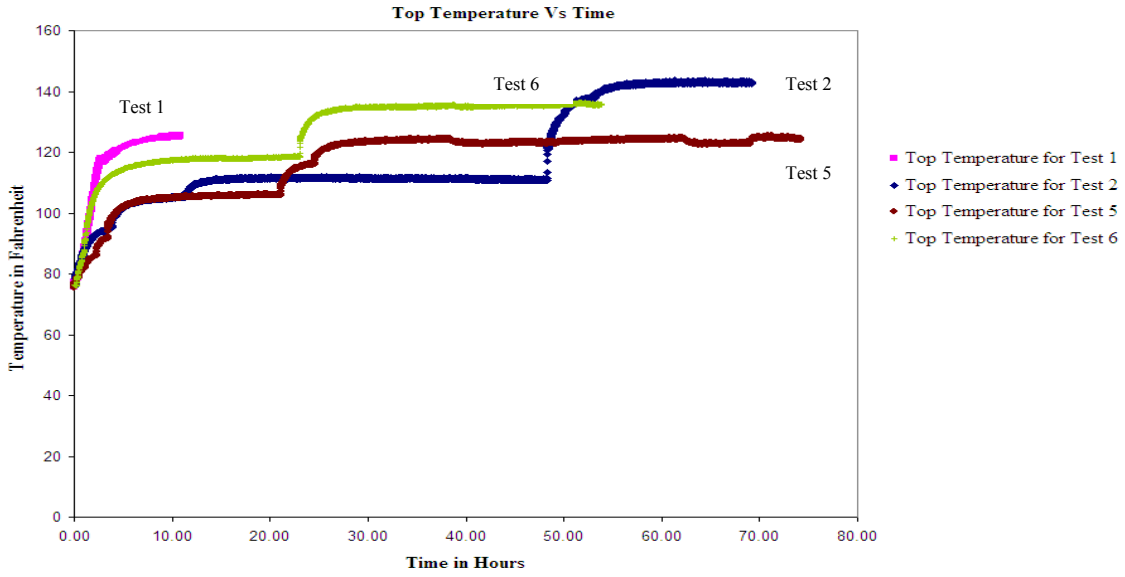

Figure 4.15: Top Temperature of Fiber Composite Deck Group with Longitudinal Ribs.

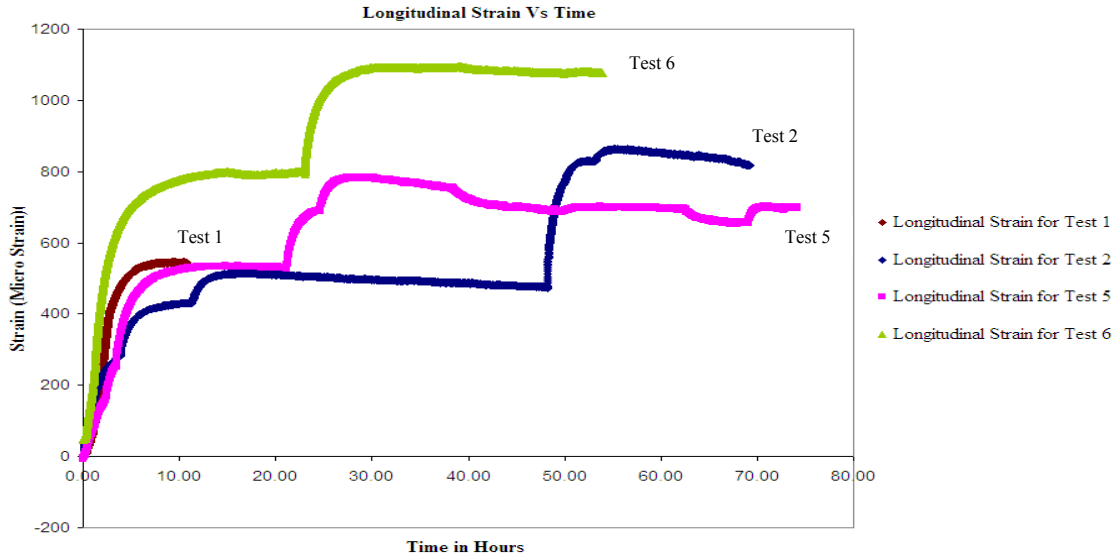

Figure 4.16: Longitudinal Strain of Fiber Composite Deck Group with Longitudinal Ribs

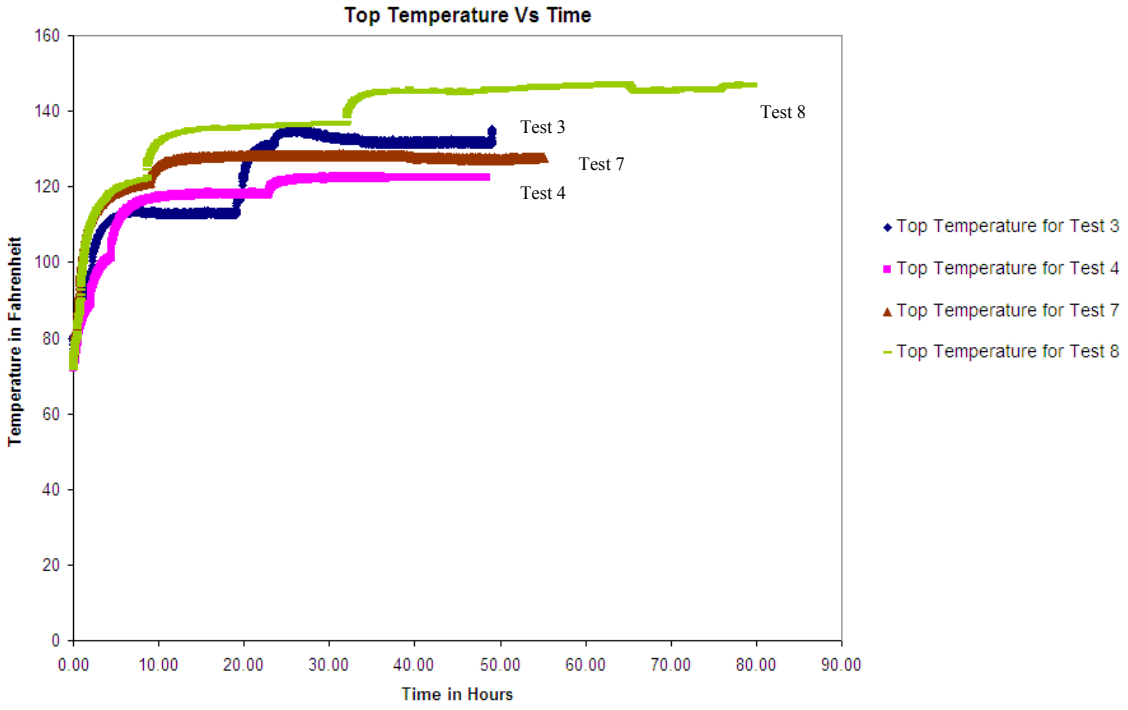

Figure 4.17: Top Temperature of Fiber Composite Deck Group with Transverse Ribs

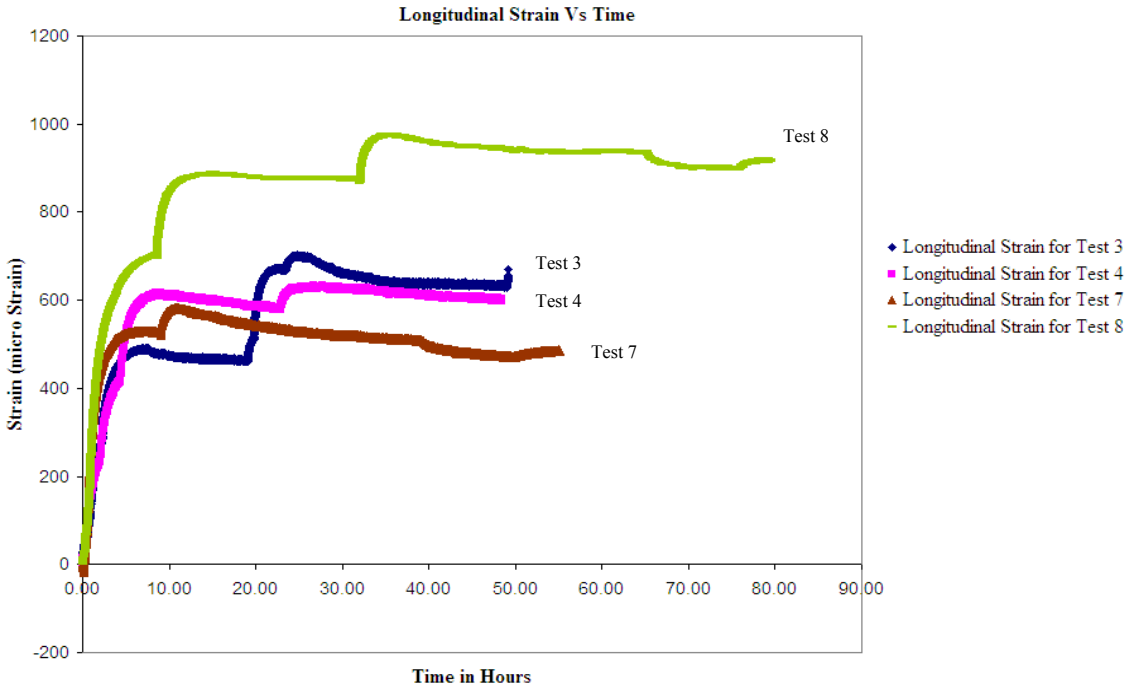

Figure 4.18: Longitudinal Strain for Fiber Composite Deck Group with Transverse Ribs.

The fiber composite decks showed a positive deflection indicating the hogging effect (bulging outward). The deflection of the decks with ribs oriented along transverse direction was twice as large as the deflection of the decks with ribs oriented along longitudinal direction. The retested fiber composite decks in test no 6 and 8 which were the same decks as those used in test no 1 and 3, yielded twice the deflection of the fiber composite decks tested for the first time with restrained ends. This indicates, the deflection of the deck could increase as it undergoes the cycle of temperature gradient and the deflection of the decks can be controlled based on the orientation of the ribs.

The coefficient of thermal expansion varied for the temperature tests with unrestrained end, where as the coefficient of thermal expansion remained the same for sets of fiber composite decks with longitudinal and transverse ribs for restrained end experiment. The difference in temperature between the top and bottom surface was

much higher for 4 x 8 decks, when compared to 2 x 8 decks and coefficient of thermal expansion remained less. The above results conclude that the coefficient of thermal expansion is also a function of orientation of the ribs and end conditions. The values have been tabulated in Table 4.6

Table 4.6: Coefficient of Thermal Expansion and Deflection for all the Tests

Test No	Duration Hours	Orientation of Ribs	T_T (˚F)	T_B (˚F)	Deflection (mm)	α
1	10.83	Longitudinal	125.4	91.2	-	9.37672E-05
2	69.18	Longitudinal	143.3	95.8	-	1.36229E-05
3	49.13	Transverse	134.9	94.1	-	1.30482E-05
4	48.39	Transverse	122.6	89.6	-	6.69028E-06
5	74.2	Longitudinal	125.2	94.3	1.10	1.55241E-05
6	53.89	Longitudinal	131.9	88.2	2.47	1.69454E-05
7	46.79	Transverse	147.4	99.5	1.90	2.14695E-05
8	79.52	Transverse	147.6	98.5	4.17	1.94984E-05
9	72.12	Transverse	145.3	101.1	-	1.087E-05

During the restrained end testing the fiber composite decks in test no 5 and 6 were restrained with a total compressive force of 200 lbs. The fiber composite deck tested in test no 5 was able to overcome the compressive force, where as the deck retested in experiment no 6 remained the same. The first test on fiber composite deck in test no 5 exhibited a increase in force with time, whereas the deck tested in test no 6 failed to exhibit an increase in force due to the heat absorption in the test no 1.The fiber composite decks restrained in test no 7 and 8 were also not able to overcome the compressive force. This behavior in test no 7 and 8 is because the ribs were arranged parallel to the restrained ends.

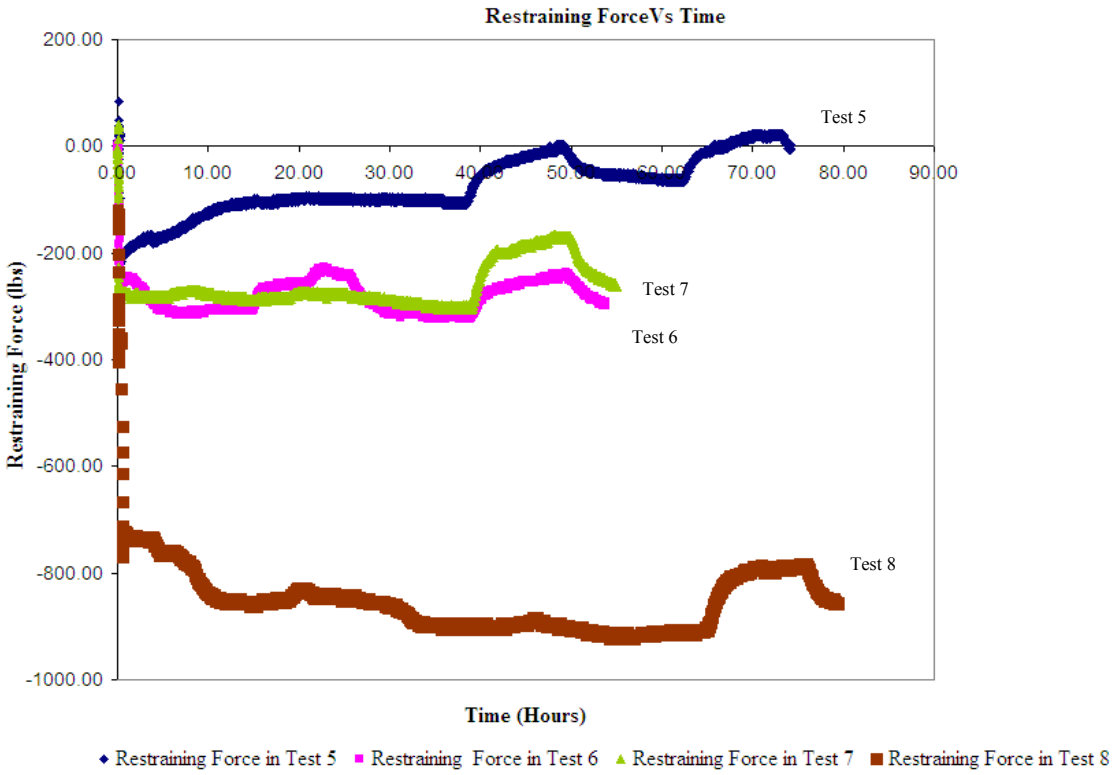

Figure 4.19: Restraining Force Vs Time for all the Restrained End Testing

4.6 Conclusion

The fiber composite decks tested showed a mean temperature difference of 33˚F between the top and bottom surfaces of the deck with a standard deviation of 2.1˚F for experimental tests and mean temperature difference of 4.78 ˚F between the top and bottom surfaces of the deck with a standard deviation of 0.75˚F during the finite element analysis. The difference between the top and bottom surface is dependent on the magnitude of temperature and time of exposure at the top surface. The decks showed a hogging effect (bulging outward) with a positive temperature difference between the top and bottom surface. The outward bulging of the deck depends on the orientation of the ribs and it is also a function of the temperature difference between the top and bottom

surface. The coefficient of thermal expansion varies with the orientation of ribs in fiber composite decks and also with the end conditions. The coefficient of thermal expansion of fiber composite decks would be less for unrestrained ends when it is compared with restrained ends. The decks exert a force if the ends are restrained; the force on these restrained ends is a function of ribs oriented in the deck. The magnitude of the exerted force is once again a function of temperature at the top surface. The decks with ribs oriented along longitudinal direction were capable of resisting thrice as much as the load of ribs oriented along transverse direction during two point bending test.

4.7 Recommendations

- The fiber composite decks are better to be unrestrained at the ends, which in turn could reduce the coefficient of thermal expansion, deflection and force transferred.
- The fiber composite decks with ribs oriented perpendicular to the support could reduce the deflection.
- Experimental tests could be carried out on repeated thermal cycles with positive and negative temperature difference between the top and bottom surface to predict the fatigue behavior of decks.
- The finite element analysis can be optimized by considering temperature dependent material properties of the fiber composite deck.
- A more precise model of the honey comb structure could be used in optimizing the finite element analysis.
- An experiment simulating the effect of temperature and live loads on composite deck could give the behavior of decks due to the two loads acting simultaneously.

APPENDIX A - EXPRESSION FOR COEFFICIENT OF THERMAL EXPRESSION

A.1 Expression for Co-Efficient of Thermal Expansion

Consider a specimen of unit volume (V = 1) in the form of rectangular parallelepiped in space with a uniform temperature, whose edges are parallel to the coordinate axis x_i (i = 1, 2, 3). The Specimen is assumed to be statistically homogeneous and composed of (N) phases (constituents), each of which has homogeneous mechanical and thermal properties.

The potential energy π for the composite section is given by

$$\pi = \int_{V=1} F_H dV - \int_S \hat{T}_i \hat{u}_i dS \qquad \text{Equation A.1}$$

Where F_H is the Helmholtz free energy density in terms of phase properties G, k and α, given by

$$F_H = G\varepsilon_{ij}\varepsilon_{ij} + (K/2 - G/3)\vartheta^2 - 3K\alpha T\vartheta \qquad \text{Equation A.2}$$

The Equation for Complementary energy is given by:

$$\pi_C = \int_{V=1} F_G dV \qquad \text{Equation A.3}$$

Where F_G is the Gibb's free energy density, given by

$$F_G = \frac{-\sigma_{ij}\sigma_{ij}}{4G} + \left(\frac{1}{12G} - \frac{1}{18K}\right)\Theta^2 - \alpha T \qquad \text{Equation A.4}$$

Displacement distribution is assumed as

$$u_i = e_{ij} x_j \qquad \text{Equation A.5}$$

Take $e_{ij} = e_{ji}$ as a constant. Therefore the six constants are defined as a constant strain distribution as given below

$$\varepsilon_{ij} = \frac{1}{2}\left(\frac{du_i}{dx_j} + \frac{du_j}{dx_i}\right) = e_{ij} \qquad \text{Equation A.6}$$

By Substituting Equations 5 and 6 into 1 and 2 yields

$$\pi^a = \bar{G} e_{ij} e_{ij} + \left(\frac{\bar{K}}{2} - \frac{\bar{G}}{3}\right) e^2 - 3\bar{K}\bar{\alpha} T e - \hat{\sigma}_{ij} e_{ij} \qquad \text{Equation A.7}$$

Where $e = e_{11} + e_{22} + e_{33}$ and bars denote volume averages,

$$\bar{G} = G_n V_n, \bar{K}\bar{\alpha} = (K\alpha)_n v_n \qquad \text{Equation A.8}$$

By differentiating Equation π^a w.r.t de_{ij} and setting $\frac{d\pi^a}{de_{ij}} = 0$, solve for e_{ij}

$$e_{ij} = \frac{\hat{\sigma}_{ij}}{2G} - \left(\frac{1}{6\bar{G}} - \frac{1}{9\bar{K}}\right)\hat{\Theta}\delta_{ij} + \frac{\bar{K}\alpha}{\bar{K}} T\delta_{ij} \qquad \text{Equation A.9}$$

This is interpreted as stress-strain relationship in terms of average properties

Substituting equation 09 in 07 yields

$$\pi^a = -\frac{\hat{\sigma}_{ij}\hat{\sigma}_{ij}}{4\bar{G}} + \left(\frac{1}{12\bar{G}} - \frac{1}{18\bar{K}}\right)\hat{\Theta}^2 - \frac{\bar{K}\bar{\alpha}}{\bar{K}} T\hat{\Theta} - \frac{9}{2}\frac{\bar{K}\bar{\alpha}^2}{\bar{K}} T^2 \qquad \text{Equation A.10}$$

An approximate complementary energy from equation 3 and 4 with constant stress distribution as $\sigma_{ij} = \hat{\sigma}_{ij}$ is given by

$$\pi_c{}^a = -\frac{\hat{\sigma}_{ij}\hat{\sigma}_{ij}}{4G_L} + \left(\frac{1}{12G_L} - \frac{1}{18K_L}\right)\hat{\Theta}^2 - \bar{\alpha} T \qquad \text{Equation A.11}$$

Where

$$\frac{1}{G_L} = \int_{V=1} \frac{dV}{G} = \frac{\upsilon_n}{G_n} \qquad \text{Equation A.12}$$

$$\frac{1}{K_L} = \int_{V=1} \frac{dV}{K} = \frac{\upsilon_n}{K_n} \qquad \text{Equation A.13}$$

By setting $\hat{\sigma}_{ij} = 0$ except $\hat{\sigma}_{11} = \sigma \neq 0$ in equation 10 and 11 .By Substituting in the below equation

$$\pi_c{}^a \leq -\frac{1}{2}\hat{S}_{ij}^{kl}\hat{\sigma}_{ij}\hat{\sigma}_{kl} - \hat{\alpha}_{ij}\hat{\sigma}_{ij}T + C \leq \pi^a + \frac{9}{2}T^2\bar{K}\bar{\alpha}^2 \qquad \text{Equation A.14}$$

Yields

$$-\frac{1}{2}\frac{\sigma^2}{E_L} - \bar{\alpha}T\sigma \leq -\frac{1}{2}\frac{\sigma^2}{\hat{E}_1} - \hat{\alpha}_{11}T\sigma + C \leq -\frac{1}{2}\frac{\sigma^2}{E_v} - \frac{\bar{K}\bar{\alpha}}{\bar{K}}T\sigma + \frac{9}{2}T^2\left(\bar{K}\bar{\alpha}^2 - \frac{\bar{K}\bar{\alpha}^2}{K}\right) \qquad \text{Equation A.15}$$

Introducing $\hat{E}_1 = \frac{1}{\hat{S}_{ii}^{jj}}$

$$\frac{1}{E_V} = \frac{1}{3}\left(\frac{1}{\bar{G}} + \frac{1}{3\bar{K}}\right); \frac{1}{E_L} = \frac{1}{3}\left(\frac{1}{G_L} + \frac{1}{3K_L}\right) = \frac{\upsilon_i}{E_i} \qquad \text{Equation A.16}$$

The significance of E_L is found by setting T=0 in equation 15 .From c = c (t), c is also equal to zero

$$E_L \leq \hat{E}_1 \leq E_V \qquad \text{Equation A.17}$$

E_L and E_V are upper and lower bounds

Similarly

$$\hat{\alpha}_{11}^{(-)} \leq \hat{\alpha}_{11} \leq \hat{\alpha}_{11}^{(+)} \qquad \text{Equation A.18}$$

Where

$$\hat{\alpha}_{11}^{(-)} = \bar{\alpha} + \left(\frac{\bar{K}\bar{\alpha}}{\bar{K}} - \bar{\alpha}\right)\frac{\left(\frac{1}{E_L} - \frac{1}{\hat{E}_1}\right)}{\left(\frac{1}{E_L} - \frac{1}{E_U}\right)} - \Delta\hat{\alpha}_{11} \qquad \text{Equation A.19}$$

$$\hat{\alpha}_{11}^{(+)} = \bar{\alpha} + \left(\frac{\bar{K}\bar{\alpha}}{\bar{K}} - \bar{\alpha}\right)\frac{\left(\frac{1}{E_L} - \frac{1}{\hat{E}_1}\right)}{\left(\frac{1}{E_L} - \frac{1}{E_U}\right)} + \Delta\hat{\alpha}_{11} \qquad \text{Equation A.20}$$

$$\Delta\hat{\alpha}_{11} = \frac{3\left(\frac{1}{\hat{E}_1} - \frac{1}{E_U}\right)^{\frac{1}{2}}\left(\frac{1}{E_L} - \frac{1}{\hat{E}_1}\right)^{\frac{1}{2}}}{\left(\frac{1}{E_L} - \frac{1}{E_U}\right)}\left[\left(\bar{K}\bar{\alpha}^2 - \frac{\bar{K}\bar{\alpha}^2}{\bar{K}}\right)\left(\frac{1}{E_L} - \frac{1}{E_U}\right) - \frac{1}{9}\left(\bar{\alpha} - \frac{\bar{K}\bar{\alpha}^2}{\bar{K}}\right)\right]^{\frac{1}{2}} \geq 0 \qquad \text{Equation A.21}$$

For a unidirectional Composite

$$\hat{E}_1 \cong E_L \qquad \text{Equation A.22}$$

$$\hat{\alpha}_{11} \cong \bar{\alpha} \qquad \text{Equation A.23}$$

When $\hat{E}_1 \cong E_V$

$$\hat{\alpha}_{11} \cong \frac{\bar{K}\bar{\alpha}}{\bar{K}} \qquad \text{Equation A.24}$$

The axial co-efficient can be expressed in terms of the young's modulus

$$\hat{\alpha}_a = \frac{\bar{E}\bar{\alpha}}{\bar{E}} = \frac{E_1\alpha_1\upsilon_1 + E_2\alpha_2\upsilon_2}{E_1\upsilon_1 + E_2\upsilon_2} \qquad \text{Equation A.25}$$

Where $\frac{\bar{E}\bar{\alpha}}{\bar{E}}$ is exact for an arbitrary number of different kinds of fibers with same poisons ratio and the composite may be orthotropic.

A.2 Nomenclature:

$\hat{E}_i =$ Composite Young's modulus in x_i direction.

E, E_n = phase Young's modulus.

F_G = Gibb's free energy density.

F_H = Helmholtz free energy density.

G, G_n = phase shear modulus.

i, j, k, l =indices associated with coordinate direction 1, 2, or 3

K, K_n = phase bulk modulus.

$\hat{K}$ = Composite bulk modulus.

m, n = indices designating a particular phase (m, n =1, 2,----N)

n_i = direction cosines of vector normal to surface

S = surface

$\hat{S}_{ij}^{kl}$ = Composite compliances.

T = temperature change from reference value.

$\hat{T}_i$ = applied surface traction.

u_i = displacement components.

$\hat{u}_i$ = Surface displacements.

$\hat{v}_n$ = Volume fraction of nth phase.

$\hat{V}$ = Specimen volume = 1

x_i = Cartesian coordinates.

α, α_n = phase linear coefficient of thermal expansion.

$\hat{\alpha}_v =$ composite volumetric expansion coefficient.

$\hat{\alpha}_{ij} =$ composite linear coefficients of thermal strain (or expansion)

$\delta_{ij} =$ Kronecker delta.

$\varepsilon_{ij} =$ strain components.

$\hat{\varepsilon}_{ij} =$ average strains in composite specimens.

$\Theta = \sigma_{11} + \sigma_{22} + \sigma_{33}$.

$\vartheta = \varepsilon_{11} + \varepsilon_{22} + \varepsilon_{33}$.

$\upsilon, \upsilon_n =$ phase Poisson's ratio.

$\hat{\upsilon} =$ composite poisson's ratio.

$\xi =$ reduced time.

$\pi, \pi_c =$ potential and complementary energies.

$\sigma_{ij} =$ stress components

$\hat{\sigma}_{ij} =$ applied stresses.

APPENDIX B - ASTM D 3039/D 3039M -00

The ASTM D 3039/D 3039 M-00 could be used to determine the in-plane tensile properties of polymer matrix composite materials reinforced by high modulus fibers. This test method could be used to obtain the tensile property of material for research and development, quality assurance and structural analysis and design. The important factors which govern the tensile properties are material, methods of material preparation and lay-up, specimen stacking sequence, specimen preparation, specimen conditioning, environment of testing, specimen alignment and gripping, speed of testing, time at temperature, void content, and volume percent reinforcement. This test is limited to composite material with continuous or discontinuous fiber in which the laminate is balanced and symmetric with respect to test direction. The minimum geometry requirement for the specimen is given below:

Table B.1: Minimum Specimen Geometry Requirements

Parameter	Requirement
Shape	Constant rectangular cross section
Minimum Length	Gripping + 2 Times width + gage length
Specimen Width	As needed
Specimen width tolerance	$\pm$ 1% of Width
Specimen thickness	As needed
Specimen thickness tolerance	$\pm$ 4 % of thickness
Specimen flatness	Flat with light finger pressure
Tab Requirement	If used
Tab Material	As needed
Fiber Orientation	As needed
Tab Thickness	As needed
Tab Thickness variation between tabs	$\pm$ 1 % tab thickness
Tab bevel angle	5 to 90°, inclusive
Tab step at level to specimen	Feathered without damaging specimen

The geometry of the coupon was derived, based upon the minimum geometry requirements by ASTM D 3039/D 3039M-00 and the ability to machine the test coupons. The geometry of fiber composite deck and fiber composite tubular section coupons is given below.

Geometry of fiber composite deck coupon: (All Dimensions are in inches)

Width of the section : .50

Gage Length : 2.00

Thickness : .50

Radius of fillet : 3.00

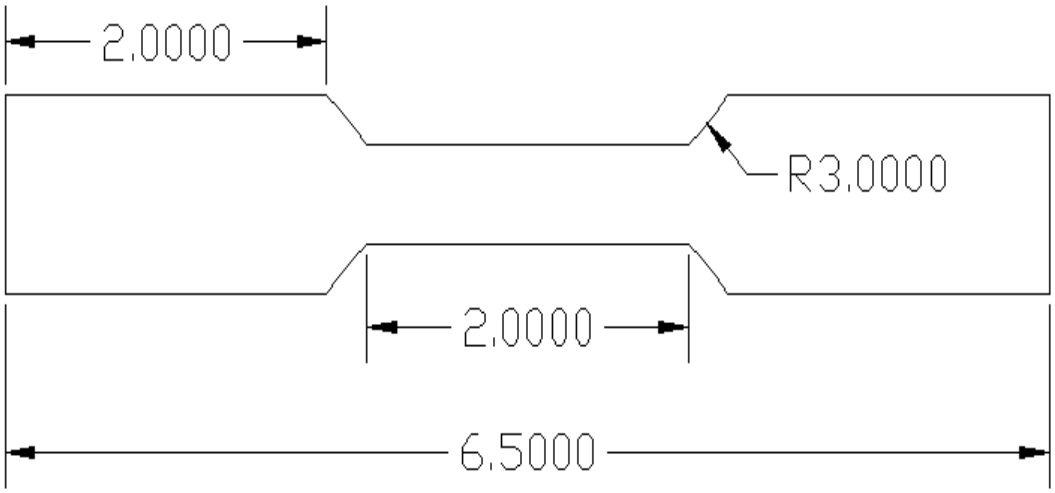

Figure B.1: Geometry of Fiber Composite Deck Coupon

Geometry of fiber composite tubular section coupon: (All Dimensions are in inches)

Width of the section : .50

Gage Length : 2.00

Thickness : .25

Radius of fillet : 3.00

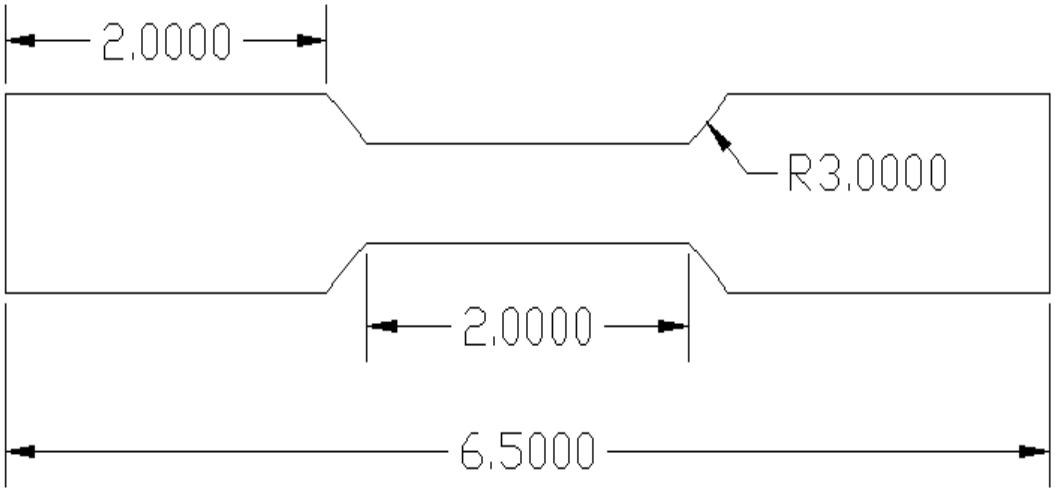

Figure B.2: Geometry of Fiber Composite Tubular Section Coupon

APPENDIX C

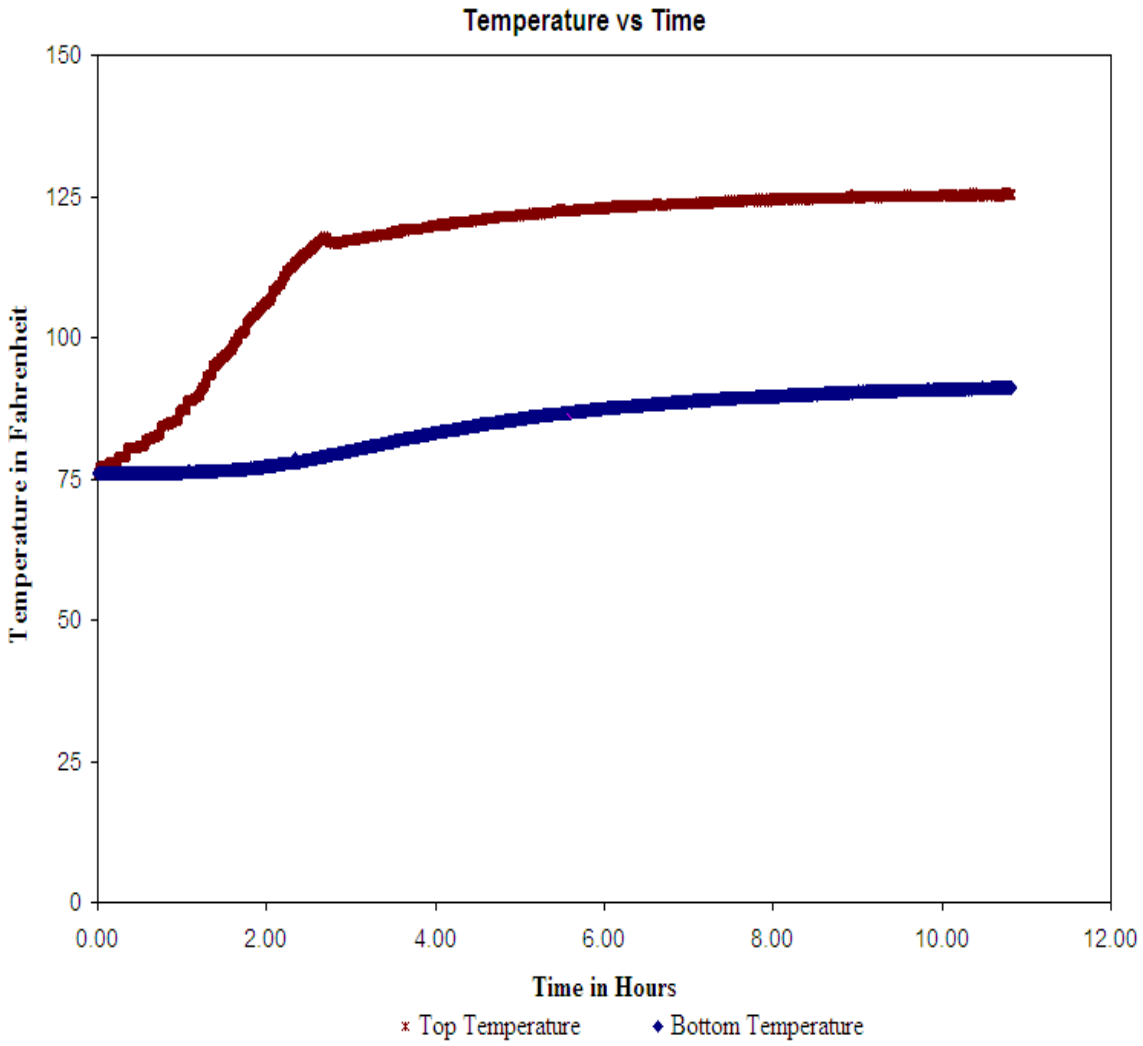

Figure C.1: Temperature vs. Time for Test # 1

The above graph shows the application of heat to the top surface and the measurement of heat at the bottom surface for fiber composite deck specimen #1 with longitudinal ribs and ends unrestrained.

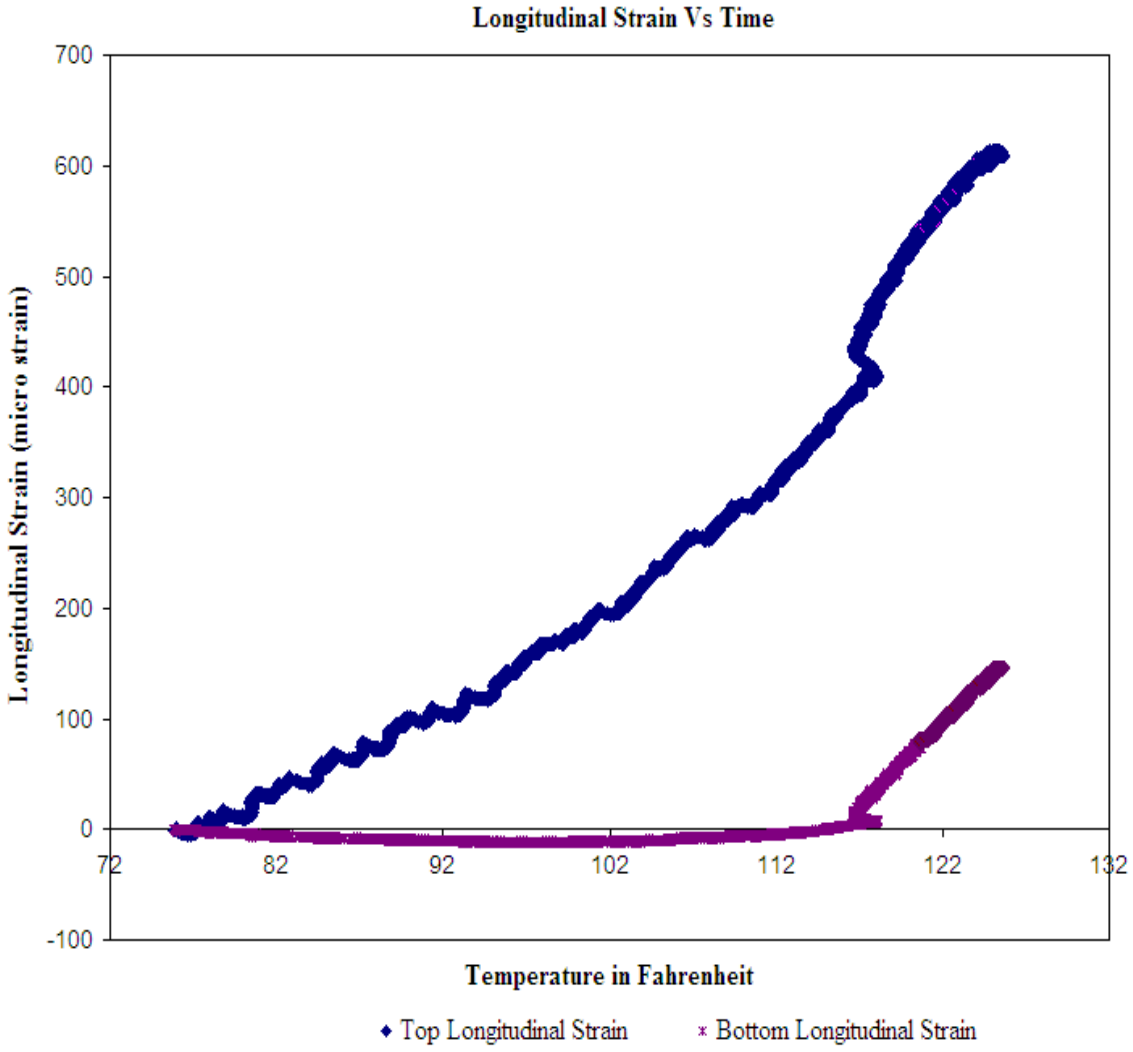

Figure C.2: Longitudinal Strain vs. Temperature for Test # 1

The above graph shows the variation of longitudinal strain at top and bottom surfaces over temperature at the top surface for the fiber composite deck with ribs oriented along longitudinal direction. The negative strain at the bottom surface indicates the compressive strain.

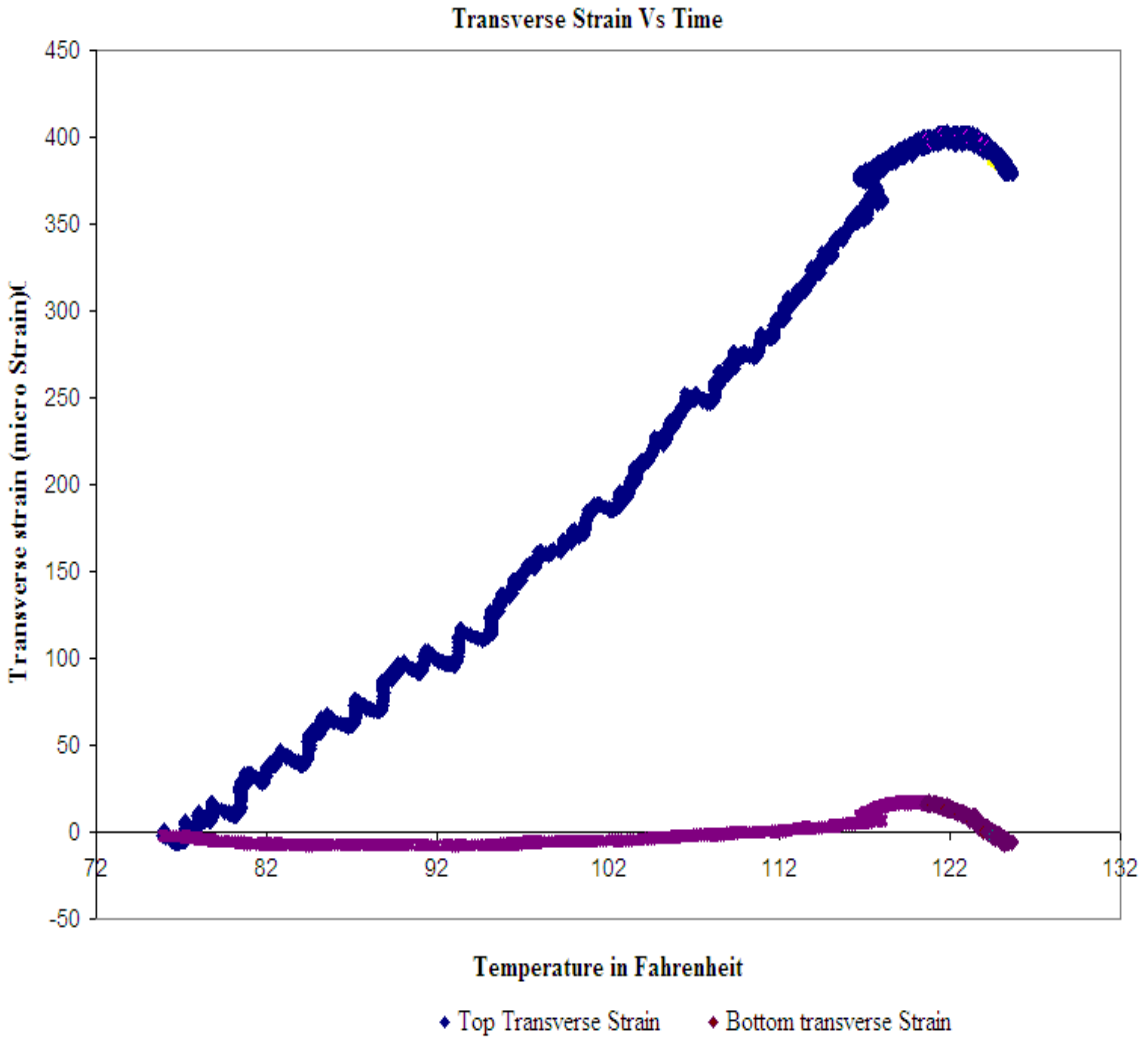

Figure C.3: Transverse Strain vs. Temperature for Test # 1

The above graph shows the variation of transverse strain at top and bottom surfaces over temperature at the top surface for the fiber composite deck with ribs oriented along longitudinal direction. The negative strain at the bottom surface indicates the compressive strain.

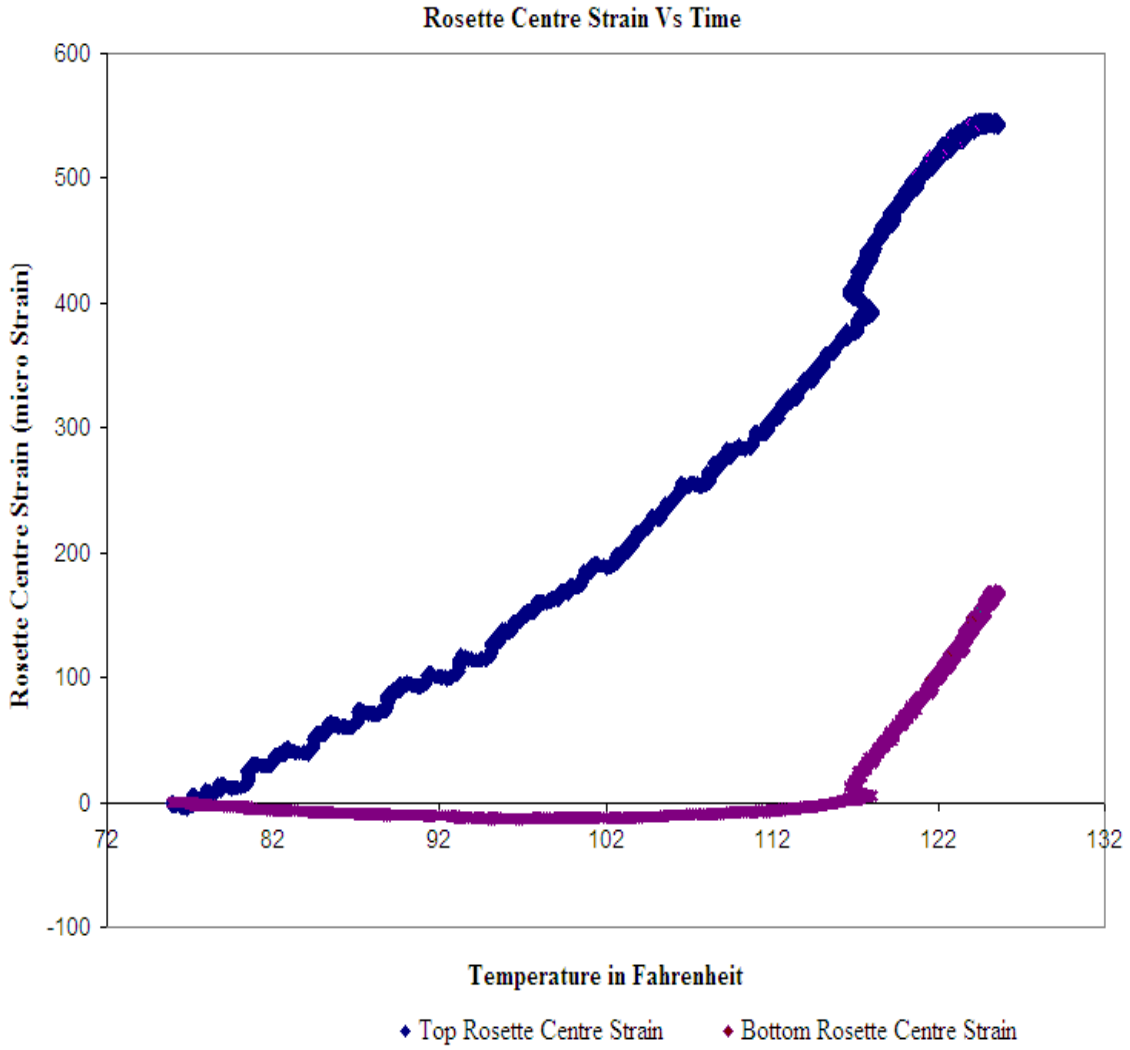

Figure C.4: Rosette Centre Strain vs. Temperature for Test # 1

The above graph shows the variation of rosette centre strain at top and bottom surfaces over temperature at the top surface for the fiber composite deck with ribs oriented along longitudinal direction. The negative strain at the bottom surface indicates the compressive strain.

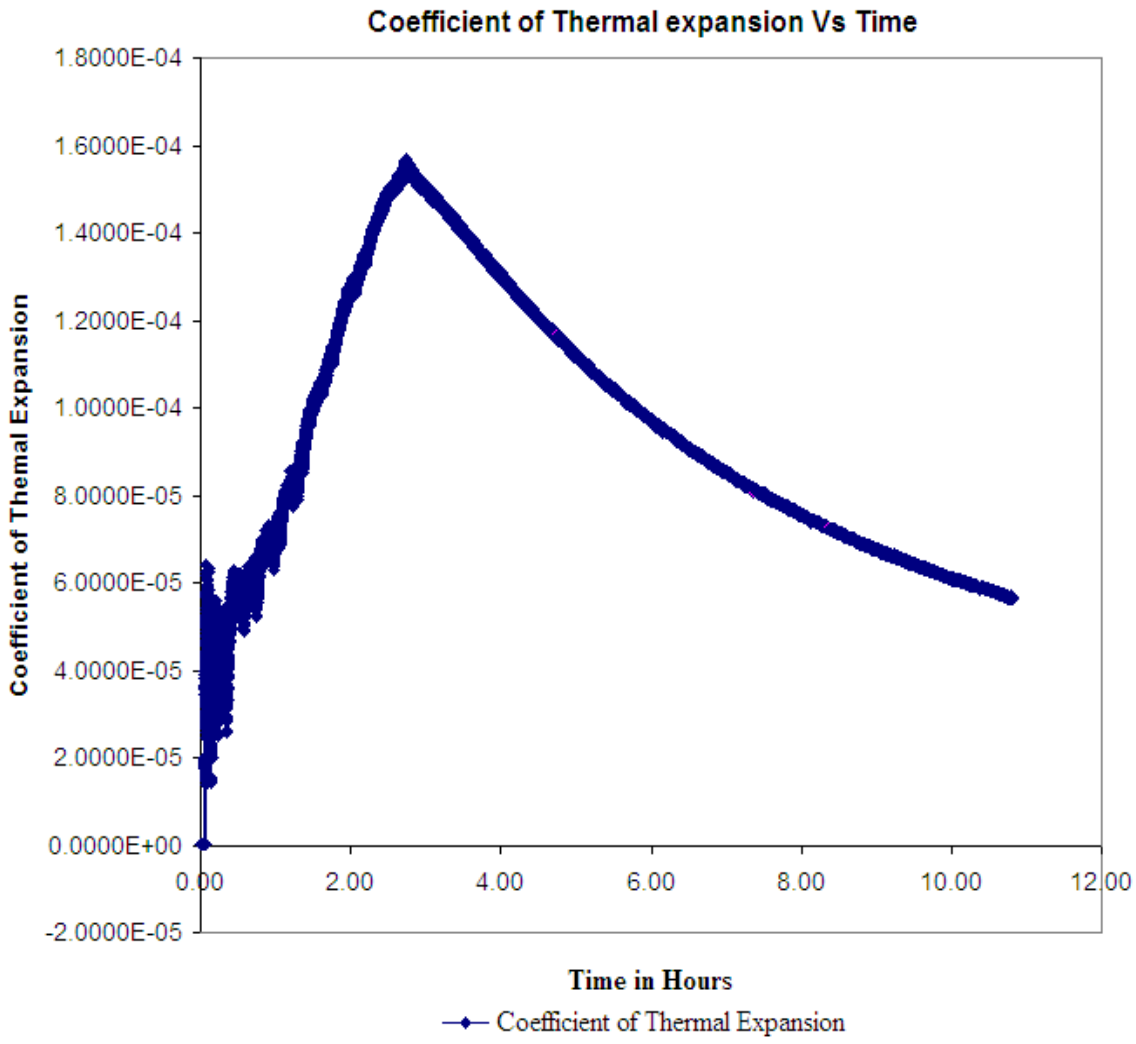

Figure C.5: Coefficient of Thermal Expansion vs. Time for Test # 1

The above graph shows the variation of coefficient of thermal expansion over time for the fiber composite deck with ribs oriented along longitudinal direction. The coefficient of thermal expansion exhibited a strange behavior of increasing with temperature and then it decreased after temperature stabilized at the top surface.

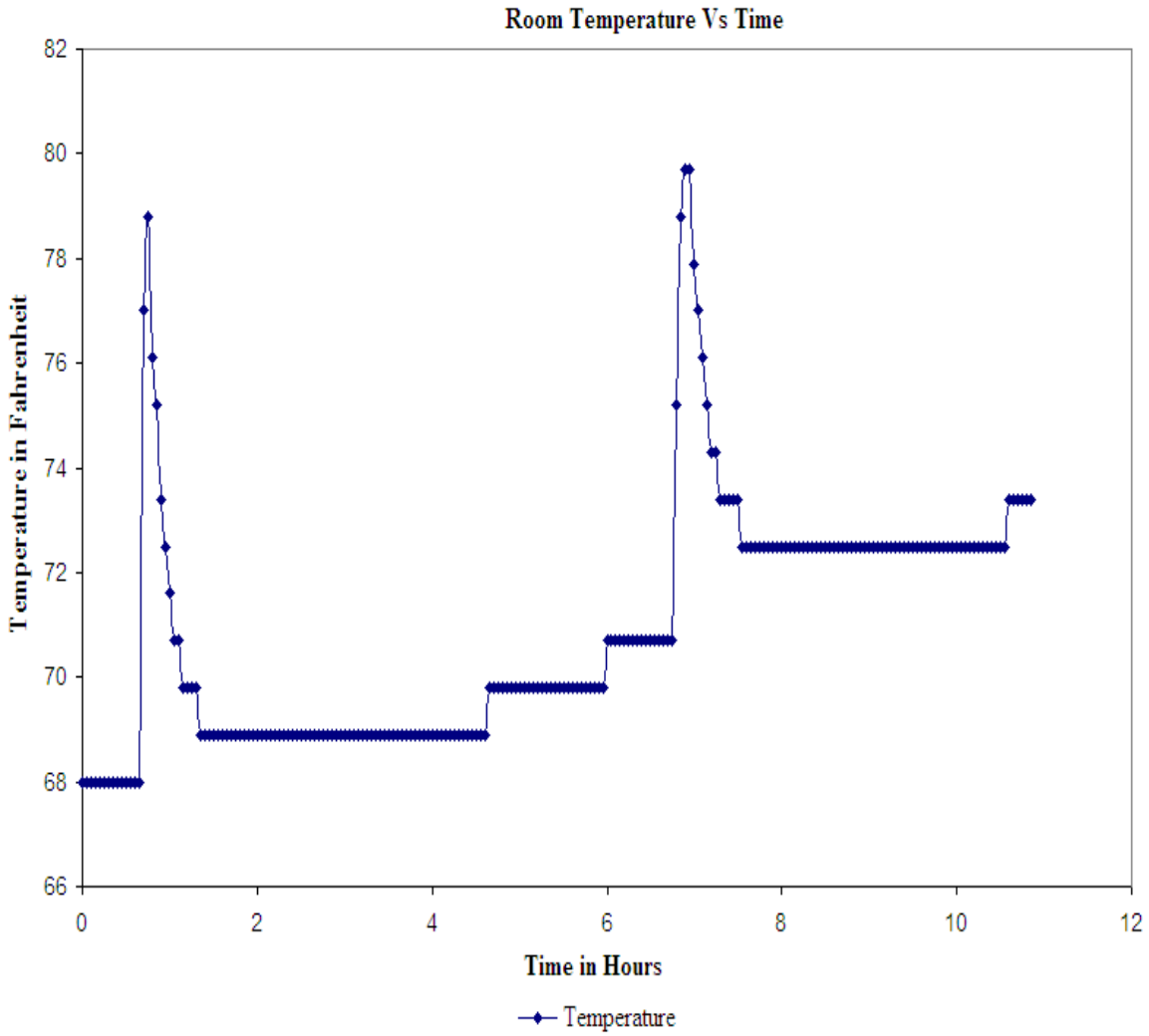

Figure C.6: Room Temperature vs. Time for Test # 1

The above graph shows the variation of temperature next to the experimental setup over time for Test # 1. The little variation of temperature for a short duration is because of the interference of the outside temperature.

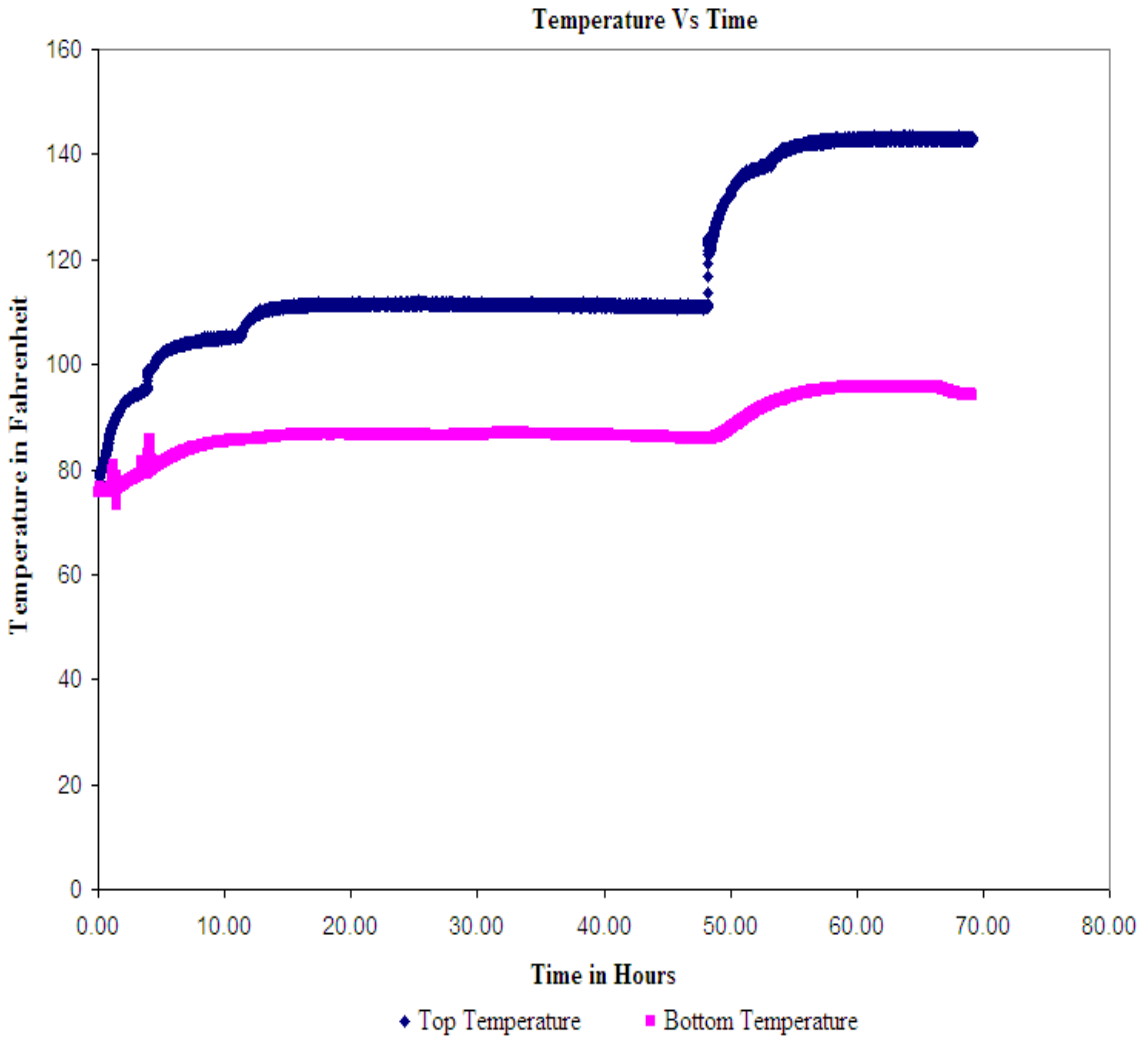

Figure C.7: Temperature vs. Time for Test # 2

The above graph shows the application of heat to the top surface and the measurement of heat at the bottom surface for fiber composite deck specimen # 2 with ribs oriented along longitudinal direction and ends unrestrained.

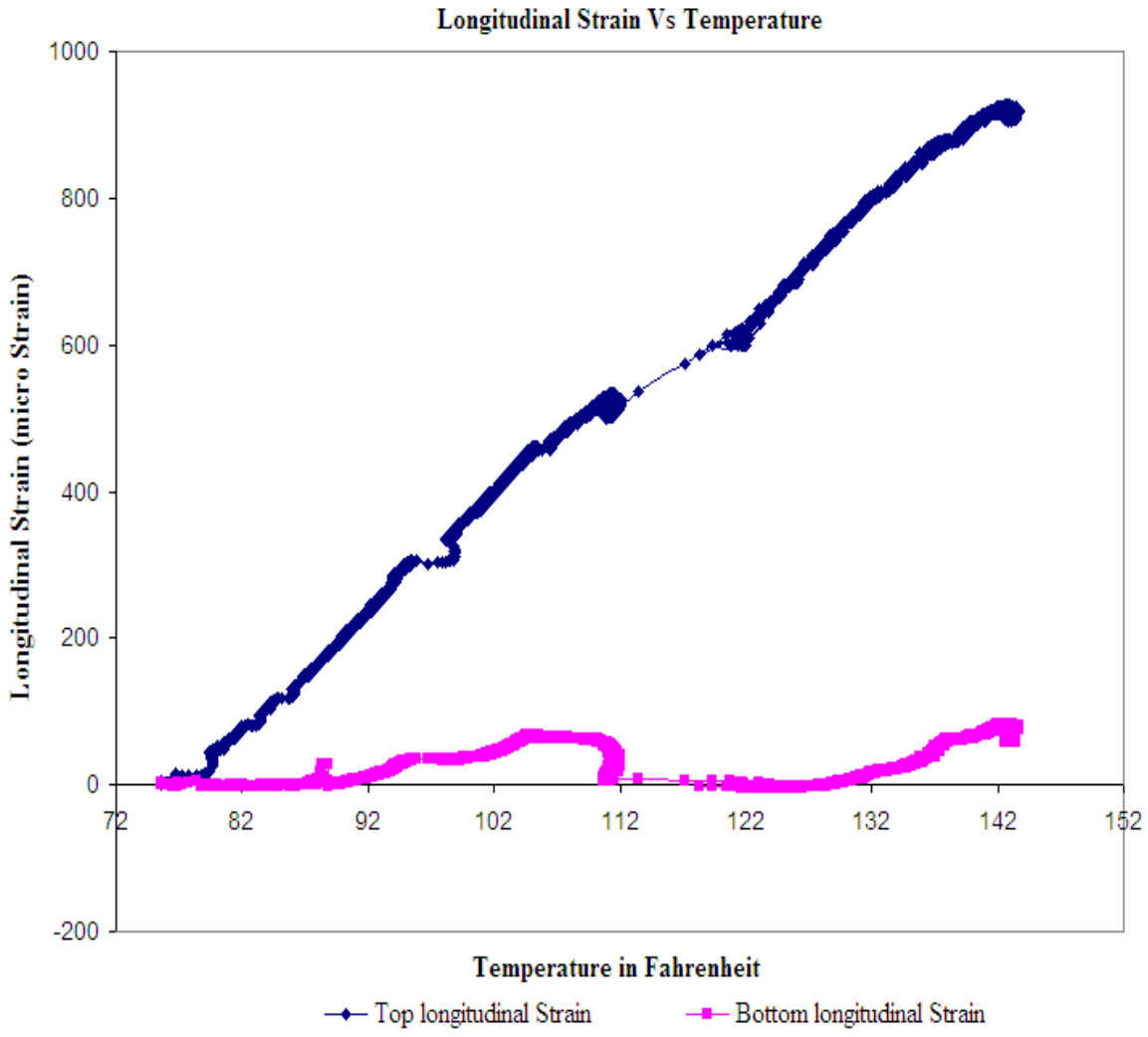

Figure C.8: Longitudinal Strain vs. Temperature for Test # 2

The above graph shows the variation of longitudinal strain at top and bottom surfaces over the temperature at the top surface for the fiber composite deck specimen # 2 with ribs oriented along longitudinal direction and ends unrestrained.

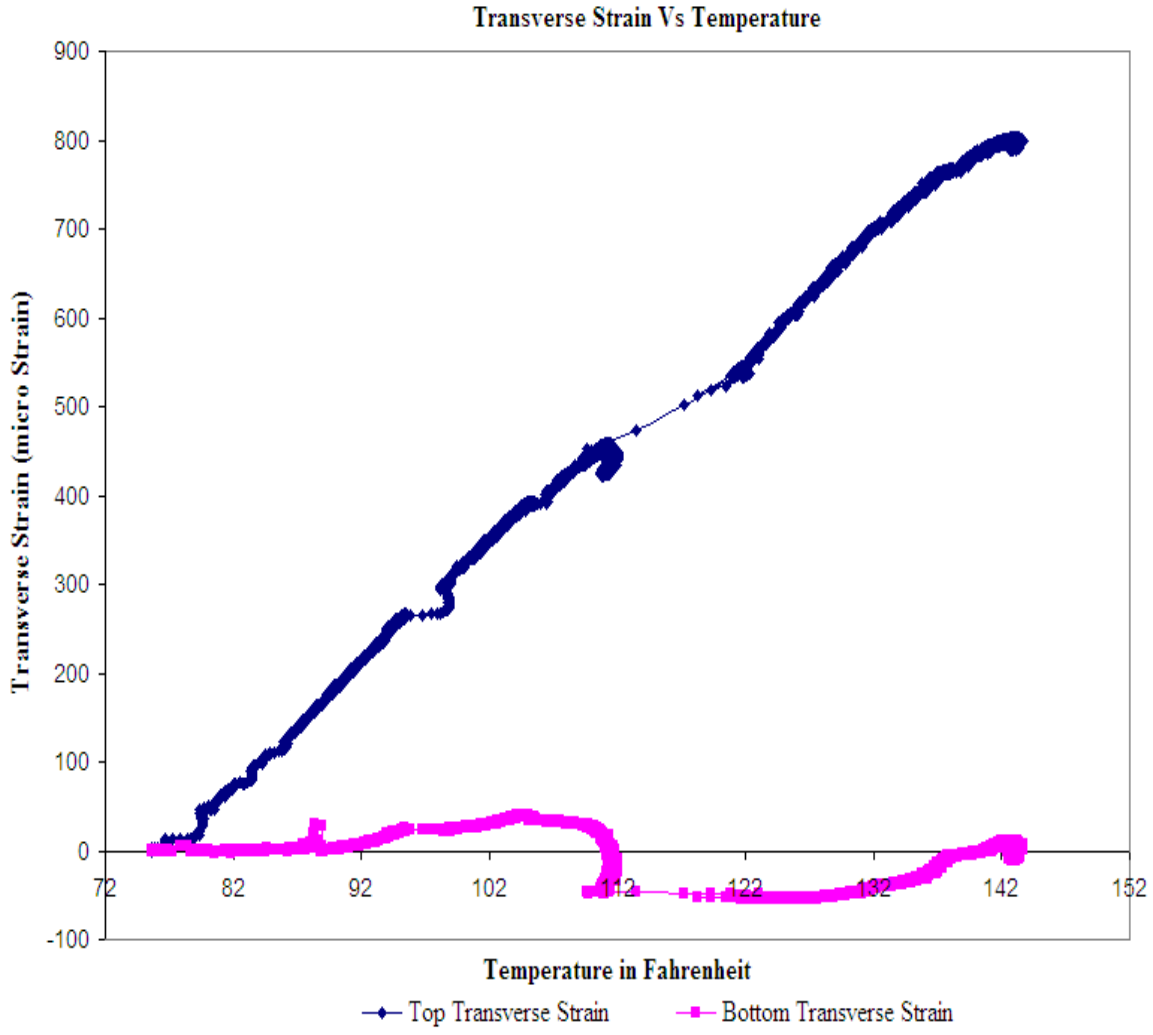

Figure C.9: Transverse Strain vs. Temperature for Test # 2

The above graph shows the variation of transverse strain at top and bottom surfaces over temperature at the top surface for the fiber composite deck specimen # 2 with ribs oriented along longitudinal direction. The negative strain at the bottom surface indicates the compressive strain.

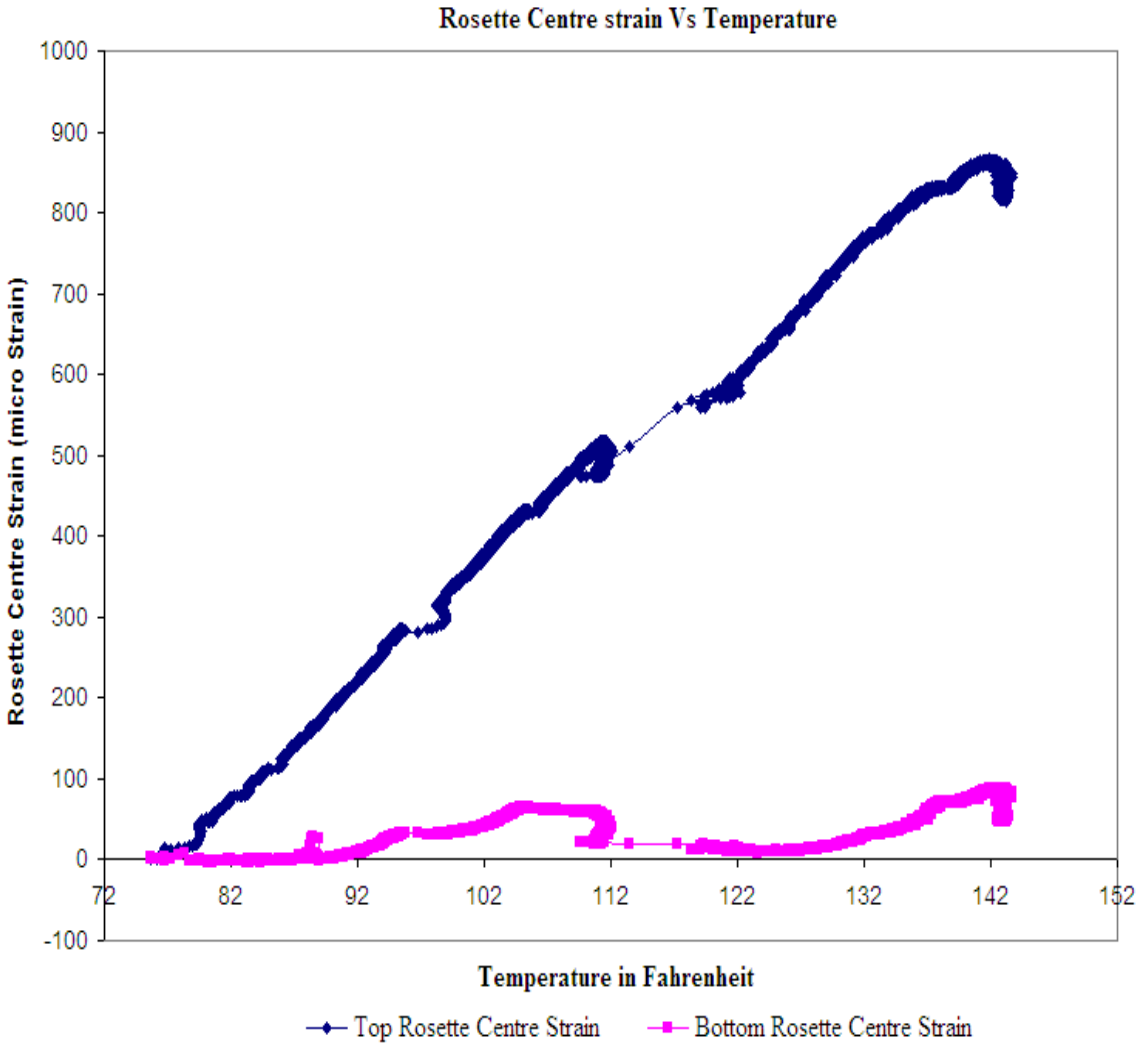

Figure C.10: Rosette Centre Strain vs. Temperature for Test # 2

The above graph shows the variation of rosette centre strain at top and bottom surfaces over temperature at the top surface for the fiber composite deck specimen # 2 with ribs oriented along longitudinal direction and ends unrestrained.

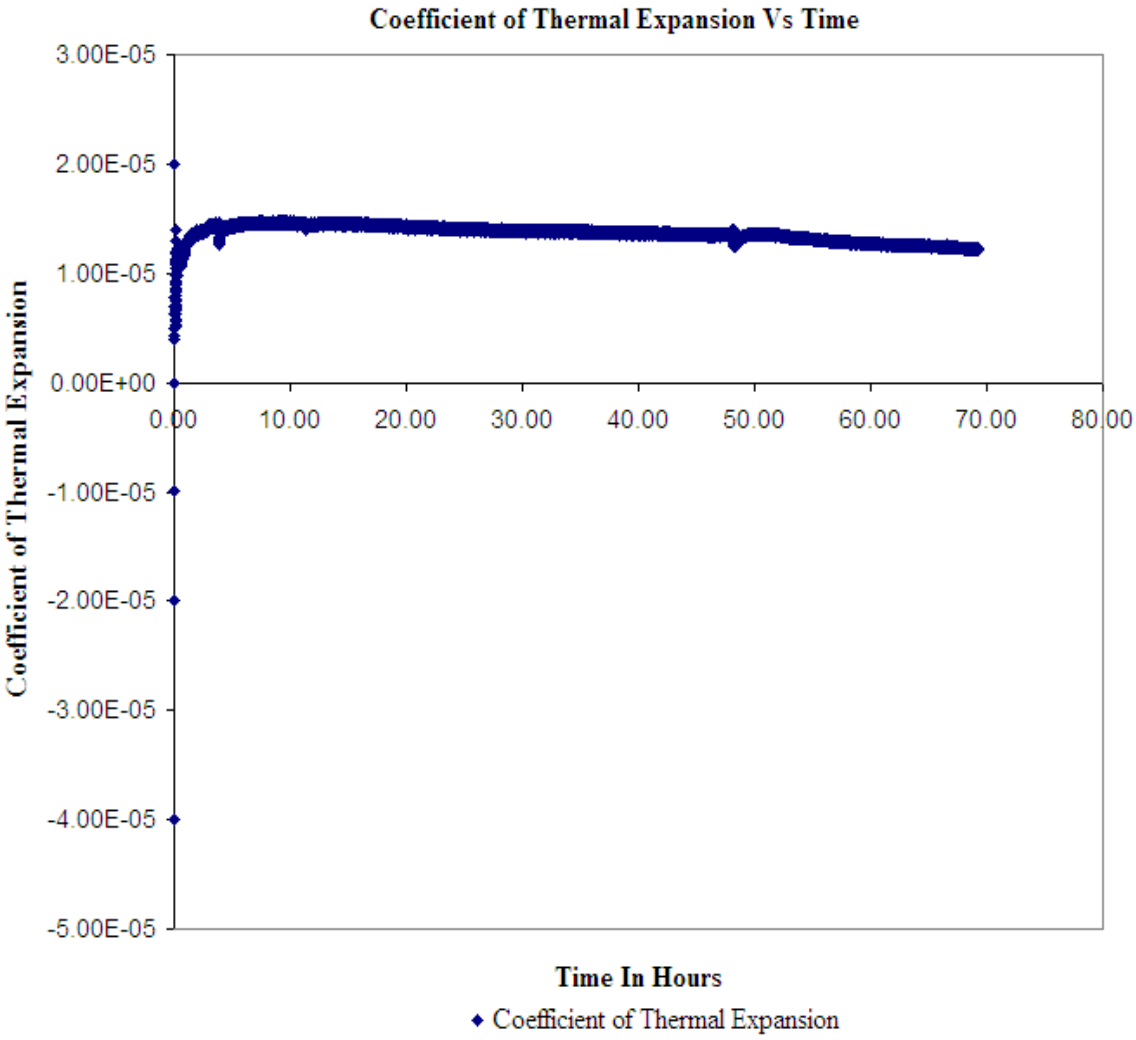

Figure C.11: Coefficient of Thermal Expansion vs. Time for Test # 2

The above graph shows the coefficient of thermal expansion over time for the fiber composite deck specimen # 2 with ribs oriented along longitudinal direction. The coefficient of thermal expansion remained constant throughout the experiment.

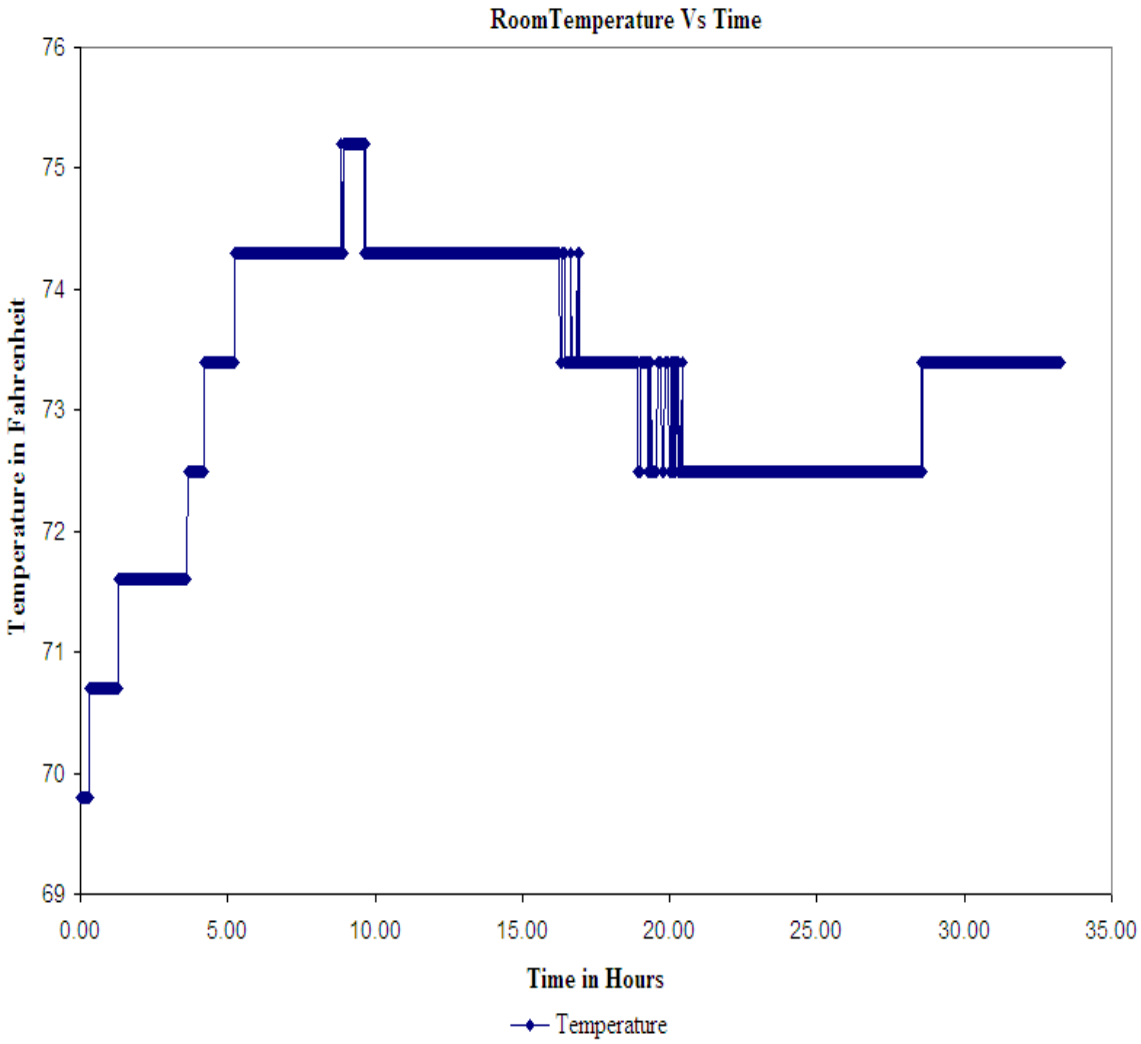

Figure C.12: Room Temperature vs. Time for Test # 2

The above graph shows the variation of temperature next to the experimental setup over time for Test # 2. The little variation of temperature for a short duration is because of the interference of the outside temperature.

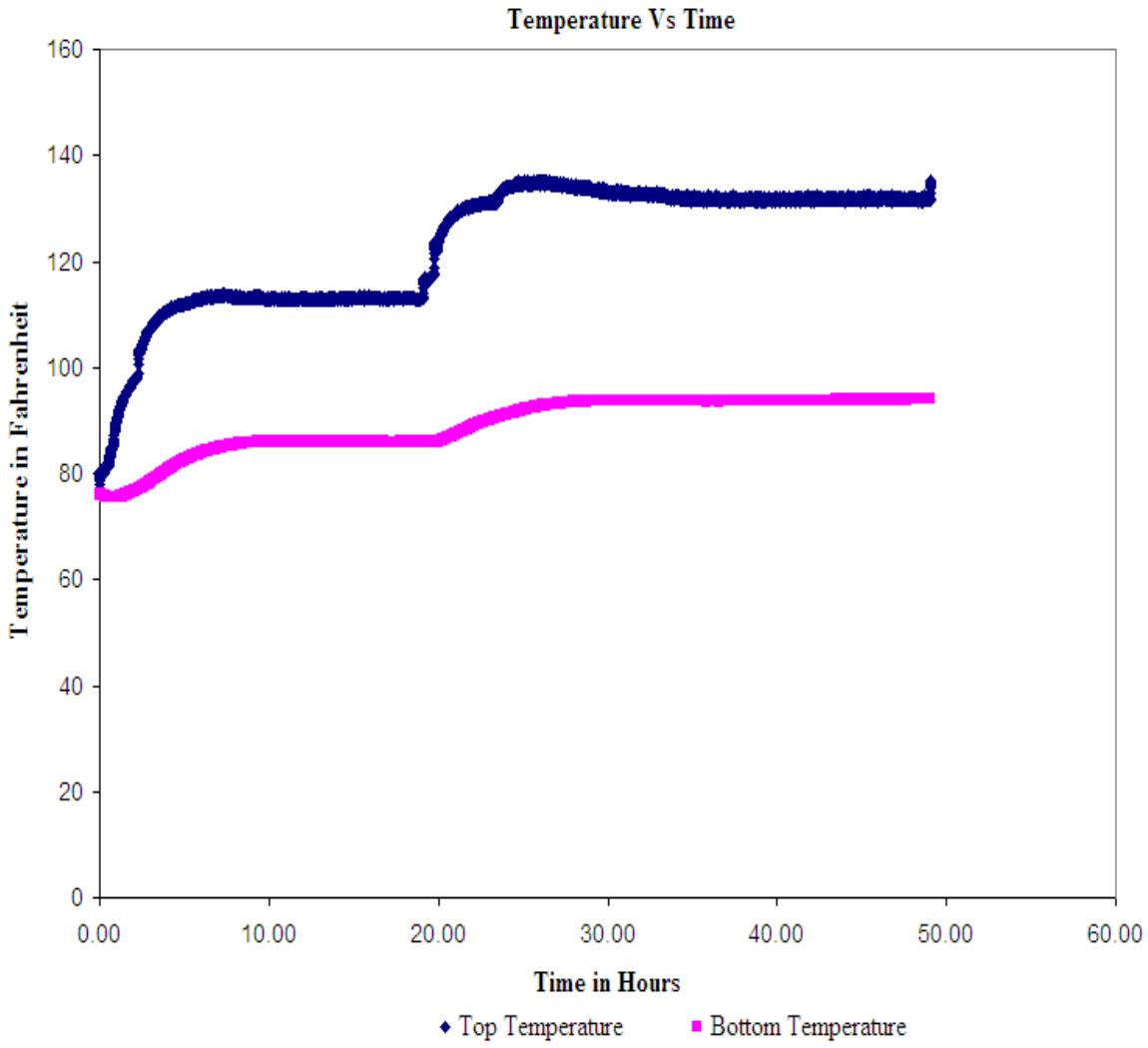

Figure C.13: Temperature vs. Time for Test # 3

The above graph shows the application of heat to the top surface and the measurement of heat at the bottom surface for the fiber composite deck specimen # 3 with transverse ribs and ends unrestrained.

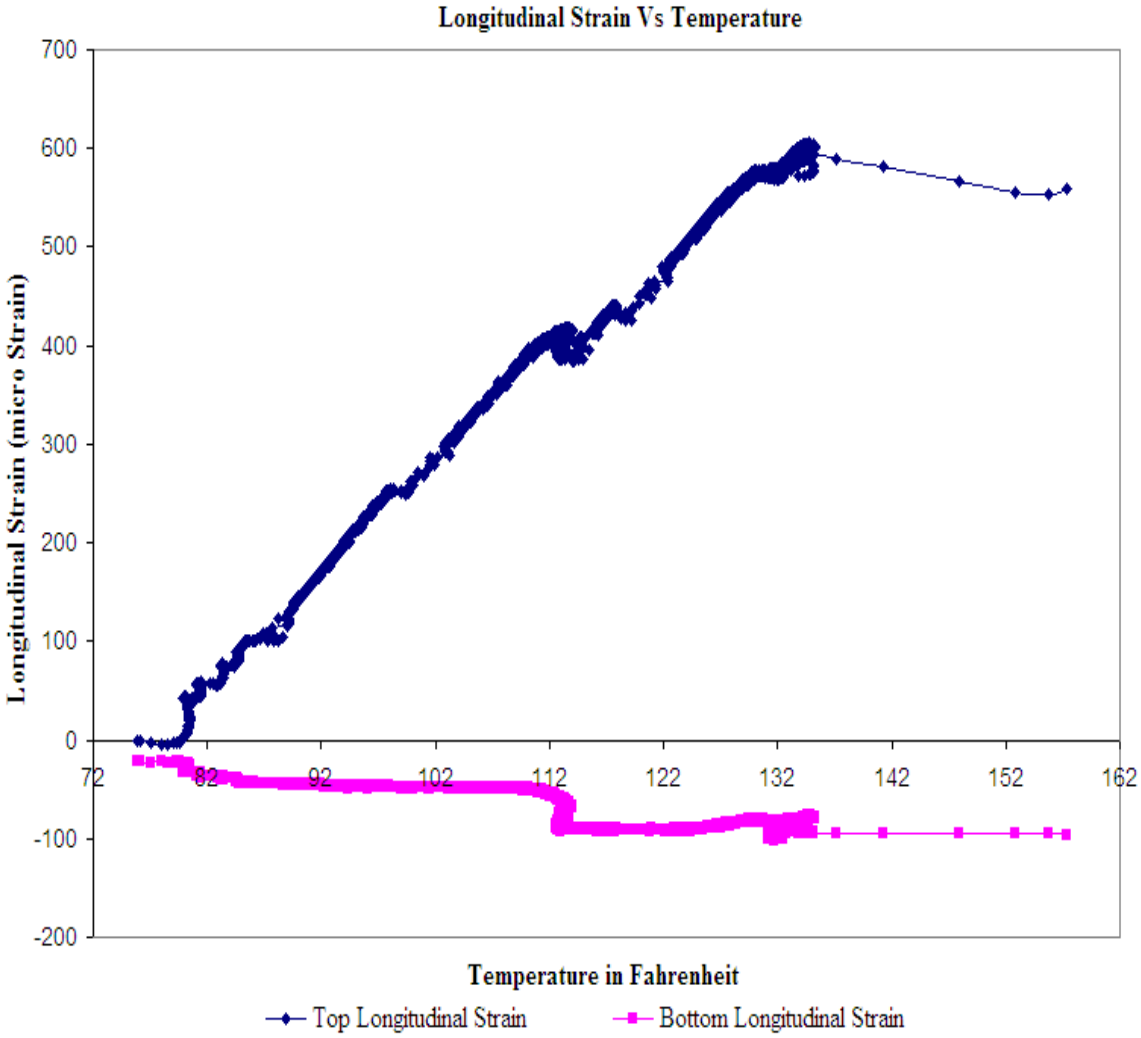

Figure C.14: Longitudinal Strain vs. Time for Test # 3

The above graph shows the variation of longitudinal strain at top and bottom surfaces over the temperature for the fiber composite deck specimen # 3 with ribs oriented along transverse direction and ends unrestrained. The negative strain at the bottom surface indicates a compressive strain.

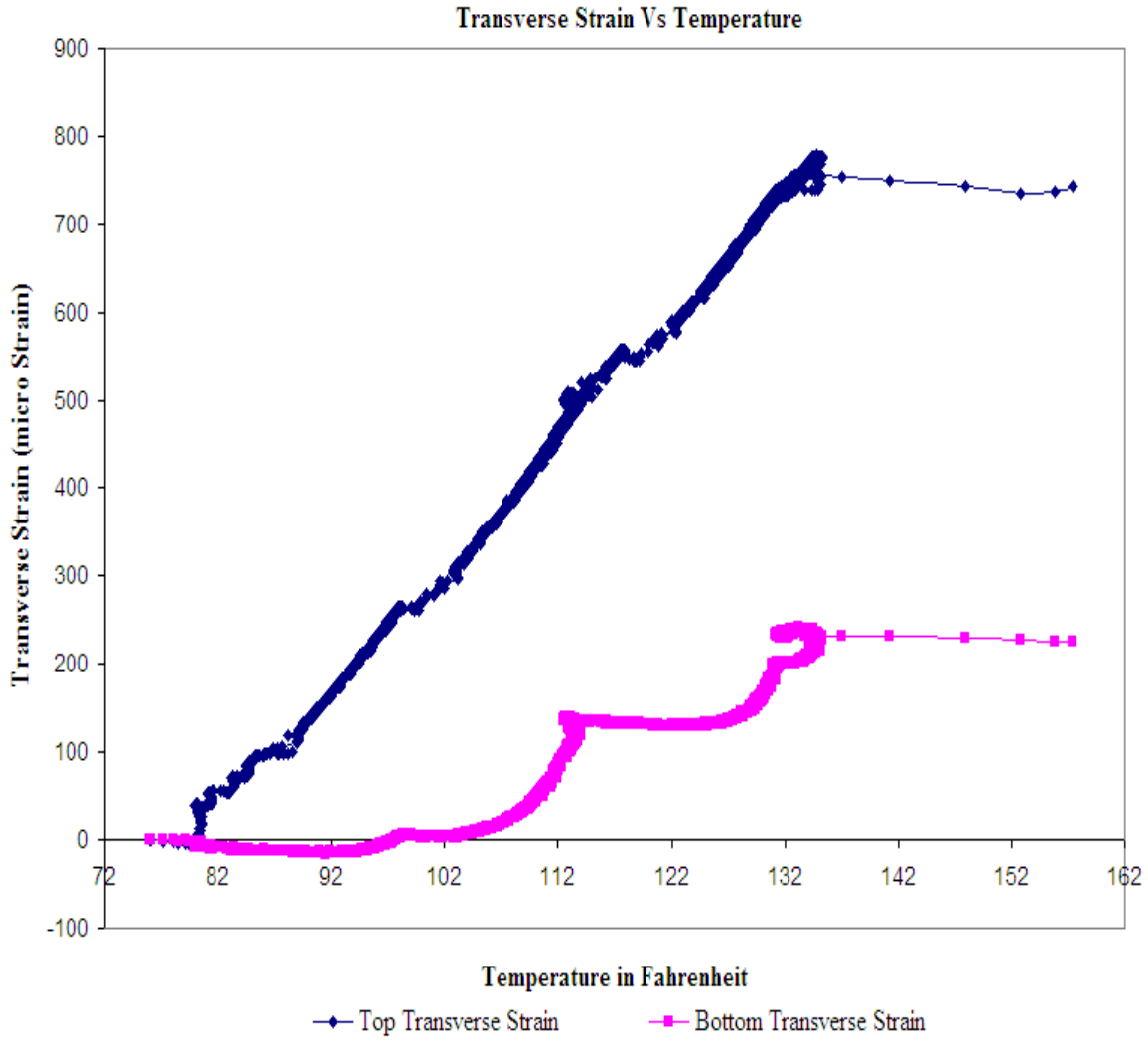

Figure C.15: Transverse Strain vs. Temperature for Test # 3

The above graph shows the variation of transverse strain at the top and bottom surfaces over the temperature at the top surface for the fiber composite deck specimen # 3 with ribs oriented along transverse direction and ends unrestrained. The negative strain at the bottom surface signifies a compressive strain

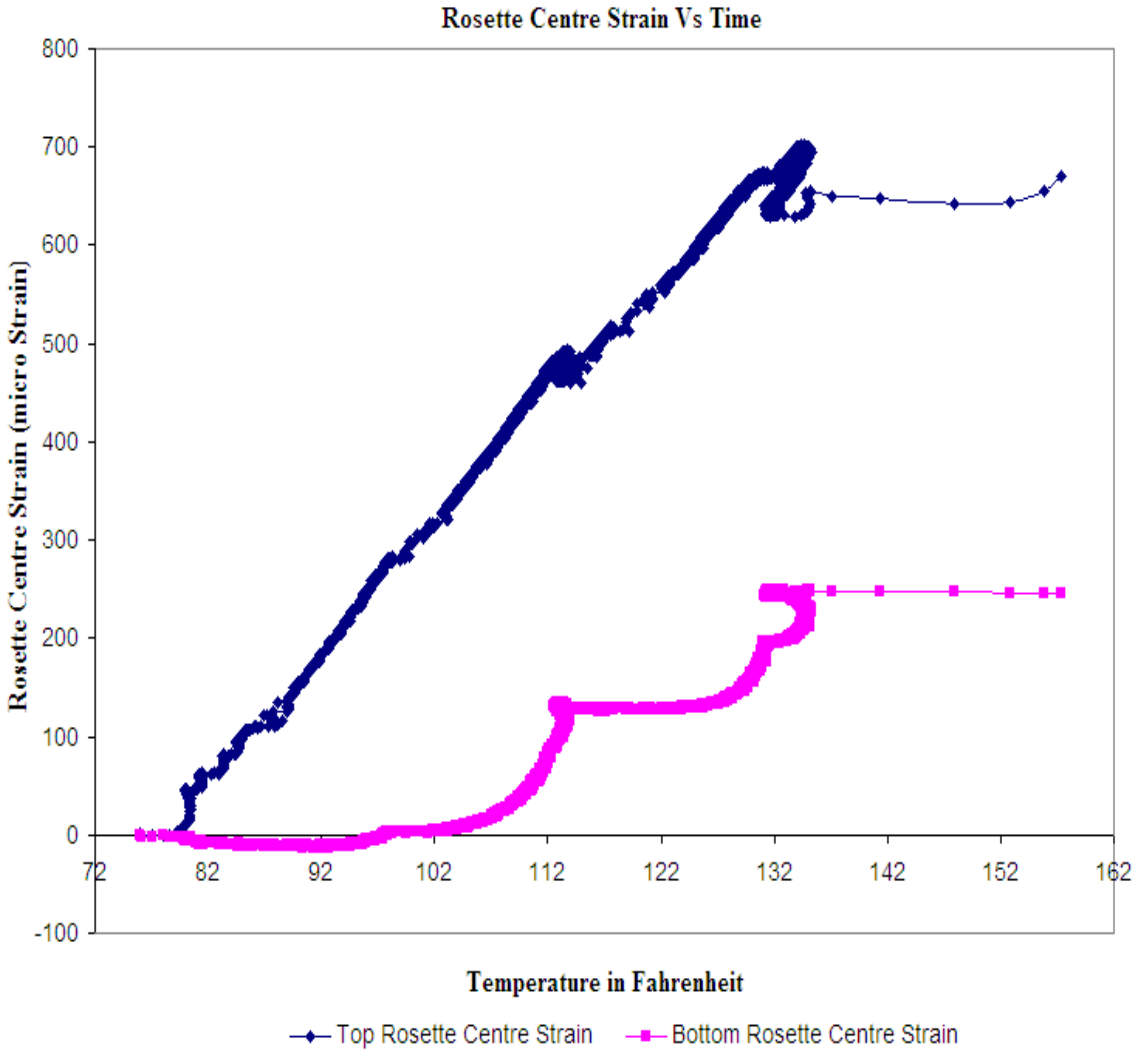

Figure C.16: Transverse Strain vs. Temperature for Test # 3

The above graph shows the variation of rosette centre strain at the top and bottom surfaces over the temperature at the top surface for the fiber composite deck specimen # 3 with ribs oriented along transverse direction and ends unrestrained.

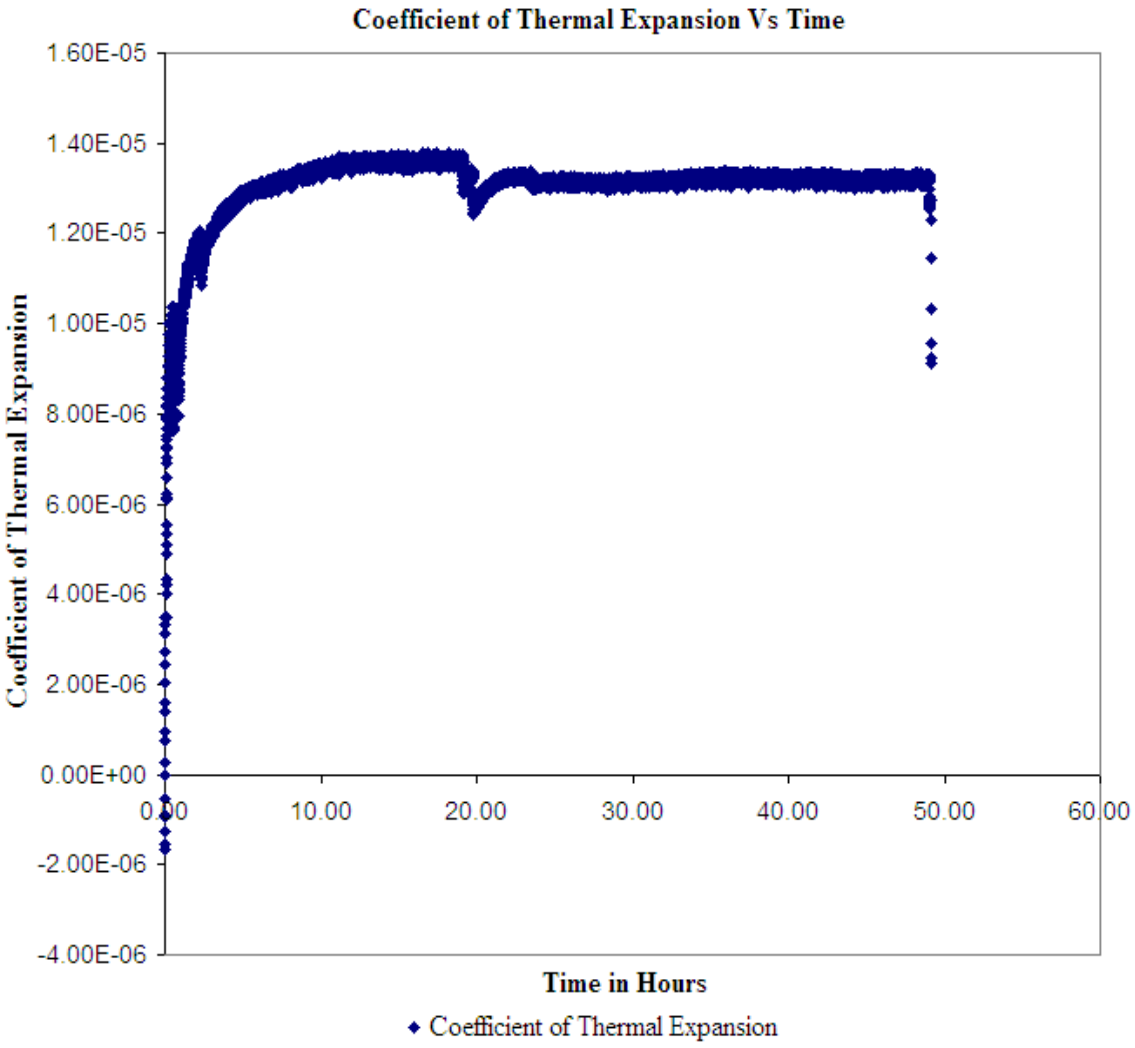

Figure C.17: Coefficient of Thermal Expansion vs. Time for Test # 3

The above graph shows the coefficient of thermal expansion over time for the fiber composite deck specimen # 3 with ribs oriented along transverse direction and ends unrestrained. The coefficient of thermal expansion remained constant throughout the experiment.

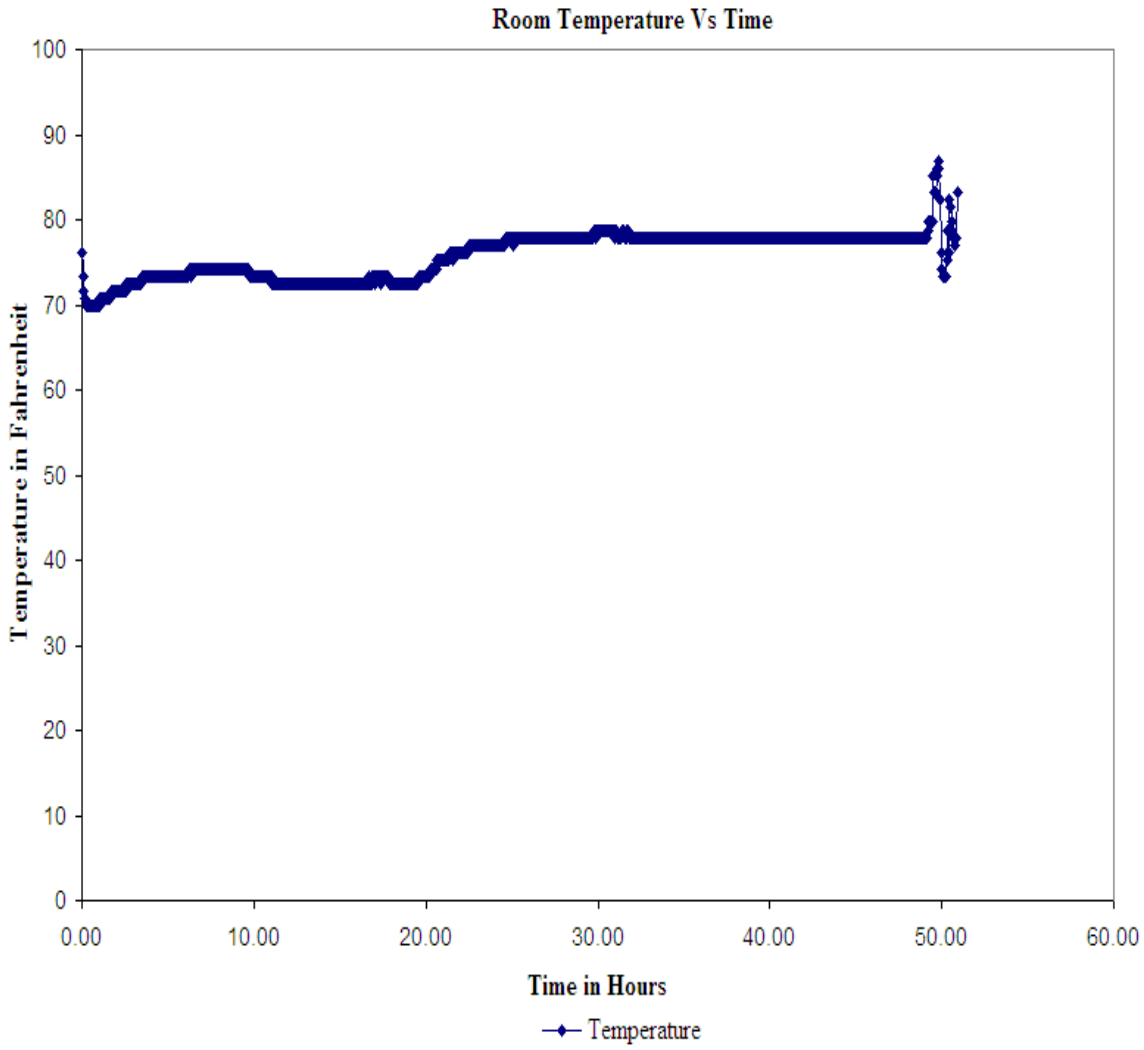

Figure C.18: Room Temperature vs. Time for Test # 3

The above graph shows the variation of temperature next to the experimental setup over time for Test # 3. The little variation is due to the interference of the outside temperature.

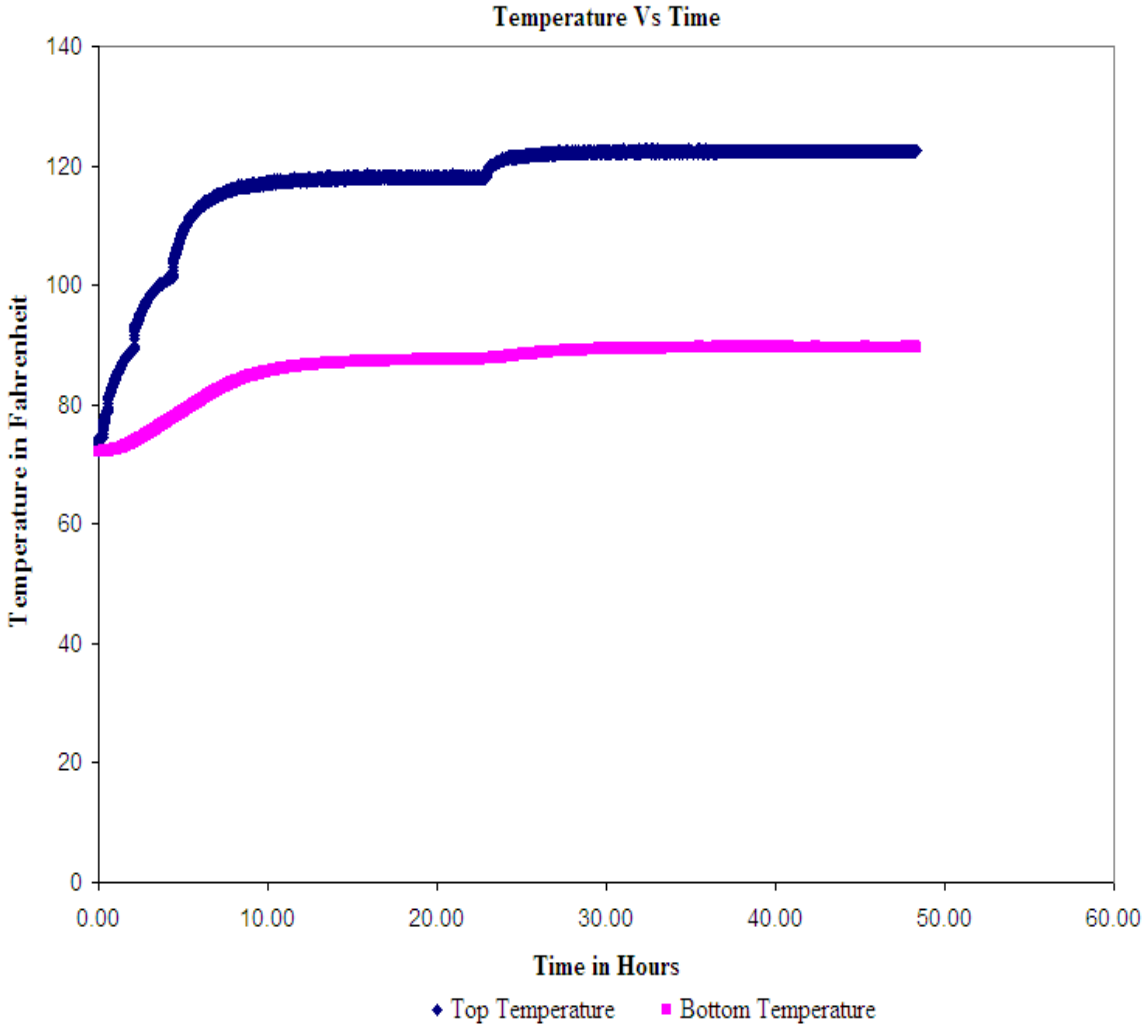

Figure C.19: Temperature Vs Time for Test # 4

The above graph shows the application of heat to the top surface and the measurement of heat at the bottom surface for fiber composite deck specimen # 4 with transverse ribs and ends unrestrained.

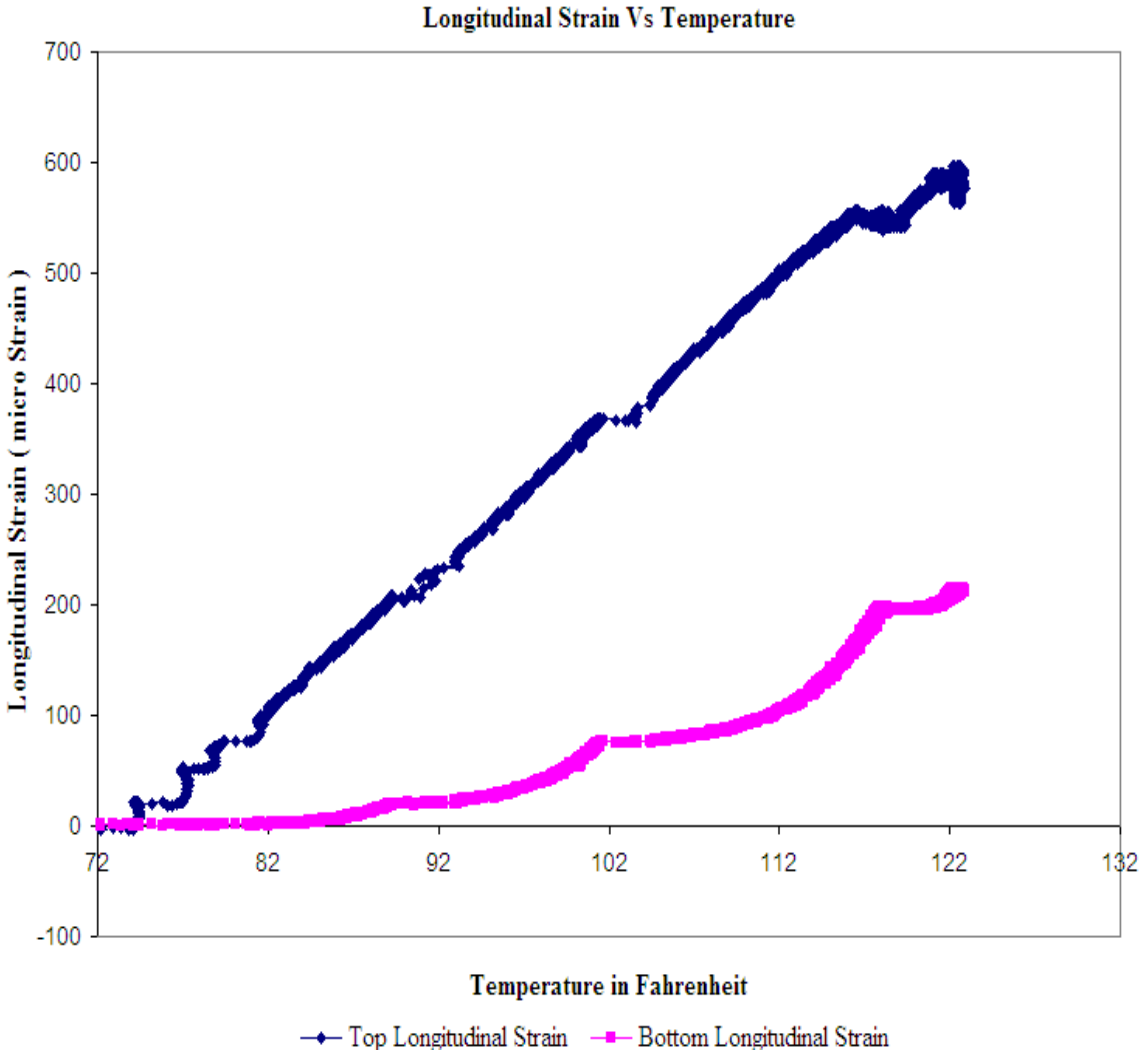

Figure C.20: Longitudinal Strain Vs Temperature for Test # 4

The above graph shows the variation of longitudinal strain at top and bottom surfaces over the temperature at the top surface for the fiber composite deck with ribs oriented along transverse direction.

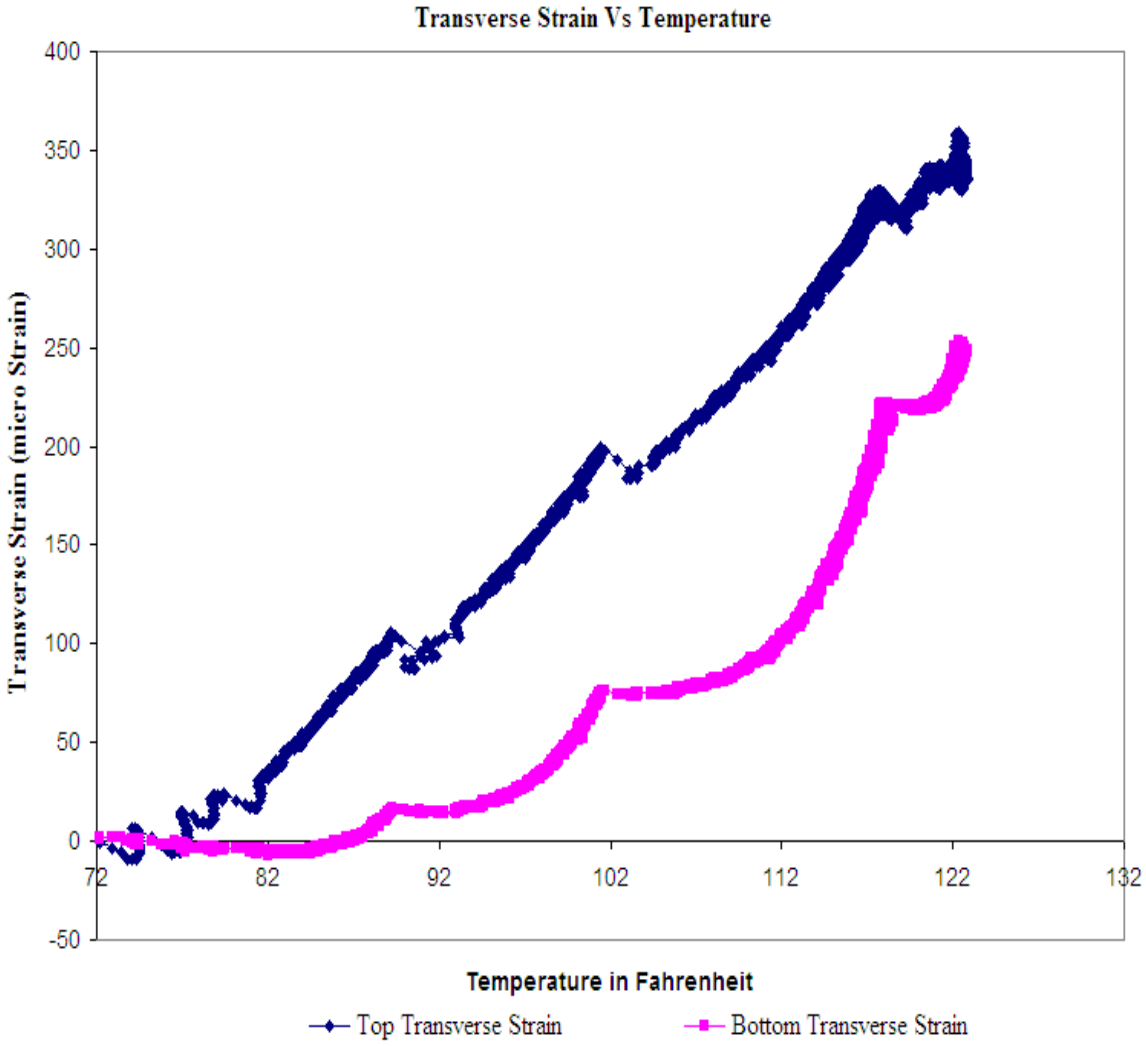

Figure C.21: Transverse Strain Vs Temperature for Test # 4

The above graph shows the variation of transverse strain at the top and bottom surfaces over the temperature at the top surface for the fiber composite deck specimen # 4 with ribs oriented along transverse direction and ends unrestrained. The negative strain at the bottom surface indicates a compressive strain.

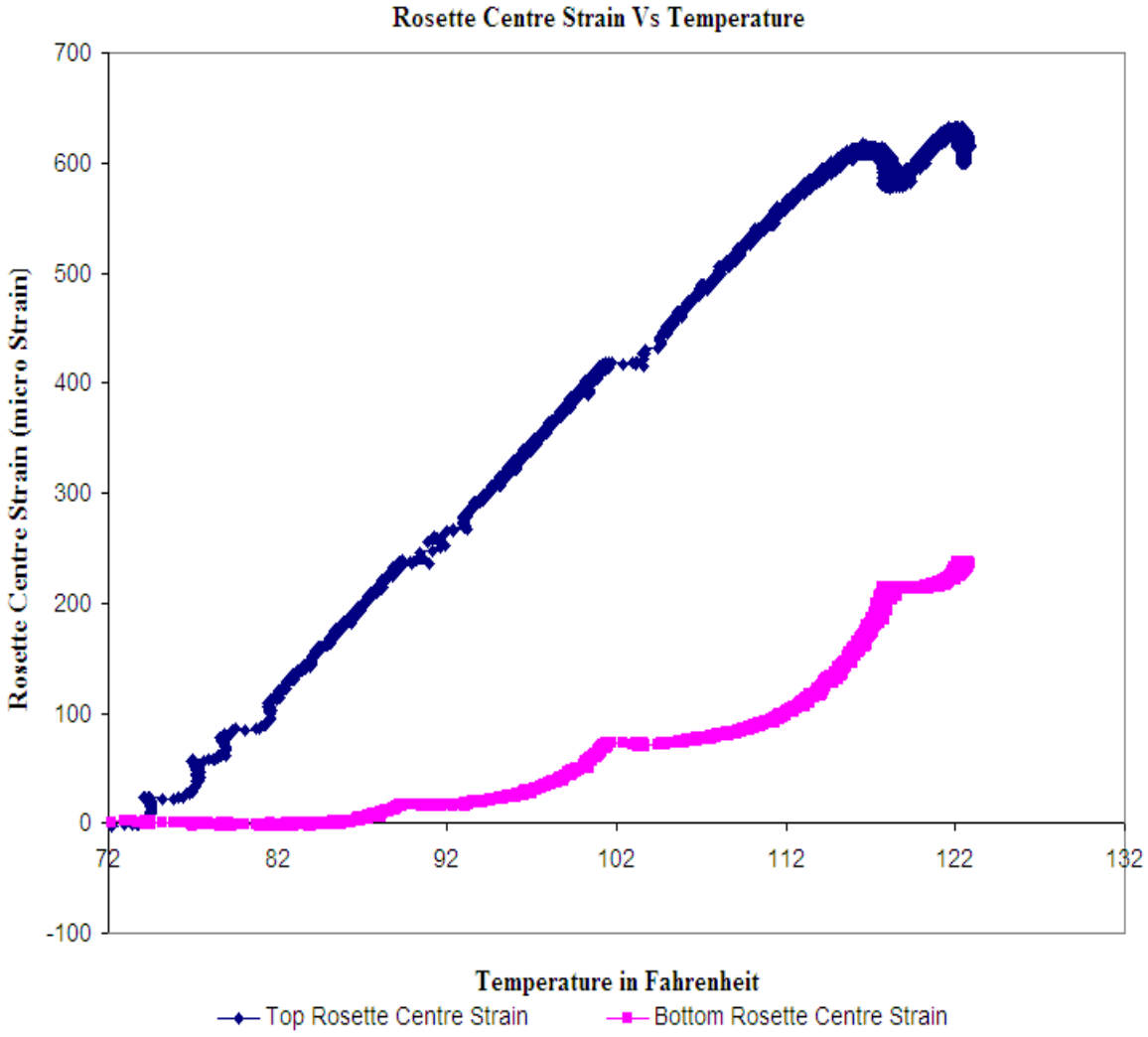

Figure C.22: Rosette Centre Strain Vs Temperature for Test # 4

The above graph shows the variation of rosette centre strain at the top and bottom surfaces over the temperature at the top surface for the fiber composite deck specimen # 4 with ribs oriented along transverse direction and ends unrestrained.

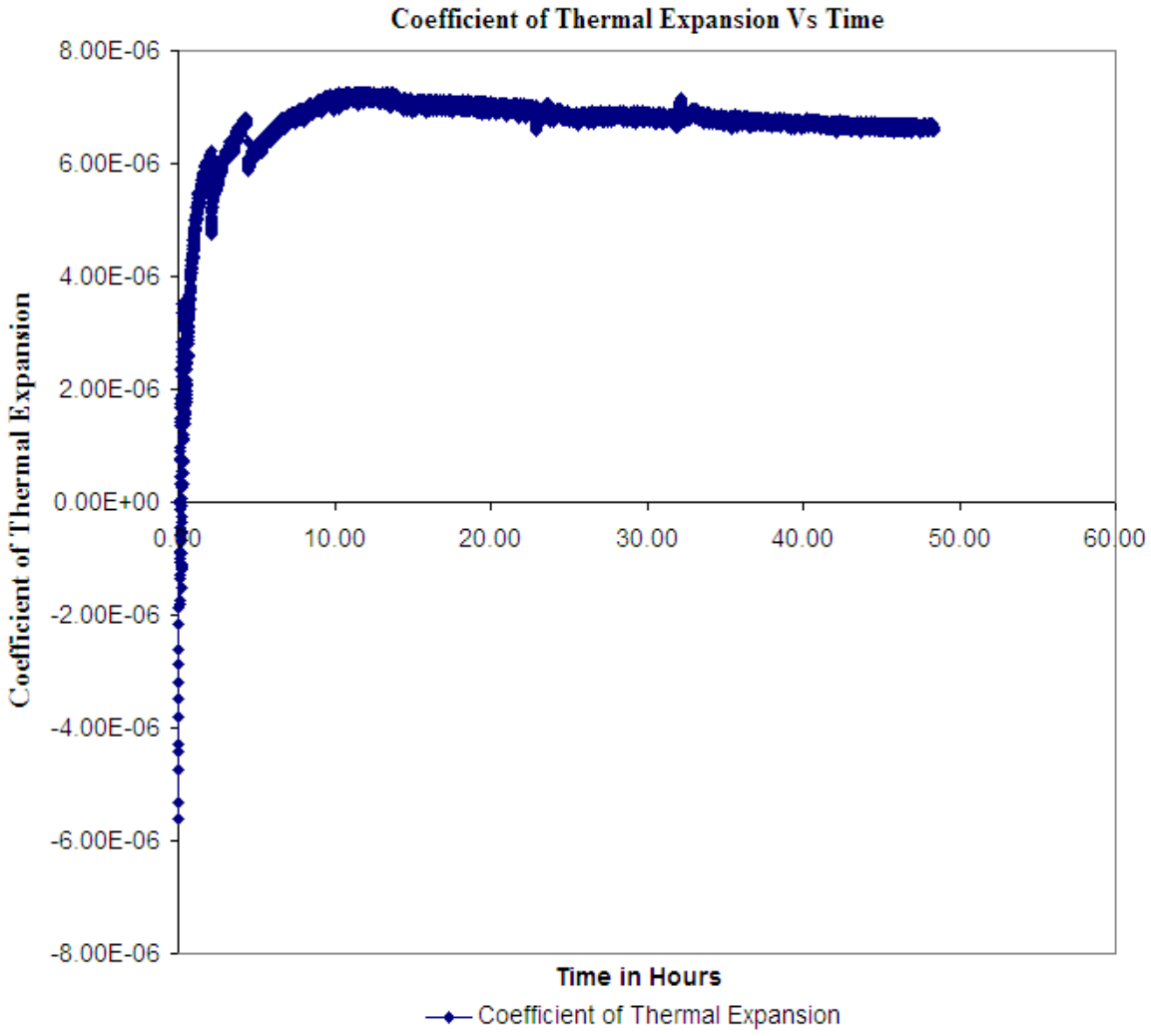

Figure C.23: Coefficient of Thermal Expansion Vs Time for Test # 4

The above graph shows the variation of coefficient of thermal expansion over time for the fiber composite deck specimen # 4 with ribs oriented along transverse direction and ends unrestrained. The coefficient of thermal expansion remained constant after the temperature stabilized at the top surface.

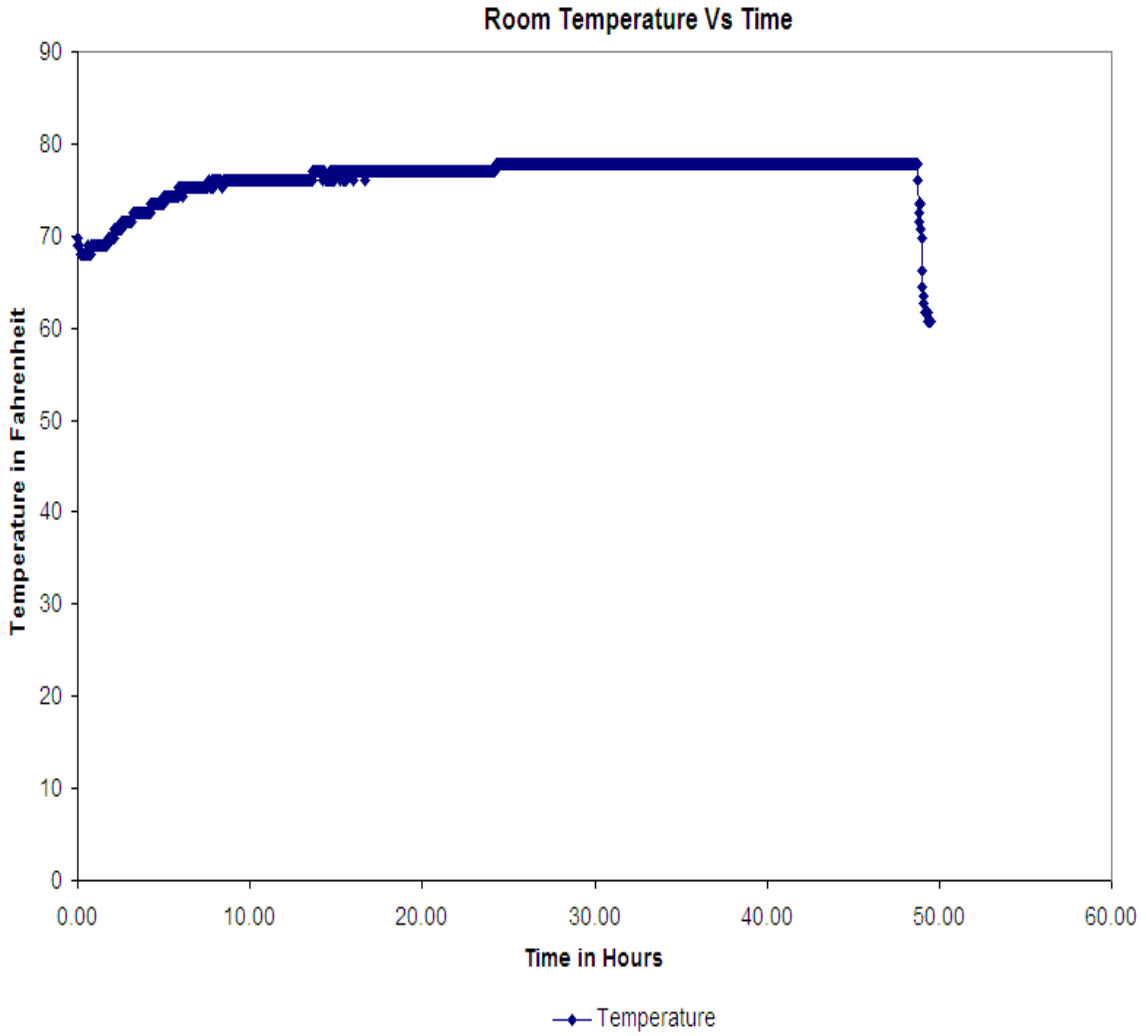

Figure C.24: Room Temperature Vs Time for Test # 4

The above graph shows the variation of temperature next to the experimental setup over time for Test # 4. The little variation of temperature for a short duration is because of the interference of the outside temperature.

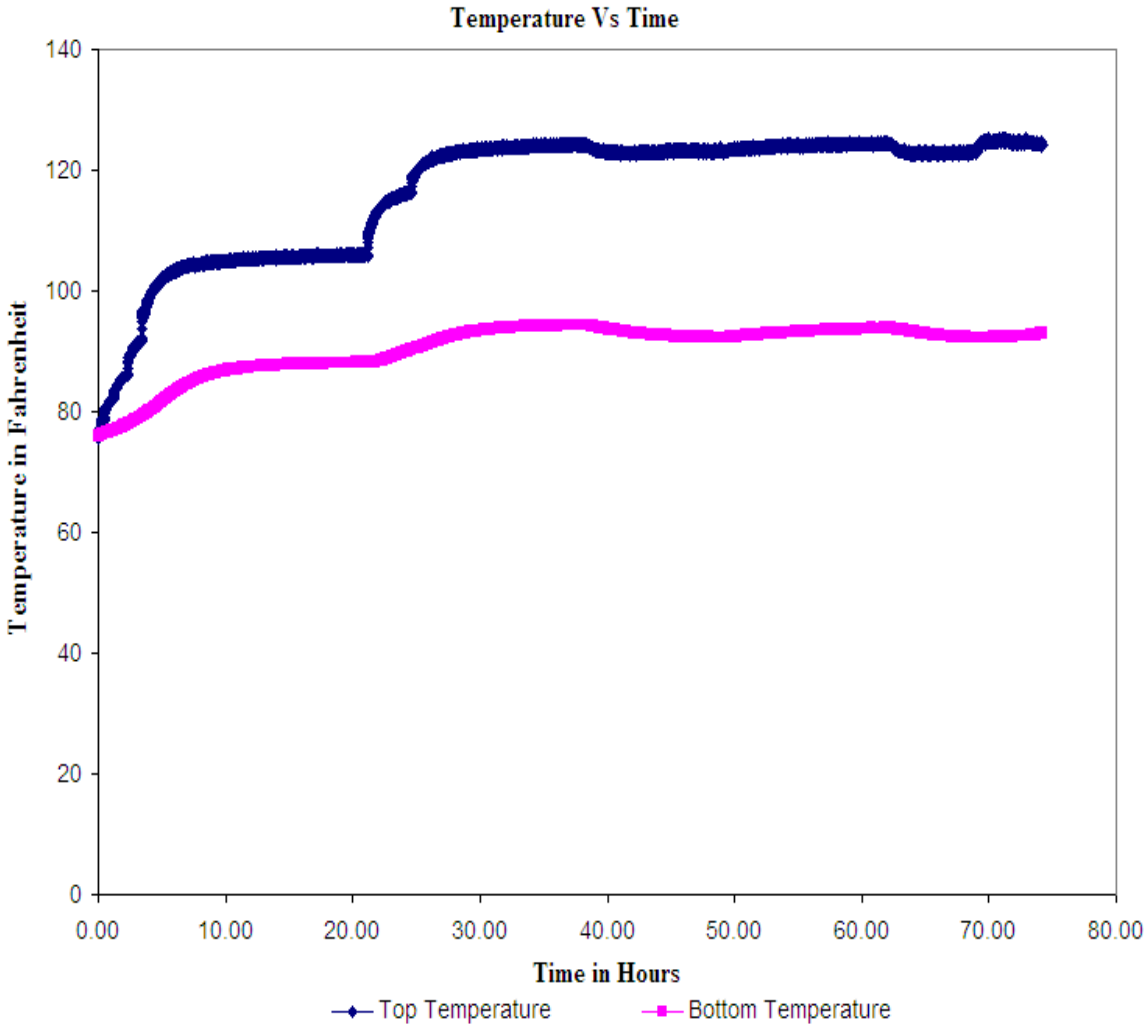

Figure C.25: Temperature Vs Time for Test # 5

The above graph shows the application of heat to the top surface and the measurement of heat at the bottom surface for fiber composite deck specimen # 5 with longitudinal ribs and ends restrained.

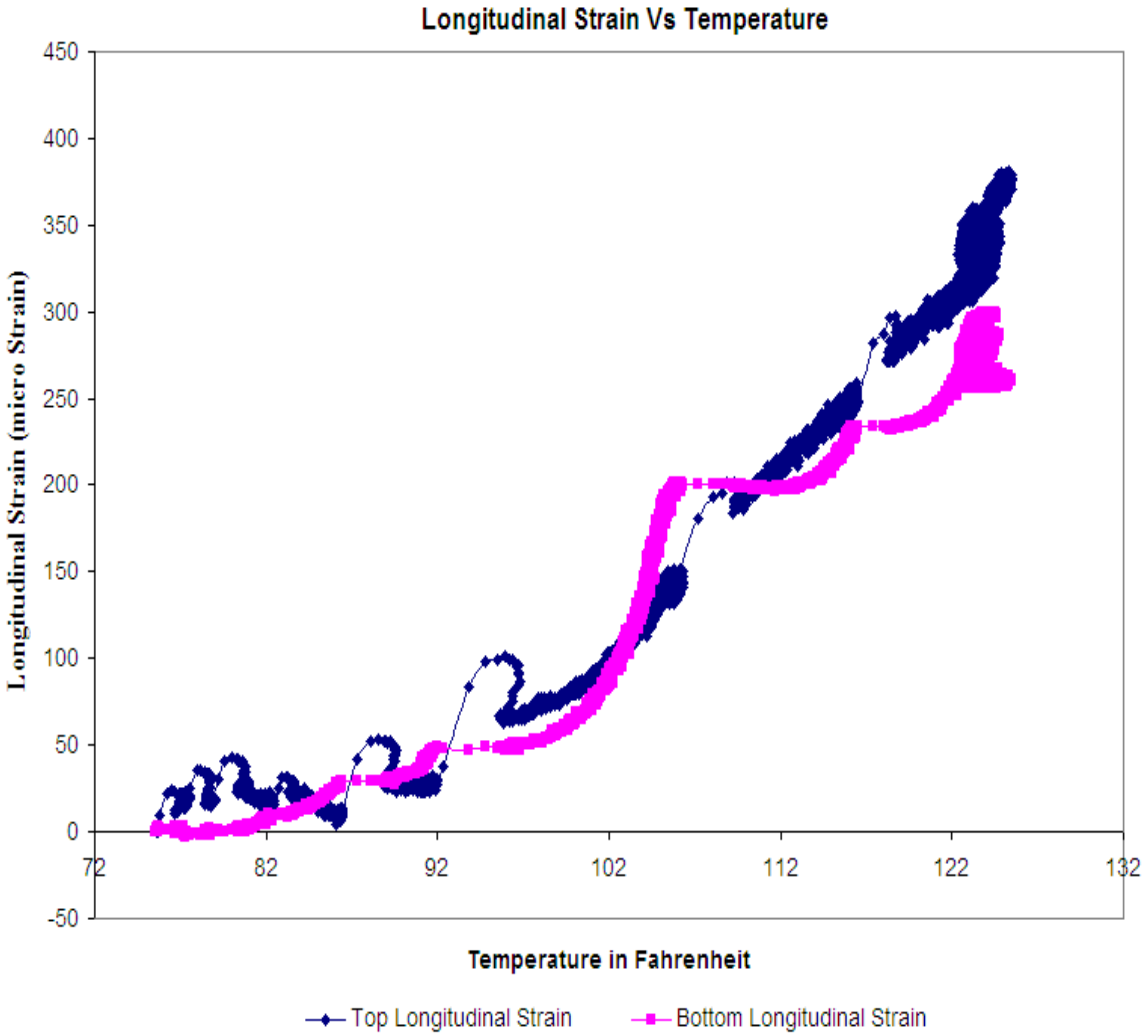

Figure C.26: Longitudinal Strain Vs Temperature for Test # 5

The above graph shows the variation of longitudinal strain at the top and bottom surfaces over the temperature at the top surface for the fiber composite deck specimen # 5 with ribs oriented along longitudinal direction and ends restrained. The graph shows a strange behavior of same strain values at some points of both the surfaces even with a different temperature.

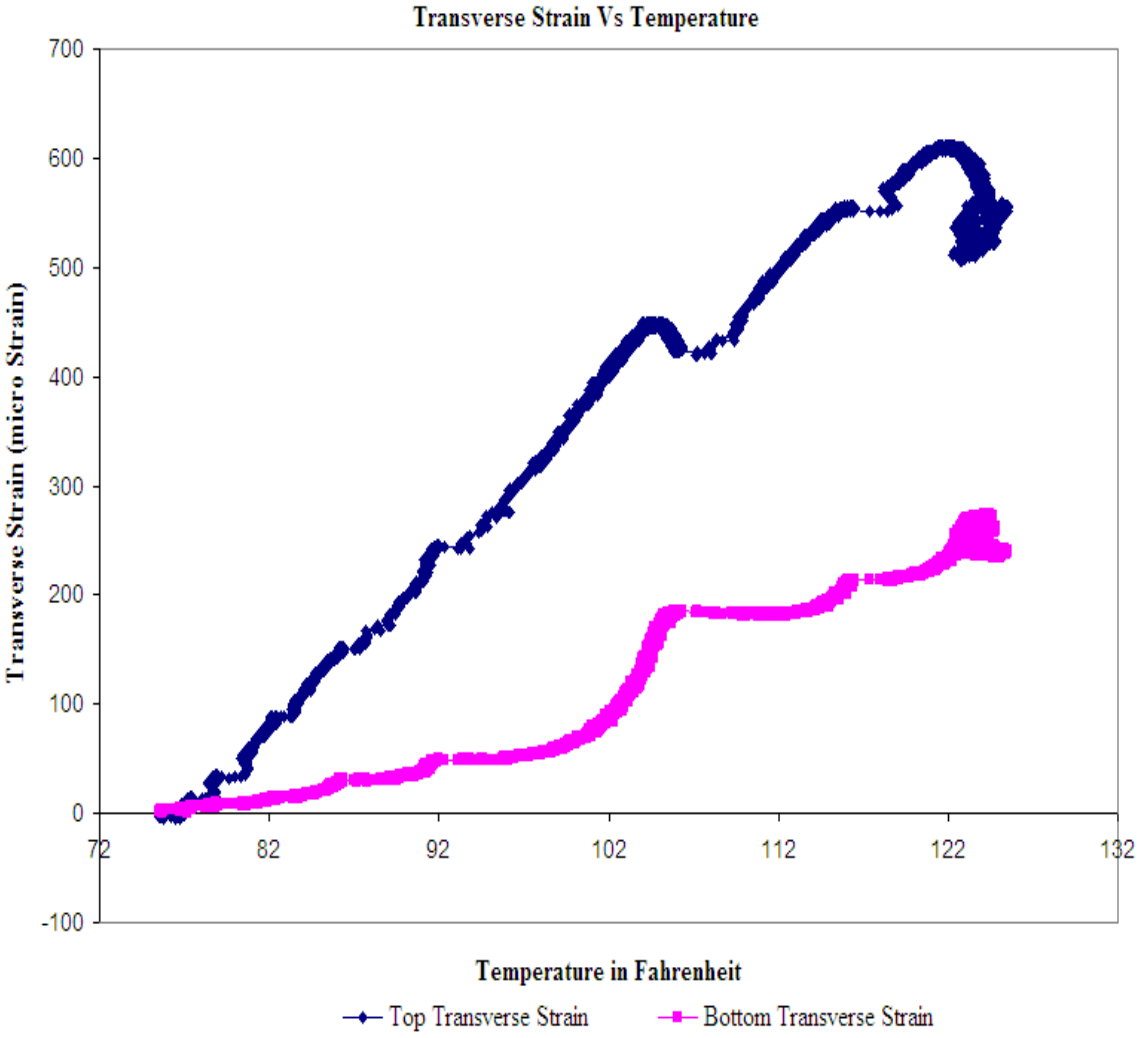

Figure: C.27: Transverse Strain Vs Temperature for Test # 5

The above graph shows the variation of transverse strain at the top and bottom surfaces over the temperature at the top surface for the fiber composite deck specimen # 5 with ribs oriented along longitudinal direction and ends restrained.

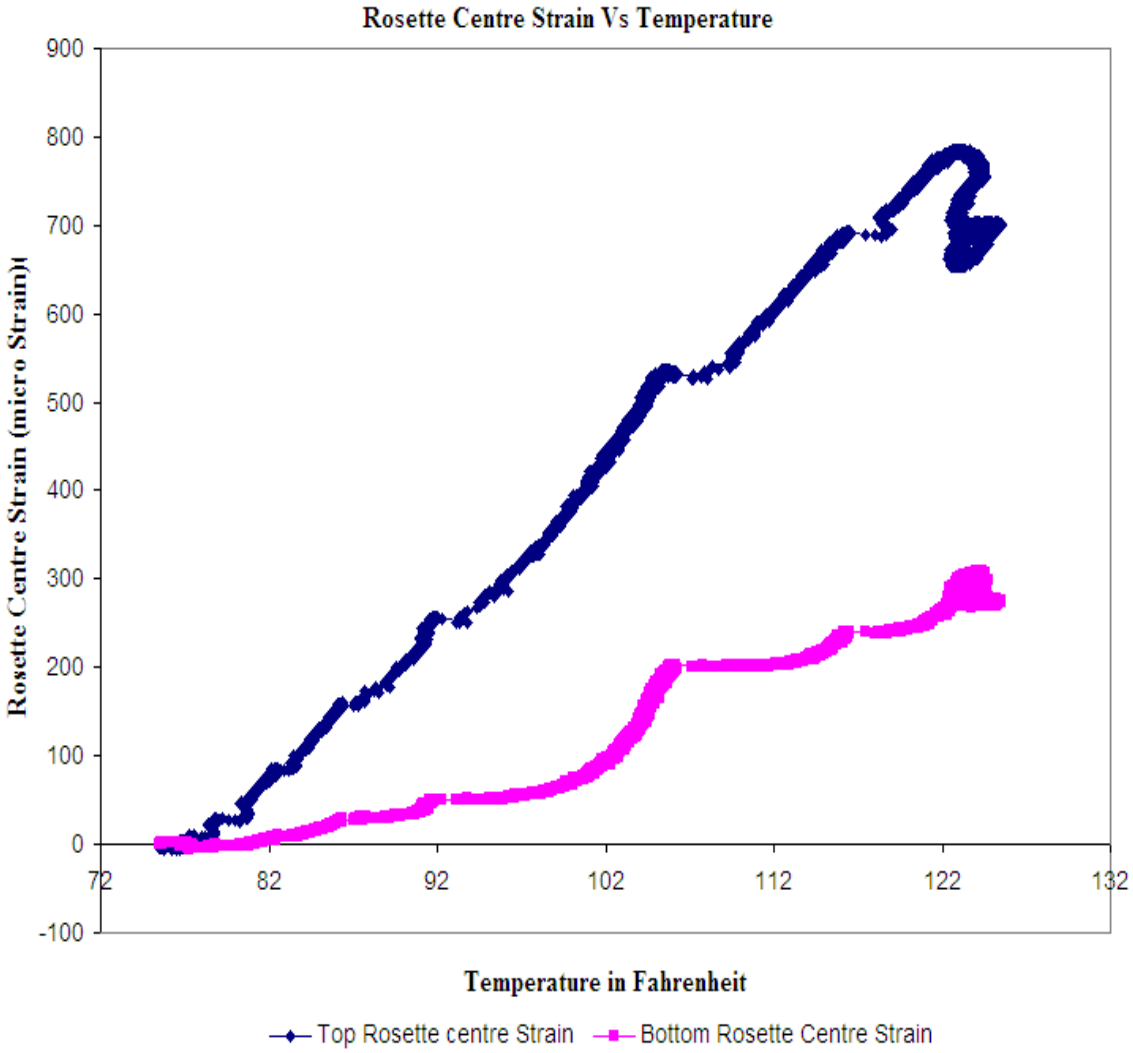

Figure C.28: Rosette Centre Strain Vs Temperature for Test # 5

The above graph shows the variation of rosette centre strain at the top and bottom surfaces over the temperature at the top surface for the fiber composite deck specimen # 5 with ribs oriented along longitudinal direction and ends restrained.

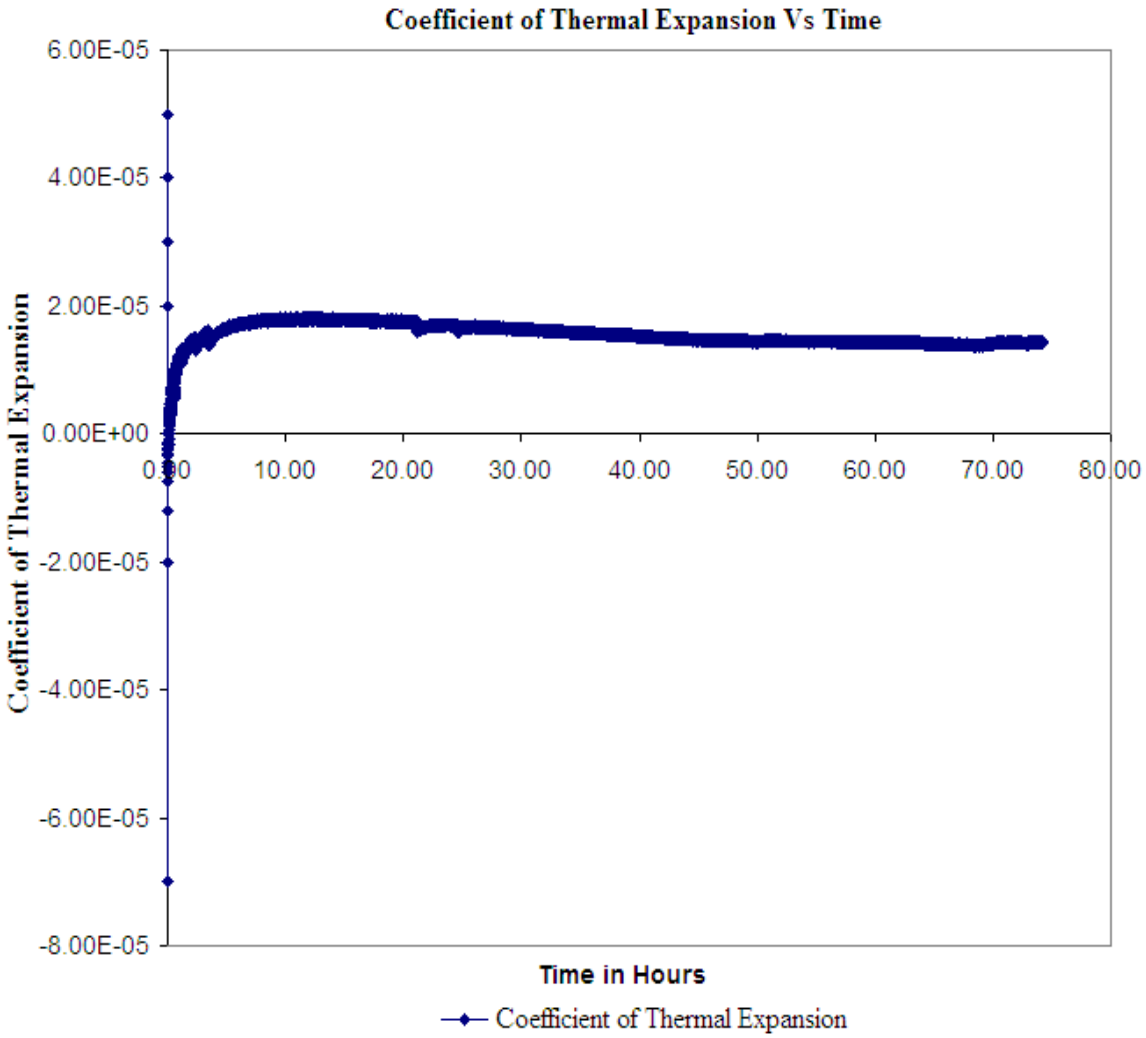

Figure C.29: Coefficient of Thermal Expansion Vs Time for Test # 5

The above graph shows the variation of coefficient of thermal expansion over time for the fiber composite deck specimen # 5 with ribs oriented along longitudinal direction. The coefficient of thermal expansion remained constant throughout the experiment.

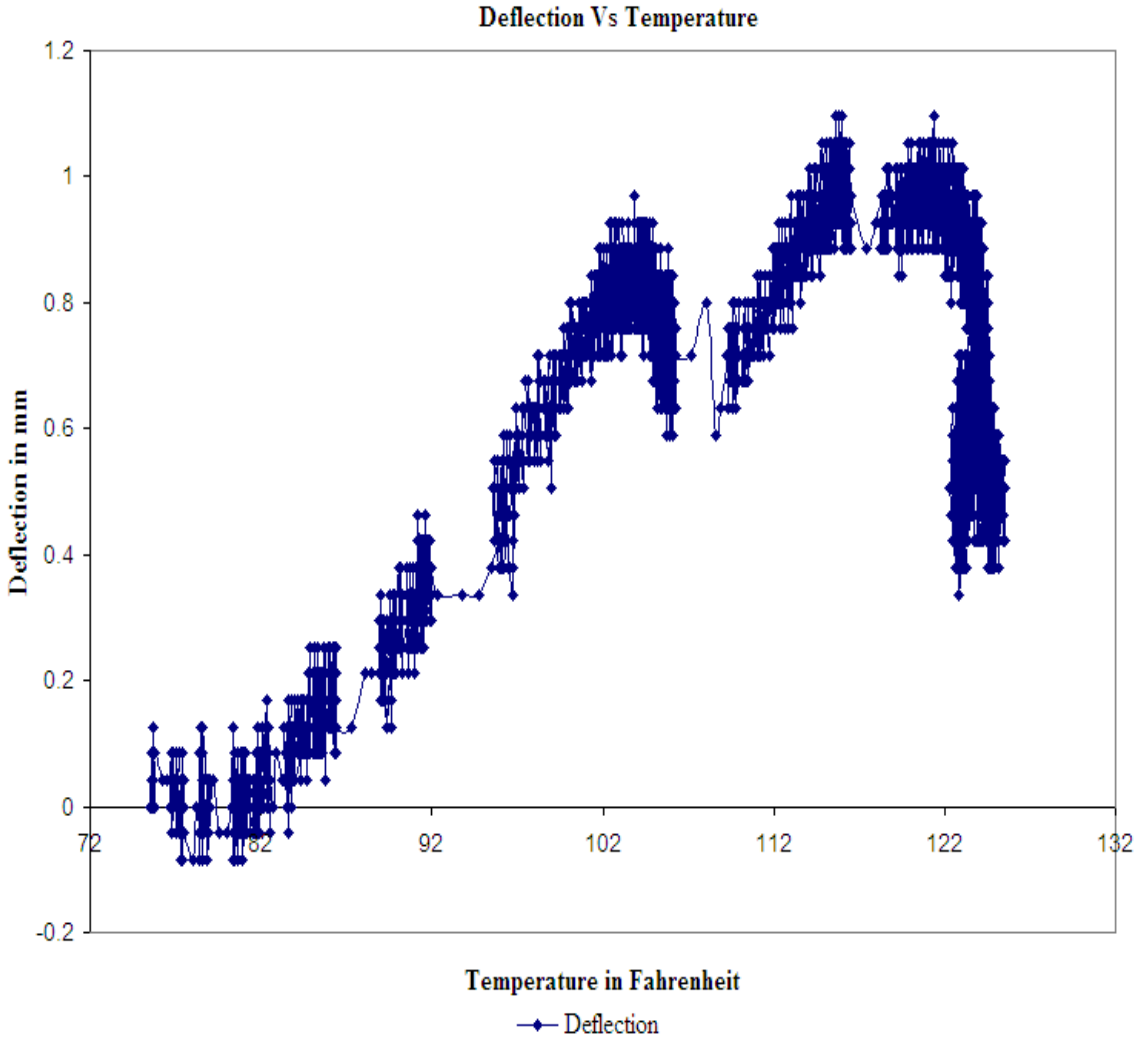

Figure C.30: Deflection Vs Temperature for Test # 5

The above graph shows the variation of deflection over temperature at the top surface for the fiber composite deck specimen # 5 with ribs oriented along longitudinal direction and ends restrained.

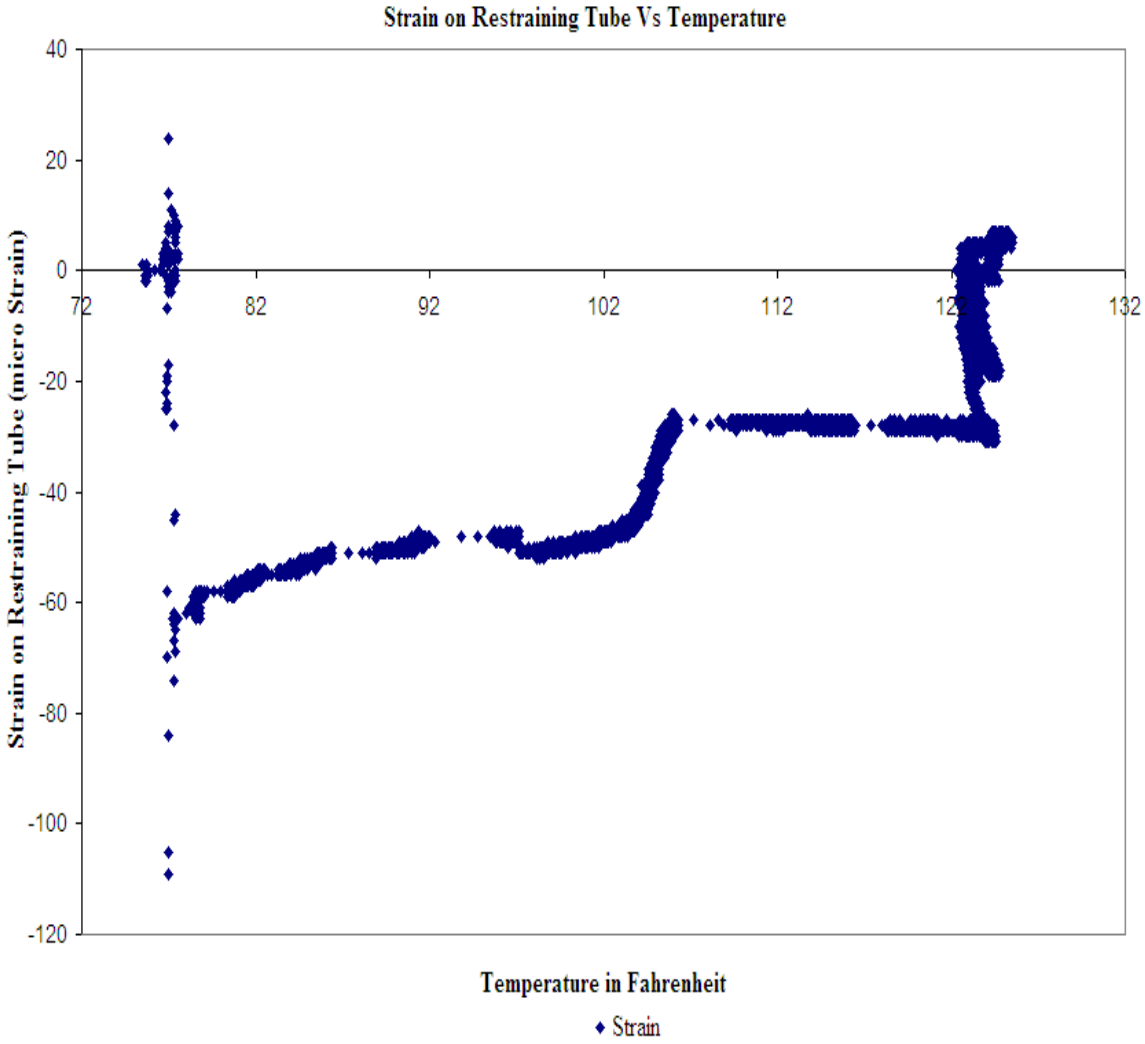

Figure C.31: Strain on Restraining Tube Vs Temperature for Test # 5

The above graph shows the variation of strain on restraining tube over temperature at the top surface for the fiber composite deck specimen # 5 with ribs oriented along longitudinal direction and ends restrained.

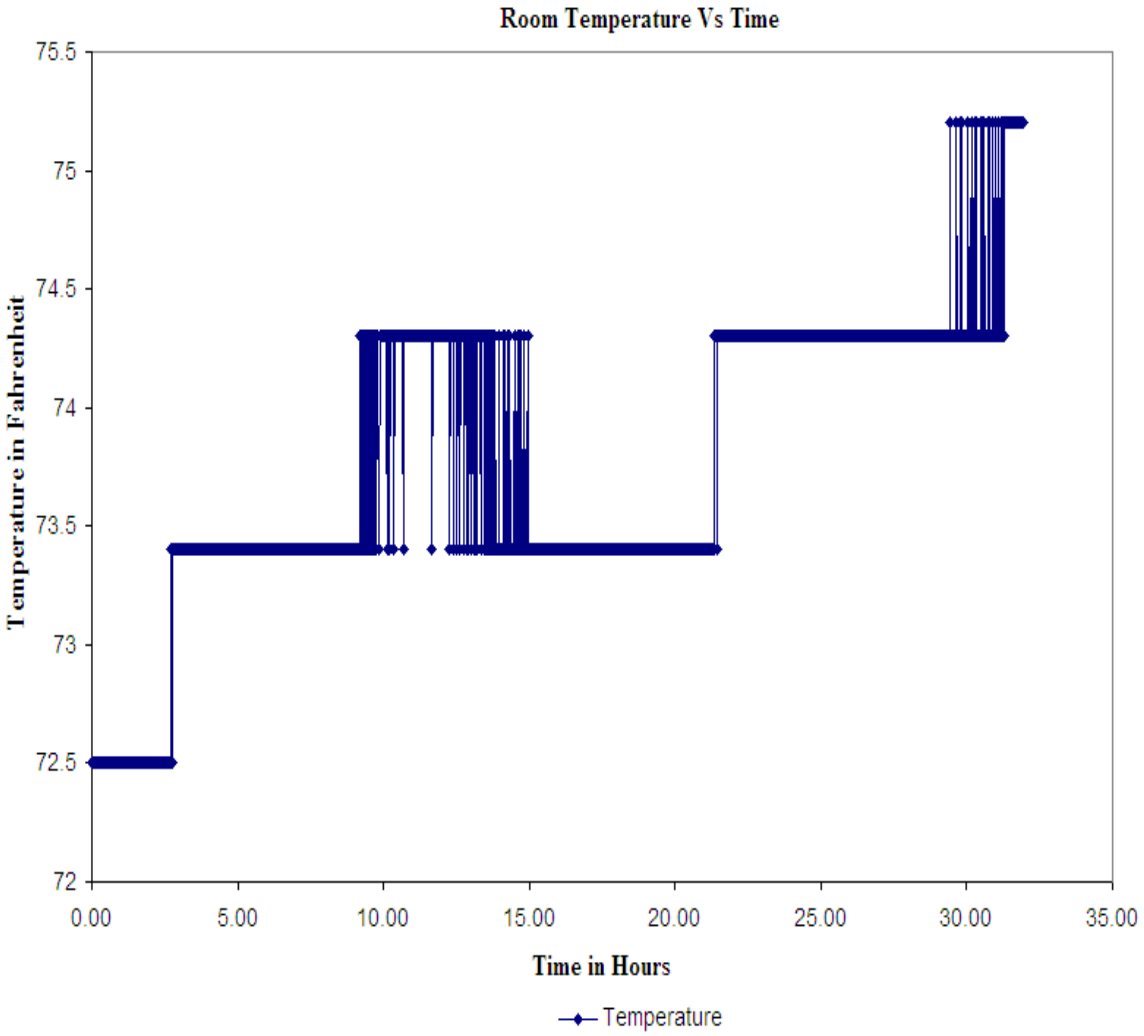

Figure C.32: Room Temperature Vs Time for Test # 5

The above graph shows the variation of temperature next to the experimental setup over time for Test # 5.

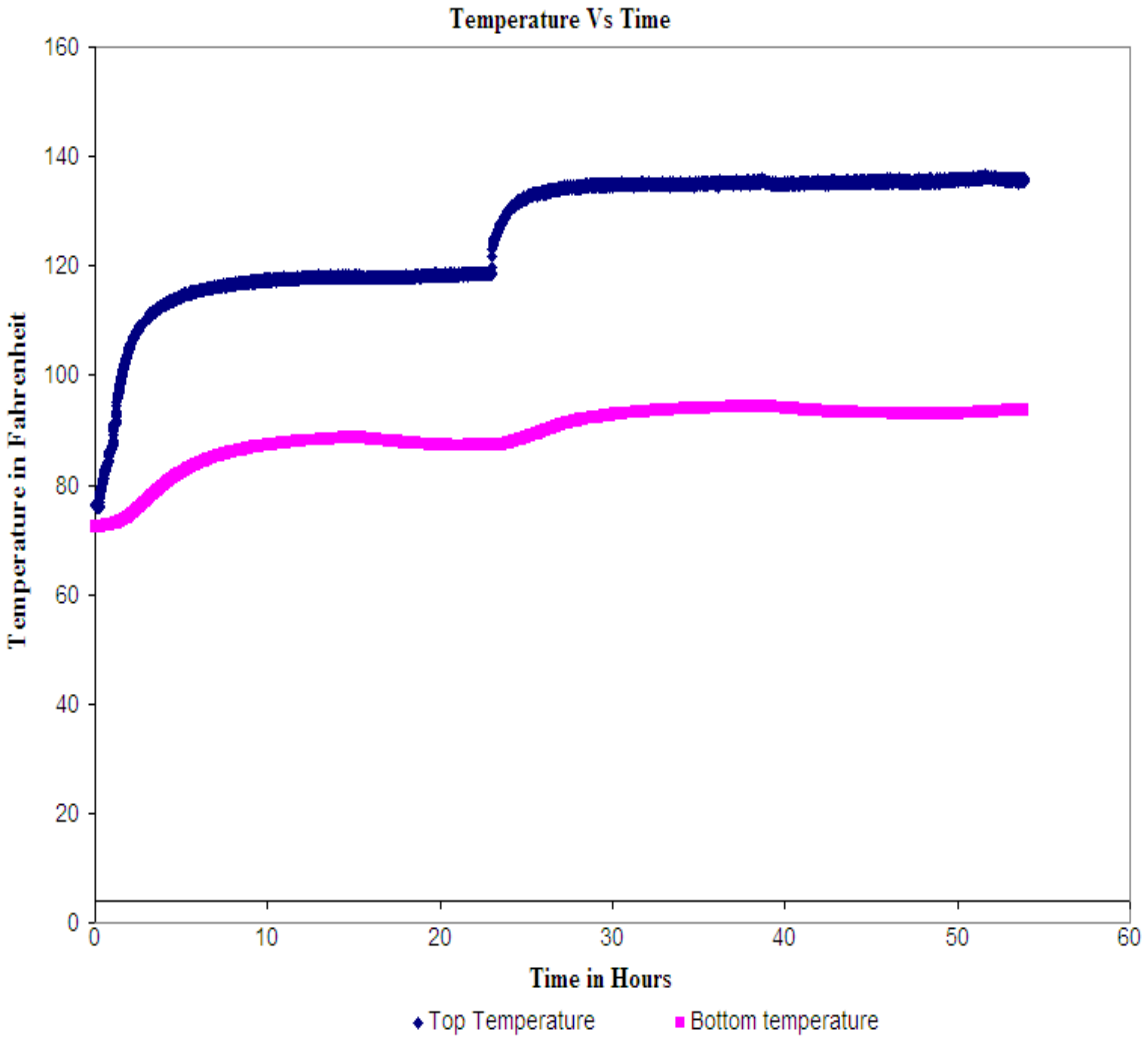

Figure C.33 Temperature Vs Time for Test # 6

The above graph shows the application of heat to the top surface and the measurement of heat at the bottom surface for the fiber composite deck specimen # 1 with ribs oriented along longitudinal direction and ends unrestrained. This specimen was also tested in Test # 1.

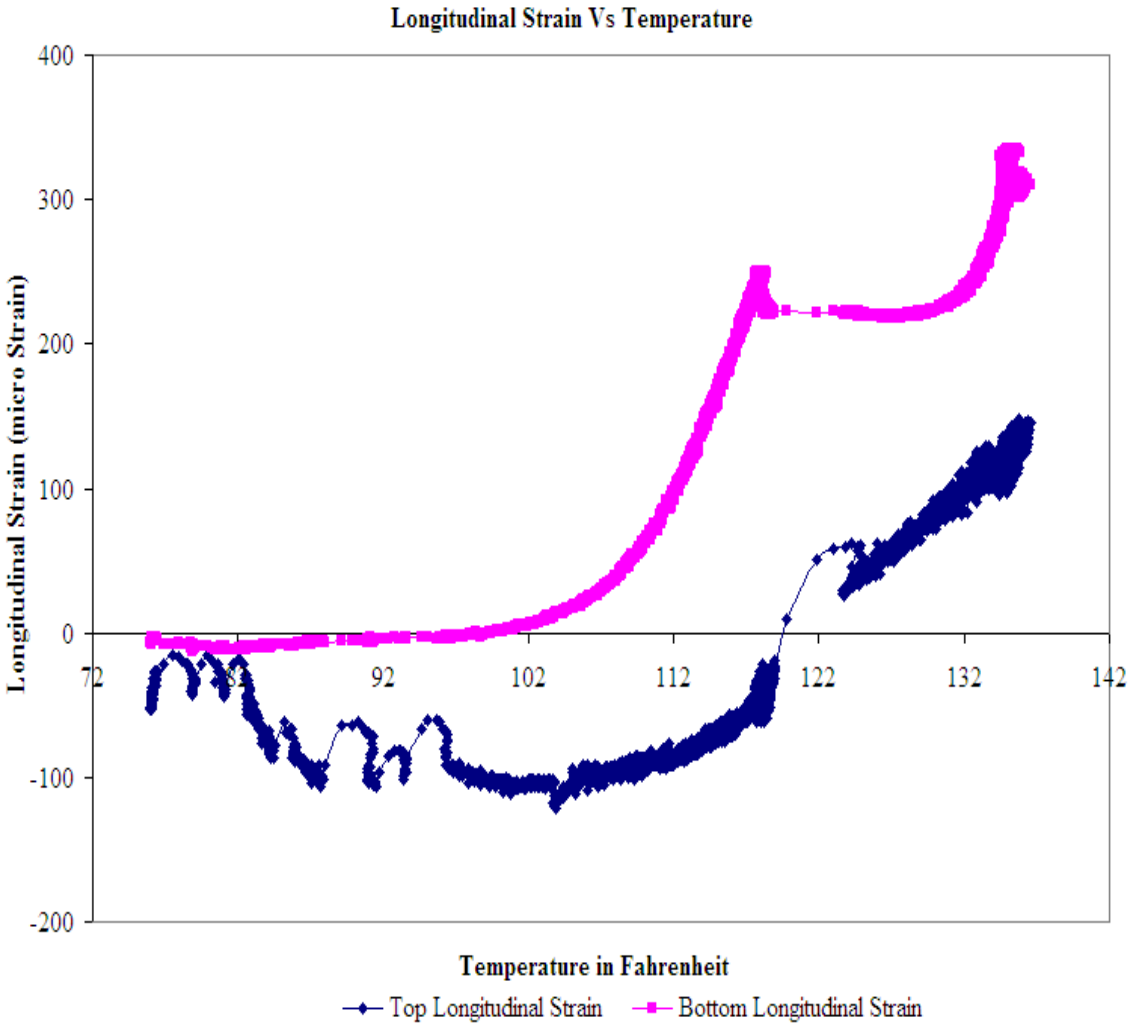

Figure C.34: Longitudinal Strain Vs Temperature for test # 6

The above graph shows the variation of longitudinal strain at top and bottom surfaces over the temperature at the top surface for the fiber composite deck specimen # 1 with ribs oriented along longitudinal direction and ends restrained. The negative strain at the bottom surface indicates a compressive strain. This specimen was also tested in Test # 1.

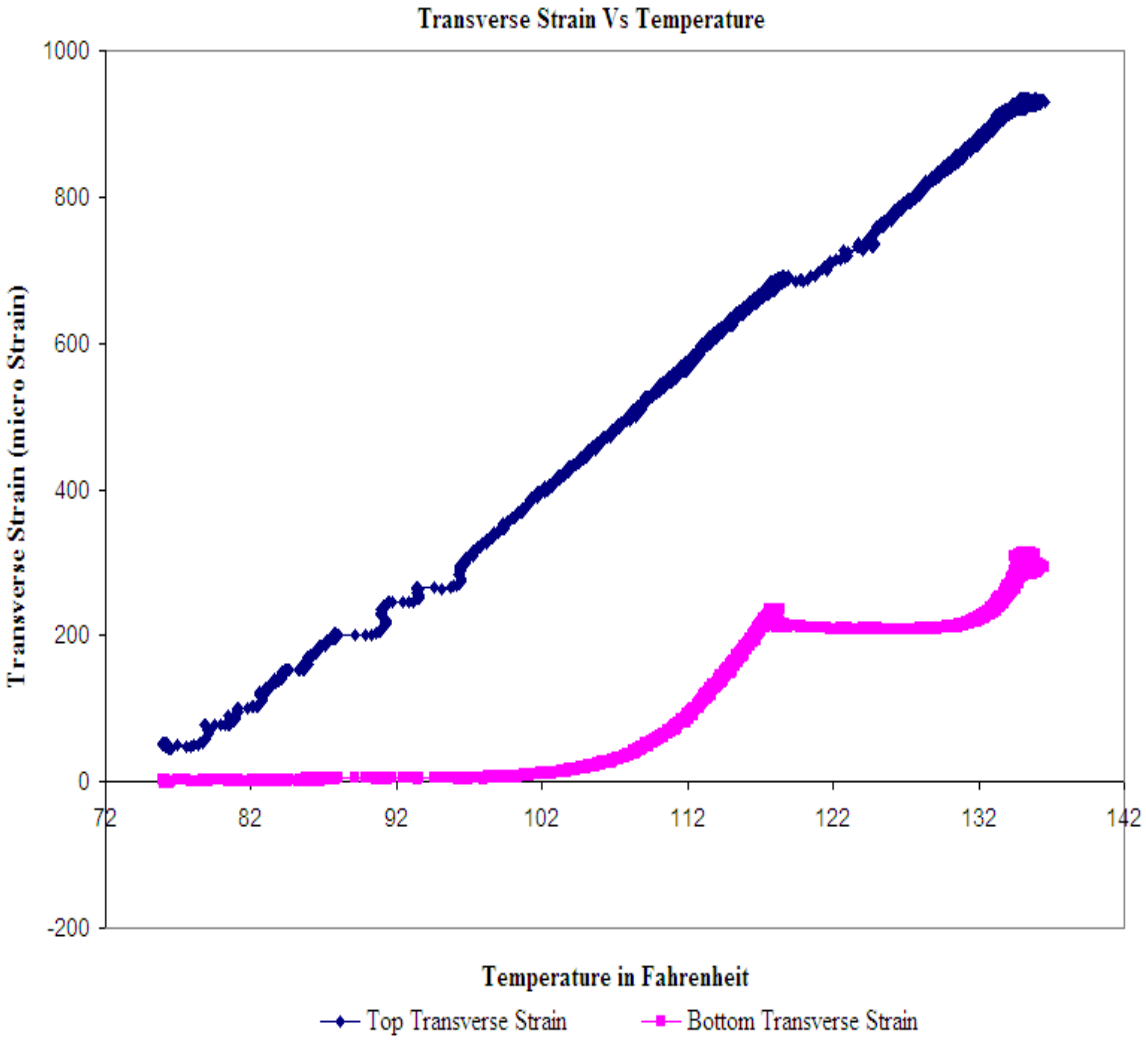

Figure C.35: Transverse Strain Vs Temperature for Test # 6

The above graph shows the variation of transverse strain at the top and bottom surfaces over the temperature at the top surface for the fiber composite deck specimen # 1 with ribs oriented along longitudinal direction and ends restrained. This specimen was also tested in Test # 1.

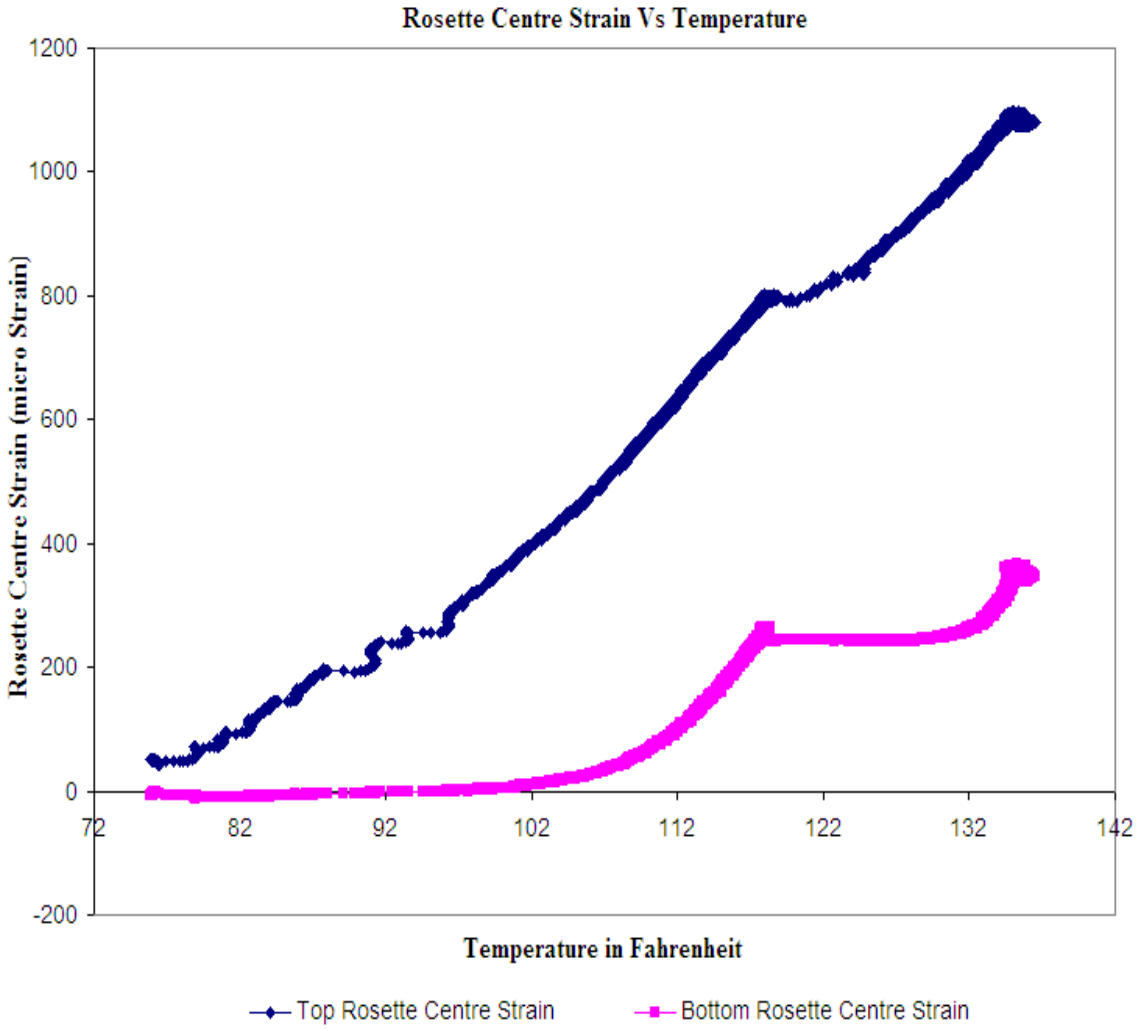

Figure C.36: Rosette Centre Strain Vs Temperature for Test # 6

The above graph shows the variation of rosette centre strain at the top and bottom surfaces over the temperature at the top surface for the fiber composite deck specimen # 1 with ribs oriented along longitudinal direction and ends restrained This specimen was also tested in Test # 1.

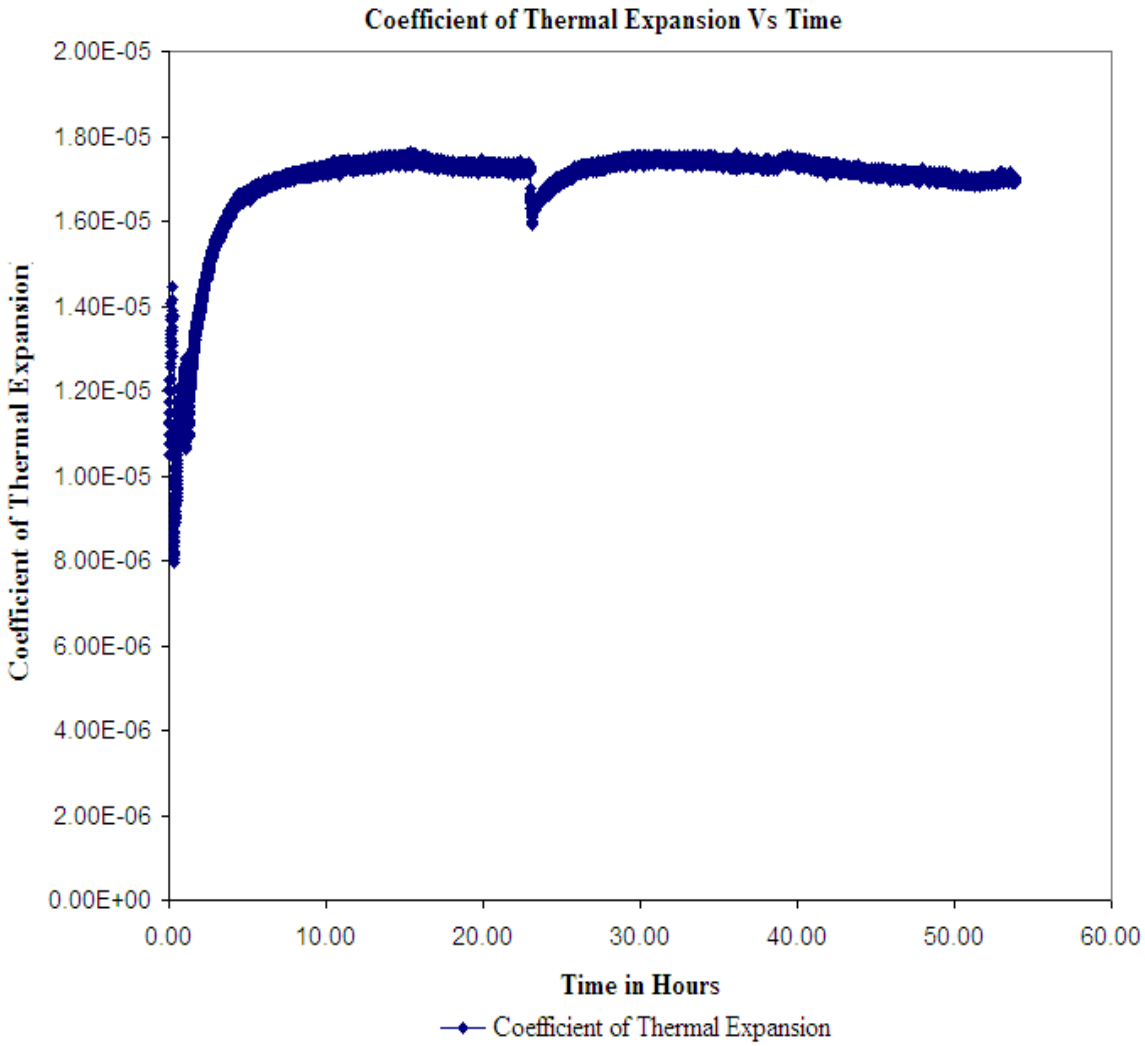

Figure C.37: Coefficient of Thermal Expansion Vs Time for Test # 6

The above graph shows the variation of coefficient of thermal expansion over time for the fiber composite deck specimen # 1 with ribs oriented along longitudinal direction and ends restrained. This specimen was also tested in Test # 1.

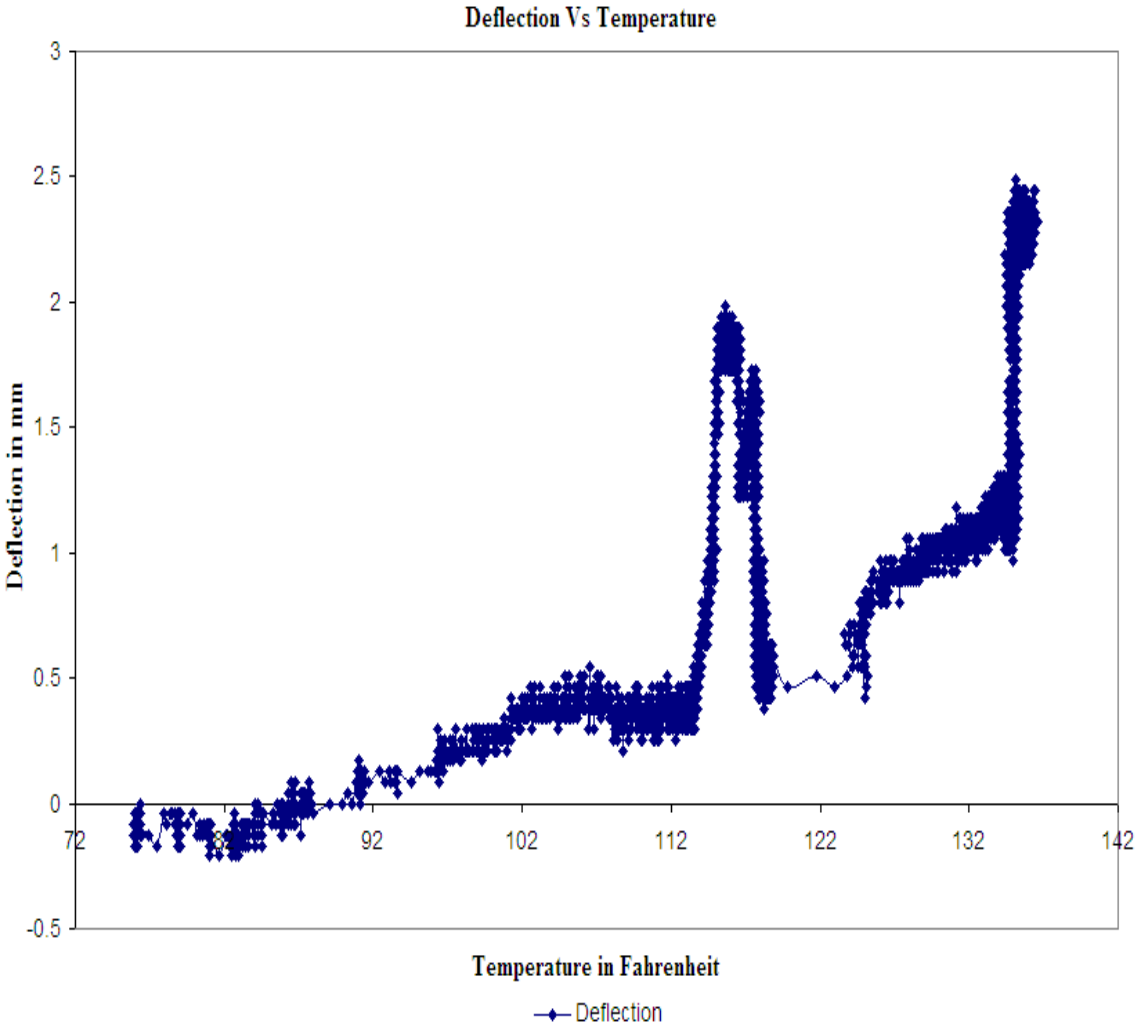

Figure C.38: Deflection Vs Temperature for Test # 6

The above graph shows the variation of deflection over temperature at the top surface for the fiber composite deck specimen # 1 with ribs oriented along longitudinal direction and ends restrained. This specimen was also tested in Test # 1.

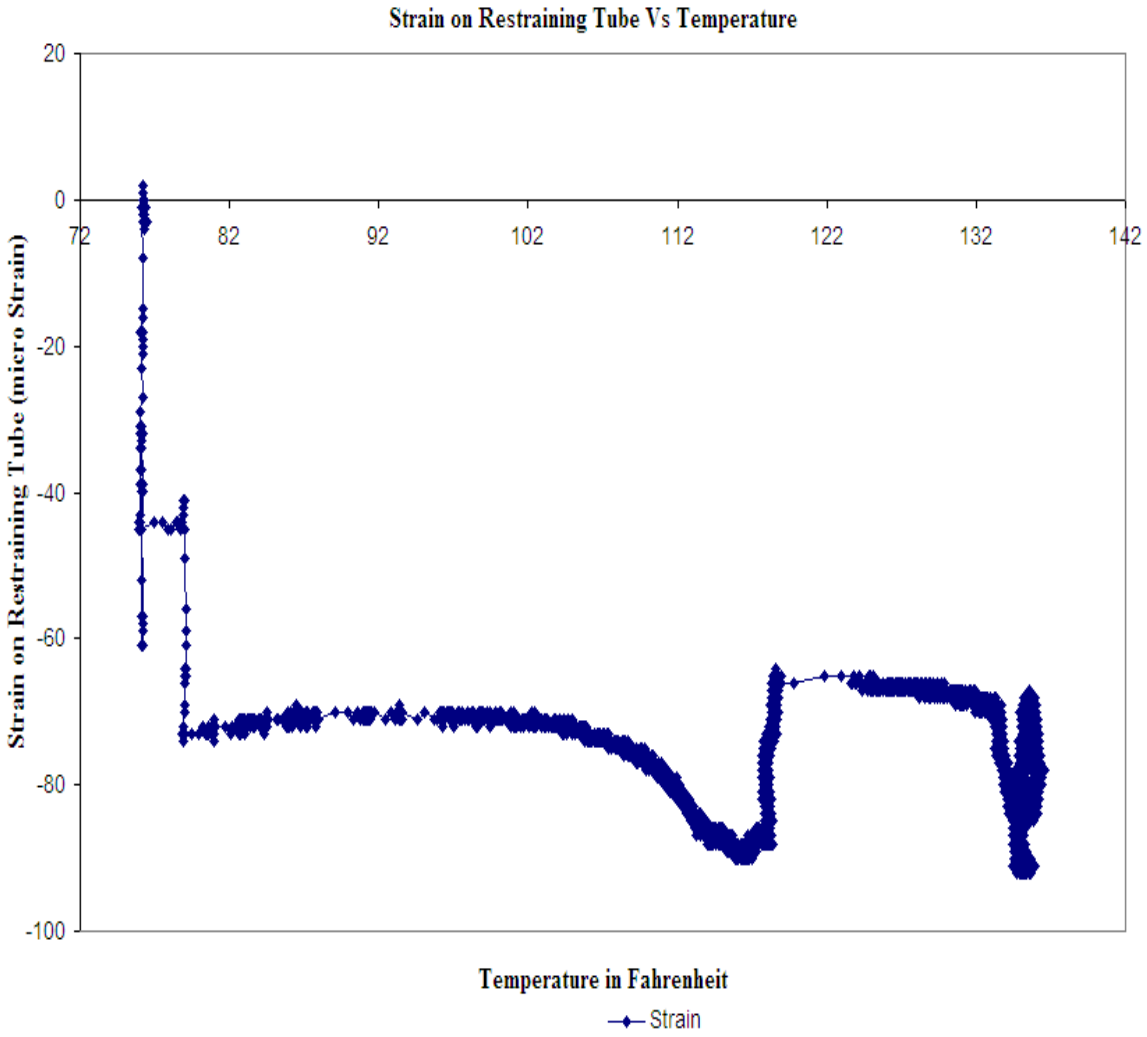

Figure C.39: Strain on Restraining Tube Vs Temperature for Test # 6

The above graph shows the variation of strain on restraining tube over temperature at the top surface for the fiber composite deck specimen # 1 with longitudinal ribs and ends restrained. This specimen was also tested in Test # 1.

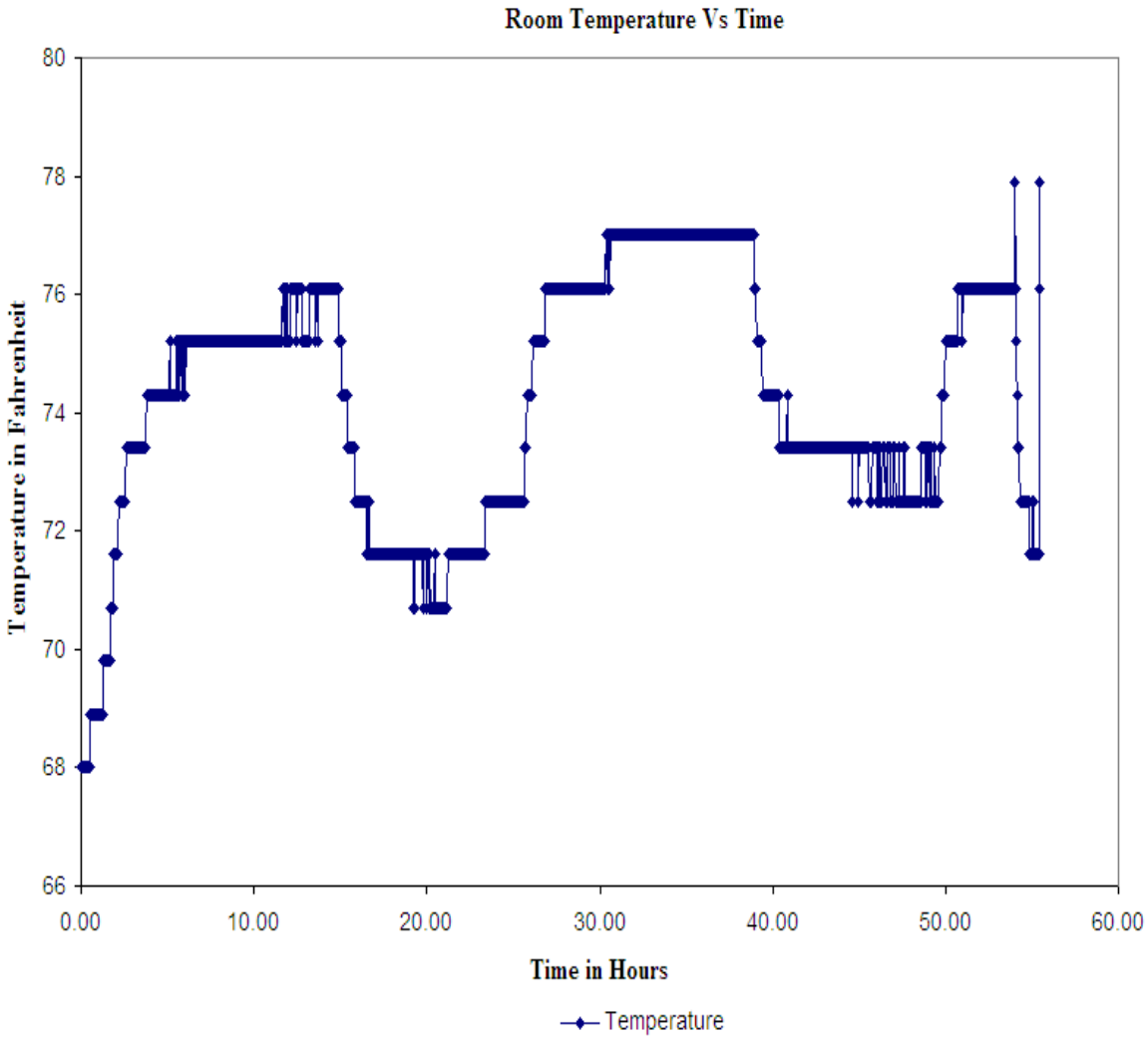

Figure C.40: Room Temperature Vs Time for Test # 6

The above graph shows the variation of temperature next to the experimental setup over time for Test # 6. The little variation of temperature for a short duration is because of the interference of the outside temperature.

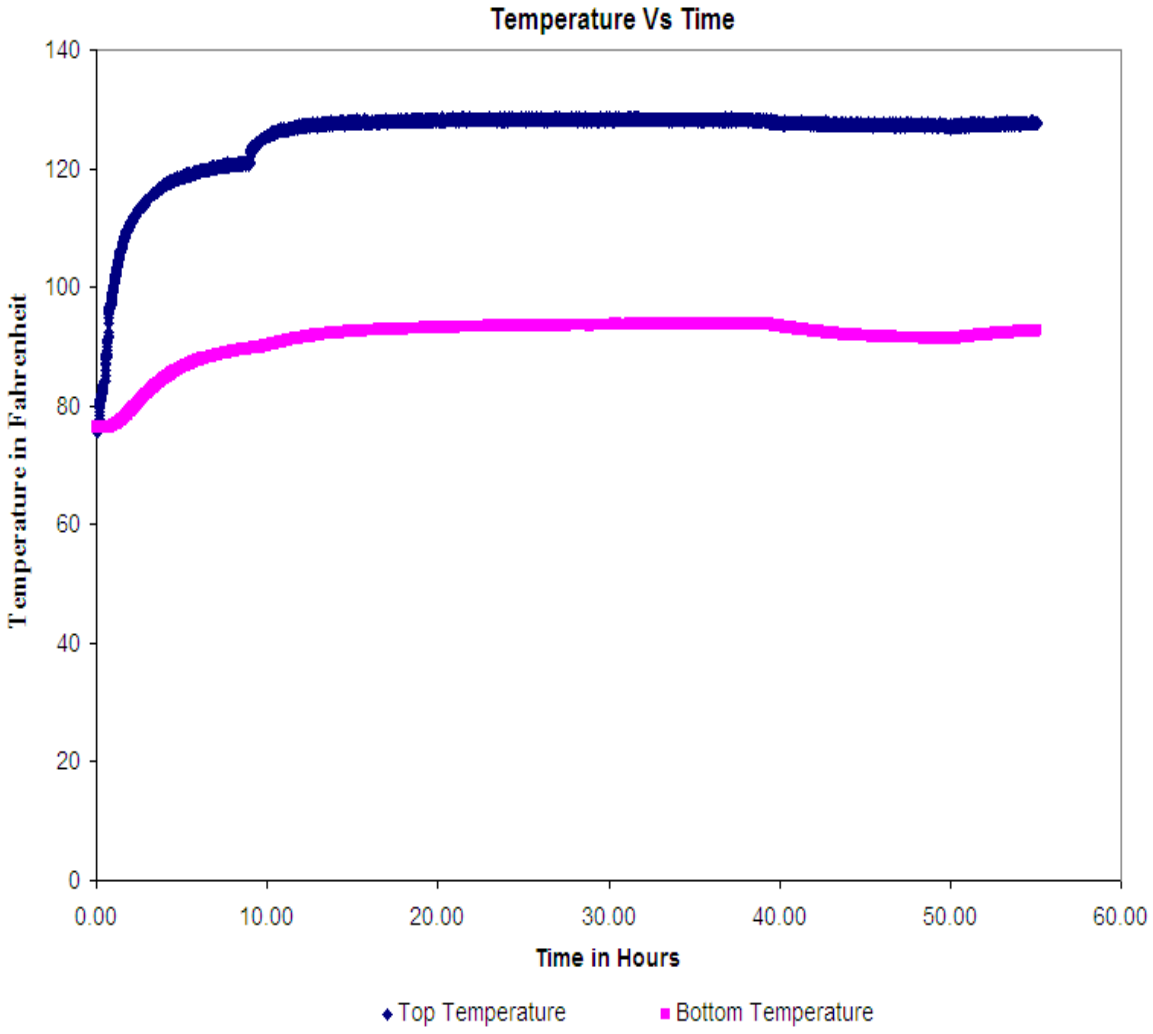

Figure C.41: Temperature Vs Time for Test # 7

The above graph shows the application of heat to the top surface and the measurement of heat at the bottom surface for the fiber composite deck specimen # 6 with transverse ribs and ends restrained.

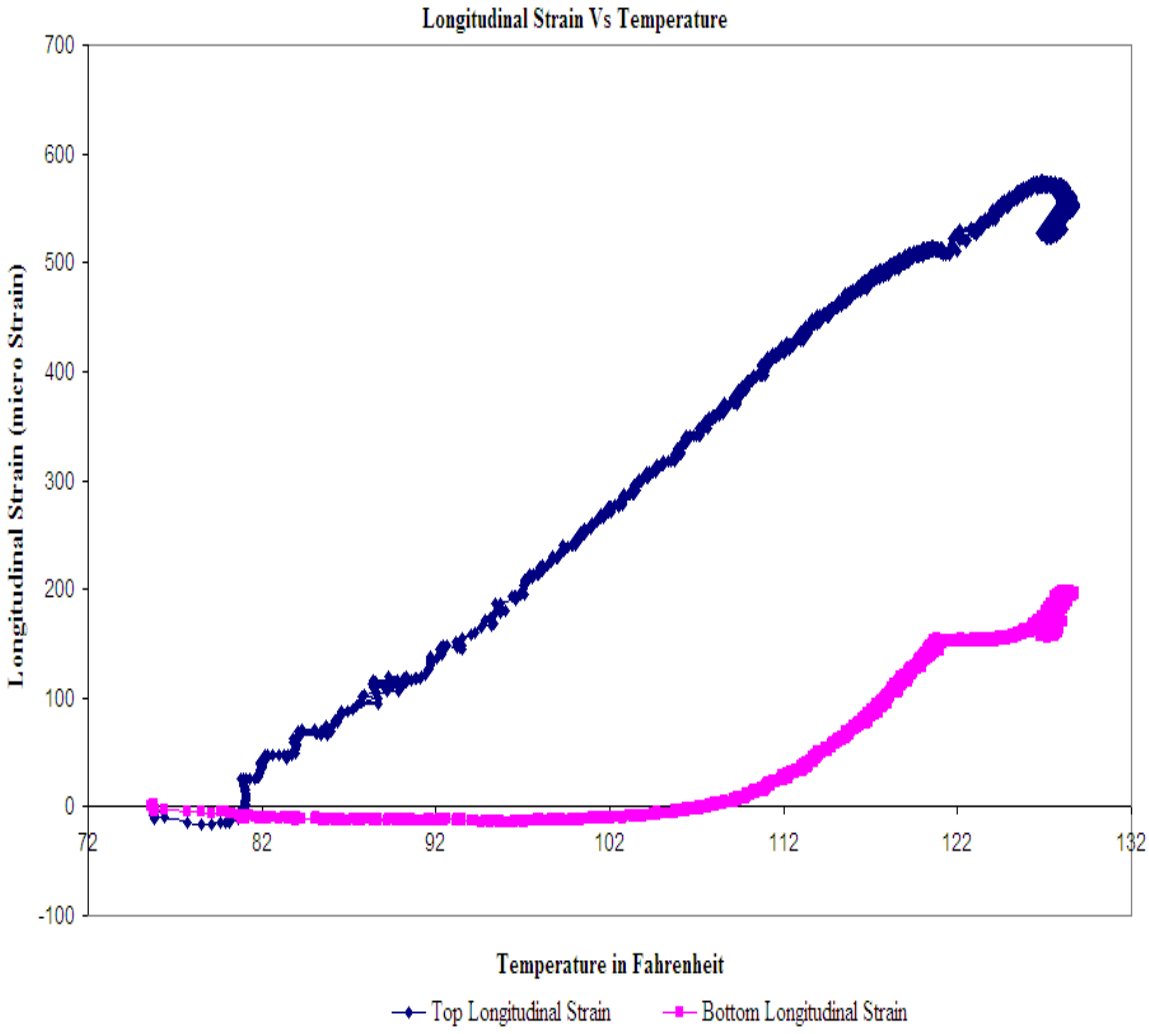

Figure C.42: Longitudinal Strain Vs Temperature for Test # 7

The above graph shows the variation of longitudinal strain at top and bottom surfaces over the temperature at the top surface for the fiber composite deck specimen # 6 with ribs oriented along transverse direction and ends restrained. The negative strain at the bottom surface indicates a compressive strain.

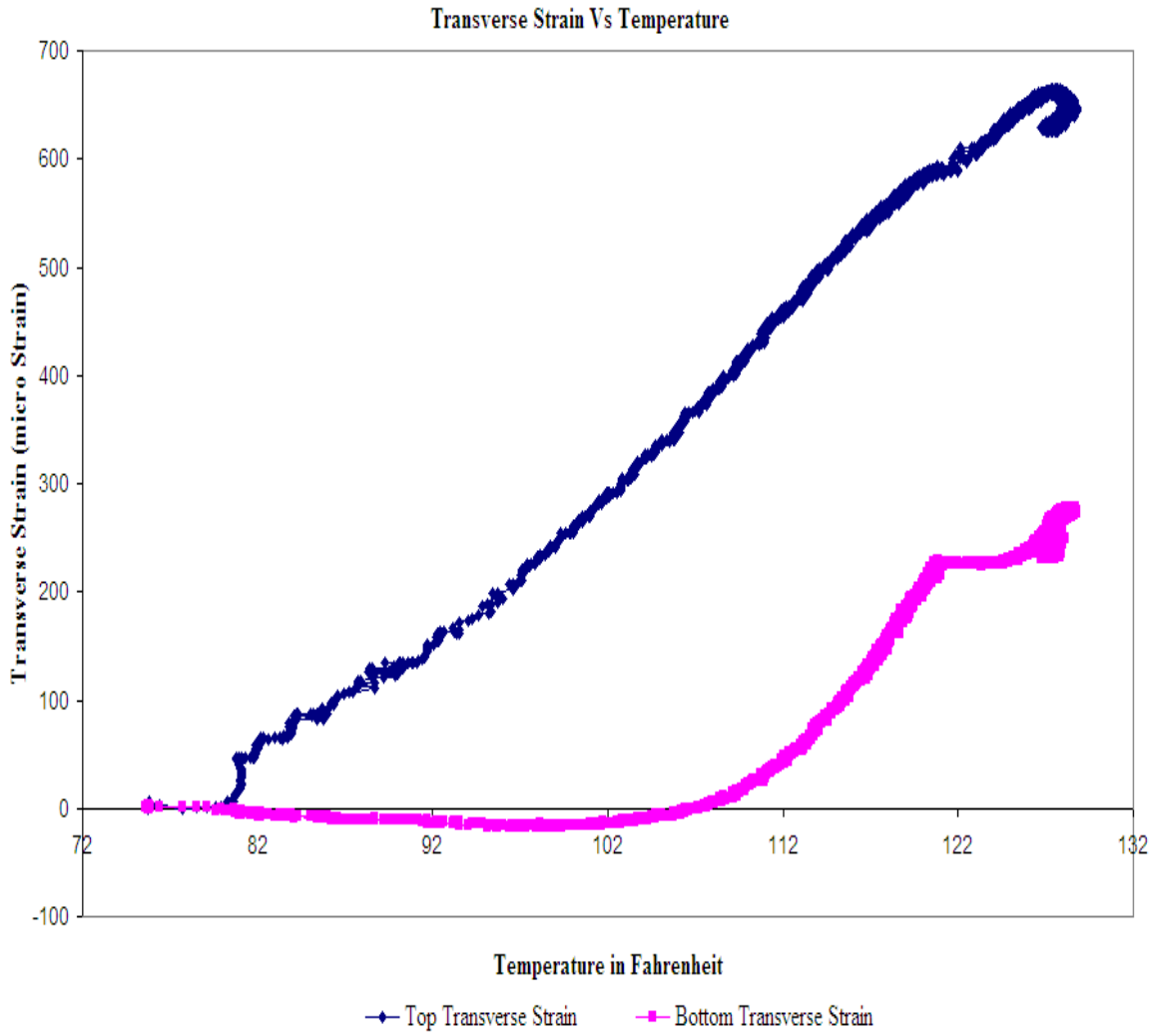

Figure C.43: Transverse Strain Vs Temperature for Test # 7

The above graph shows the variation of transverse strain at top and bottom surfaces over the temperature at the top surface for the fiber composite deck specimen # 6 with ribs oriented along transverse direction and ends restrained. The negative strain at the bottom surface indicates a compressive strain.

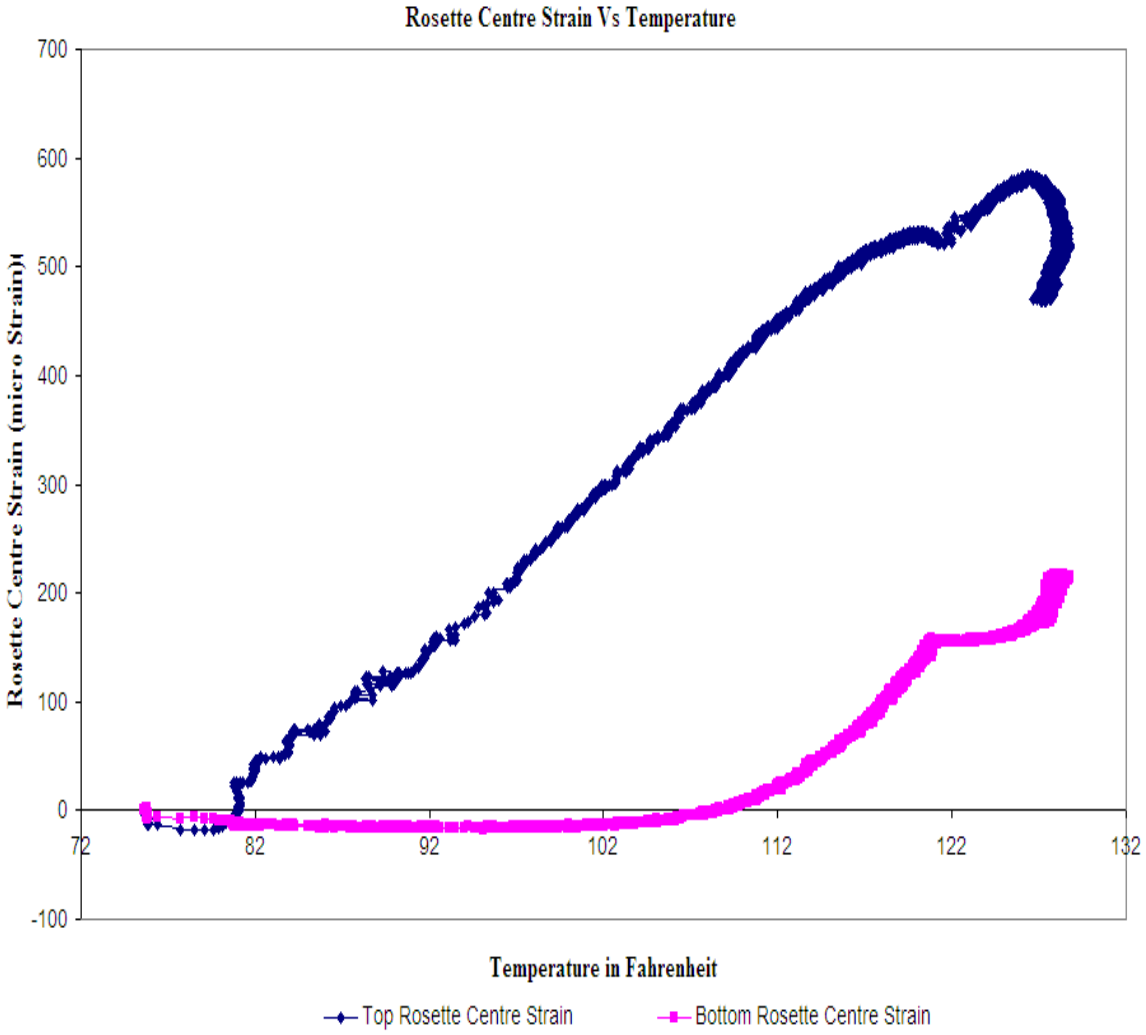

Figure C.44: Rosette Centre Strain Vs Temperature for Test # 7

The above graph shows the variation of rosette centre strain at top and bottom surfaces over the temperature at the top surface for the fiber composite deck specimen # 6 with ribs oriented along transverse direction and ends restrained. The negative strain at the bottom surface indicates a compressive strain.

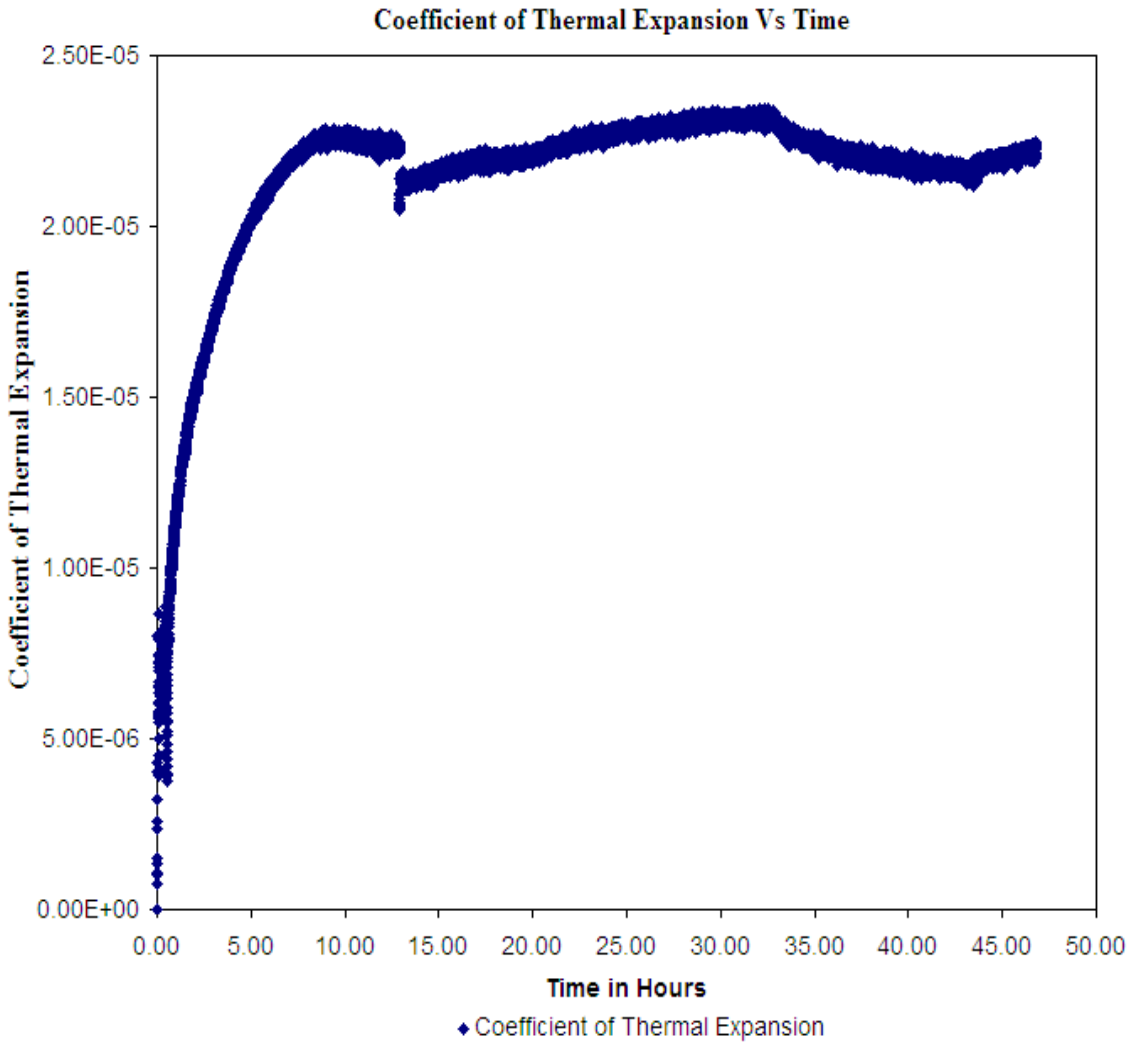

Figure C.45: Coefficient of Thermal Expansion Vs Time for Test # 7

The above graph shows the variation of coefficient of thermal expansion over temperature at top surface for the fiber composite deck specimen # 6 with ribs oriented along transverse direction and ends restrained.

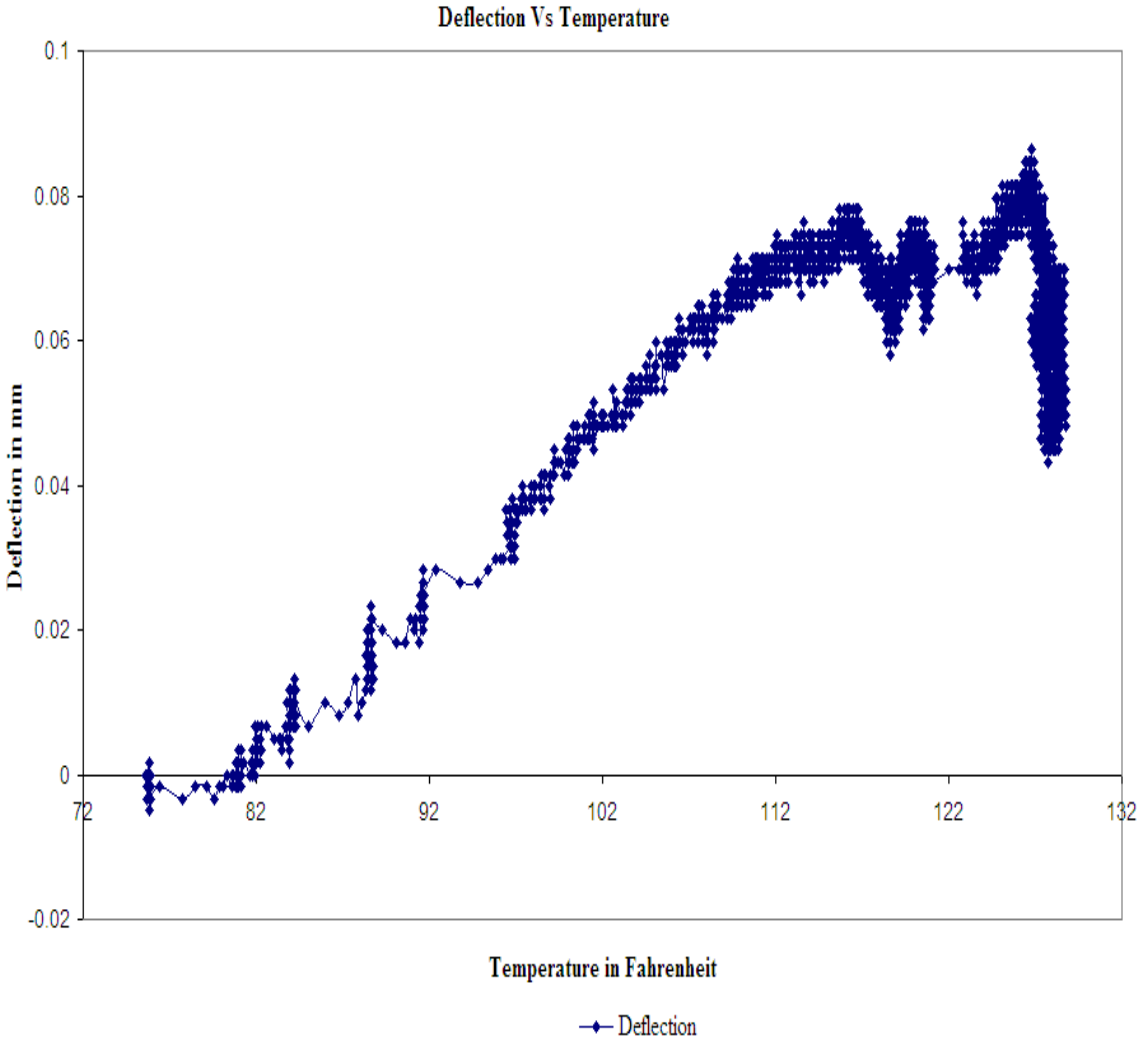

Figure C.46: Deflection Vs Time for Test # 7

The above graph shows the variation of deflection over temperature at the top surface for the fiber composite deck specimen # 6 with ribs oriented along transverse direction and ends restrained.

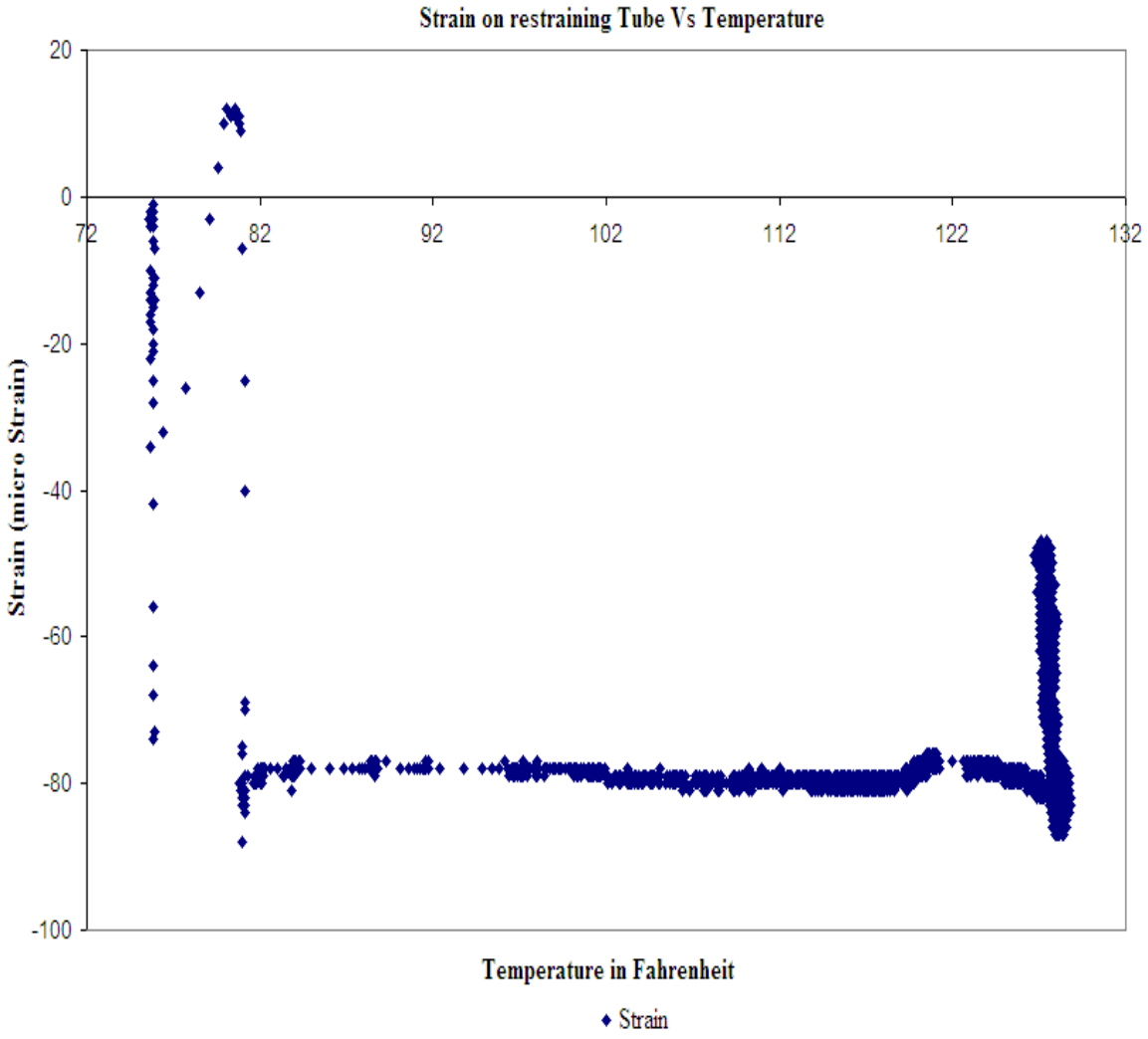

Figure C.47: Strain on Restraining Tube Vs Temperature for Test # 7

The above graph shows the variation of strain on restraining tube over temperature at the top surface for the fiber composite deck specimen # 6 with ribs oriented along transverse direction and ends restrained.

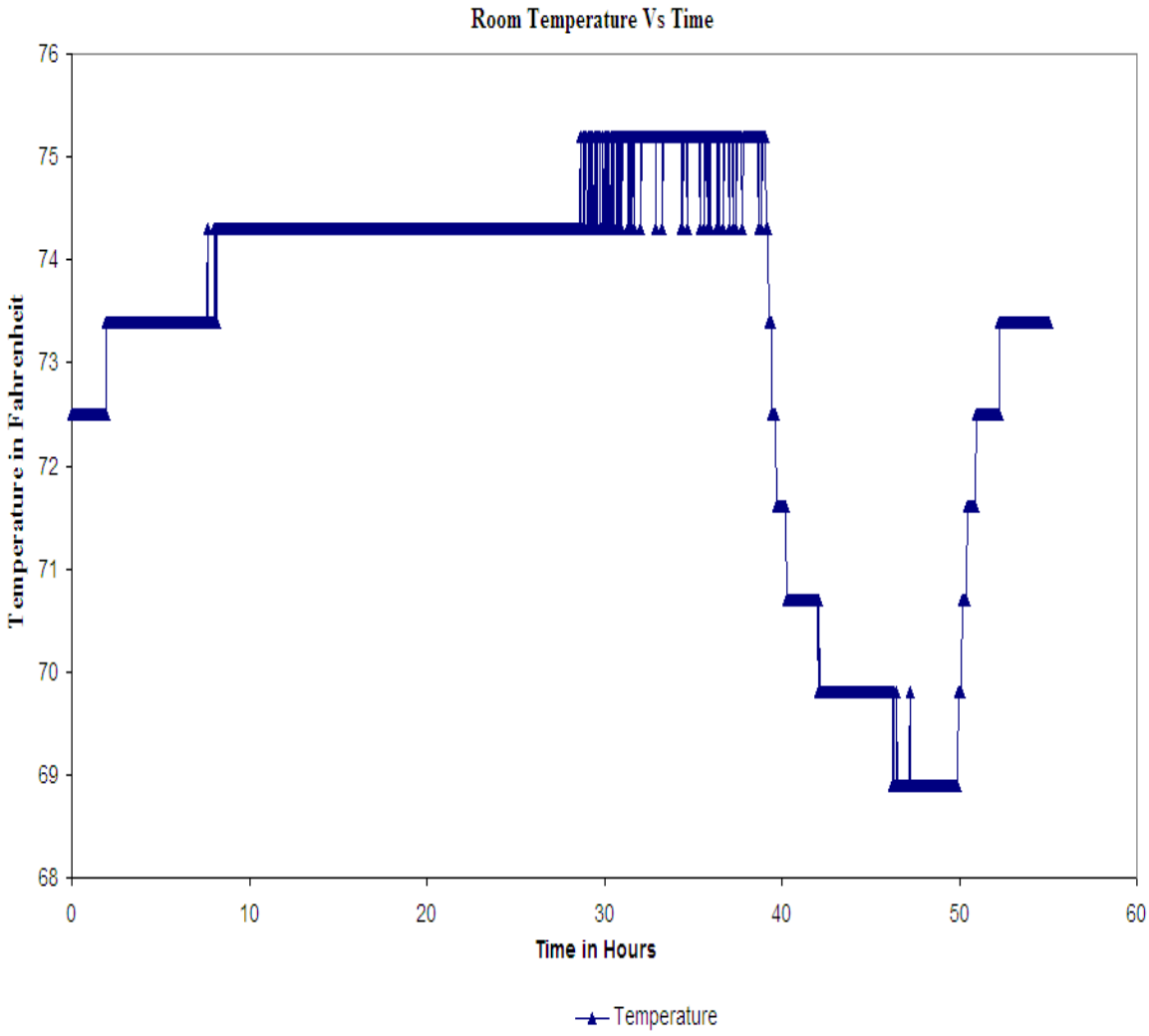

Figure C.48: Room Temperature Vs Time for Test # 7

The above graph shows the variation of temperature next to the experimental setup over time for Test # 7.

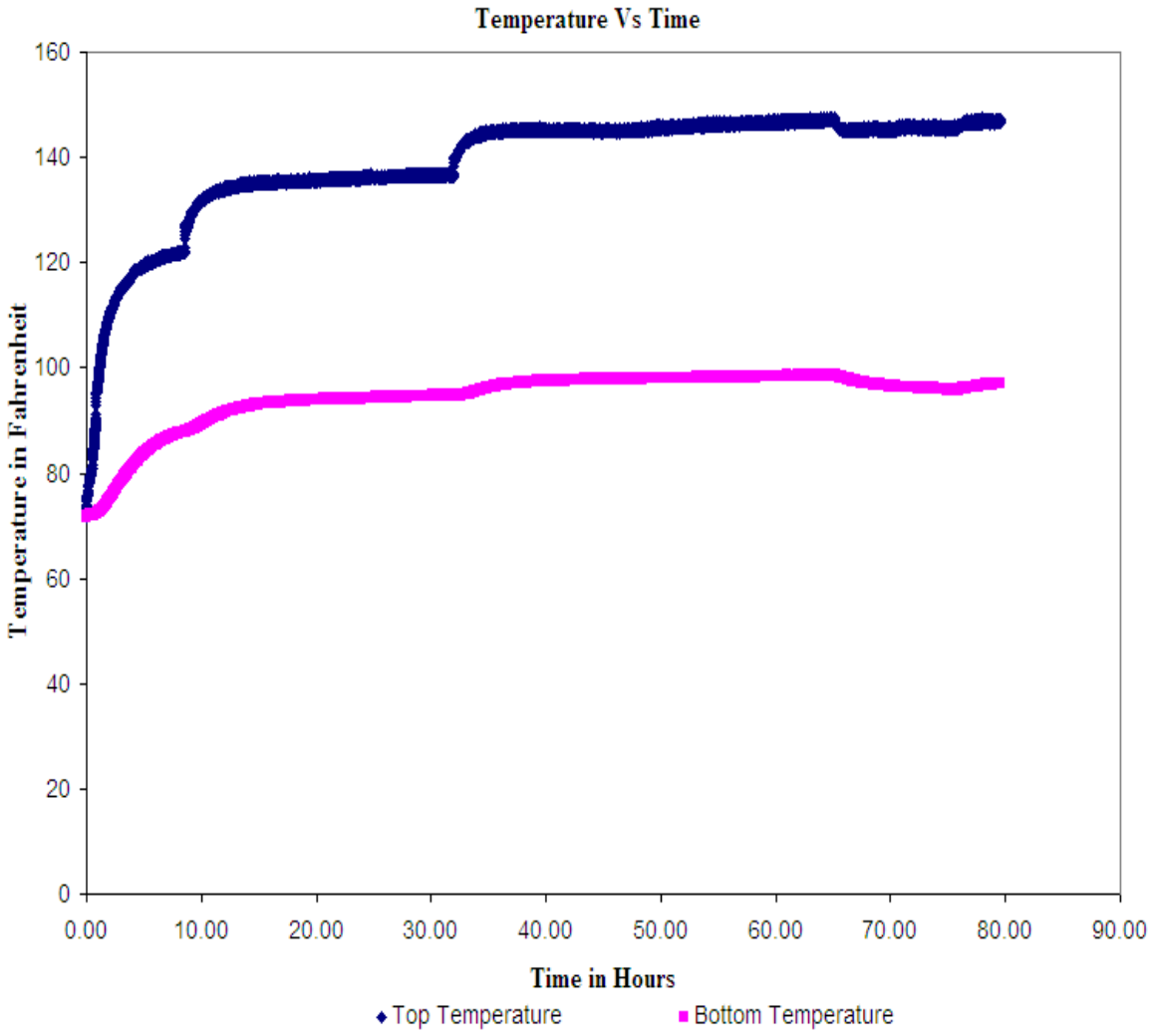

Figure C.49: Temperature Vs Time for Test # 8

The above graph shows the application of heat to the top surface and the measurement of heat at the bottom surface for fiber composite deck specimen # 3 with transverse ribs and ends restrained. This specimen was also tested in Test # 3 for unrestrained condition.

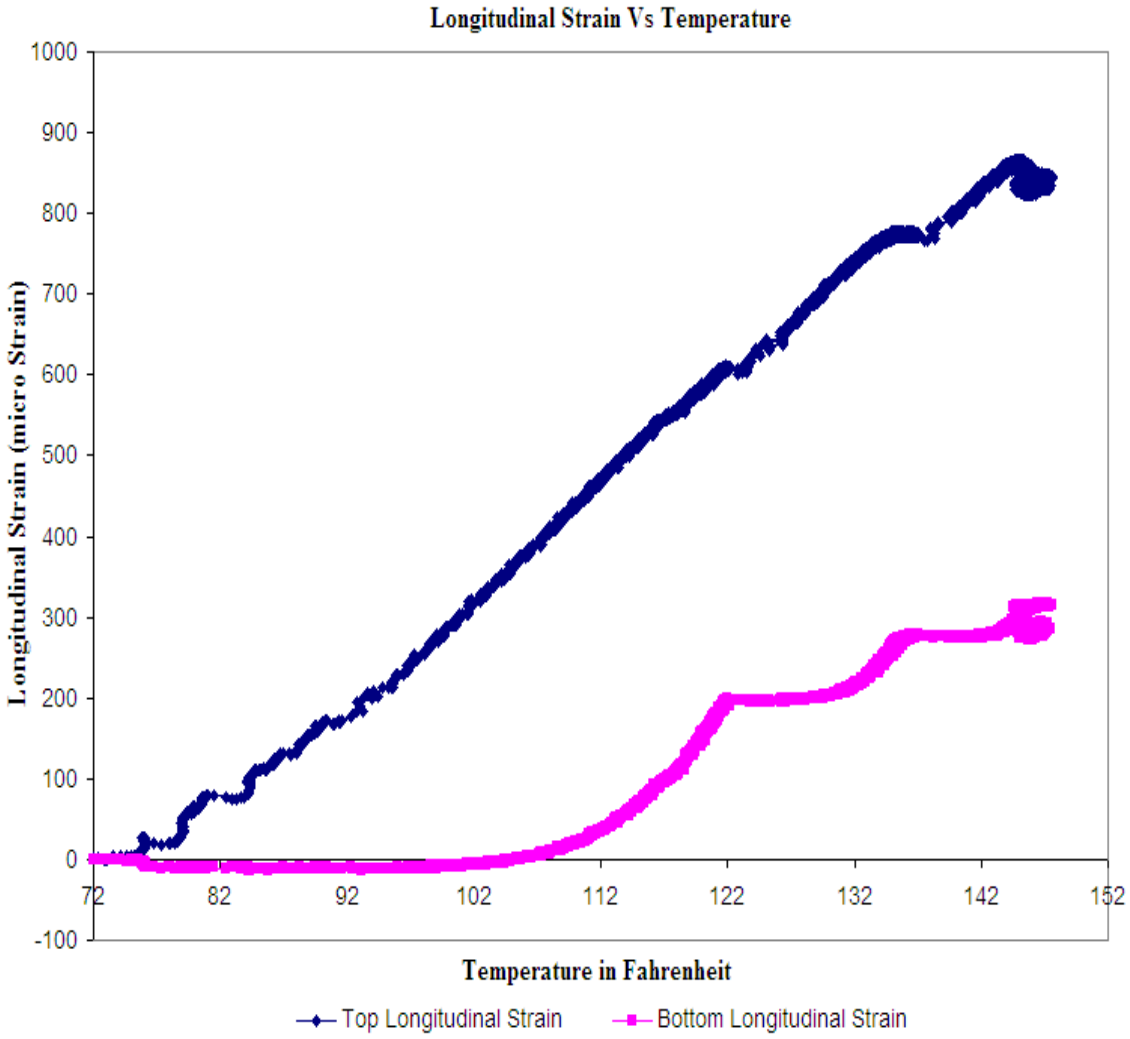

Figure C.50: Longitudinal Strain Vs Temperature for Test # 8

The above graph shows the variation of longitudinal strain at top and bottom surfaces over temperature at the top surface for the fiber composite deck with ribs oriented along transverse direction and ends restrained. The negative strain at the bottom surface indicates a compressive strain. This specimen was also tested in Test # 3 for unrestrained condition.

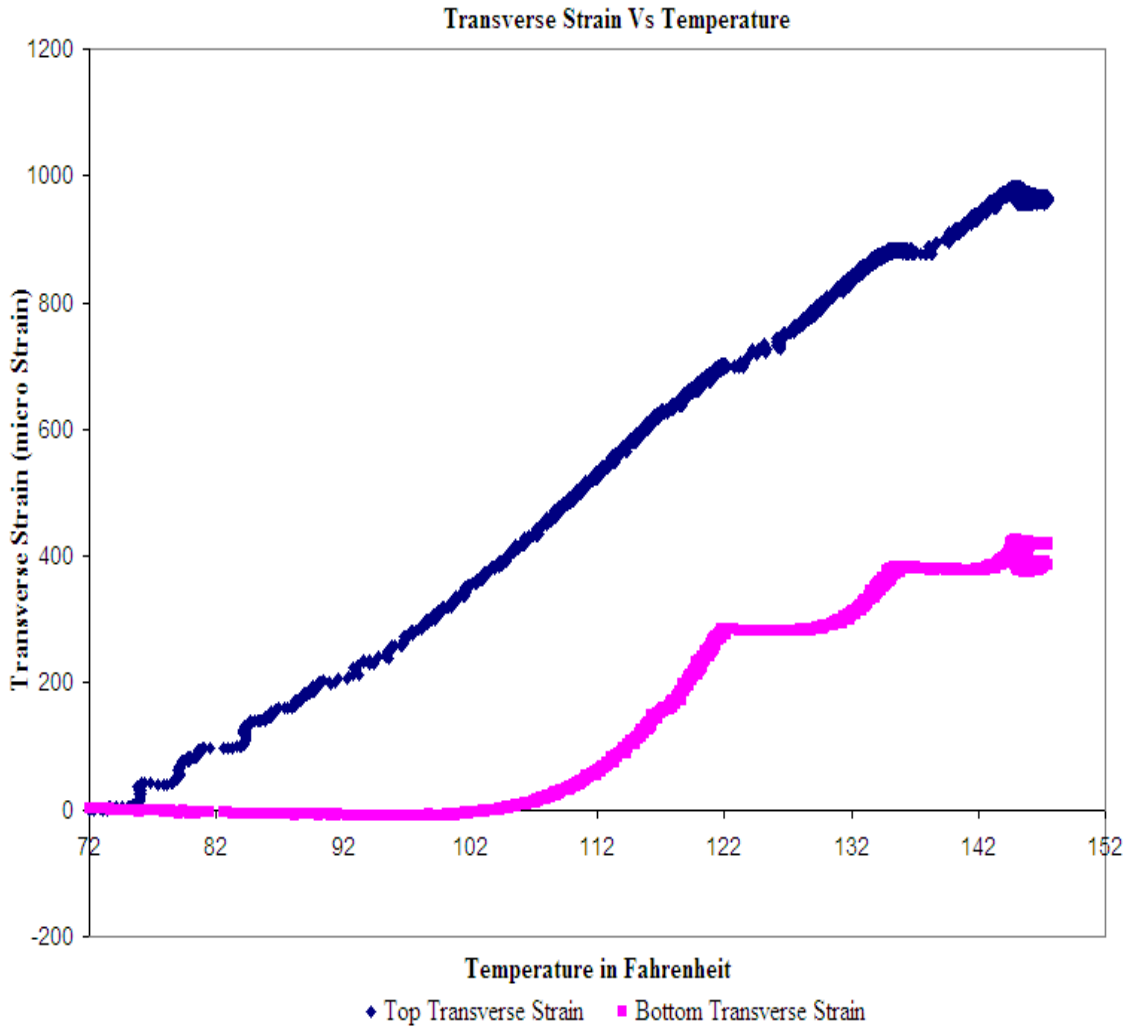

Figure C.51: Transverse Strain Vs Temperature for Test # 8

The above graph shows the variation of transverse strain at top and bottom surfaces over temperature at the top surface for the fiber composite deck specimen # 3 with ribs oriented along transverse direction and ends restrained. The negative strain at the bottom surface indicates a compressive strain. This specimen was also tested in Test # 3 for unrestrained condition.

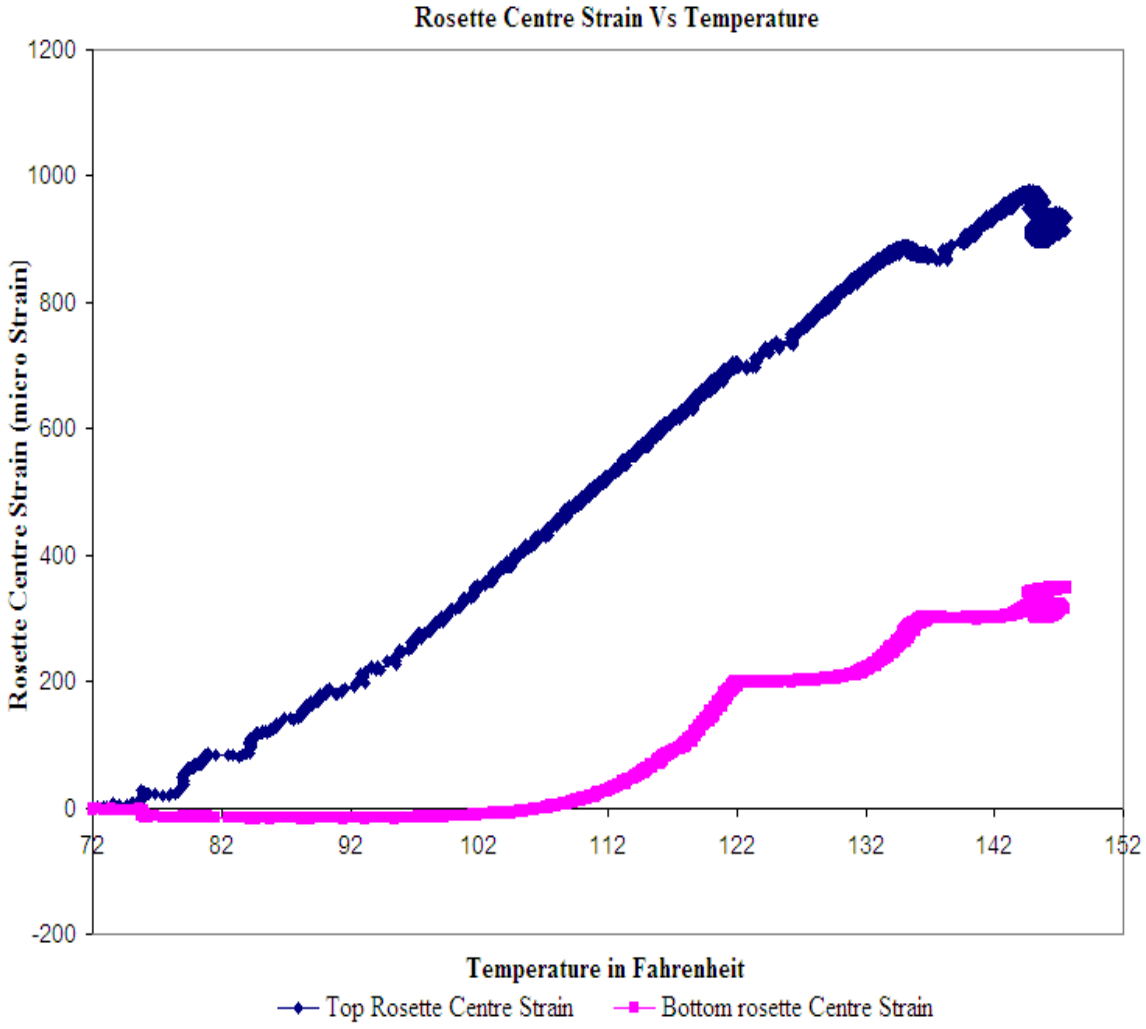

Figure C.52: Rosette Centre Strain Vs Temperature for Test # 8

The above graph shows the variation of rosette centre strain at top and bottom surfaces over temperature at the top surface for the fiber composite deck specimen # 6 with ribs oriented along transverse direction and ends restrained. The negative strain at the bottom surface indicates a compressive strain. This specimen was also tested in Test # 3 for unrestrained condition.

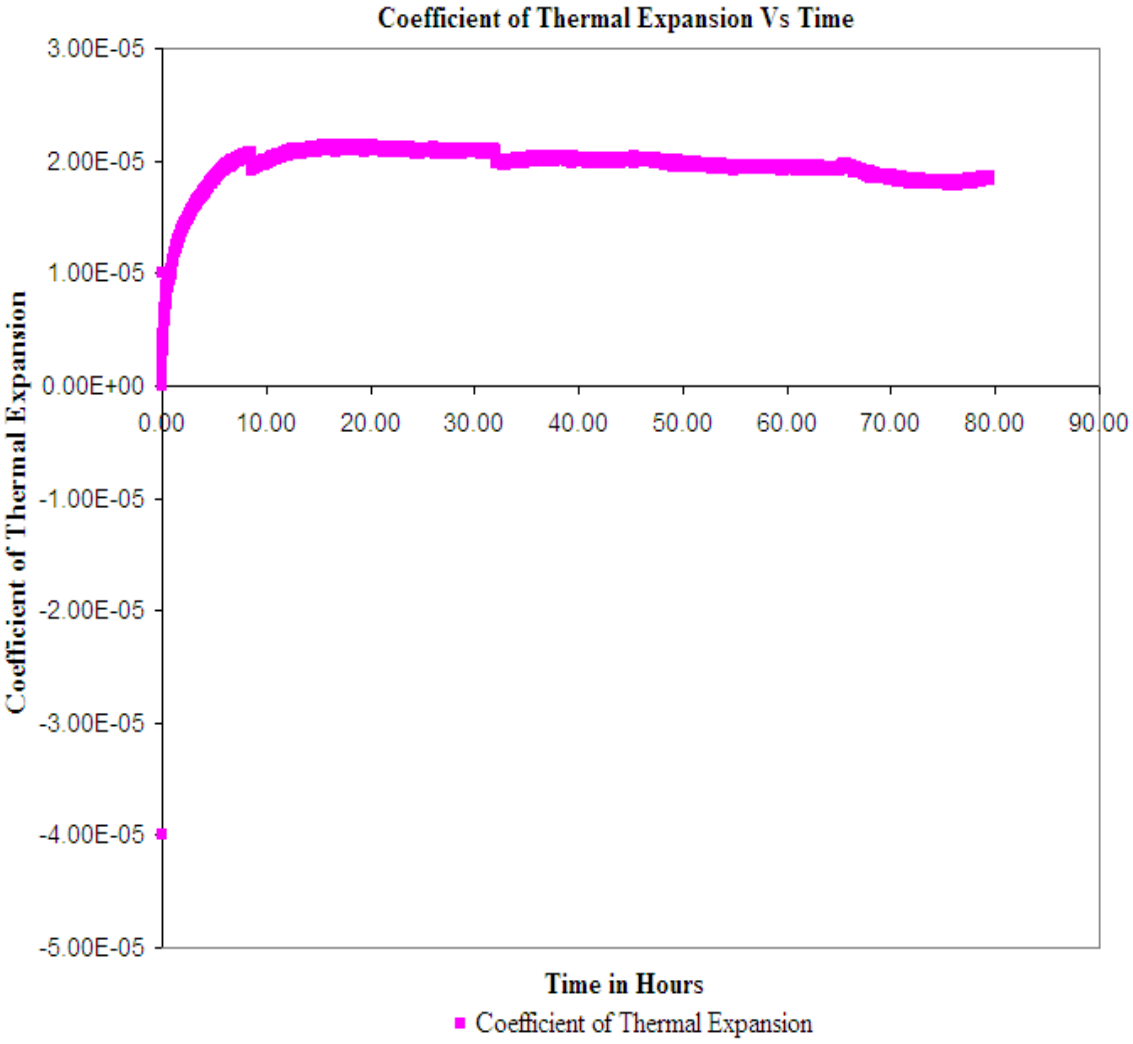

Figure C.53: Coefficient of Thermal expansion Vs Time for Test # 8

The above graph shows the variation of coefficient of thermal expansion over time for the fiber composite deck specimen # 3 with ribs oriented along transverse direction and ends restrained. This specimen was also tested in Test # 3 for unrestrained condition.

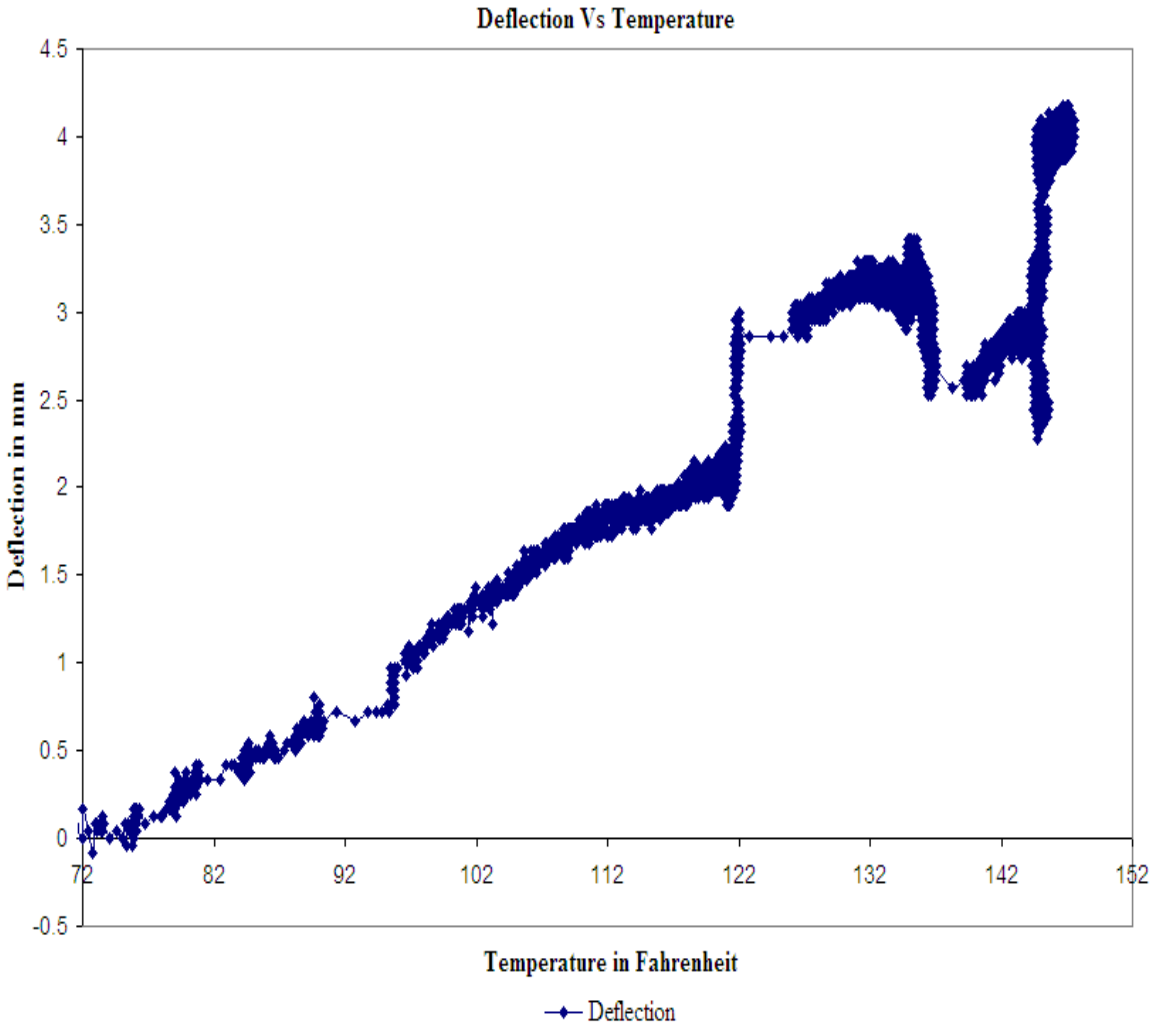

Figure C.54: Deflection Vs Temperature for Test # 8

The above graph shows the variation of deflection over temperature at the top surface for the fiber composite deck specimen # 3 with ribs oriented along transverse direction and ends restrained. This specimen was also tested in Test # 3 for unrestrained condition.

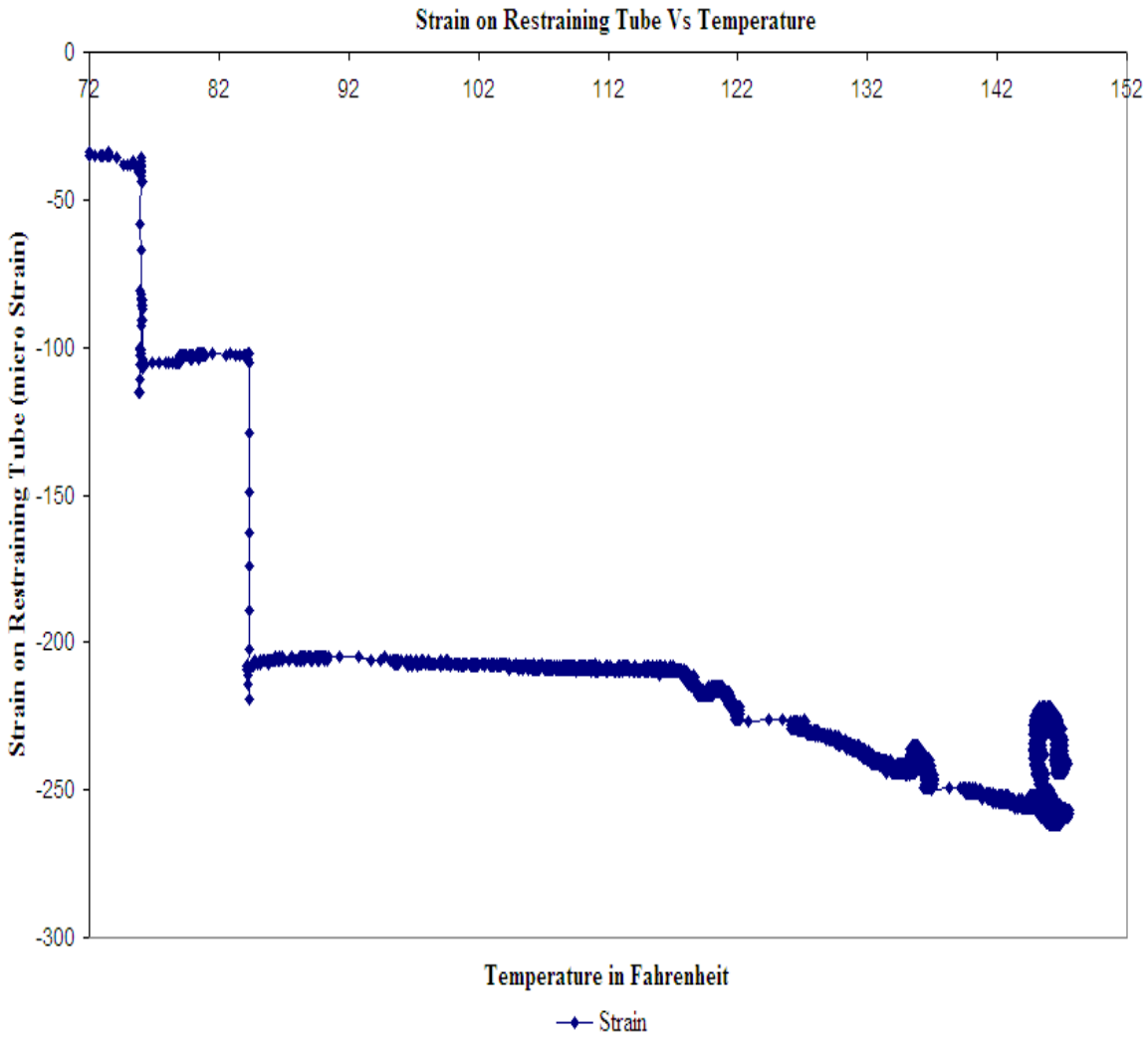

Figure: C.55: Strain on Restraining Tube Vs Temperature for Test # 8

The above graph shows the variation of strain on restraining tube over temperature at the top surface for the fiber composite deck specimen # 3 with ribs oriented along transverse direction and ends restrained. This specimen was also tested in Test # 3 for unrestrained condition.

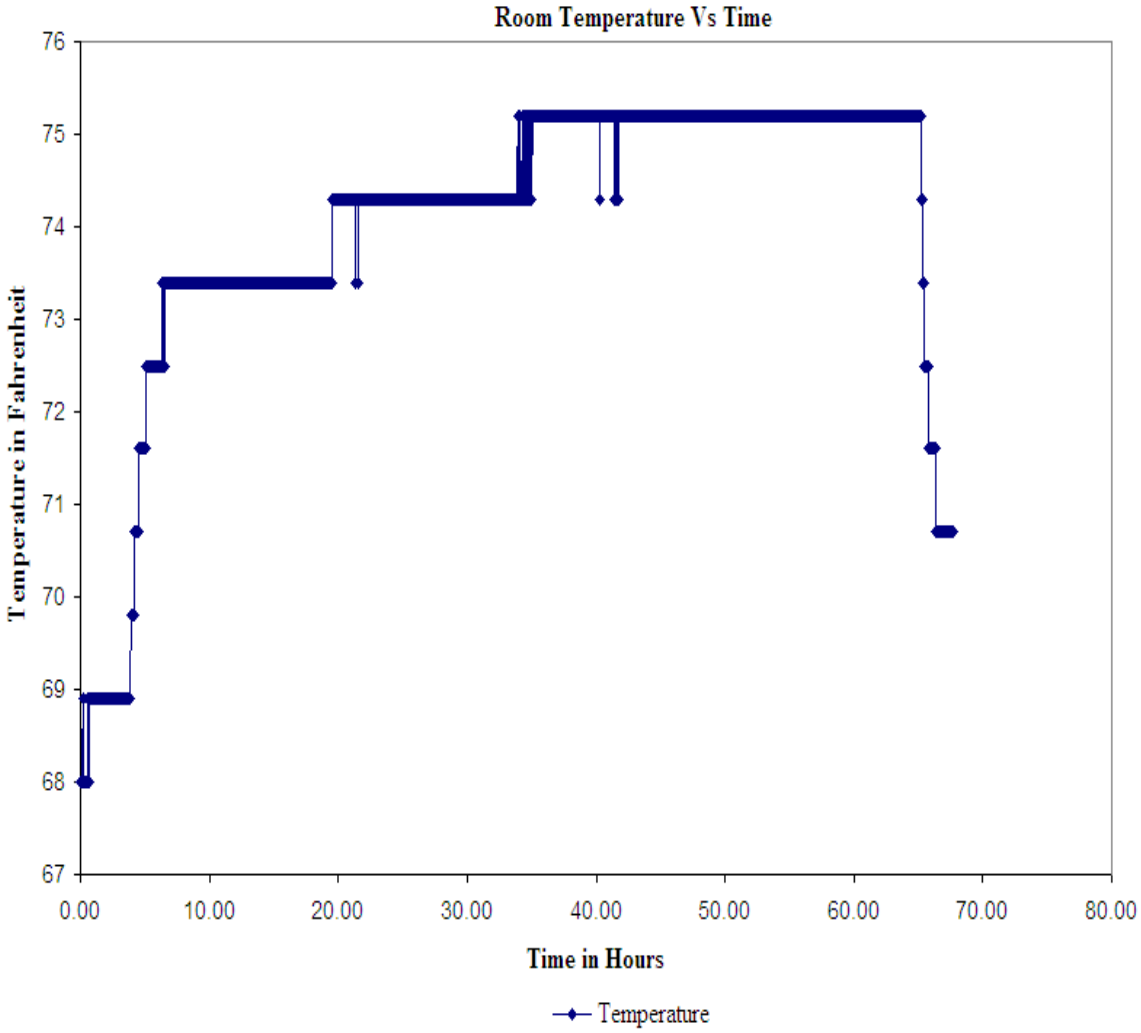

Figure: C.56: Room Temperature Vs Time for Test # 8

The above graph shows the variation of temperature next to the experimental setup over time for Test # 8.

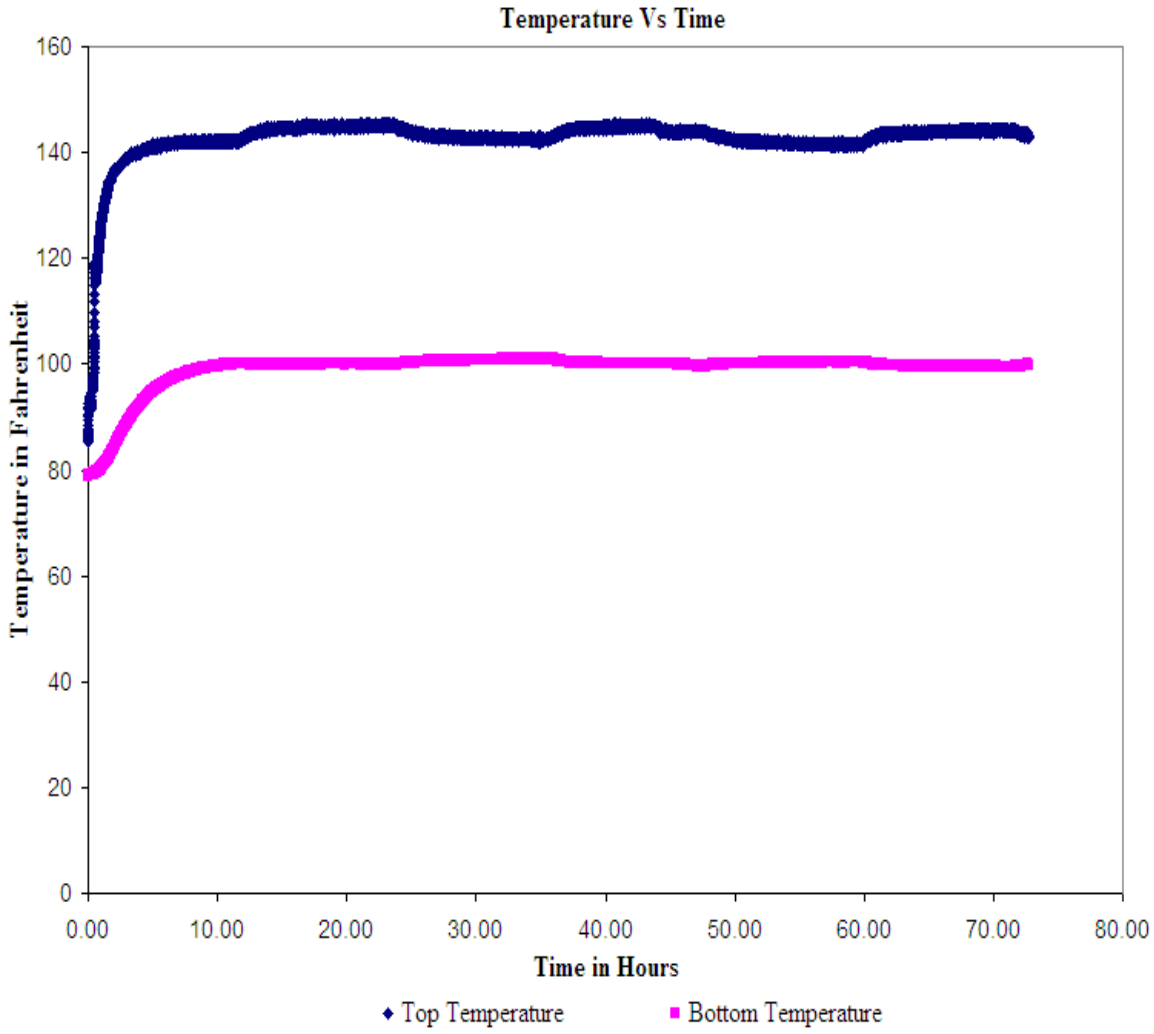

Figure C.57: Temperature Vs Time for Test # 9

The above graph shows the application of heat to the top surface and the measurement of heat at the bottom surface for fiber composite deck specimen # 1 with longitudinal ribs and ends unrestrained.

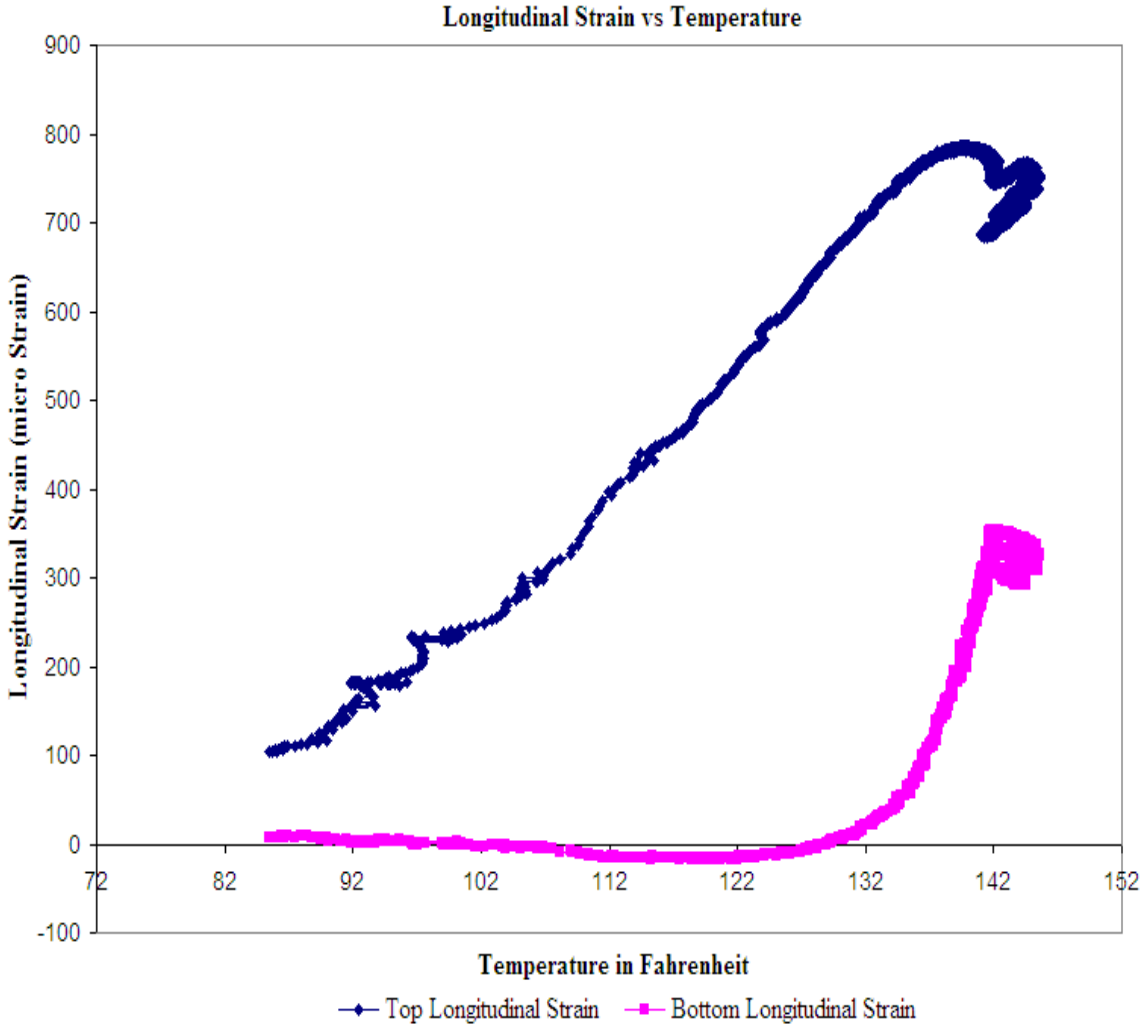

Figure C.58: Longitudinal Strain Vs Temperature for Test # 9

The above graph shows the variation of longitudinal strain at top and bottom surfaces over the temperature for the fiber composite deck specimen # 7 with ribs oriented along transverse direction and ends unrestrained. The negative strain at the bottom surface indicates a compressive strain.

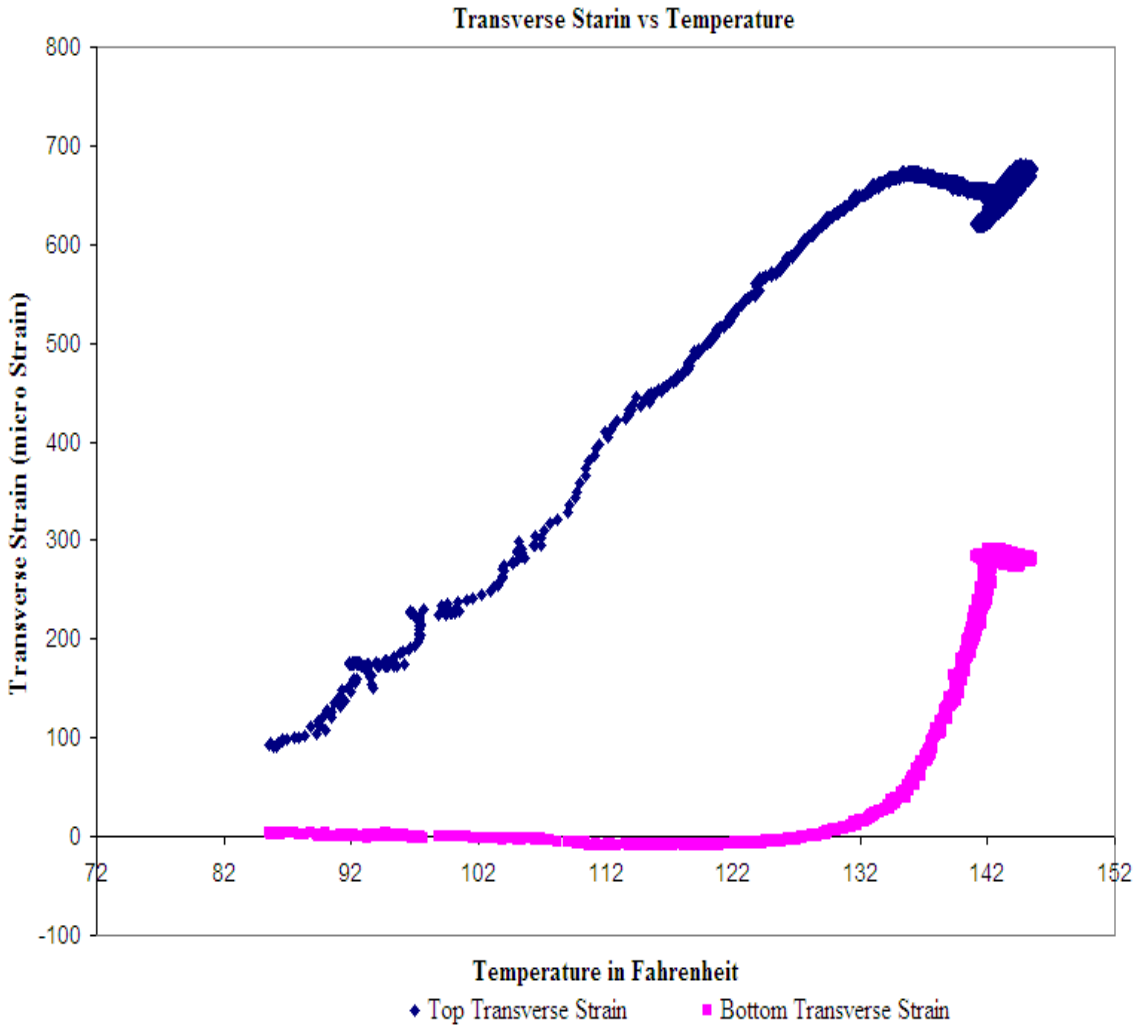

Figure C.59: Transverse Strain Vs Temperature for Test # 9

The above graph shows the variation of transverse strain at top and bottom surfaces over temperature at the top surface for the fiber composite deck specimen # 7 with ribs oriented along transverse direction and ends unrestrained. The negative strain at the bottom surface indicates a compressive strain.

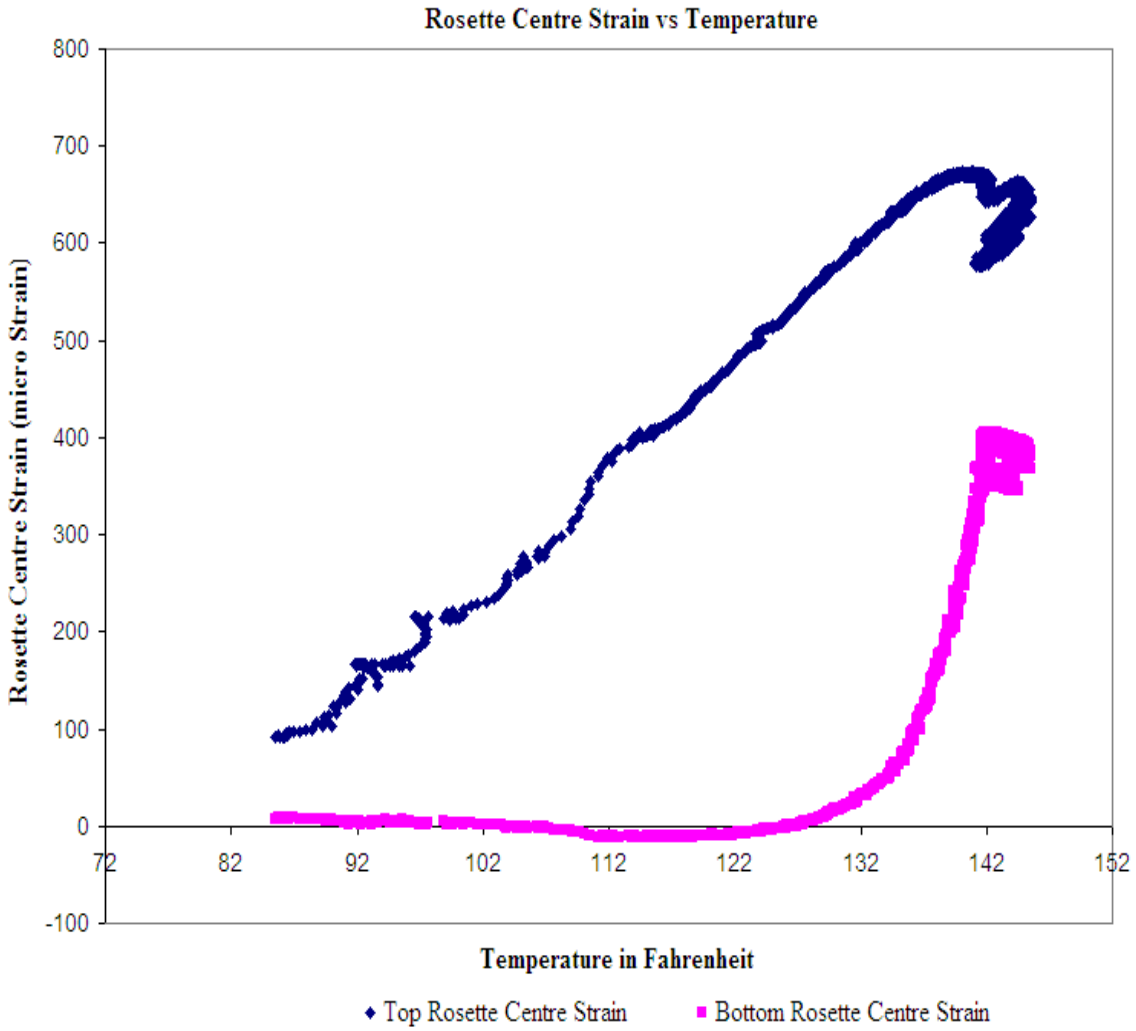

Figure C.60: Rosette Centre Strain Vs Temperature for Test # 9

The above graph shows the variation of rosette centre strain at top and bottom surfaces over temperature at the top surface for the fiber composite deck specimen # 7 with ribs oriented along transverse direction and ends unrestrained. The negative strain at the bottom surface indicates a compressive strain.

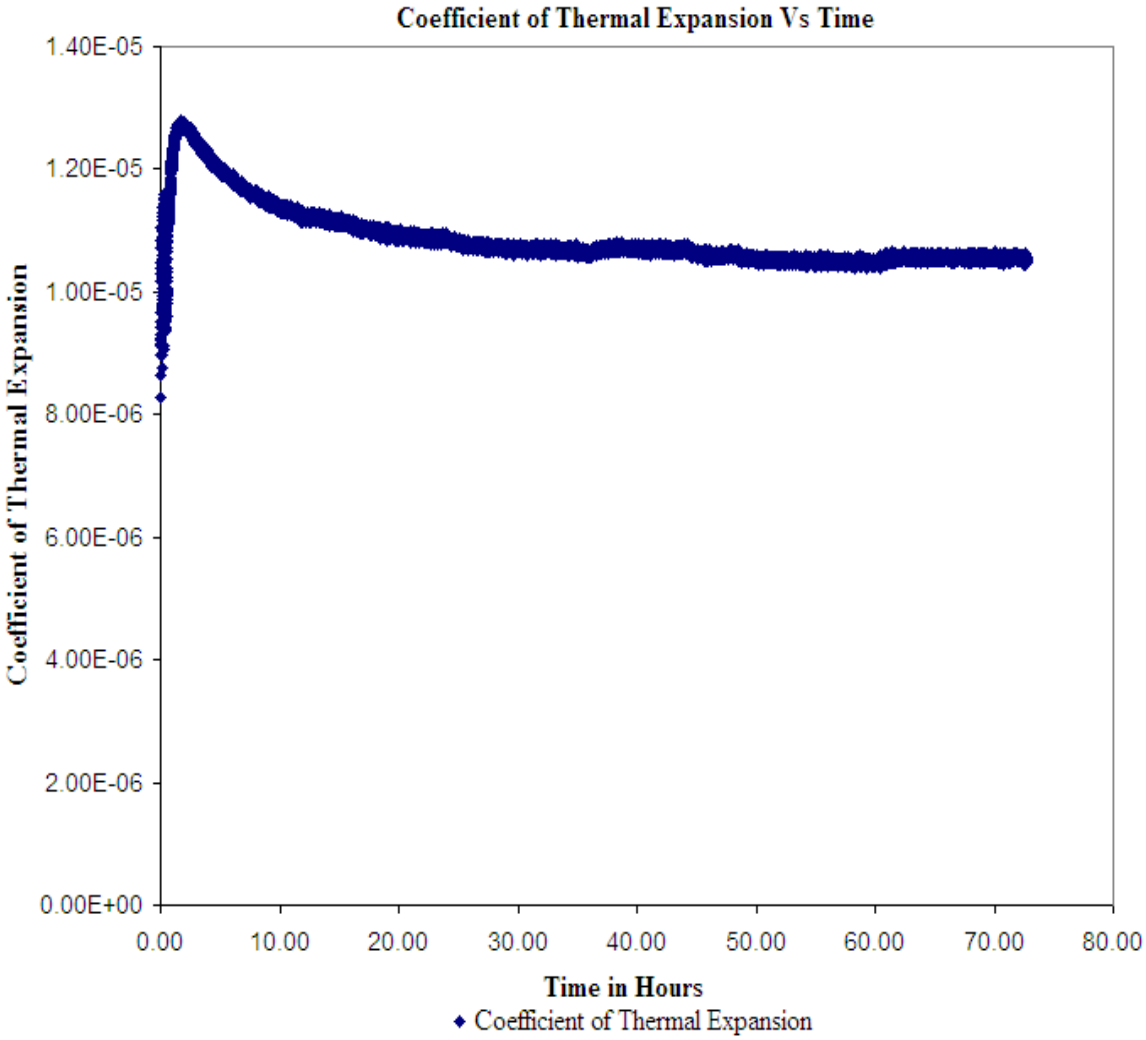

Figure C.61: Coefficient of Thermal Expansion Vs Time for Test # 9

The above graph shows the variation of coefficient of thermal expansion over time for the fiber composite deck specimen # 7 with ribs oriented along transverse direction and ends unrestrained.

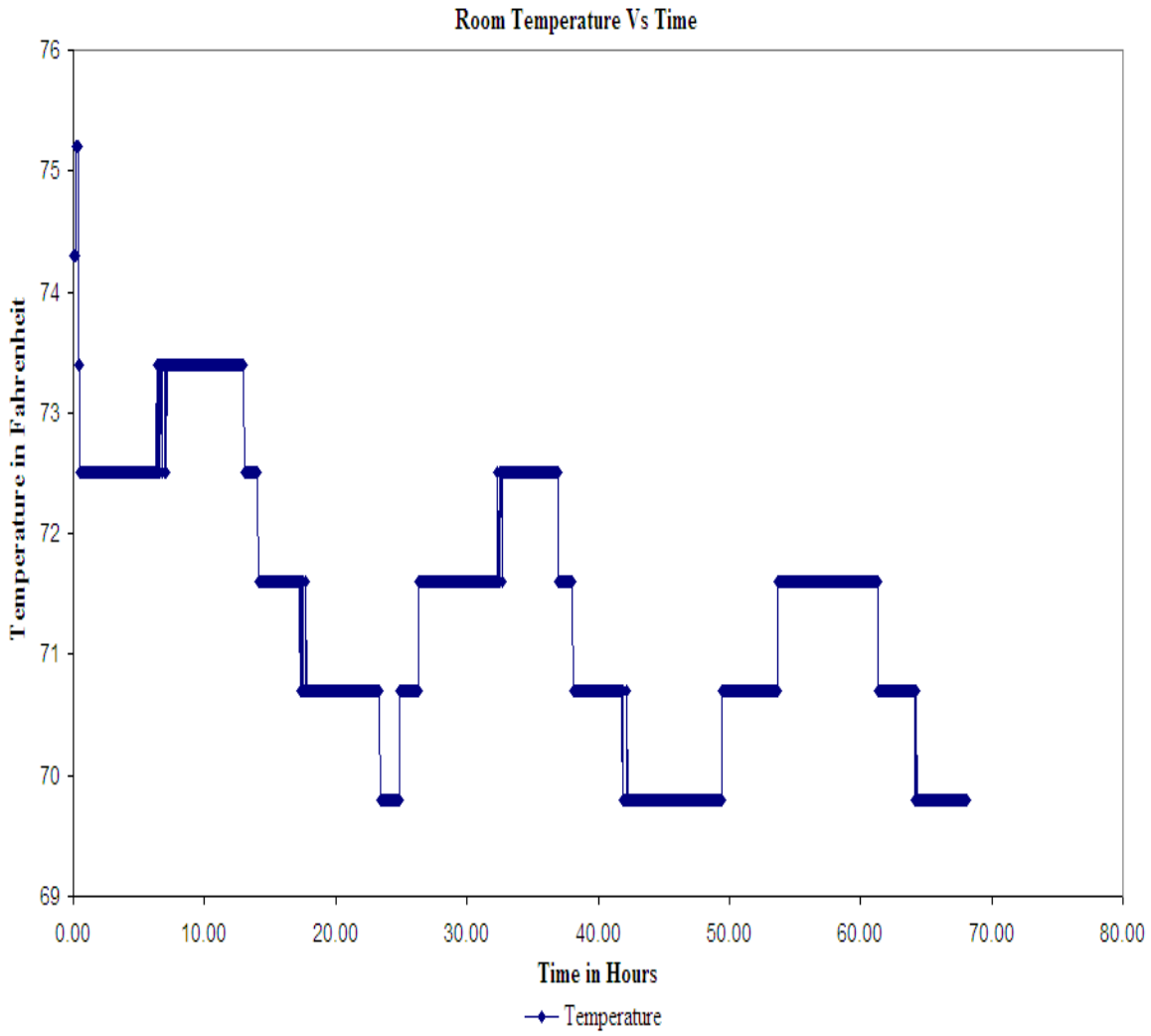

Figure: C.62: Room Temperature Vs Time for Test # 9

The above graph shows the variation of temperature next to the experimental setup over time for Test # 9. The little variation of temperature for a short duration is because of the interference of the outside temperature.

Coupon #1

Geometry:

Width: .5010 in

Thickness: .4505 in

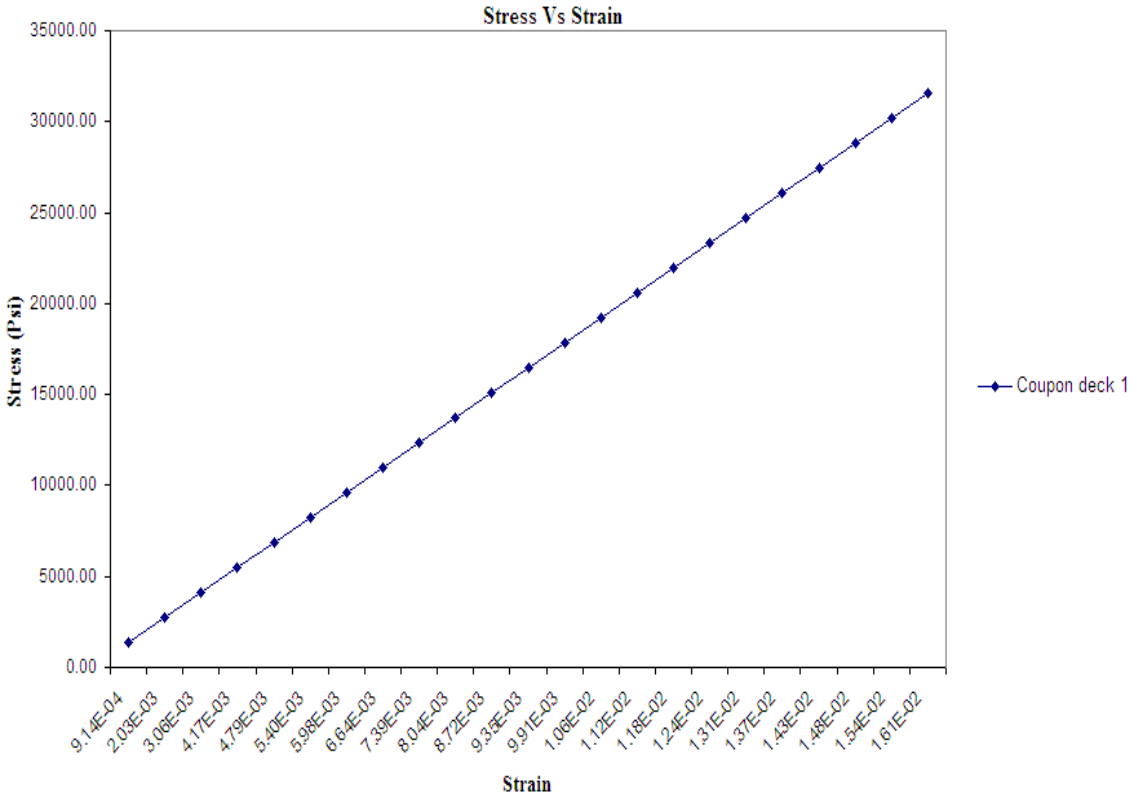

Figure C.63: Stress Vs Strain for Fiber Deck Coupon 1

Modulus of Elasticity of a material is given by

$$E = \frac{\text{Stress}}{\text{Strain}}$$

The calculated modulus of elasticity from the graph for fiber deck coupon 1 is

E = 2.28 E+06 Psi

Coupon #2

Geometry:

Width: .5060 in

Thickness: .4550 in

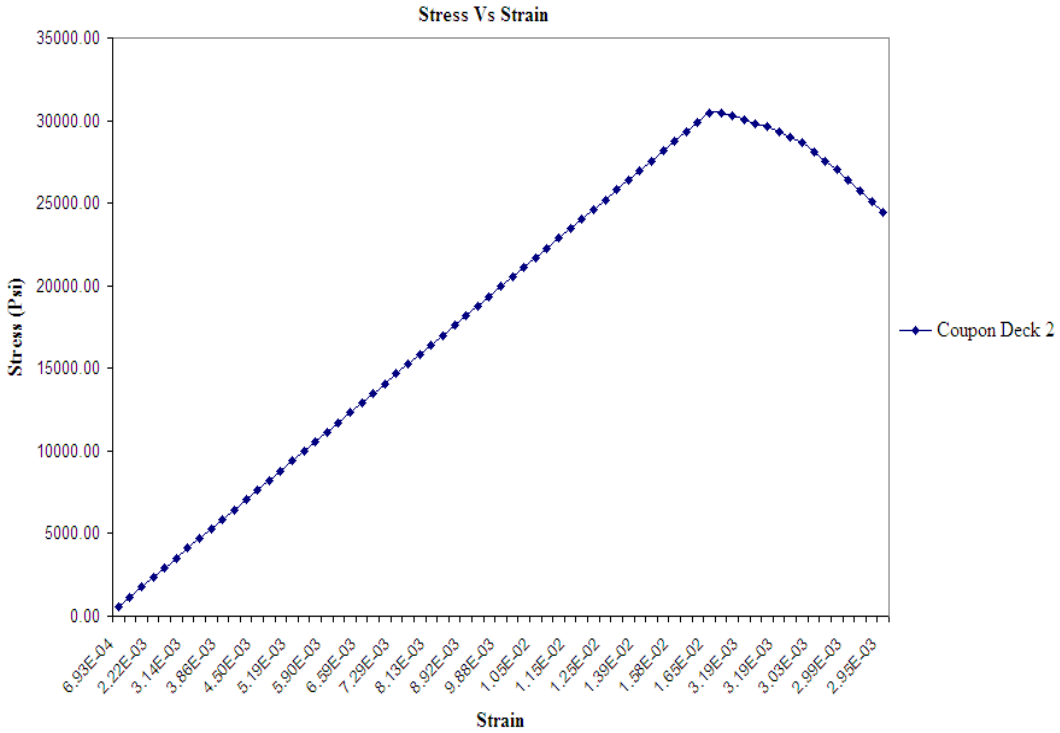

Figure C.64: Stress Vs Strain for Fiber Deck Coupon 2

The calculated modulus of elasticity from the graph for fiber deck coupon 2 is E = 2.46 E+06 Psi

Coupon #1

Geometry:

Width: .5010 in

Thickness: .2650 in

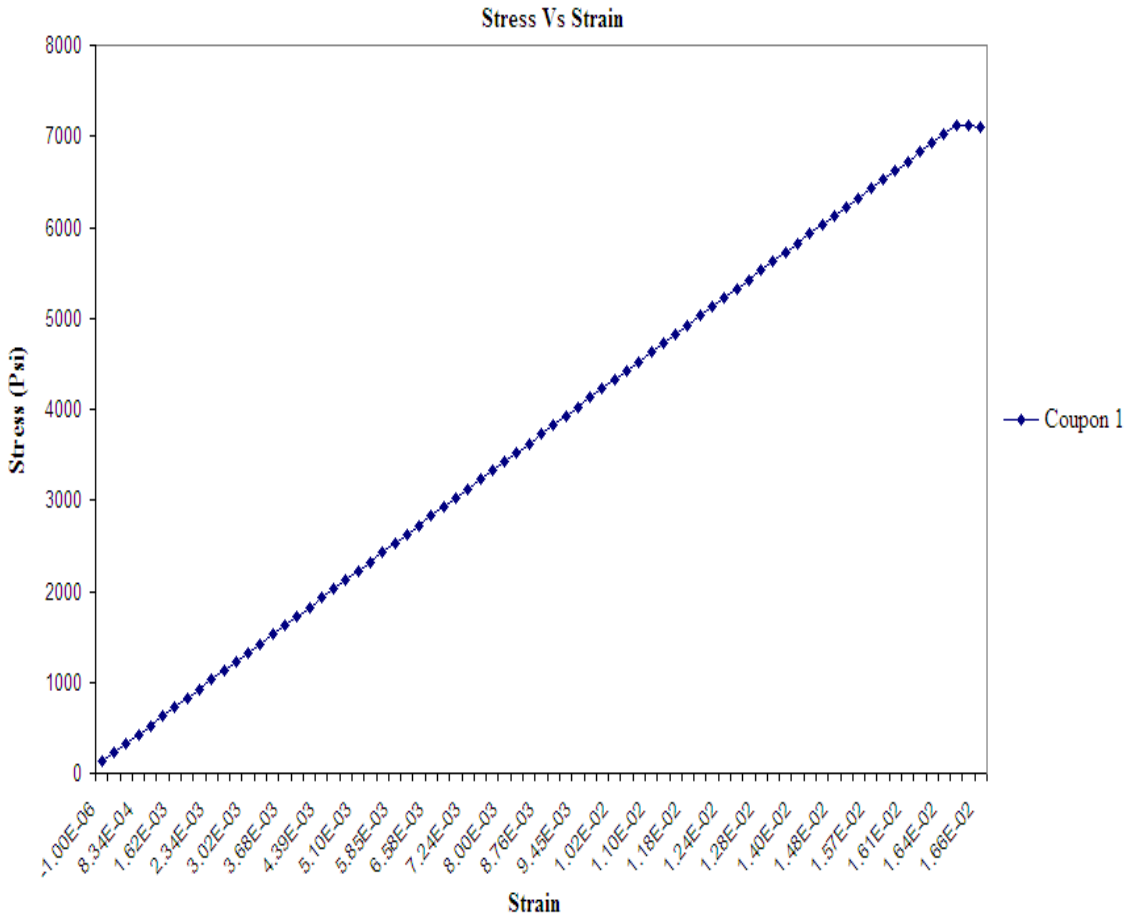

Figure C.65: Stress Vs Strain for Fiber Composite Tubular Section Coupon 1

The calculated modulus of elasticity from the graph for fiber composite tubular section coupon 1 is E = 4.16 E+05 Psi

Coupon #2

Geometry:

Width: .5030 in

Thickness: .2650 in

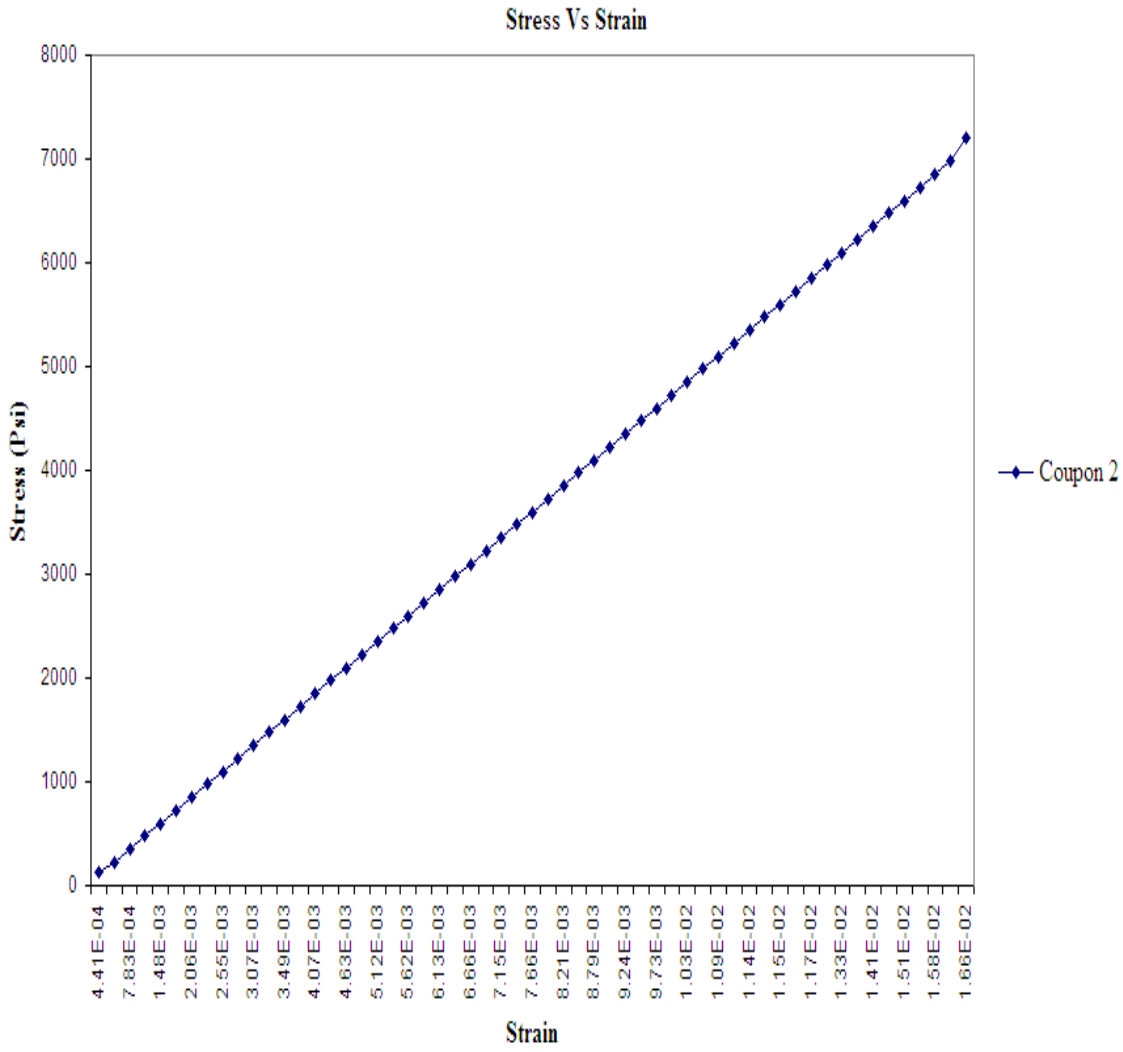

Figure C.66: Stress Vs Strain for Fiber Composite Tubular Section Coupon 2

The calculated modulus of elasticity from the graph for fiber composite tubular section coupon 2 is E = 4.79 E+05 Psi

Analysis of a Prototype using Ansys Fem Software

In this part of the section, the models were generated and analyzed using the finite element software ANSYS^{TM} Classic 10.0. The models were analyzed for thermal loading. Three models were generated using Pro-E software. The three models used in the analysis are as shown in figure C.71 and C.72. The models were meshed as solid 90 and subjected to transient temperature loading. The temperature was varied linearly with time for the first 23400 seconds from the room temperature 75.7˚F to maximum temperature 140˚F and then the temperature was stabilized to 140˚F for the next 48600 for Type I, Type II and Type III Models .The process was repeated for Type II model with different exposure times after stabilizing as 84600, 252000 and 383400 seconds.

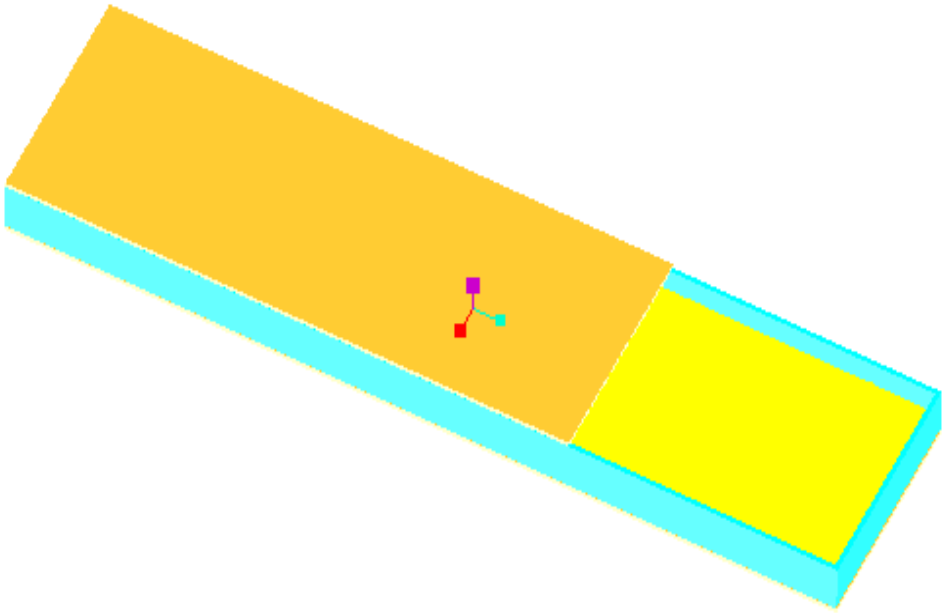

Figure C.67: Type I Model

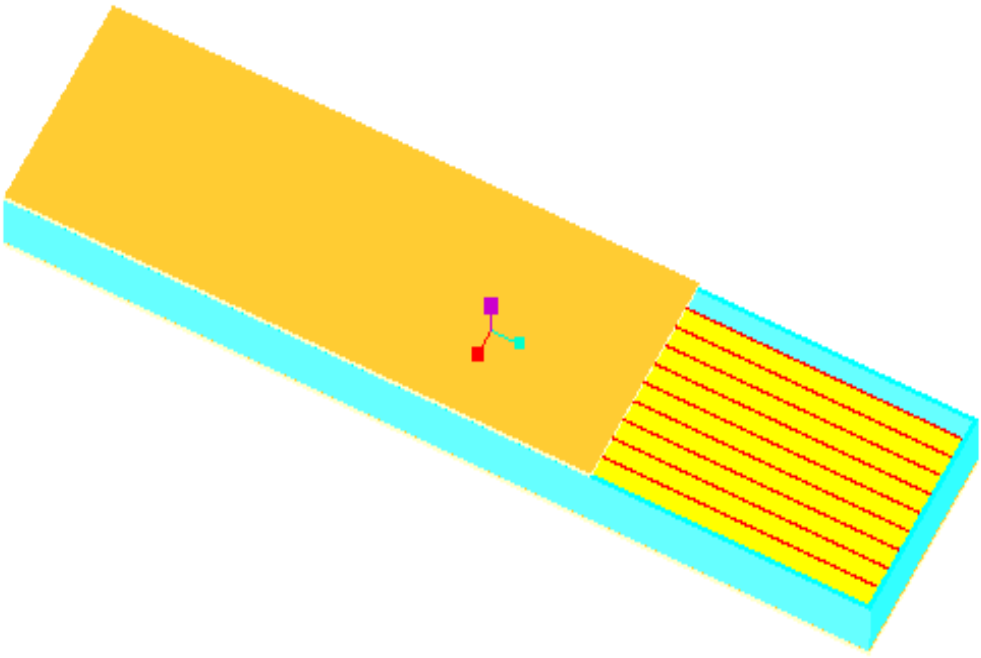

Figure C.68: Type II and Type III Model

Models

Table C.1: Models used in the FEM Analysis

Models	Type I	Type II	Type III
Shape	Rectangular Hollow Box	Rectangular Hollow Box	Rectangular Hollow Box
Width, feet	1.975	1.975	1.975
Length, feet	8	8	8
Depth, inches	6	6	8
Thickness of plate, inches	.5	.5	.5
Core	Filled with air	Rectangular plates of .3 inches placed at 2.3 inches C/C	Rectangular plates of .3 inches placed at 2.3 inches C/C

Material Properties used in the Analysis:

Table C.2: Material Properties

Properties	Air at Room temperature	Chopped Strand Mat
Specific Heat, $Jg^{-1}K^{-1}$ **(** $J/Kg.C^{o}$ **)**	1.012 (1012)	1.55 (1550)
Thermal Conductivity, W/ (m-K) (W/m-C˚)	0.025 (0.025)	0.85 (0.85)
Density lb/ft^3 (Kg/m^3)	0.0737 (1.18)	0.469 (7.51)

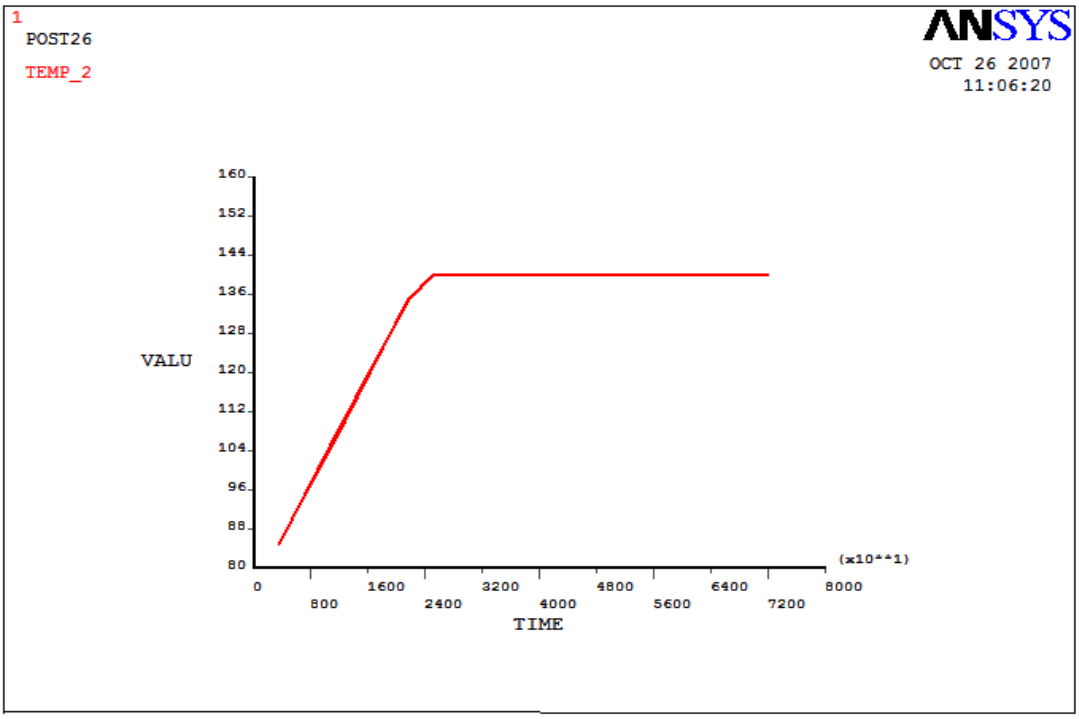

Figure C.69: Top Temperature of Type I Subjected to 72000 Seconds

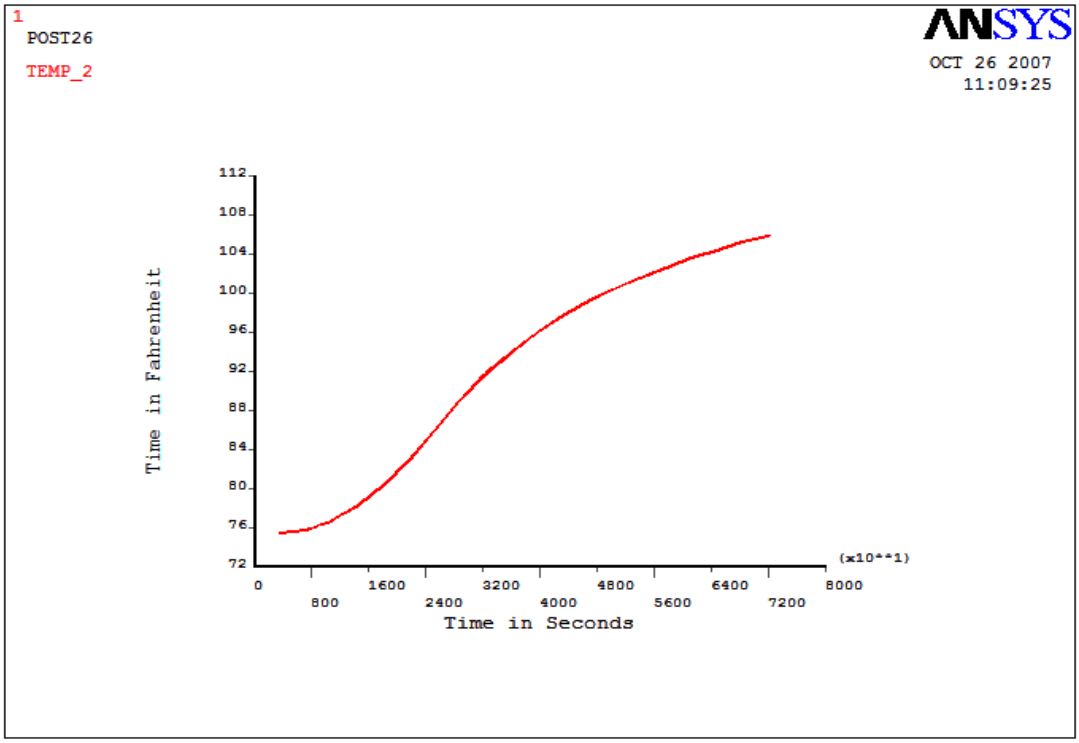

Figure C.70: Center Temperature of Type I Subjected to 72000 Seconds

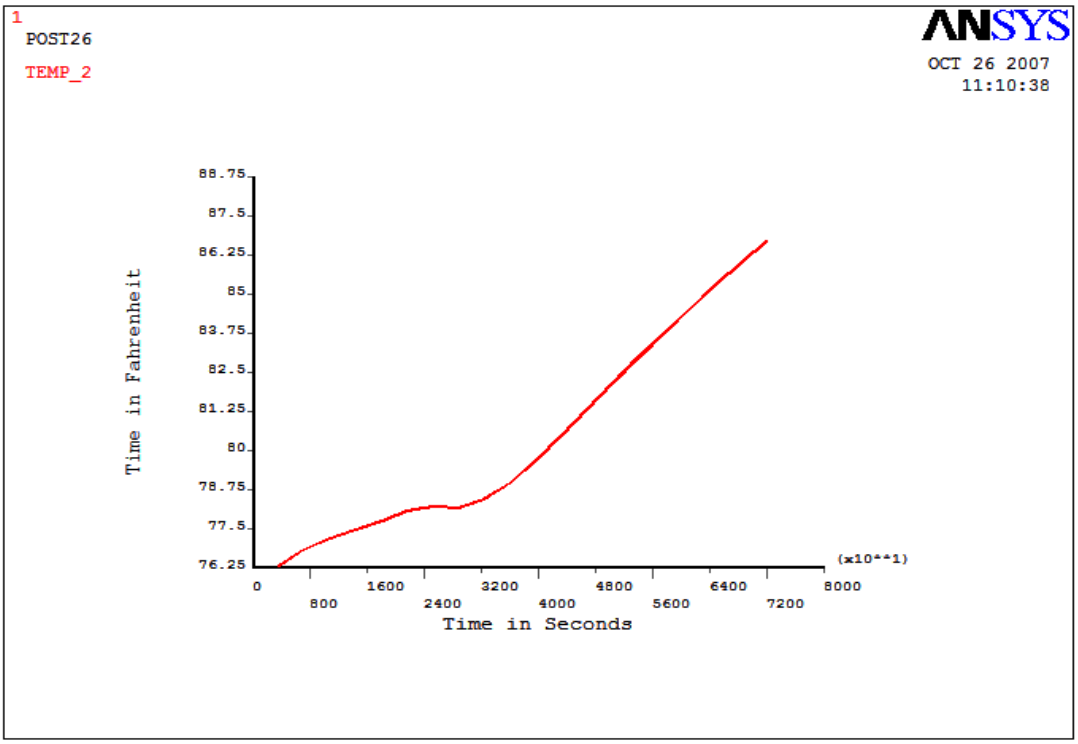

Figure C.71: Bottom Temperature of Type I Subjected to 72000 Seconds

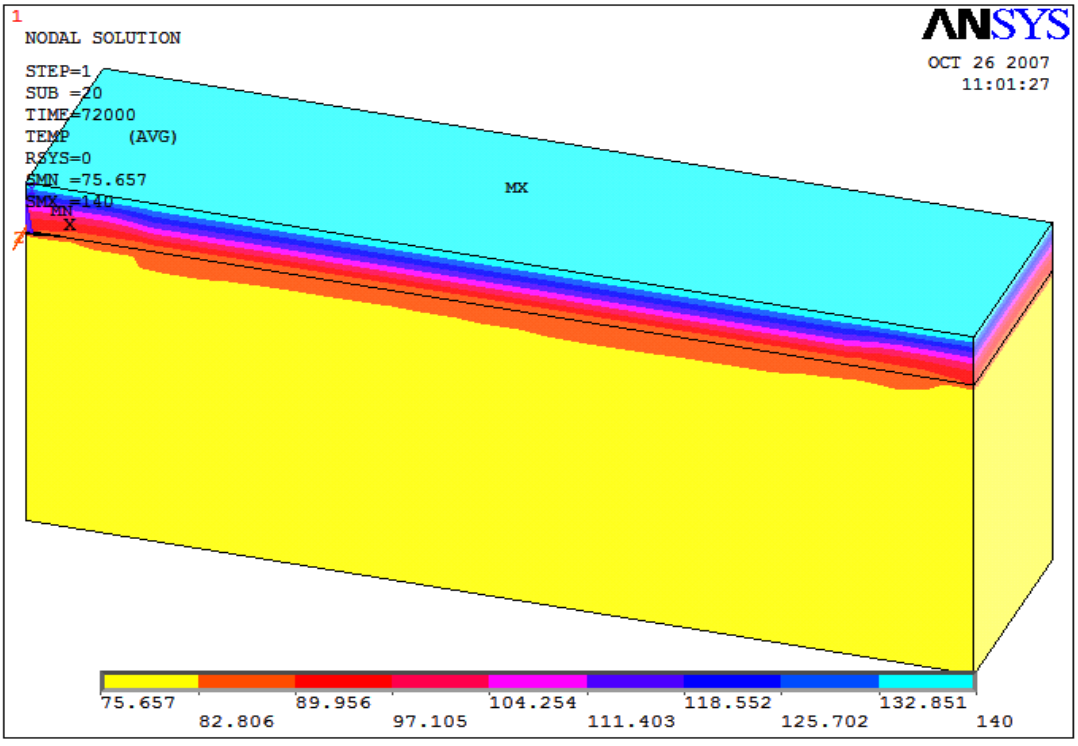

Figure C.72: Change in Temperature over Depth for Type I Subjected to 72000 Seconds

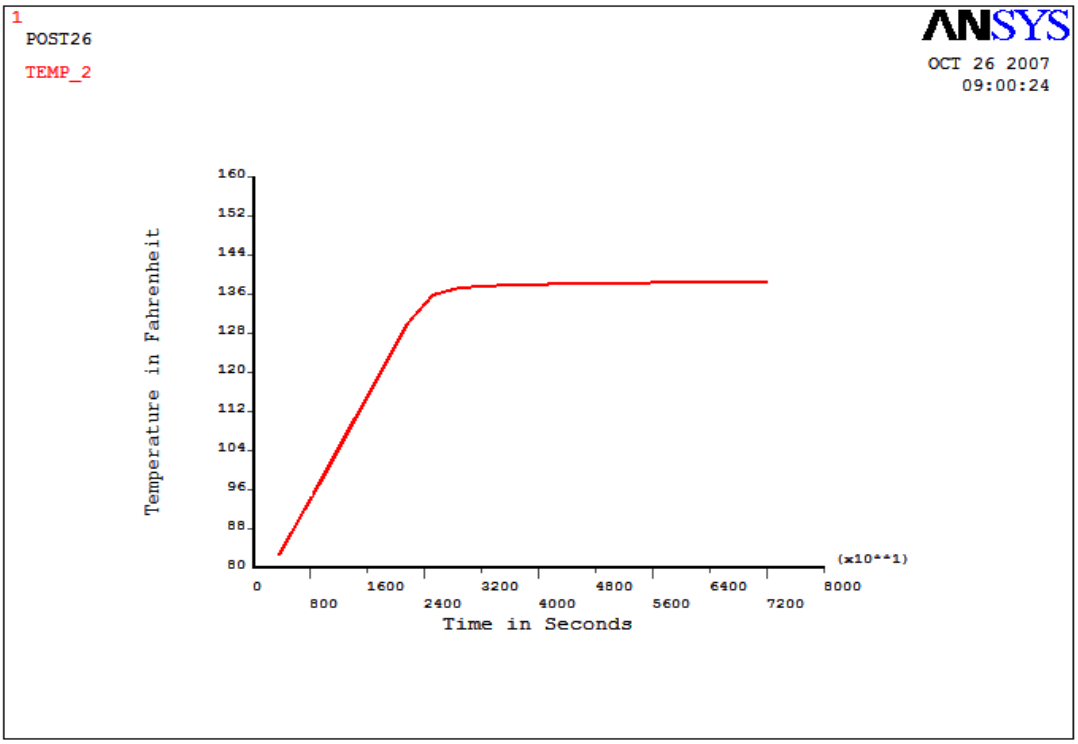

Figure C.73: Top Temperature of Type II Subjected to 72000 Seconds

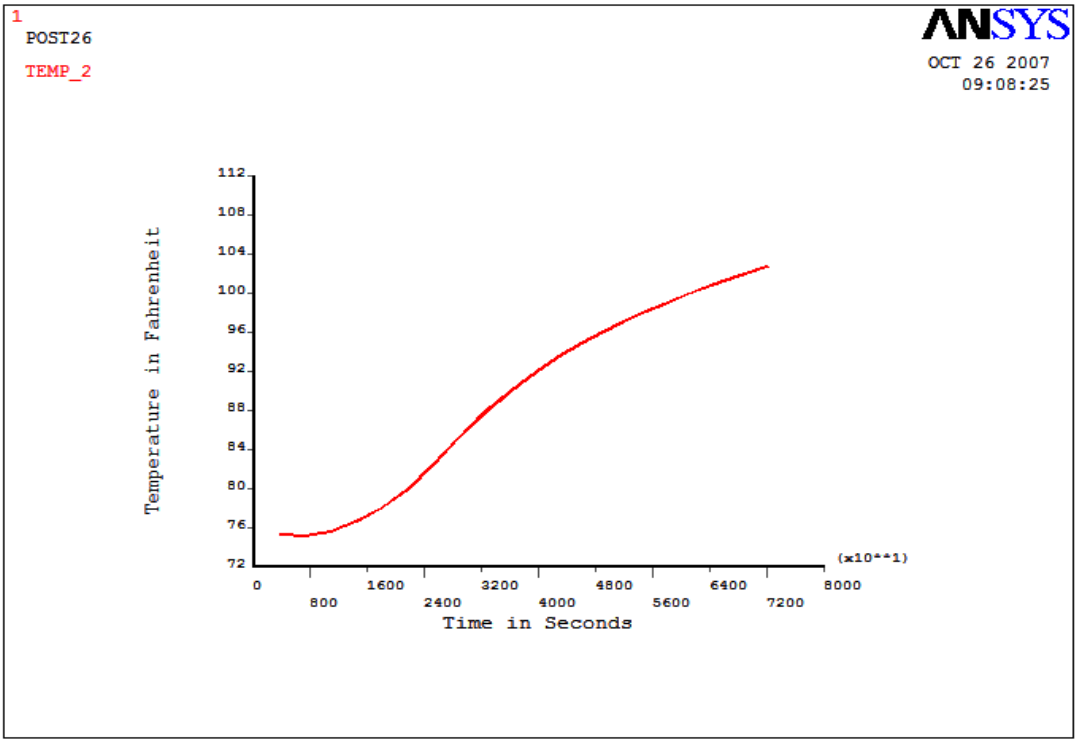

Figure C.74: Center Temperature of Type II Subjected to 72000 Seconds

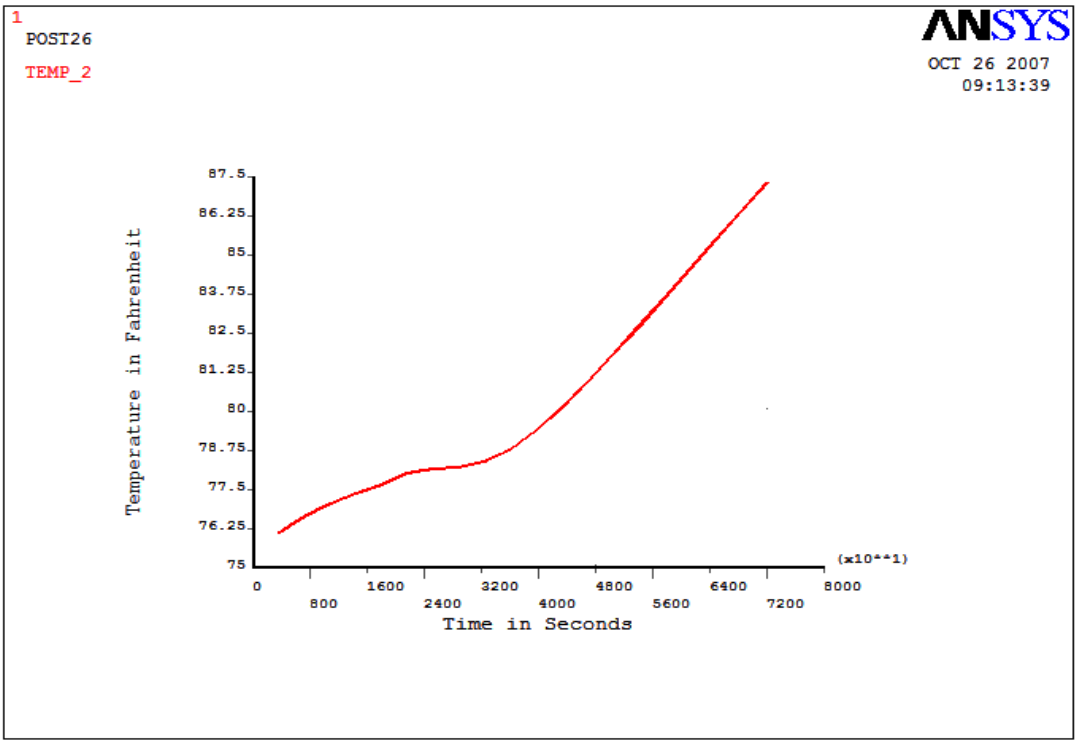

Figure C.75: Bottom Temperature of Type II Subjected to 72000 Seconds

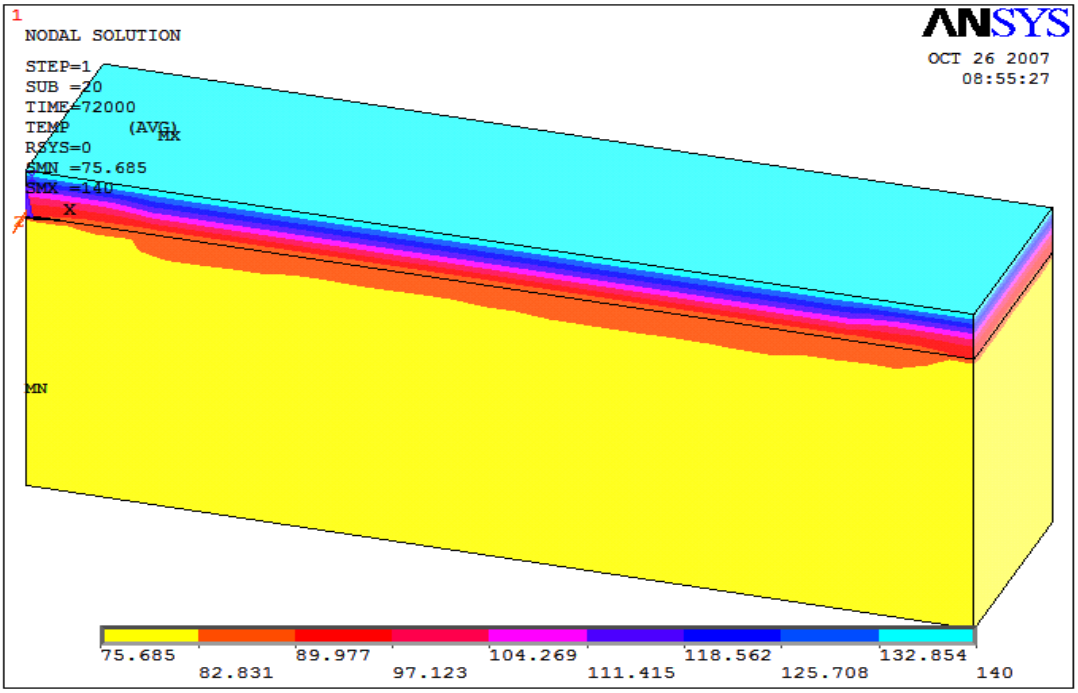

Figure C.76: Change in Temperature over Depth for Type II Subjected to 72000 Seconds

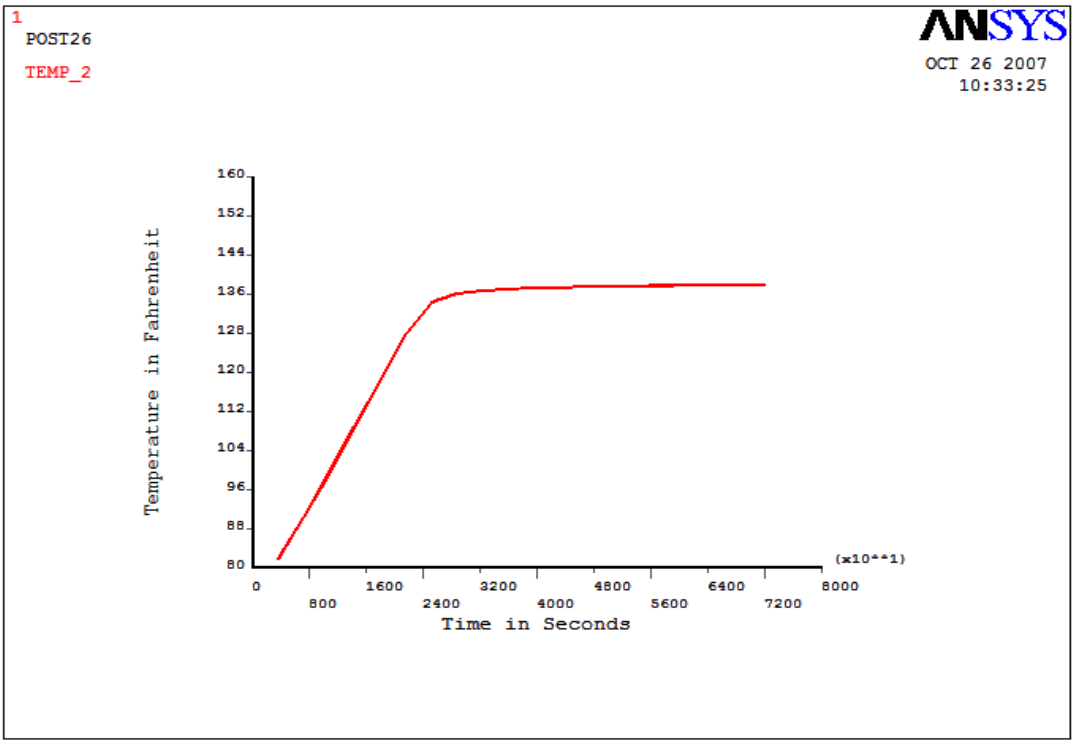

Figure C.77: Top Temperature of Type III Subjected to 72000 Seconds

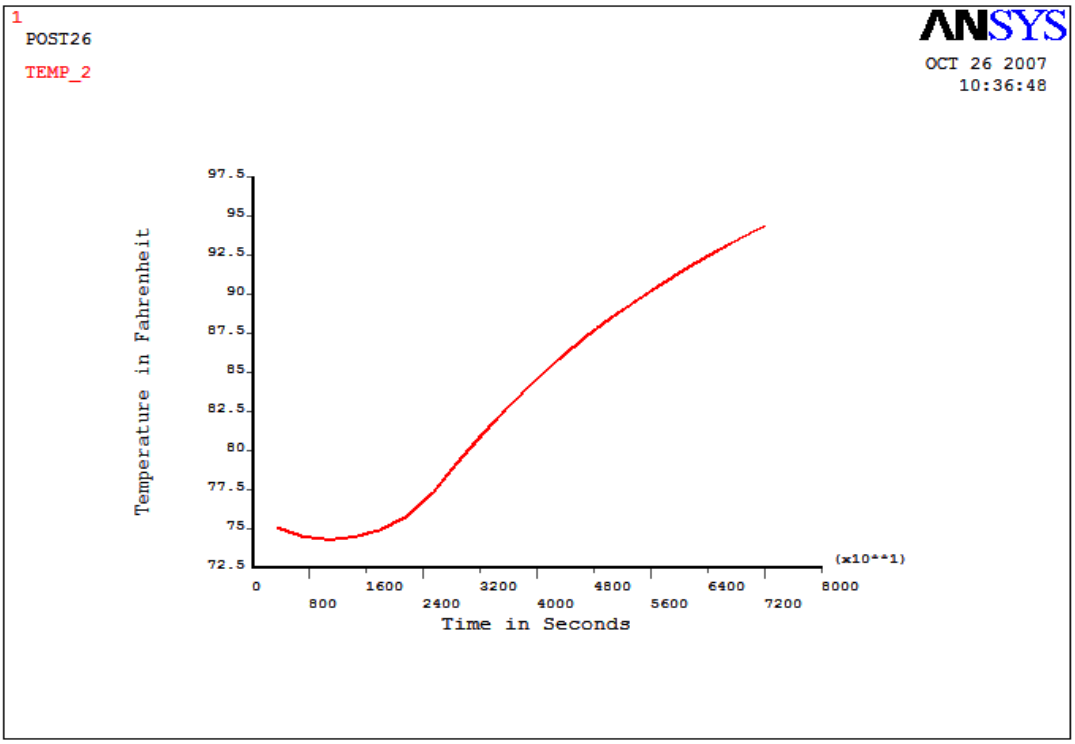

Figure C.78: Center Temperature of Type III Subjected to 72000 Seconds

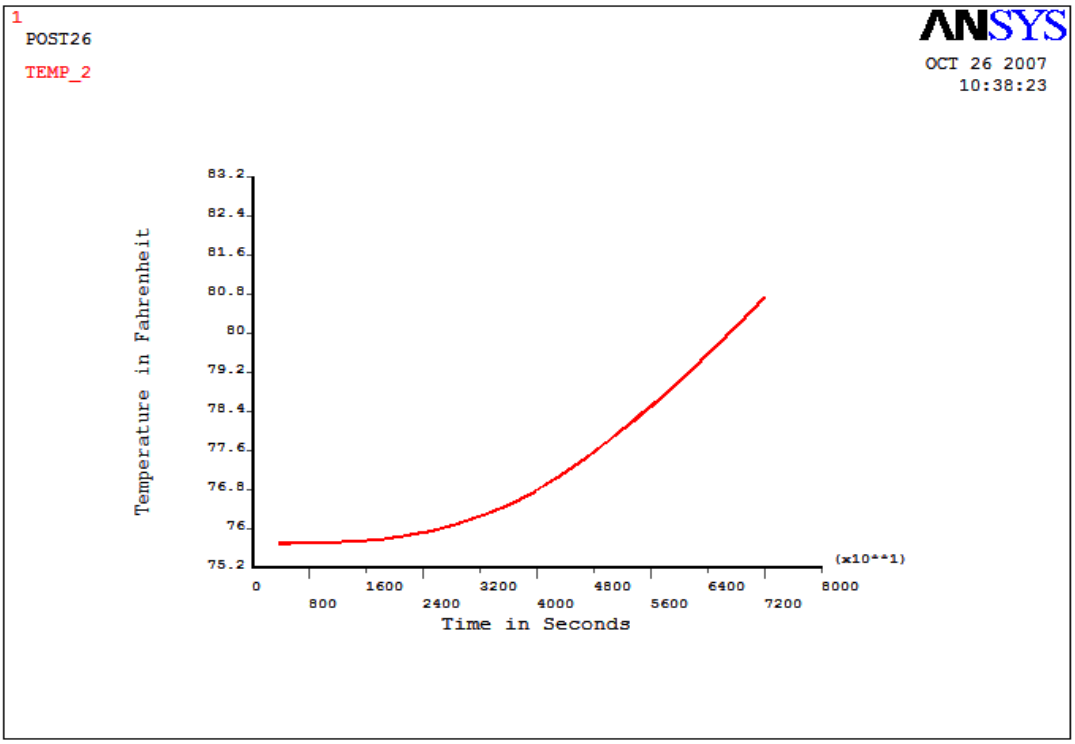

Figure C.79: Bottom Temperature of Type III Subjected to 72000 Seconds

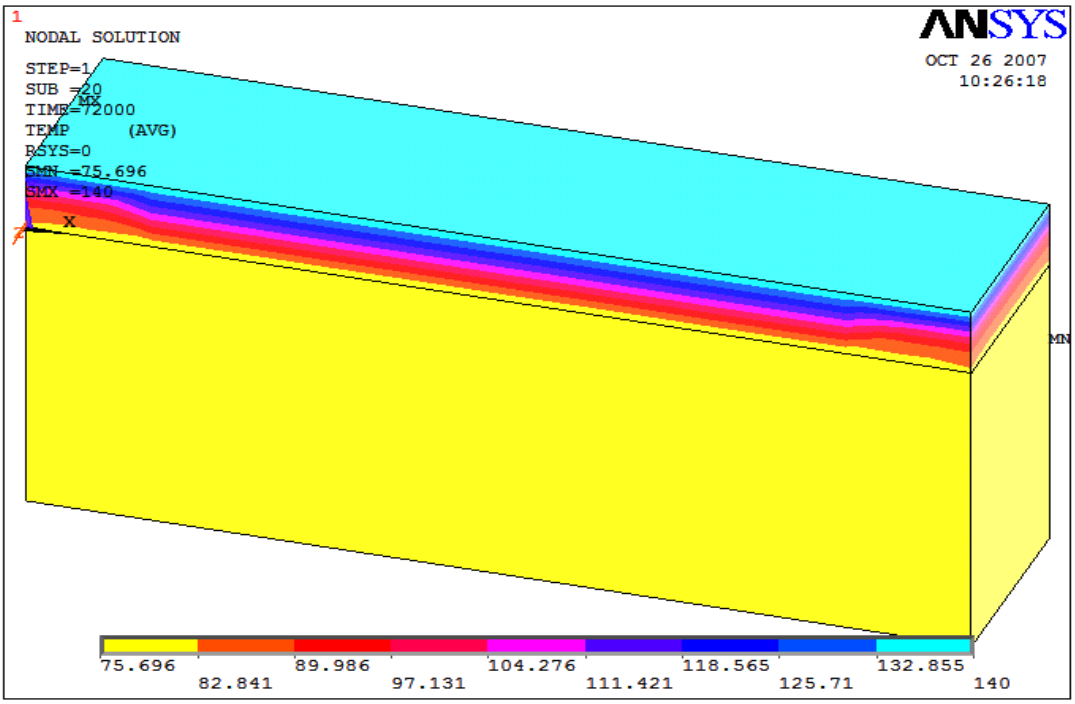

Figure C.80: Change in Temperature over Depth for Type III Subjected to 72000 Seconds

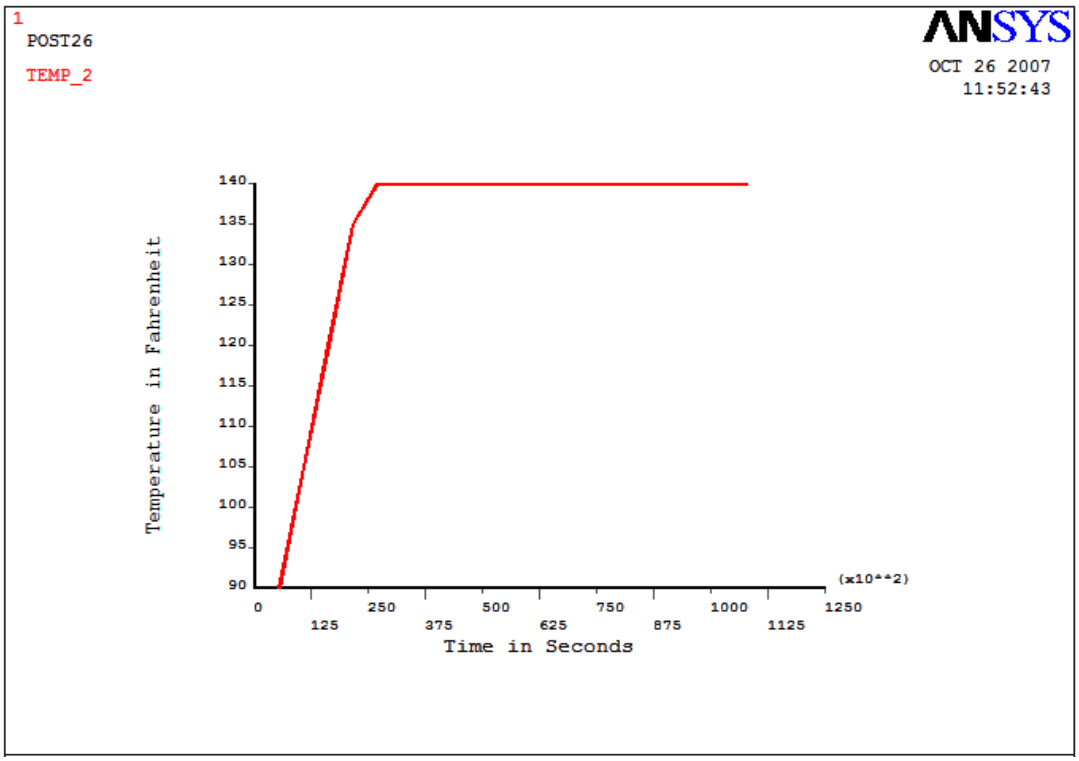

Figure C.81: Top Temperature of Type II Subjected to 108000 Seconds

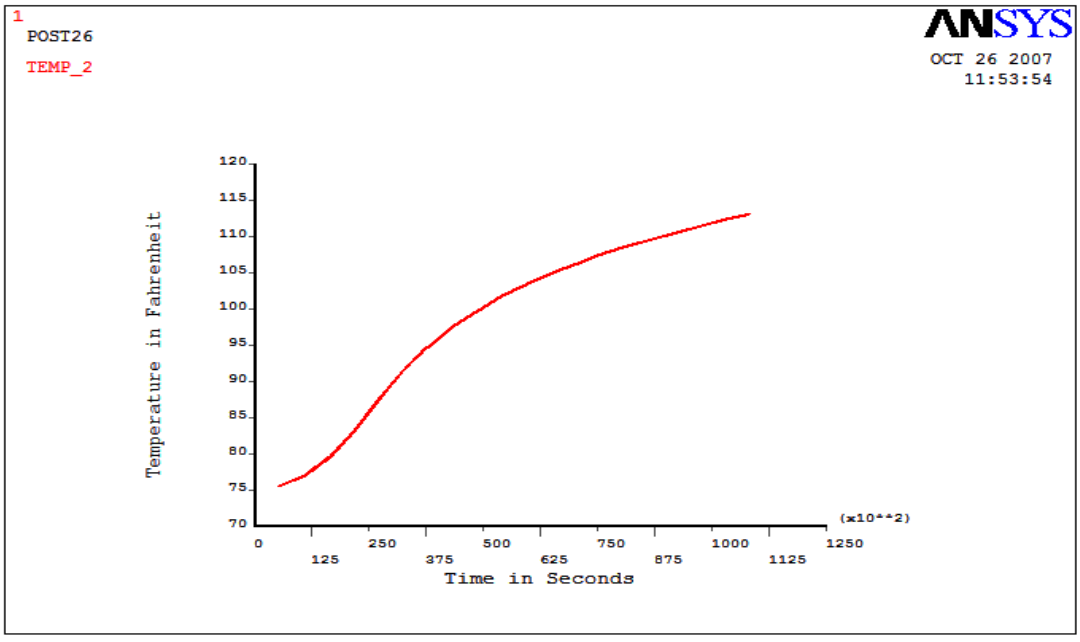

Figure C.82: Center Temperature of Type II Subjected to 108000 Seconds

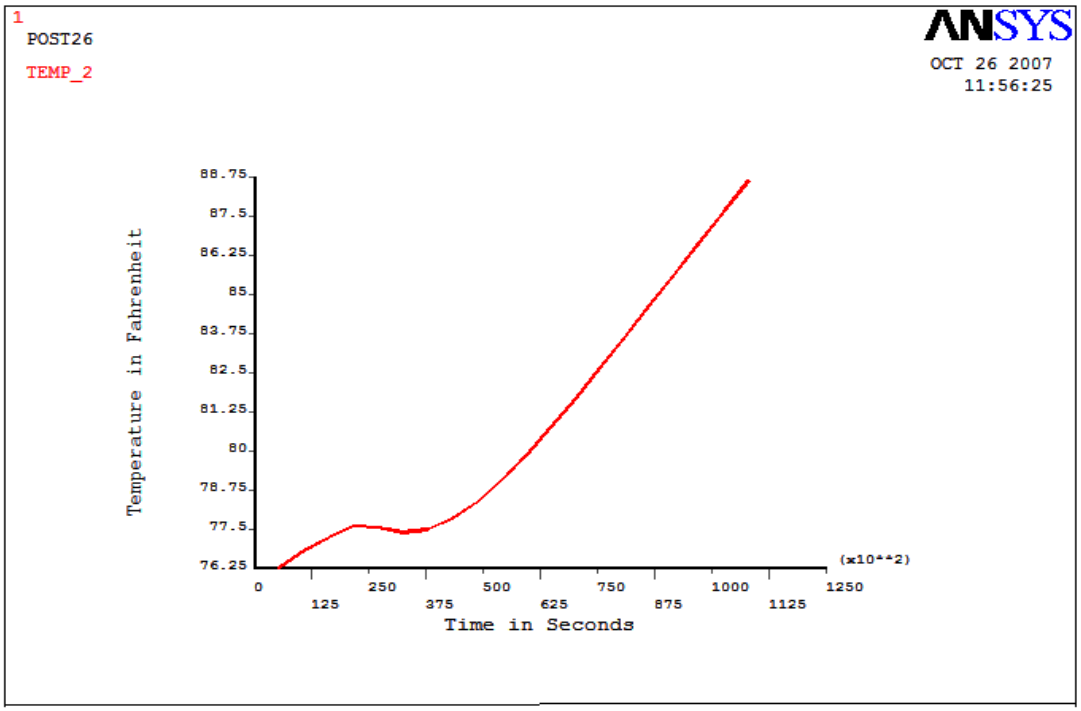

Figure C.83: Bottom Temperature of Type II Subjected to 108000 Seconds

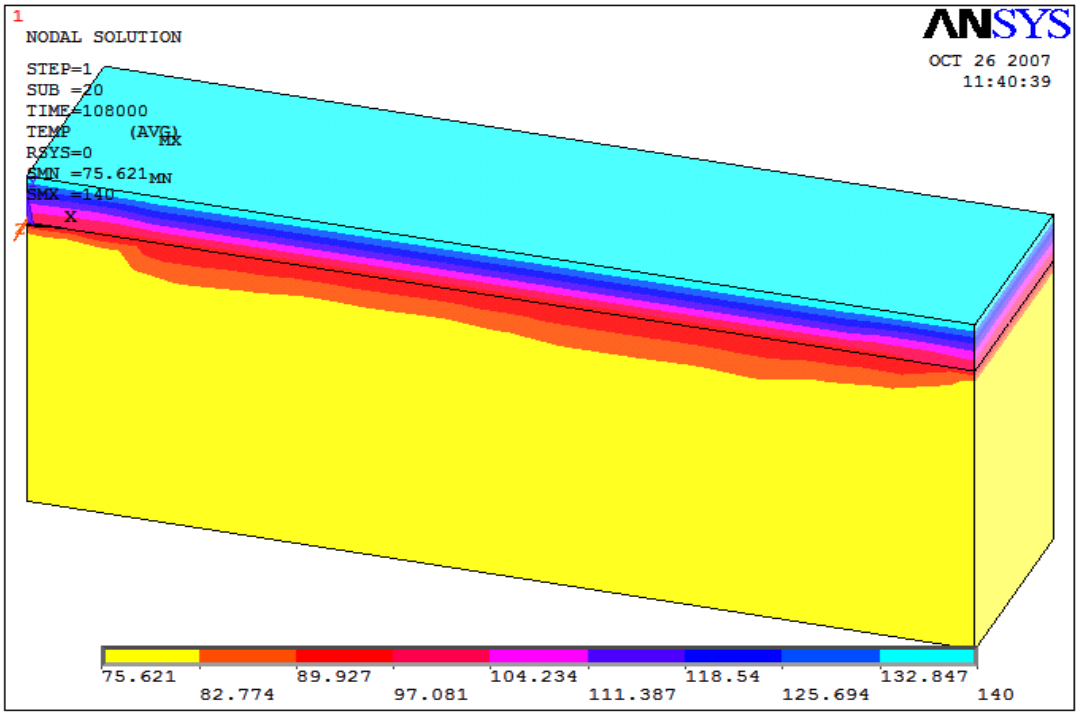

Figure C.84: Change in Temperature over Depth for Type II Subjected to 108000 Seconds

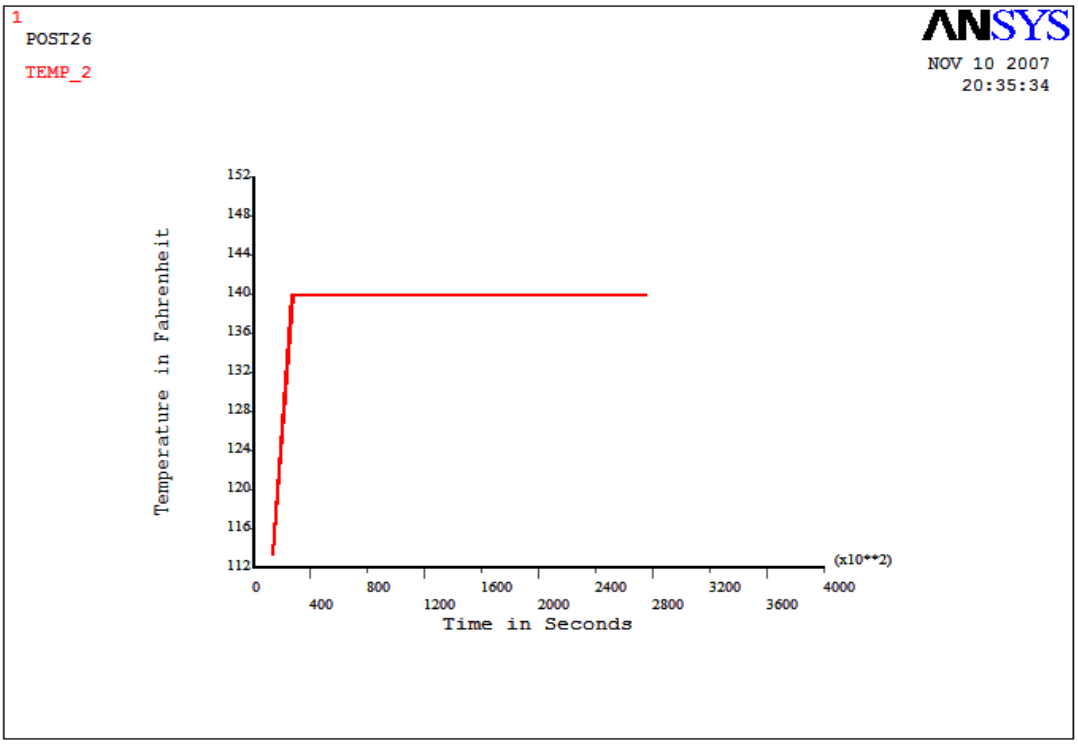

Figure C.85: Top Temperature of Type II Subjected to 275400 Seconds

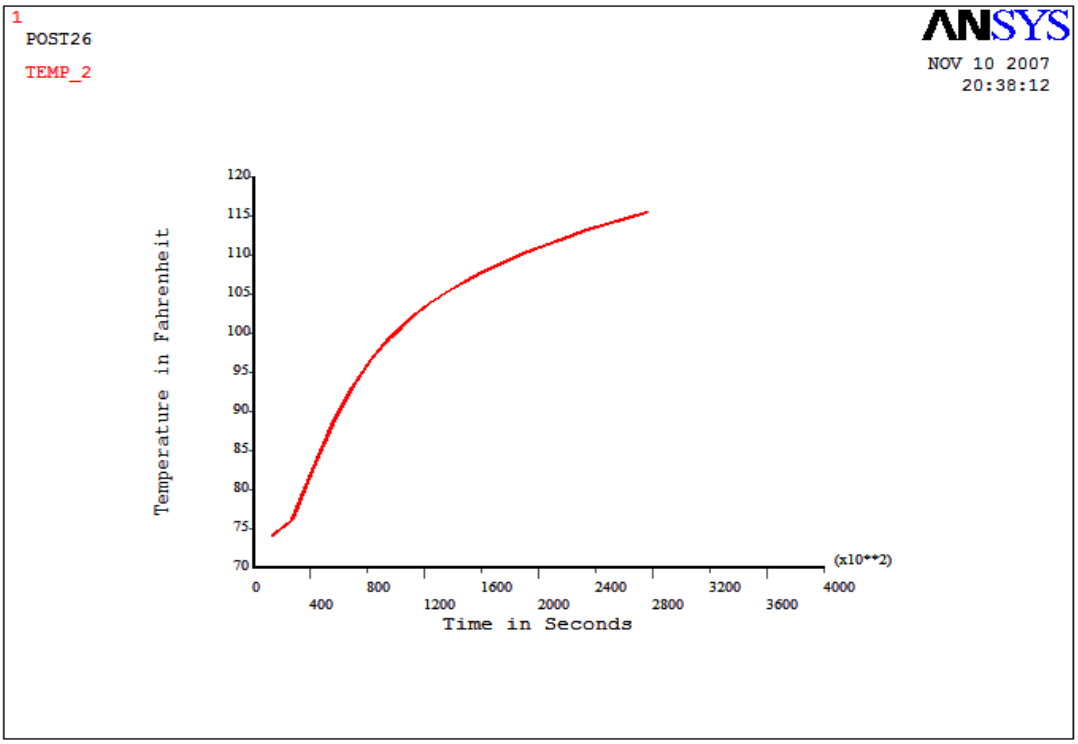

Figure C.86: Center Temperature of Type II Subjected to 275400 Seconds

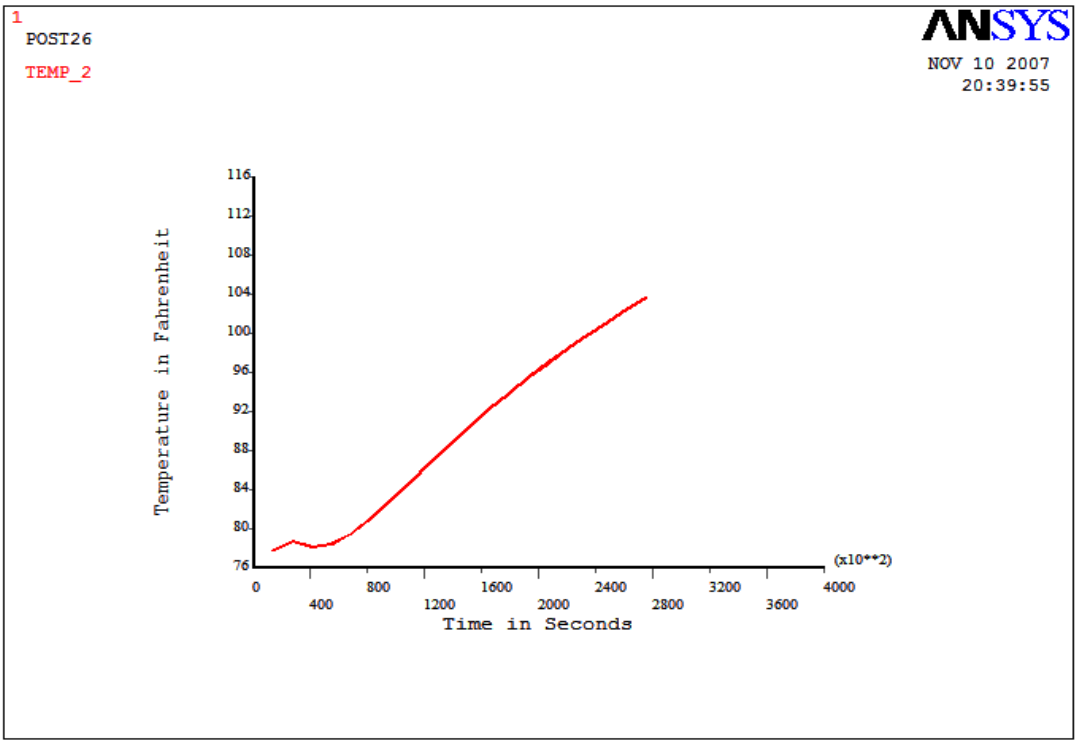

Figure C.87: Bottom Temperature of Type II Subjected to 275400 Seconds

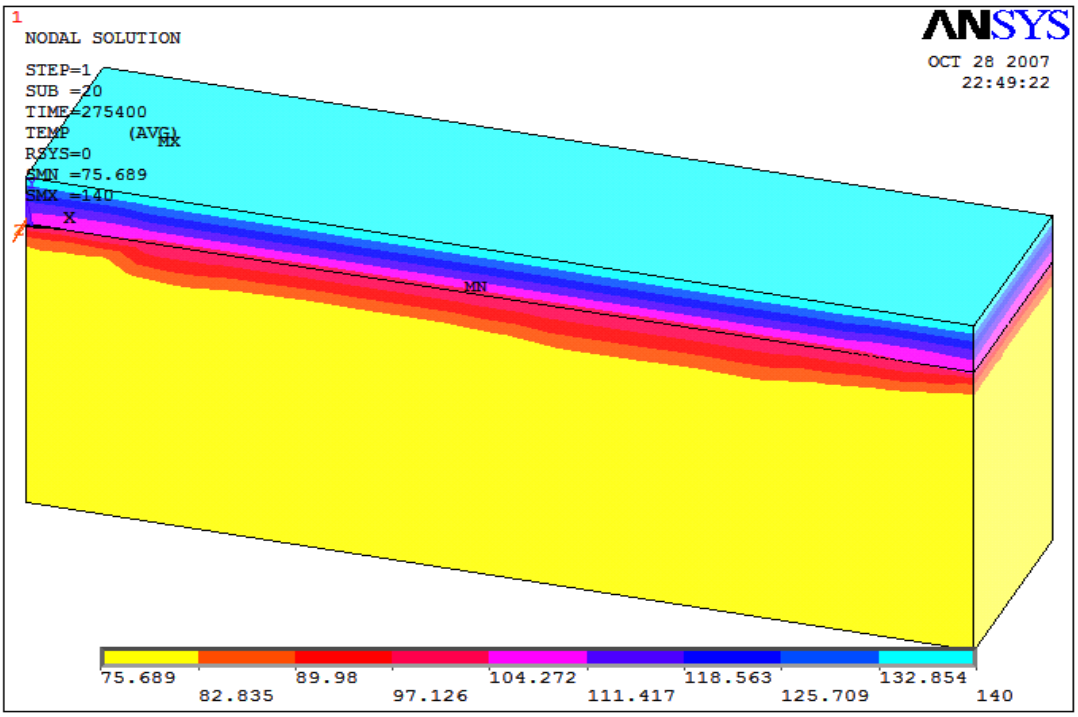

Figure C.88: Change in Temperature over Depth for Type II Subjected to 108000 Seconds

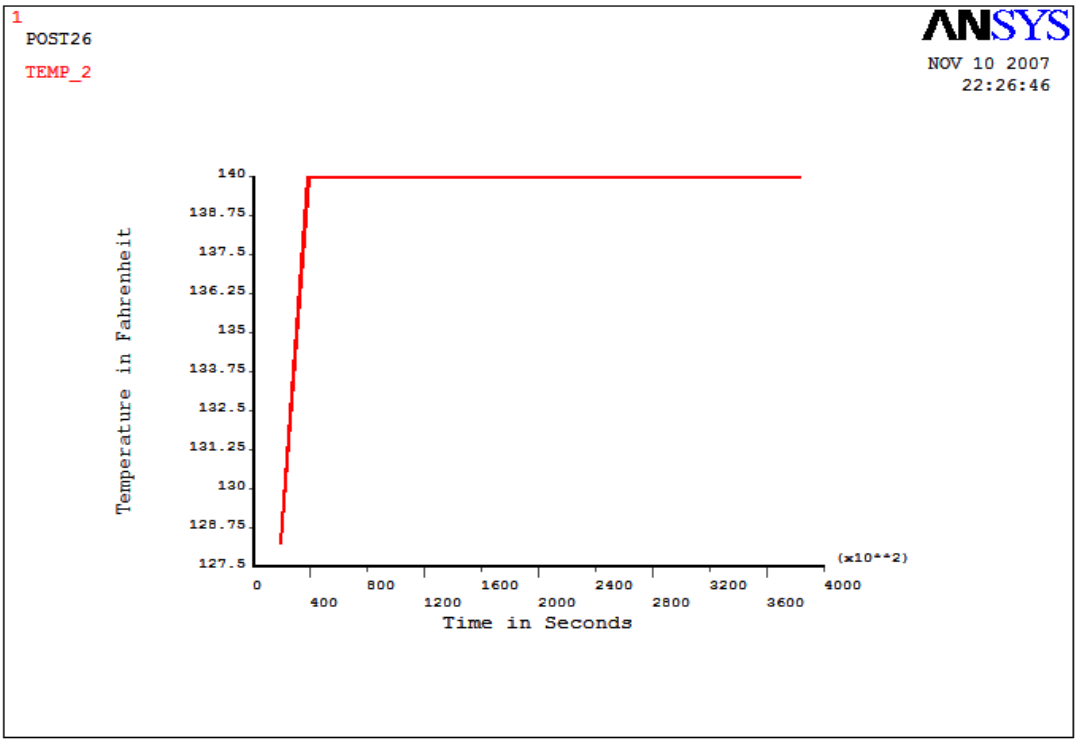

Figure C.89: Top Temperature of Type II Subjected to 383400 Seconds

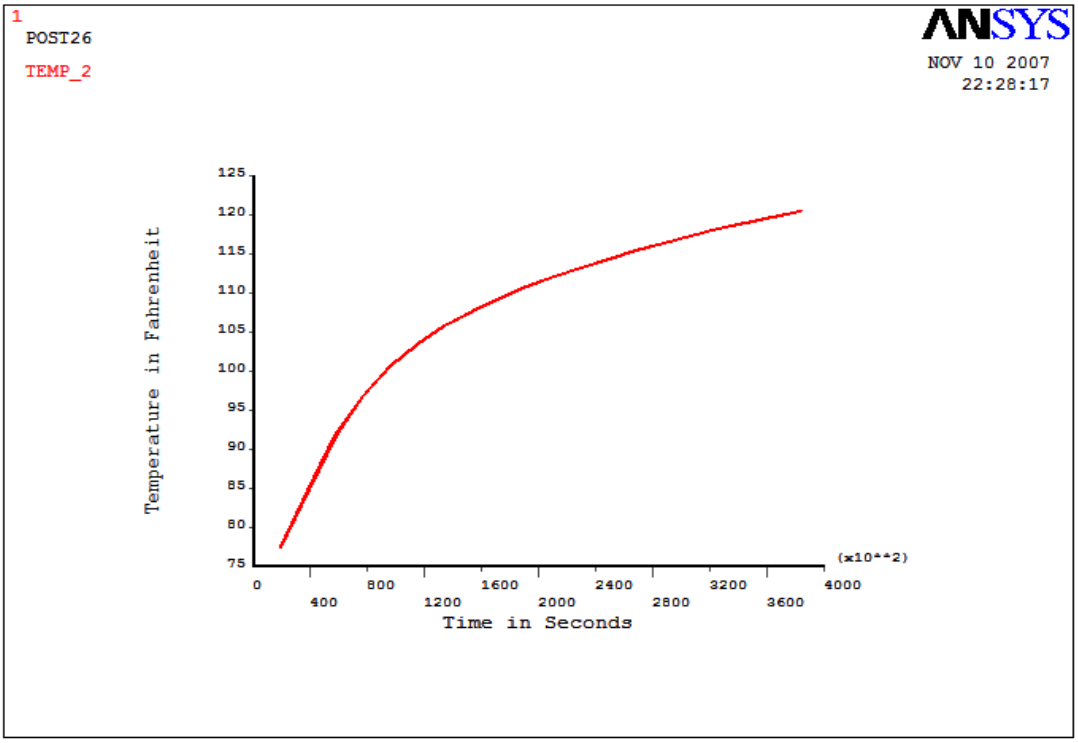

Figure C.90: Center Temperature of Type II Subjected to 383400 Seconds

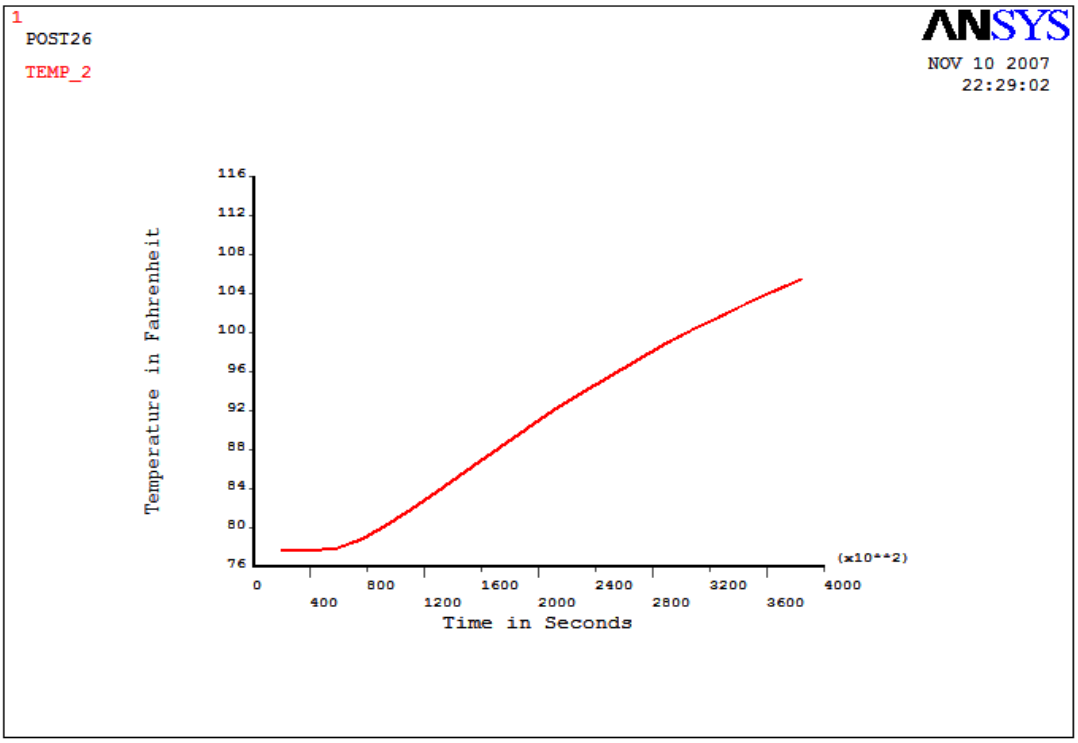

Figure C.91: Bottom Temperature of Type II Subjected to 383400 Seconds

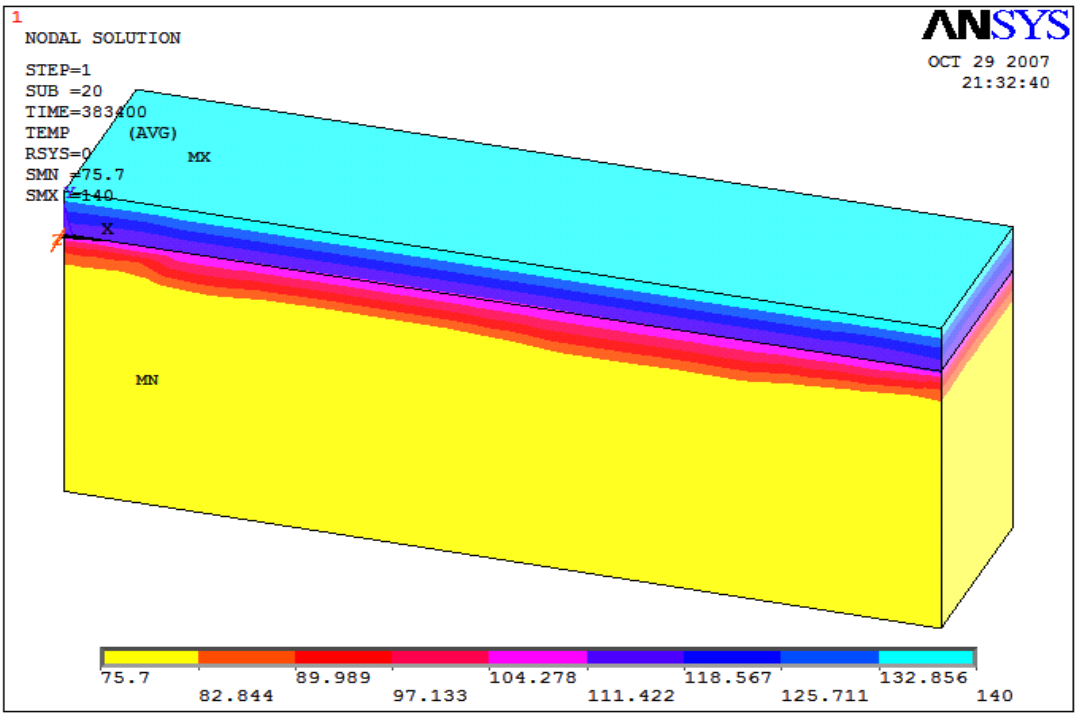

Figure C.92: Change in Temperature over Depth for Type II Subjected to 383400 Seconds

REFERENCES

1. Emanuel, Jack H. and Taylor, Charles M. (1985), “Length-Thermal Stress Relations for Composite Bridges”, Journal of Structural Engineering, Vol. 111, No. 4, April, 1985
2. Emanuel, Jack H. and Hulsey, J.L. (1978), “Temperature Distribution in Composite Bridges”, Journal of the Structural Division, Vol. 104, No. 1, January, 1978
3. Kennedy, John B. and Soliman, Mohamed H. (1987), “Temperature Distribution in Composite Bridges”, Journal of the Structural Division, Vol. 113, No. 3, March 1987
4. Zuk, W. (1965). “Thermal Behaviour of Composite Bridges-Insulated and Uninsulated” Highway Research Record. T6.
5. Zuk, W. (1965). “Simplified Design Check of Thermal Stresses in Composite Highway Bridges.” Highway Research Record. 103.
6. Churchward, A., and Sokal, Y., “Prediction of Temperatures in Concrete Bridges,” Journal of the Structural Division, ASCE, Vol. 107, No. ST11, Proc Paper 16676, Nov., 1981, pp. 2163-2176.
7. Piyush K. Dutta, Soon-Chul Kwon and Roberto Lopez Anido, “Fatigue Performance Evaluation of FRP Composite Bridge Deck Prototype Under High and Low Temperatures”, Transportation Research Board, 82nd Annual Meeting, Washington, D.C, January, 2003

8. S.C.Kwon, P.K.Dutta, Y.H.Kim, S.H.Eum, D.H.Shin and R.Lopez-Anido, “Fatigue Studies of FRP Composite Decks at Extreme Environmental Conditions”, Key Engineering Materials Vol. 261-263 (2004) pp. 1301-1306
9. Vishay Micro Measurements Tech note TN-513-1 “Measurement of Thermal Coefficient using Strain Gages”.
10. Vishay Micro Measurements Tech note TN-506-3 “Bondable Resistance Temperature Sensors and Associated Circuitry”.
11. ASTM D 3039/D 3039 M, Standard Test Method for Tensile Properties of Polymer Matrix Composite Materials.
12. Plunkett JD. Fiber-Reinforcement Polymer Honeycomb Short Span Bridge for Rapid Installation. IDEA Project Report, November 1997.
13. Julio F. Davalos, Pizahong Qiao, X. Frank Xu, Justin Robinson, Karl E. Barth. “Modeling and Characterization of Fiber-Reinforced Plastic Honeycomb Sandwich Panels for Highway Bridge Applications”
14. http://www.mece.ualberta.ca/tutorials/ansys/
15. Incropera, Frank P.; DeWitt, David P. (August 9 2001). Fundamentals of Heat and Mass Transfer, 5th Edition
16. R.A.Schapery, “Thermal Expansion Coefficients of Composite Materials Based on Energy Principles,” J. Compos. Mater., 2(3), 280-404(1986).
17. www.intekcorp.com
18. www.amazon.com
19. www.ibutton.com

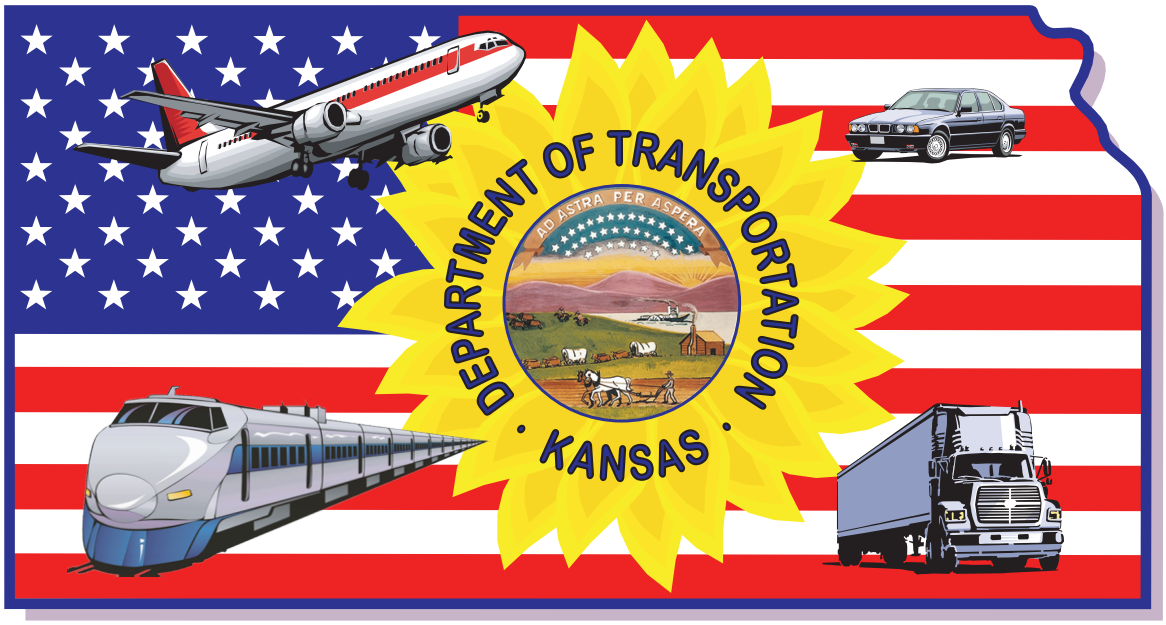
DEPARTMENT OF TRANSPORTATION
KANSAS
AD ASTRA PER ASPERA